

GL-TR-90-0332(A)
ENVIRONMENTAL RESEARCH PAPERS, NO. 1073

1

Proceedings of the 10th Annual DARPA/AFGL Seismic
Research Symposium, 3-5 May 1988
ADDENDUM

DTIC FILE COPY

Editors:

JAMES F. LEWKOWICZ
JEANNE M. McPHETRES

DTIC
ELECTE
DEC 31 1990
S D & D



17 December 1990



Approved for public release; distribution unlimited.




EARTH SCIENCES DIVISION
GEOPHYSICS LABORATORY
PROJECT 7600
HANSCOM AFB, MA 01731-5000

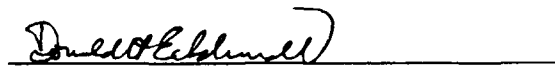
90 12 26 181

AD-A230 066

"This technical report has been reviewed and is approved for publication."

FOR THE COMMANDER


JAMES F. LEWKOWICZ
Branch Chief
Solid Earth Geophysics Branch
Earth Sciences Division


DONALD H. ECKHARDT
Director
Earth Sciences Division

This report has been reviewed by the ESD Public Affairs Office (PA) and is releasable to the National Technical Information Service (NTIS).

Qualified requestors may obtain additional copies from the Defense Technical Information Center. All others should apply to the National Technical Information Service.

If your address has changed, or if you wish to be removed from the mailing list, or if the addressee is no longer employed by your organization, please notify GL/IMA, Hanscom AFB, MA 01731-5000. This will assist us in maintaining a current mailing list.

Do not return copies of this report unless contractual obligations or notices on a specific document requires that it be returned.

17 December 1990 Scientific, Interim

Proceedings of the 10th Annual DARPA/AFGL Seismic
Research Symposium, 3-5 May 1988
ADDENDUM

PE 62101F
PR 7600
TA 09
WU 08

Editors: James F. Lewkowicz
Jeanne M. McPhetres

Air Force Geophysics Laboratory, AFSC
AFGL/LWH
Hanscom AFB, MA 01731-5000

GL-TR-90-0332(A)
ERP, No. 1073

DARPA/NMRO
1400 Wilson Boulevard
Arlington, VA 22209-2308

This research was supported by DARPA under PE 61101E and 62714E.

Approved for Public Release; distribution unlimited

This Addendum contains the following:

Slides and overheads presented as part of the special session entitled, "Current Research Issues in Nuclear Test Ban Treaty Monitoring"

Late papers that were part of the general technical session.

Poster papers presented at the poster session.

Critical Reviews of the meeting.

underground nuclear explosion, seismic waves, regional
seismology arrays, yield estimation, source coupling

250

UNCLASSIFIED

UNCLASSIFIED

UNCLASSIFIED

UL

GENERAL INSTRUCTIONS FOR COMPLETING SF 298

The Report Documentation Page (RDP) is used in announcing and cataloging reports. It is important that this information be consistent with the rest of the report, particularly the cover and title page. Instructions for filling in each block of the form follow. It is important to stay within the lines to meet optical scanning requirements.

Block 1. Agency Use Only (Leave Blank)

Block 2. Report Date. Full publication date including day, month, and year, if available (e.g. 1 Jan 88). Must cite at least the year.

Block 3. Type of Report and Dates Covered. State whether report is interim, final, etc. If applicable, enter inclusive report dates (e.g. 10 Jun 87 - 30 Jun 88).

Block 4. Title and Subtitle. A title is taken from the part of the report that provides the most meaningful and complete information. When a report is prepared in more than one volume, repeat the primary title, add volume number, and include subtitle for the specific volume. On classified documents enter the title classification in parentheses.

Block 5. Funding Numbers. To include contract and grant numbers; may include program element number(s), project number(s), task number(s), and work unit number(s). Use the following labels:

C - Contract	PR - Project
G - Grant	TA - Task
PE - Program Element	WU - Work Unit Accession No.

Block 6. Author(s). Name(s) of person(s) responsible for writing the report, performing the research, or credited with the content of the report. If editor or compiler, this should follow the name(s).

Block 7. Performing Organization Name(s) and Address(es). Self-explanatory.

Block 8. Performing Organization Report Number. Enter the unique alphanumeric report number(s) assigned by the organization performing the report.

Block 9. Sponsoring/Monitoring Agency Names(s) and Address(es). Self-explanatory.

Block 10. Sponsoring/Monitoring Agency Report Number. (If known)

Block 11. Supplementary Notes. Enter information not included elsewhere such as: Prepared in cooperation with...; Trans. of ..., To be published in When a report is revised, include a statement whether the new report supersedes or supplements the older report.

Block 12a. Distribution/Availability Statement.

Denote public availability or limitation. Cite any availability to the public. Enter additional limitations or special markings in all capitals (e.g. NOFORN, REL, ITAR)

DOD - See DoDD 5230.24, "Distribution Statements on Technical Documents."

DOE - See authorities

NASA - See Handbook NHB 2200.2.

NTIS - Leave blank.

Block 12b. Distribution Code.

DOD - DOD - Leave blank

DOE - DOE - Enter DOE distribution categories from the Standard Distribution for Unclassified Scientific and Technical Reports

NASA - NASA - Leave blank

NTIS - NTIS - Leave blank.

Block 13. Abstract. Include a brief (Maximum 200 words) factual summary of the most significant information contained in the report.

Block 14. Subject Terms. Keywords or phrases identifying major subjects in the report.

Block 15. Number of Pages. Enter the total number of pages.

Block 16. Price Code. Enter appropriate price code (NTIS only).

Blocks 17. - 19. Security Classifications. Self-explanatory. Enter U.S. Security Classification in accordance with U.S. Security Regulations (i.e., UNCLASSIFIED). If form contains classified information, stamp classification on the top and bottom of the page.

Block 20. Limitation of Abstract. This block must be completed to assign a limitation to the abstract. Enter either UL (unlimited) or SAR (same as report). An entry in this block is necessary if the abstract is to be limited. If blank, the abstract is assumed to be unlimited.



DEPARTMENT OF THE AIR FORCE
AIR FORCE GEOPHYSICS LABORATORY (AFSC)
HANSCOM AIR FORCE BASE, MASSACHUSETTS 01731-5000

This addendum contains the following:

* Slides and overheads presented as part of the special session entitled, "Current Research Issues in Nuclear Test Ban Treaty Monitoring"

* Late papers that were part of the general technical session

* Poster papers presented at the poster session

* Critical reviews of the meeting

I want to thank Charles Archambeau, Brian Stump, Jack Murphy, William Farrell Gerard Leies, Gregory van der Vink, Christopher Paine and Harold Agnew for their efforts and insightful presentations. The session was very informative and productive for the audience.

I also appreciate the time and thought that went into the critical reviews and thank Lane Johnson and Karl Veith for their frank and constructive comments.

JAMES F. LEWKOWICZ
Program Manager

Accession For	
NTIS ORARI	J
DTIC TAB	11
Unannounced	11
Justification	
By	
Distribution	
Availability Codes	
Dist	Availability Codes
A-1	



10TH ANNUAL AFGL/DARPA SEISMIC RESEARCH SYMPOSIUM

3-5 MAY 1988
PALA MESA RESORT
FALLBROOK, CA

TABLE OF CONTENTS

<u>CURRENT RESEARCH ISSUES IN NUCLEAR TEST BAN TREATY MONITORING</u>	<u>PAGE</u>
ARCHAMBEAU, CHARLES, What's Needed for a Quantitative and Confident Specification of a Verifiable Low Threshold Test Ban Treaty	1
STUMP, BRIAN, Wave Propagation Issues Associated with Explosive Sources	27
MURPHY, JOHN, Current Research Issues in Nuclear Test Limitation Treaty Monitoring	44
FARRELL, WILLIAM, Engineering Perspectives on Seismic Monitoring of the Soviet Union	53

PAPERS

COYNER, KARL B. and RANDOLPH J. MARTIN III, Attenuation and Moduli from Hysteresis Loops at 0.1 Hz	66
JOSWIG, MANFRED, Pattern Recognition for Earthquake Detection	75

POSTER PAPERS

on

HIGH FREQUENCY SEISMOLOGY AND NUCLEAR TEST BAN MONITORING

MCCARTOR, G.D and W.R. WORTMAN, Nonlinear Constitutive Relations at Moderate Strain - 10^{-3} to 10^{-6} in Salt	88
HERRIN, EUGENE, Development of an Intelligent Seismic Facility	100
BURDICK, L.J., The Fine Structure of P_n and P_g	118
McLAUGHLIN, K., T. BARKER, S. DAY, J. STEVENS and B. SHKOLLER Effects of Depth of Burial and Tectonic Release on Explosion and Earthquake Regional Seismograms	140
FERGUSON, JOHN, ALLEN H. COGBILL, RUSSELL J. HEIDESCH and HERBERT D. AXILROD, Geophysical Structure at Pahute Mesa, Nevada	158
SEARFUS, ROBERT, DARREL LAGER, CINDY L. MASON, TOM CANALES and ROWLAND JOHNSON, SEA - An Automated Event Analyzer for Seismic Arrays	175

	<u>PAGE</u>
CSS, Databases and Software Support at the Center for Seismic Studies	197
CHAEI, ERIC, Discrimination of NTS Explosions and Earthquakes Using High-Frequency Regional Data	236

CRITICAL REVIEWS

JOHNSON, LANE, University of California, Berkeley	244
VEITH, KARL F., Pacific-Sierra Research Corporation	246

What's Needed for a Quantitative and Confident Specification of a Verifiable Low Threshold Test Ban Treaty

I. Objectives

II. Problems

III. Current Status

IV. Directions for Future Work

I. Objectives: Essential Questions

I. Objective is to answer the following "bottom line" questions:

- (1.) To what threshold is a test ban effectively verifiable"? (eg. A 90% probability of identification of all shallow events.)**
- 2.) How many in-country stations are required, where should they be located and what instrumentation must be used. (eg. 20-30 in-country high-performance seismic stations for a 3-5 kt threshold.)**
- 3.) What additional treaty conditions are necessary to insure verification to a low threshold. (eg. Numbers of on-site inspections, requirements for a-priori announcements, or banning, of large industrial explosions in areas where decoupling above the threshold level is possible, constraints on area of allowed testing and on rock type/depths where testing can take place, etc.)**

II. Problems in Monitoring a Low Threshold Test Ban

Principal Problems in Monitoring a Low Threshold Nuclear Test Ban

I. Evasion of Detection

1. Nuclear Explosions in Large Underground Cavities - "Decoupling"
2. Nuclear Explosion (Coupled/Decoupled) Detonated with a Large Industrial (Chemical) Explosion. ("Hide in industrial Explosion")
3. Nuclear Explosion (Coupled/Decoupled) Detonated During a Large Earthquake ("Hide in Earthquake")

II. Operational Difficulties

1. Overloading due to large number of small earthquakes and industrial explosions to be located and identified
2. Identification of "earthquake-like" explosions and "explosion-like" earthquakes (In - depth analysis required)

III. False Alarms

1. Mistaking an earthquake for a nuclear test
2. Mistaking a large industrial explosion for a nuclear test

III. Current Status: Technical Details

Principal Problems in Monitoring a Low Threshold Nuclear Test Ban

IV. Uncertainties in Yield Estimates

1. Systematic Under or Over Estimates (Biased estimates)
2. Higher than desirable uncertainty (Random error large)

V. Systematically Missed Detections or Erroneous Identifications

1. Blind area for the Seismic Network - with no or few detections in a particular region
2. Consistent mis-identifications of events from a special area. (Network coverage biased or structure/source unusually "complex")

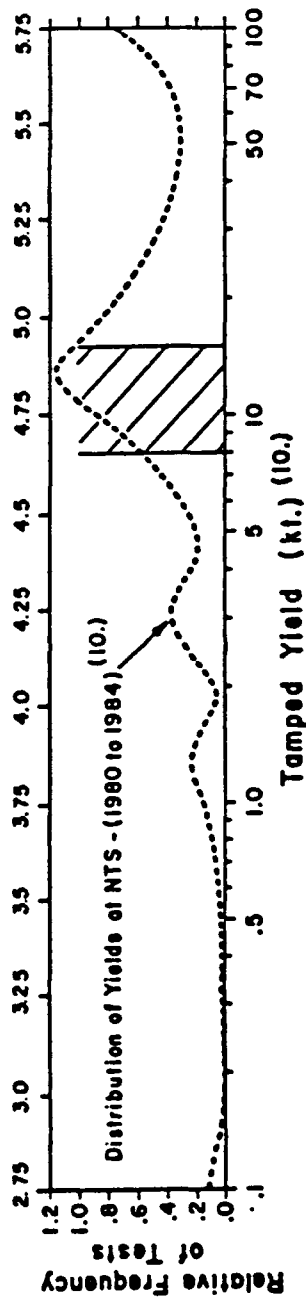
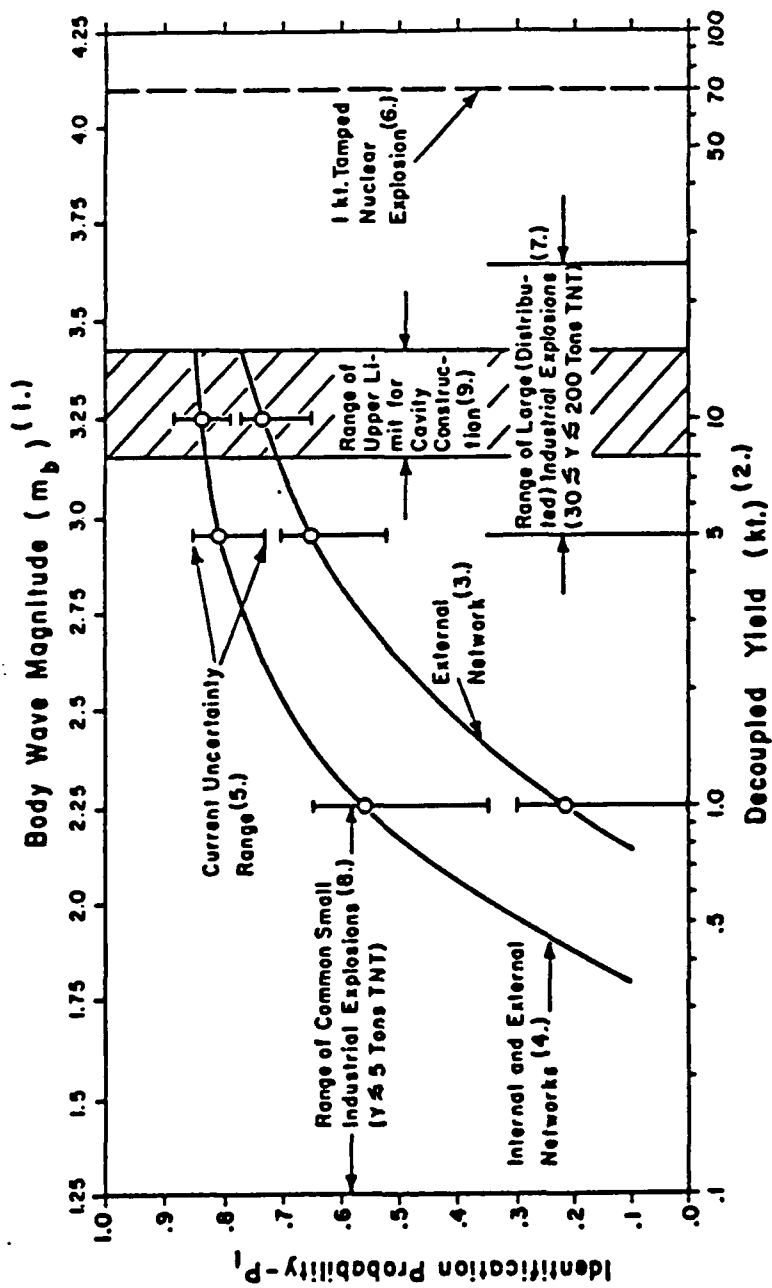


Figure 1: (a) Probability of Identification of Decoupled Nuclear Tests under Test Ban Treaty constraints on Large Industrial Explosions; and (b) Relative Frequency of Test Yields at the Nevada Test Site, 1980-84. The identification probability applies to previously located shallow continental events (earthquakes with depths less than 20 km., earthquakes with unknown depths and all types of industrial explosions as well as possible decoupled nuclear tests) within areas suitable for cavity decoupling.

Probability of Identification of Decoupled Nuclear Tests with Treaty Constraints on Industrial Explosions

The "Identification Probability of Decoupled Nuclear Tests", denoted as P_1 , is here defined to be the same as the probability of identification of shallow (less than 20 km. depth) seismic events within the areas in the USSR/US where decoupling is possible. (The list of shallow seismic events includes not only natural seismic events, but various types of industrial explosions as well.) This identification probability includes use of all national technical means, but here seismic methods dominate. However the probability estimate also assumes that large industrial explosions are banned, or must be announced and inspected, *in those (designated) areas where decoupling in the yield range above 5 kt is deemed possible*. In this case P_1 then represents the probability of distinguishing between only shallow earthquakes and explosions (of all types) in the magnitude range above about 3. (In this range any large unannounced explosion within regions designated as possible high yield decoupling areas would be a violation, whether it was a tamped or decoupled nuclear test or a chemical explosion.) The restricted areas within each country, where decoupling is possible, are quite well defined for large yield decoupling, and are limited to two or three areas that are not highly active seismically. As the yield is lowered however, more sites of greater area and of more diverse geologic characteristics must be included, with some of these potential decoupling sites being in tectonically active areas with high seismicity. Further, very large numbers of industrial explosions with seismic magnitudes in the range of importance would be encountered and would have to be distinguished from decoupled nuclear tests, since banning or inspecting them is impractical. Therefore, the number of shallow events that would have to be identified will increase rapidly (exponentially) as lower decoupling yields are considered and identification of any one of them would be fundamentally more difficult, since possible nuclear explosions must be distinguished from industrial explosions as well as earthquakes. It is estimated that the number of shallow seismic events per year of all types with magnitudes above 3.25, within potential decoupling areas for a decoupled test with magnitude of 3.25 or larger (10 kt. or larger), is about 10. The number becomes about 1000 for magnitudes of 2.25 and larger (1 kt. and larger decoupled nuclear explosions). Since the number of *unidentified events* (N_u) that can be expected is $N_u = N_o (1 - P_1)$, where N_o denotes the number of shallow seismic events in potential decoupling areas; then at $m_b = 3.25$ one can normally expect 3-4 unidentified events per year and, at $m_b = 2.25$, about 500. The latter (rather large) number is primarily a consequence of the large numbers of small industrial explosions at this magnitude level within the more numerous areas of potential decoupling at 1 kt. (See also Figure 2.) However, it should be noted that we have assumed a rather low probability of discriminating between decoupled nuclear explosions and industrial explosions. This could improve dramatically as particular seismic and non-seismic methods are tested more extensively. (See note 7. below). In the best case one might expect something like 50 unidentified events at $m_b = 2.25$, as an upper bound.

- (1.) The body wave magnitude (m_b) values are teleseismic magnitudes for decoupled explosions in stable continental areas. For such explosions in tectonically active regions, subtract .35 (approximate) from the magnitude values on the scale to adjust for greater upper mantle attenuation in such regions. It is assumed that the receivers producing the (averaged) m_b values are (predominantly) in stable continental areas. If most receivers are in tectonic areas, then the averaged m_b value would be reduced by an additional .35 magnitude units. The probability curves shown assume that none of these latter restrictions are necessary when applied to available decoupling areas and receivers in the US or USSR.
- (2.) When referred to the identification probability curves, this scale indicated yields for fully decoupled nuclear explosions. Yields of corresponding *tamped nuclear explosions* (ie. corresponding in the sense that they have the same m_b values given on the upper scale) are approximately obtained by dividing the decoupled yields by a factor of 70. (eg. A 7 kt. decoupled nuclear explosion corresponds in m_b value to a .1 kt. tamped nuclear explosion.) Yields of corresponding *tamped chemical (TNT) explosions*, having approximately the same m_b values as given on the upper scale,

are obtained by dividing the decoupled yield values on the lower scale by a factor of 175. (eg. A 7 kt. decoupled nuclear explosion corresponds to about a 40 ton TNT explosion, with both giving m_b values of slightly over 3.0.)

- (3.) The identification probability curve for the "External Network" case is based on an external seismic monitoring network of 15 to 20 arrays, or high performance stations, and assumes treaty constraints requiring testing below a threshold at only *one* designated test site of limited area and (known) uniform high coupling characteristics. Further, it is assumed that a reasonably high number (eg. ten per year) of unrestricted inspections would be allowed. In addition, treaty constraints on large industrial explosions are assumed, prohibiting certain types of large explosions from areas in which decoupling is possible, or that the treaty requires prior announcement and allowed special inspections; or a combination of such conditions for the variety of potential decoupling areas in each country. Both m_b vs M_s and spectral discrimination methods (UFM and others) are considered applicable over a broad frequency band, up to moderately high frequencies.
- (4.) The identification probability curve for the "Internal and External Networks" case is based on 15-20 external arrays plus from 25 to 30 internal high performance stations within the country in question (US or USSR). The same treaty constraints described for the external network case, in (3.), are assumed to apply. Both m_b vs M_s and spectral discrimination methods, applied over a frequency band to high frequencies, are considered applicable. (This identification probability curve turns out to be quite similar to that estimated for the *detection probability* of the external network alone.)
- (5.) The "current uncertainty range" is estimated in terms of a range for the identification probability at particular yields and reflects optimistic and pessimistic extremes from a large group of experts. The range results from a number of considerations, including efficiency of wave propagation within particular areas of the U.S./USSR (particularly at high frequencies), noise levels and their variations at the required widely distributed receivers, uncertainties in identification capabilities and false alarm rates versus inspection opportunities, and the effectiveness of treaty constraints on (and discrimination of) large industrial explosions. The probability curves themselves are estimates of an "average" of the estimates expressed by experts. (A "consensus curve, representing a large majority of experts agreeing that the identification probability is no worse than the "consensus curve," would result in a curve nearer to the lower bound of the uncertainty range shown.) The larger uncertainty range at lower yields, and the lower probabilities for identification indicated by the "average" identification probability curves, reflect not only the greater difficulty of achieving confident identification in a rapidly increasing population of ever smaller seismic events, but also the impossibility of constraining, by treaty, the many small industrial explosions that are seismically similar to small decoupled nuclear explosions. This circumstance results in an ever increasing number of false alarms at lower yields (see Figure 2), which would eventually overwhelm identification capabilities deriving from on-site inspections. The optimistic (upper) value indicated by the uncertainty range at the low yield levels anticipates that high frequency spectral discrimination will allow discrimination of *distributed* chemical explosions from decoupled nuclear tests, with such high frequencies observable at rather large distances from small explosions. (In this case only concentrated "point" detonated chemical explosions, that only occur frequently at very low yields, would appear seismically similar to decoupled nuclear explosions.)
- (6.) The scale position of the "1 kt. Tamped Nuclear Explosion" is shown for reference and is located at the *decoupled yield* value of 70 kt.; in view of the factor of 70 used for decoupling efficiency at low frequencies. The corresponding m_b value is about 4.15 units and is appropriate to a

detonation in a high coupling medium in a stable continental area. (See (1.) for adjustments required when detonations are in tectonic regions.)

- (7.) The indicated range of "Large (Distributed) Industrial Explosions" produce m_b values as indicated on the upper magnitude scale. Their yields range from about 30 tons to 200 tons of TNT and, as noted in (1.), correspond to the decoupled yield scale divided by a factor of about 175. These large chemical explosions are almost always distributed explosions, with partial charges emplaced in many separate drill holes that are well separated spatially. These separate charges are often detonated with time delays between each ("ripple fired"), but in any case are always spatially separated when detonated. Consequently they are a special class of explosion that is expected to be seismically distinguishable from decoupled nuclear tests for a number of reasons. (Less high frequency content in the directly radiated compressional seismic wave, due to non-linear shock wave interference between the separate charges and related high deformational losses in the local medium, as well as higher levels of shear wave production.) Further, large near surface chemical explosions typically produce acoustic waves in the atmosphere, and ultimately in the ionosphere. The atmospheric waves can be measured directly at large distances from large shallow explosions and, along with the seismic signals received, would allow identification of the event as a surface explosion rather than a muffled decoupled nuclear test at depth. On the other hand, the acoustic wave propagating upward into the ionosphere is greatly amplified, due to the decreasing density of the atmosphere with height, and even a rather small surface disturbance causes a significant disturbance in the ionosphere, which in turn produces a high frequency electromagnetic disturbance that can be measured. Again, observation of such an electromagnetic disturbance, in conjunction with a seismic disturbance from the same region, would be characteristic of a large near surface industrial explosion. (The estimated yields where these acoustic related identification methods could be applicable is from about 25 tons of TNT and above.) Nevertheless, large explosions could be used to obscure signals from co-located smaller decoupled nuclear tests or, in at least some instances, might be seismically and acoustically similar enough to decoupled tests to result in false alarms. Consequently these explosions should, in the short term at least, be restricted by treaty agreement (as described in (3.)) as insurance against evasion when a treaty threshold is set below about 15 kt. (As noted the identification probability estimates assume such treaty restrictions.)
- (8.) "Common Small Industrial Explosions" are taken to be those that are often simple point-like explosions, where the charge is concentrated in one relatively small volume, and detonated all at one time. Such explosions would also be expected to occur at a variety of depths, rather than very near the surface as is common for the large industrial explosions. They are also much more frequent and widespread. Therefore, as a class, they would be difficult to discriminate from small decoupled nuclear explosions below 1 kt. and so common that they could not be restricted by workable treaty constraints. Their presence would therefore result in so many false alarms that any reasonable number of on-site inspections would clearly be ineffective. Therefore, they set a lower limit for a verifiable threshold treaty. As indicated by the estimated identification probability curves, this limit would be near .5 kt., at the least. (Ability to identify in this low yield range is based mainly on on-site inspections of events identified as possible decoupled tests by seismic and other methods.)
- (9.) The upper limit for the radius of a stable cavity that can be constructed for decoupling is generally agreed to be about 50 meters. A cavity of such size could be used to fully decouple a nuclear explosion of about 10 kt. Given the uncertainties in this technology however, and the possibilities for partial decoupling, a range for the upper limit of decoupling is from about 8 to 15 kt. It is evident from the figure that this range of decoupled explosions will produce seismic magnitudes within the same range as large industrial explosions. Thus, it is particularly

imperative that special treaty constraints be applied to industrial explosions if the large industrial explosions are not clearly identifiable by seismic and/or other monitoring methods. (As noted earlier, treaty constraints on large industrial explosions are assumed in estimating the identification probability curves since, at this time, it is not clear to what degree seismic and other methods, discussed earlier, will be able to distinguish between decoupled explosions and the various types of industrial explosions.)

- (10.) The distribution of yields for U.S. Nevada Test Site nuclear explosions, in 1980-84, is based on the figure given by Kidder (1985) and is considered representative of the relative frequency of tests at different yields under current testing conditions. The yield scale shown is for *tamped* tests and so the corresponding seismic magnitude scale for these *tamped* explosions at NTS (a *tectonic* area) is uniformly 1.5 units higher than those given for the decoupled tests in a *stable* continental area. (To obtain approximate seismic magnitudes for *tamped* tests in a *stable* continental area, such as in appropriate for Soviet test sites, add .35 magnitude units to the values on the magnitude scale shown.) The Soviet test pattern as a function of yield is similar to that for the U.S. Therefore it is reasonable to assume that the peaks in the relative frequency curve near 13, 3 and 1.5 kt. are associated with narrow ranges of test yields that are particularly important in weapons development and maintenance. The lineup of these peaks with the decoupled yield scale, and other features shown in the (upper) identification probability figure, therefore indicates at what yields decoupling would be attempted by an evader, and how well a monitoring system would be able to cope with such attempts. Further, given the presumed importance of tests at the peaks in the test frequency curve, it would follow that the choice of any treaty threshold be as far from any of the peaks as possible, since one would want to minimize possible exploitation of uncertainties in yield estimation (see Figure 2) by an evader who might test in the uncertainty zone of yield estimation *above* the threshold, if some advantage could be gained. This implies that a threshold for a low threshold treaty should be set at, or somewhat below, one of the minima in the frequency curve; which are near .5, 2 and 5 kt. in the low yield range below 15 kt. Considering the form of the identification probability curves, the best thresholds for a treaty appear to be near either 2 or 5 kt. Obviously the most confident verification can be achieved near the 5 kt. threshold level, in any circumstance. However, reduction of the threshold for a verifiable treaty to about 2 kt., or even .5 kt., could be a possibility if discrimination of the various types of industrial explosions and decoupled explosions at low yield levels is thoroughly demonstrated in the future. In any case, with a threshold near (slightly below) 5 kt. an evader would be most likely to only attempt decoupling evasion if one or more decoupled tests in the range from 10 to 15 kt. could be conducted without much chance of identification. Certainly the identification probability curve for the case of both internal and external seismic monitoring precludes the likelihood of such successful evasion for even one such decoupled test. Further, several of these tests would present an exceedingly high probability that at least one of them would be identified. Therefore, on this basis a 5 kt. threshold treaty appears verifiable with high confidence, with lower thresholds at least good possibilities.

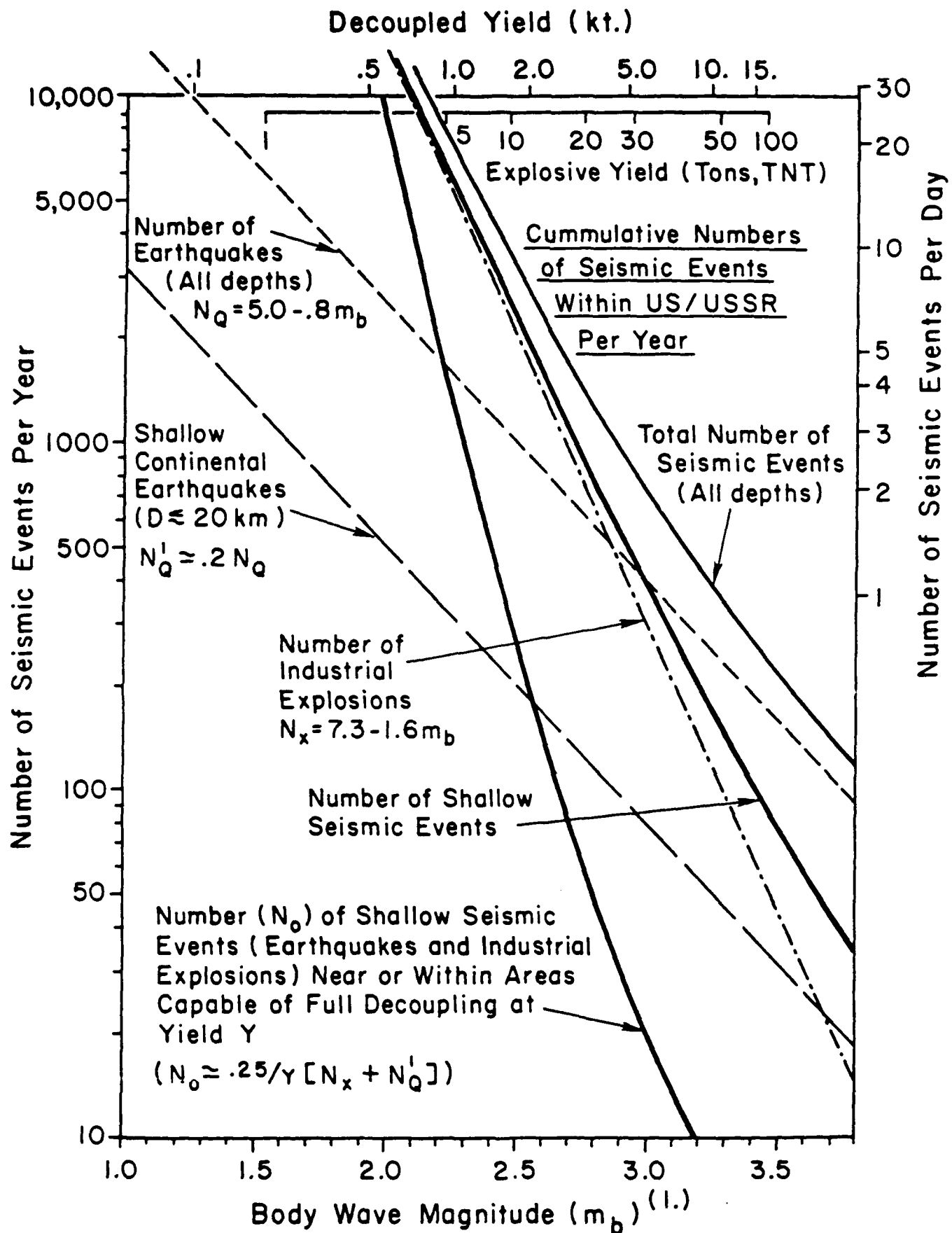


Figure (2 - a) - Numbers of seismic events in the US/USSR per year versus seismic body wave magnitude and explosive yield for fully decoupled nuclear explosions and chemical explosions.

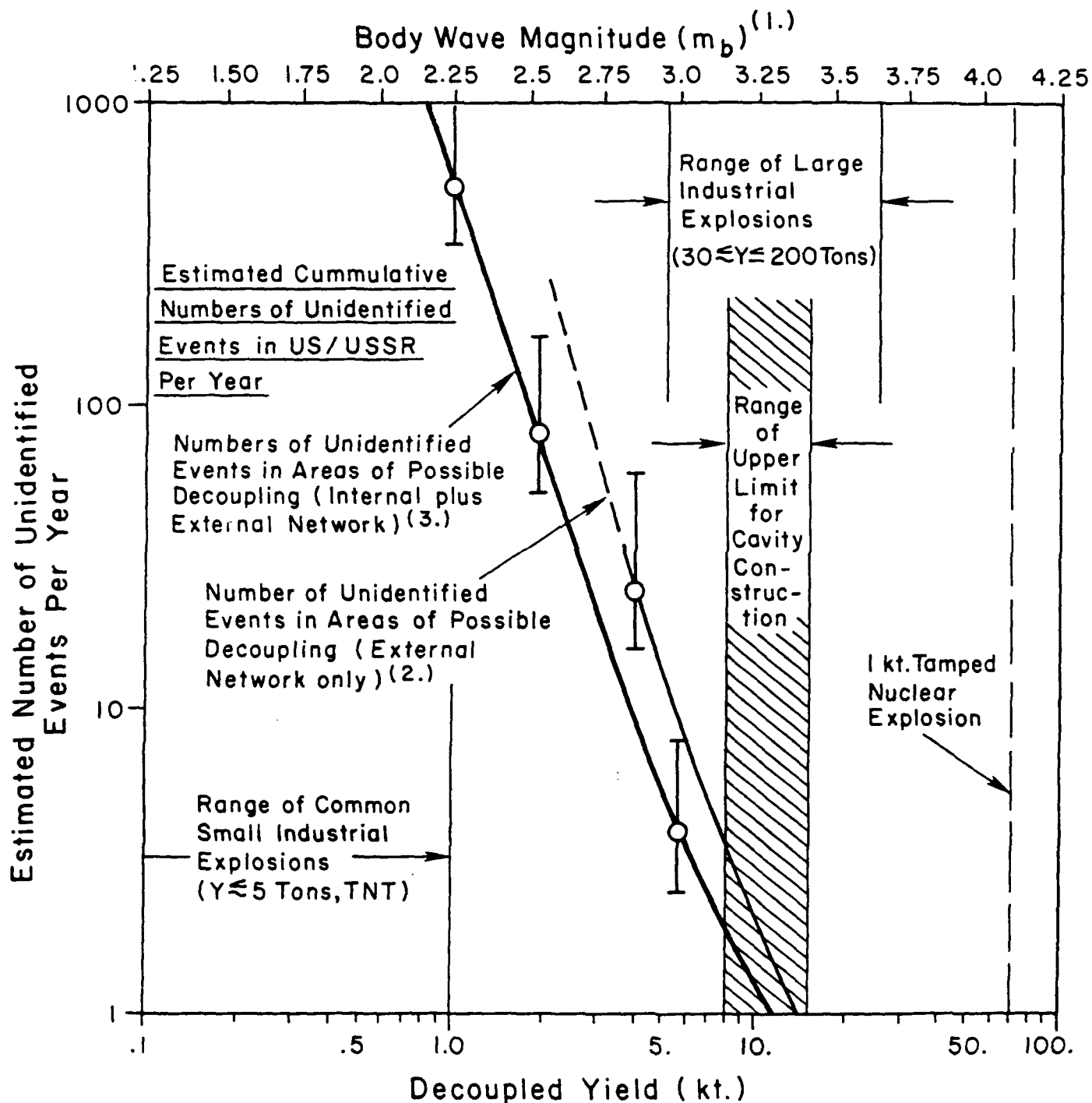


Figure (2 - b) - Estimated cumulative numbers of unidentified seismic events in the US/USSR per year versus decoupled yield or body wave magnitude for different seismic monitoring networks.

Estimated Cumulative Number of Unidentified Events per Year

The numbers of unidentified events (N_u) that can be expected at a particular body wave magnitude is given by $N_u = N_o (1 - P_i)$, where $P_i(m_b)$ is the probability of identification of events at magnitudes above a particular m_b value and $N_o(m_b)$ is the total number of shallow seismic events, within areas of possible decoupling, with magnitudes larger than the particular m_b value. Since the yield of decoupled (as well as tamped) nuclear explosions and industrial explosions is directly related to an observable m_b value, then the probability and numbers of shallow events within potential decoupling areas can be related to yield values, as well as to seismic magnitude values. (The yield scale shown in the figure illustrates this relationship for fully decoupled nuclear tests in stable continental areas. For tamped tests divide this scale by 70, for chemical explosions divide the scale by a factor of 175. It is also assumed, with engineering justification, that cavity decoupled tests would be in hard rock environments, so that these and other explosions in such areas would couple to strong rock.)

An estimate of the probability function $P_i(m_b)$ is shown in Figure 1. The number of shallow earthquakes is estimated using appropriate empirical seismicity relations for the USSR/US. In particular, the number of earthquakes (N_Q) at all depths, with magnitudes greater than a particular magnitude m_b , is given by a relation of the form, $\text{Log } N_Q = a - b \cdot m_b$, where a and b are constants characteristic of a particular seismic region. Such a relation applies to natural seismic activity, that is earthquakes. However, it is expected that industrial explosion activity obeys a similar relationship, so that a relation of the form $\text{Log } N_x = A - B \cdot m_b$ can be used to estimate the total number of industrial explosions (N_x) with magnitudes larger than a particular m_b value. Here again A and B are constants. The total number of shallow events (including those of unknown depth as well as those of known depth less than 20 km.) can be estimated by:

$$N_o = N_x \cdot f_D + N_Q \cdot f_s \cdot f_D = f_D(N_x + f_s \cdot N_Q)$$

where N_Q and N_x are as given above and f_s is the fraction of the earthquakes with unknown depths, or known depths less than 20 km, and f_D is the fraction of the events that occur in the areas that contain potential decoupling sites for tests with yields up to a particular value Y . Thus f_D changes with yield (or magnitude), with an appropriate approximate relationship having a form $f_D = .25/Y$, for yields Y in the range from 1 to 15 kt. (In this case potential decoupling of 1 kt. tests are estimated to be possible within about 25% of the total areas of either the US or USSR, but in only 2.5% of the total areas of either country for 10 kt tests.) On the other hand f_s appears to be a fixed number independent of magnitude, with a reasonable estimate being about .2. That is, about 20% of all the earthquakes, with epicentral locations on land, are shallow or have unknown depths, while the rest are known to have depths greater than 20 km, or are known to have epicenters off the sea coasts of the countries to be monitored, based on detection-location capabilities of the seismic networks. The resulting estimate for N_Q , based on the relation given and the estimated constants in it, is of course approximate but is designed to provide a reasonable upper bound (maximum value).

To make specific estimates of the numbers of unidentified events to be expected, it is only necessary to estimate appropriate constants in the relations for N_x and N_Q from available seismicity data. For both the US and USSR the number of continental earthquakes per year, with magnitudes greater than 2.5, is about 1000. Further, for earthquakes on land the value of the constant b , appearing in the relation for N_Q , ranges from about .65 to .9, depending on the geologic region within the countries. Given the locations of the restricted areas in each country that have rock types suitable for decoupling cavity construction, a reasonable choice for the average value of the constant b , describing the seismicity of these areas, appears to be about .8. Using these estimates for the number of events per year with magnitudes above 2.5 and the b value, then the seismicity relation given earlier permits computation of the expected number of earthquakes above any magnitude. (eg. There would be about 10,000 continental earthquakes above magnitude 1.25 in each country per year.)

Similarly, the numbers of industrial explosions, above any magnitude, can be estimated by noting that there are known to be about 20 per year at, or above, magnitude 3.75 in each country. Also a reasonable estimate of B in the seismicity relation for explosions appears to be about twice that for earthquakes, that is about 1.6. These conditions now allow computation of the expected numbers of industrial explosions, above any seismic magnitude value, from the seismicity relation given earlier. (We get: $a = 5.0$ and $A = 7.3$ for the two other constants in the seismicity relations for earthquakes and

industrial explosions. For industrial explosions this leads to an estimate of about 200,000 explosions per year, or about 550 per day, above magnitude 1.25.) The number of events above any magnitude level that would require identification at the low magnitude levels appropriate for decoupled nuclear tests is obtained from the relation for N_0 given earlier. (At a 5kt yield for a fully decoupled test, which produces an observed seismic body wave magnitude somewhat less than 3.0, there are expected to be about 30 "shallow" earthquakes and explosions per year within areas that would require identification.) Figure (2-a.) shows the variation in the total numbers of earthquakes (at all depths), industrial explosions, shallow earthquakes and the total cumulative number of seismic events, all as functions of magnitude and explosion yield; with yields corresponding to particular seismic magnitudes and given for the cases of fully decoupled nuclear explosions and industrial explosions. From these fundamental variations in the numbers of seismic events versus magnitude (m_b), the variation in the number of *shallow* events versus magnitude, within either the US or USSR, can be estimated (they are about the same in both countries at all magnitude levels) and, from this, the number (N_0) of shallow events *within areas capable of full decoupling at a given yield, Y*, can be estimated. These latter two curves are shown as heavy solid lines in Figure (2-a.).

The total number of unidentified shallow events (N_u) to be expected at a given yield (or magnitude) threshold is obtained using (N_0) in the relation $N_u = N_0(1 - P_I)$, and using the identification probability functions shown in Figure 1. The resulting numbers of expected unidentified events are plotted in Figure 2-b., along with the uncertainty ranges implied by the uncertainty in identification probabilities, described in connection with Figure 1. (The number N_0 also has uncertainty connected with its estimate as well, and this is included in the range of uncertainty for N_u also.)

- (1.) The body wave magnitude scale is appropriate to that expected for seismic events in stable continental areas with receivers also in stable areas. If the seismic events are in certain tectonically active areas, in either the U.S. or USSR, then these teleseismic magnitude values should be decreased by about 0.35 in order to correspond to the yield scale shown.
- (2.) When events are all within tectonic areas with high signal attenuation, so that teleseismic magnitudes would decrease as described in (1.), then this situation would require a shift in the curve for the number of unidentified events using an external seismic network. That is, a shift of the curve laterally along the magnitude/yield scale so that it coincided with the same magnitude on the new magnitude scale as it did on the old scale, since estimates for numbers of unidentified events are based on observed seismic magnitudes rather than on yields. This would result in larger numbers of unidentified events at a particular yield threshold. (If all events were from tectonic areas with high mantle attenuation characteristics, the number of unidentified events to be expected at a 5 kt. threshold would be roughly the same as those shown at 3 kt in the figure as it stands.)
- (3.) For the case in which both internal and external networks are used the situation would not change as much as described in (2.), since even when most of the events are from the limited highly attenuating tectonic areas the use of higher densities of in-country receivers at shorter ranges in such areas reduces the negative effects of signal transmission losses on detection - identification capabilities. Thus, while an adjustment leading to higher numbers of unidentified events would occur at all yield thresholds, the adjustment would not be large and should only change (increase) the numbers of unidentified events by about 10%, or so, when relatively large numbers of internal receivers (of the order of 30) are judiciously deployed. Further, the areas in both the US and USSR where high yield decoupling is possible in the yield range from 5-15 kt are quite limited and are not in tectonic regions where high attenuation is expected. Thus the curves, as shown, should be applicable to test identification for thresholds near 5 kt and above, and only when the capability of an external network for thresholds below 5 kt is considered would it be clearly necessary to adjust the expected numbers of unidentified events to somewhat higher values, as described in (2.). It is clear, however, that a fair number of internal stations are required to provide the short range coverage in tectonic areas, particularly for thresholds well below 5 kt.

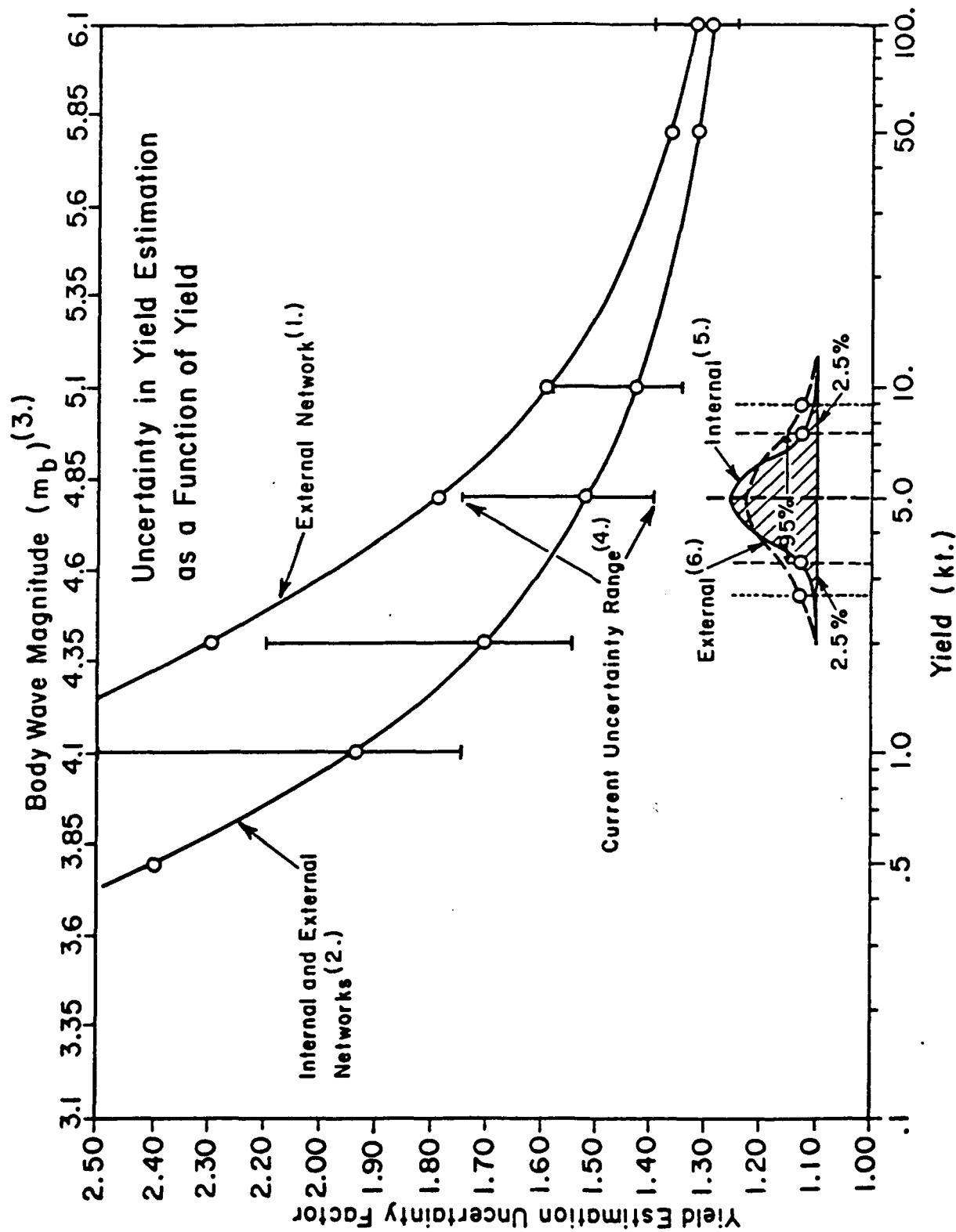


Figure (3): Uncertainty in yield estimation as a function of yield, for both internal and external monitoring cases, expressed in terms of an "uncertainty factor." The factor is a quantitative measure of the scatter that occurs in yield estimates. Specifically, this factor, when multiplied and divided into a yield value on the lower scale, gives the range in yield within which there is a .95 probability that a single estimate of yield will lie. (This yield interval is called that required for a "95% confidence level.") The probability distribution of yield estimates for a test at 5 kt. is shown in the inset, for both in-country and external monitoring cases, and the interval for a 95% confidence level is indicated for the "internal" monitoring case.

Uncertainty in Yield Estimation as a Function of Yield

The uncertainty in yield estimation is expressed as an "uncertainty factor" which, when multiplied and divided into a particular yield value on the lower scale, gives the range within which 95% of all seismic yield estimates would fall, based on observations from many tests at that yield level. It is assumed here that, by treaty limitation, all tests would be made in a limited area that had been seismically calibrated and was known to consist of material with quite uniform explosion coupling characteristics. (Such an area will be termed a "designated test site.") Thus, as illustrated in the inset, at 5 kt. the curves for external (dashed line) and internal plus external (solid line) networks indicate expected uncertainty factors of about 1.8 and 1.5 respectively and the bell-shaped distributions of yield estimates, ranging from below 2 kt. to above 10 kt., show the expected distribution of yields that would be seismically estimated from a large population of actual 5 kt. tests within the designated test area. The height of the curves is, roughly speaking, a measure of the probability of an estimate occurring at any yield within this range or, alternately, a measure of the relative frequency with which a given estimated value would occur within a large population of observed 5 kt. tests. More rigorously, the area under any portion of the curves (however narrow or wide in yield) is equal to the probability that yields in the range selected along the yield axis will occur in the observed population of estimates.

The "uncertainty factor" given here gives the yield range over which 95% of the estimates of the yield would occur and is indicated in the inset by the cross-hatched area under the curve for the "internal network" case; that is for the case in which seismic receivers at both near and regional distances, as well as teleseismic distances, are used to obtain yield estimates. (This range corresponds to two standard deviations from the mean of the population in either direction.) The inset shows that for 5 kt. tests the expected uncertainty range, where 95% of the estimates will fall, is from about 3.3 kt. to 7.5 kt. when the internal and external network is used, while it is from about 2.8 to 9 kt. when only an external network is used. It is also evident from the relative height of the curves that fewer of the estimates from an external network alone will fall at, or very near, the central value of 5 kt. than is the case when an internal network is used as well.

It is common usage to express the scatter in estimates in terms of confidence levels. Specifically, in the case at hand, a 95% confidence level defines a yield interval around the central (or mean) value in which 95% of all the estimates will occur and this yield interval is given by the "uncertainty factor" shown in the figure. Put another way, it defines an interval within which there is a .95 probability that any *one* measurement will fall. When one is concerned with the meaning of a single yield estimate from one nuclear test, it is obvious that this latter definition is of the most importance. That is, we usually ask what is the 95% confidence level for estimates of yield at, say, 5 kt. When we know something about the statistics of yield estimation at that yield level we can answer the question. In the case illustrated here we can say that the interval is from about 3.3 to 7.5 kt. when an appropriate internal seismic network is used and when certain other conditions are met (*ie.* tests must be conducted at a designated site, etc.). Then we know that there is a .95 probability that one estimate from a single test at 5 kt. will be in this interval. Further we know that there will be only a .05 probability that such a measurement will fall outside this range, with (only) a .025 probability that it will be higher than 7.5 kt. and a .025 probability that it will be lower than 3.3 kt. The same description applies at all yield levels, in particular the distribution of yield estimates when repeated for a large number of tests at any fixed yield will, under the conditions prescribed for a "designated test site," result in a central value very near the known yield value with a more or less symmetric distribution of yield estimates around this value. (*ie.* The distribution is nearly *normal* with respect to the logarithm of the yield because seismic magnitudes, which are proportional to the logarithm of the yield, are used to estimate yields.) However, as the figure shows, the uncertainty factor, and therefore the yield interval for a 95% confidence level, changes with yield; increasing quite rapidly with decreasing yield. (This means that the distributions associated with yield estimates at a given fixed yield become relatively wider, or more spread out in yield, as the yield value at which estimates are made decreases.)

At the critical lower yield levels (2 kt. and .5 kt.) it is evident from the form of the uncertainty curves for the two cases that a relatively larger "spread" in the range of values for estimates can be

expected. At 2 kt. the uncertainty factor for the internal and external network case is 1.7 so that the interval defining a 95% confidence level is from about 1.2 to 3.4 kt., while at .5 kt. it is from about .2 to 1.2 kt.

In terms of monitoring to insure compliance with a low threshold treaty one would have to evaluate whether a given yield estimate was or was not within the allowed yield range for testing. If the threshold were at 5 kt., for example, then only yield estimates exceeding 5 kt. by about 60% (ie. yield estimates at and above 8 kt.) would be of concern in view of the test frequency curve given in Figure (1). From the previous discussion it is known that one test at 5 kt. has less than one chance in forty of being estimated at a level at, or above, 8 kt. since the upper limit of the 95% confidence level is at about 7.5 kt. Therefore, if the monitor were to obtain an estimate above 8 kt., it is quite possible that a violation has taken place and that an on-site inspection should be called to confirm or further evaluate the assessment. (Note, however, that if 40 tests were conducted at 5 kt. then it is nearly certain that at least one of them would be estimated to have had a yield above 8 kt.) Similar conditions and criteria would apply at the other possible low threshold levels at around .5 and 2 kt.

- (1) The uncertainty factor versus yield curve for the external network is based on estimates of signal recording capabilities at multiple seismic stations at distances greater than 2000 km. from a designated test area within the USSR. (The likely site is the Kazakh test site in eastern Kazakhstan.) A similar estimate for the US is not given, but the uncertainty factors are expected to be significantly higher, particularly if (a part of) NTS is used as the "designated test site." The specific signal magnitudes that would be involved in a single yield estimate would be those from the direct compressional (P) wave, the Rayleigh type surface wave and from the large (crustal) Lg phase, when available.
- (2) The uncertainty factor for the internal plus external stations assumes seismic receivers in nearly all distance ranges, that is in the regional (300 to 2000 km.) and teleseismic (beyond 2000 km.) ranges and applies to both US and USSR test sites that could be used. Generally the three wave types described in (2) would be used at each receiver to obtain (independent) signal magnitudes which would be corrected and separately averaged among all stations to provide average magnitudes to be used to obtain a "multi-variant yield estimate." Stations are assumed distributed so that nearly full azimuth coverage by both regional and teleseismic stations is available and that data would also be obtained at several distances, with at least four regional stations providing data for each of the three seismic signals in the yield estimate.
- (3) The body wave magnitude (m_b) scale shown is appropriate to tamped explosions in high coupling media (strong, competent rock with low porosity and fracture density, such as most granites, and/or in rocks with higher porosity or fracture density that are water saturated, such as the sedimentary rocks at depth at NTS). Such high coupling is assumed to prevail uniformly within the limited areas of a "designated test site." The values, as shown, are close to those for high coupling conditions at the eastern Kazakh test site in the USSR. At NTS the teleseismic magnitudes for high coupling tests are observed to be about .35 magnitude units lower than those indicated in this figure, due to strong attenuation in the earth's upper mantle beneath this site. Corrections for such observed magnitude differences (bias effects) are, however, part of the procedure used to correct the observed signal magnitudes to a reference, such as the magnitude scale shown in the figure. Thus, when magnitude bias factors are known for a particular test area, they are removed and do not systematically bias the yield estimates and do not affect the yield estimation uncertainty factor. Consequently the magnitude scale in the figure, and its relation to the yield scale shown, can be regarded as a standard reference magnitude scale for yield estimation, with bias corrections applied to data from other areas to bring them into correspondence with this scale. The objective of treaty required calibration explosions (of known yield) at designated test sites is

to determine the size of these bias corrections so that these adjustments to the observations can be accurately and confidently made.

- (4) The "current range of uncertainty" is the "uncertainty in the uncertainty factor." (Or, alternately, the uncertainty in the 95% confidence level.) That is, it corresponds to the range of uncertainty factors that would be obtained from a large group of experts. It is therefore a similar measure of uncertainty as was given for the identification probability in Figure 1. In this case also, uncertainty arises from a variety of causes, but primarily from a lack of experience in estimating yields at low magnitude levels. The uncertainty factor curve itself is what can be described as an average of the expert assessments. As with the identification probability discussed in Figure 1, a "consensus curve" reflecting a large majority assessment that the yield estimation factors were no larger than as indicated by such a "consensus curve," would produce a result somewhat closer to the more pessimistic side of the uncertainty range than does this "average" curve. (ie. The result would be larger uncertainty factors.)
- (5) The probability density distribution curve labeled "Internal" corresponds to that which would be obtained using a network of stations at regional and teleseismic distances, that is from an internal plus external station network. The curve itself would be obtained, ideally, by estimating yields from a large number of tests at a known fixed yield (such as 5 kt.) and plotting the number of times a yield of a particular value was obtained versus the yield estimate obtained. The result would be a distribution like that shown "centered" at, or very near, the known yield. To obtain the "probability density" curve one would then normalize the numbers of observational estimates at each yield by dividing them by the total number of tests conducted. The "spread" in the distribution of estimated yields would be expected to occur because of (small) measurement errors, the effects of background noise contaminating the measurements of signal amplitudes, variable signal attenuation between the detonation point and the different stations in the network and because of differences in seismic coupling due to local medium variability between the different points of detonation of the explosions, among other effects. While some of the effects leading to inaccurate yield estimates can be minimized by restricting tests to well calibrated and uniform test sites and by correcting the data for differential signal propagation effects, the presence of noise and so on; there is uncertainty in these corrections and constraints as well, so that there is always some "scatter" in the estimates. Further, some of the physical effects accounting for this variability are essentially impossible to quantitatively account for in practice. But, by making a series of quite routine adjustments to the observations it is possible to remove all significant systematic effects, with the result that the variations in yield estimates from the known value are essentially random. Such random appearing variations in the estimates result in a "Gaussian" or "Normal" distribution of estimates, of the form illustrated in the figure. (As noted earlier, the distribution of estimates is Gaussian with respect to the magnitude value associated with the signals from the explosion. Since the formal definition for computation of a seismic magnitude specifies that it be proportional to the logarithm of the amplitude of the seismic wave and since such amplitudes are directly proportional to the explosion yield, then it follows that the distribution of estimates of yield is Gaussian with respect to the logarithm of the yield.)

In practice the distribution of estimates at any one particular low yield is not inferred from a large number of tests at that yield, but from observations of measured seismic magnitude scatter from a series of single tests at different yields, in a yield range larger than 1 to 5 kt. Therefore the probability distributions shown at 5 kt. in the figure, and those implied at other yields in this low yield range, are inferred from observations at larger yield. Further, the probability distributions at larger yield are themselves inferred indirectly. Nevertheless there is little doubt that the low yield probability distributions will be nearly Gaussian (or "Normal") when appropriate corrections to observed signal magnitude data are made and when such tests are conducted in areas with uniform rock properties. What is more uncertain is how wide the distribution will be at a given yield; where the uncertainty factor plotted in the figure is a measure of this width and the "current

range of uncertainty" in this factor, discussed previously in (4), is a measure of the uncertainty in the width of scatter to be expected. It can be anticipated, however, that the uncertainty in this factor will decrease dramatically as more low yield estimates are made using regional seismic data.

- (6) The probability distribution for the external network case is estimated in the same way as was that for the internal and external network. (See (5) above). The major difference is in the broader range expected for estimated yields at a given yield level. Further, while the uncertainty ranges for the uncertainty factor for external network yield estimation are not shown, they are generally larger than those that are shown for the internal plus external network case. Therefore the estimate of the "width" of the distribution (or yield range for the 95% confidence level) is not as certain as for the "internal network" case discussed above. Nevertheless, the trend toward significantly wider yield ranges for the same confidence levels is a certainty and is at least approximately of the order indicated.

IV. Directions for Future Work: Some Specific Areas for Investigation Based on Current Capabilities

IV. Directions for Future Work: Overview (1)

- **Capability is assured if threshold is at, or above, 10-15 kt.** (There is general agreement that evasion is not a significant problem at this yield level and that event identification/yield estimation could be accomplished with "National Technical Means" plus a few internal seismic stations near test areas. Research needs would be for confidence building through understanding of physics involved, "precise" knowledge of limitations of methods and inherent uncertainties. Network testing and operational optimization would also be essential.)

- **A threshold in the 1-10 kt range introduces the clear possibility for evasion.** Major problem is possible clandestine decoupled tests in a background of increasing numbers of large industrial explosions. (In 5-10 kt range problem may (probably) be managed by in-country stations and constraints on very large industrial explosions in the limited areas available for decoupling at this yield level. In 1-5 kt range basic research on industrial explosion I.D. needed.)

IV. Directions for Future Work: Overview (2)

- **A threshold much below 1 kt. will present difficulties for the same reasons as in the 1-10 kt range, but they will be more severe because of decreasing S/N and larger numbers of industrial explosions and earthquakes. (The I.D. probability will be well below 90%. The practical limit for "effective verification" is likely to be no lower than 1/2 to 1 kt. and may be somewhat higher.)**

IV. Directions for Future Work: Some Specific Areas for New Initiatives and Focused Basic Research (1)

- **Joint US-USSR experiments and analysis using regional in-country stations.** (Focus on signal propagation, industrial explosion I.D., explosion-earthquake I.D., noise levels, yield estimation in both countries.)
- **Establish a world-wide high performance seismic network focusing first on the US and USSR and then on other locations outside these countries.** (Test capabilities for a multi-lateral treaty; test capabilities of both internal and external high-performance networks for international monitoring; basic science studies of seismic sources, signal propagation and noise characteristics in different geologic environments.)
- **Initiate a series of blind verification experiments for small seismic events in the magnitude range 2 to 4 using teams of scientists employing different methods.** Re-evaluate/develop models and expand in-depth understanding, as well as to obtain empirical results. (Single task, special project funding.)

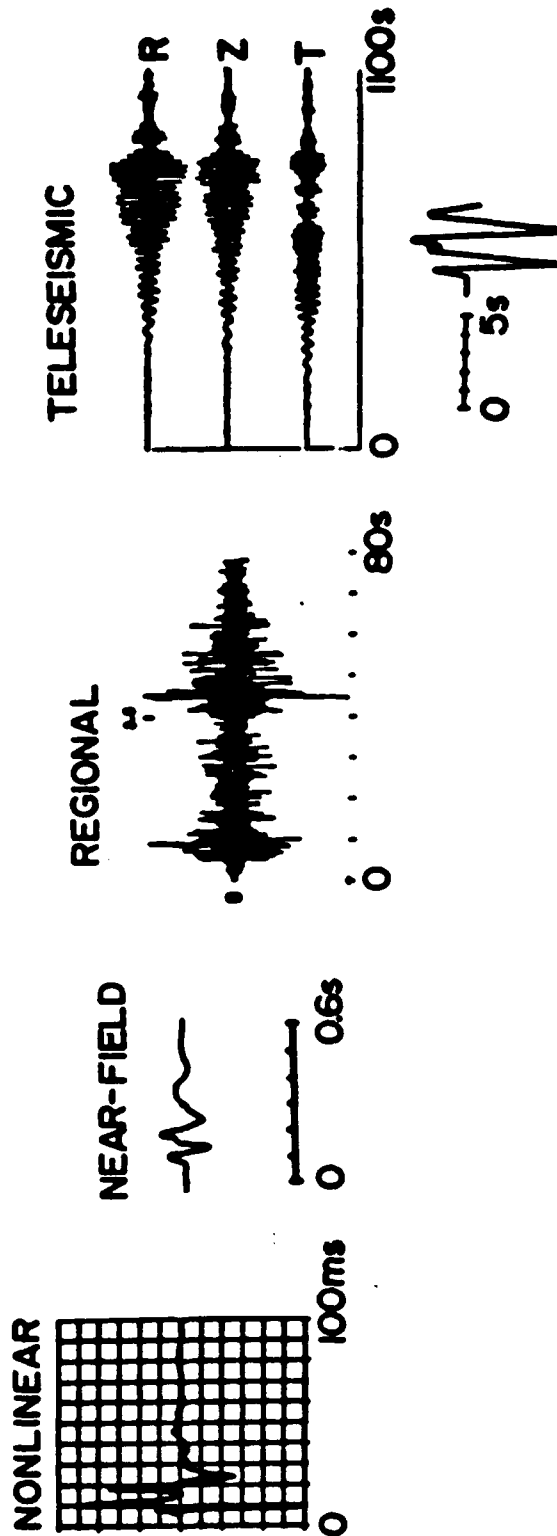
IV. Directions for Future Work: Specific Areas for New Initiatives and Focused Basic Research (2)

- **In-depth studies of differences between industrial types of explosions versus (simulated) decoupled explosions and small earthquakes.** Evaluate both seismic and non-seismic (acoustic, E-M sensing) methods for joint I.D. Use co-located explosions in controlled field experiments with high-performance equipment, followed by analysis and theoretical model generation. (Also use co-located explosions with previously recorded earthquakes when possible, so common path techniques can be applied in the earthquake-explosion cases as well.) - Single task, special project funding.

- **Test joint seismic yield estimation capabilities using P_n , P_g , L_g and Rayleigh surface waves at different regional distances and at different frequencies.** Compare to other available yield estimates (*eg.* Corrtex).

- **Deploy a small portable network of high-performance seismic systems (*eg.* five surface plus bore-hole b.b. and high frequency receivers) in linear arrays within particular geologic regions in the US/Canada (Basin and range, shield, coastal plains, central plains, mountain regions, etc.) to determine signal propagation and noise characteristics using explosion and earthquake sources.** (Use signal ratio techniques.) Move the whole network from province to province in order to seismically characterize each. (Single task, special project funding.)

WAVE PROPAGATION ISSUES ASSOCIATED WITH EXPLOSIVE SOURCES



CHEMICAL (10's μ s to ms RT)
NUCLEAR (μ s rise time RT)

150 KILOTON

- ④ MAGNITUDE-YIELD RELATIVELY WELL UNDERSTOOD
- ④ TEST SITE EFFECTS CALIBRATED
 - material effects
 - local structure
- ④ TECTONIC STRESS RELEASE CHARACTERIZED
- ④ MULTIPLE MEASURES OF YIELD
 - body waves
 - surface waves
 - L_g
 - isotropic moment

FUNDAMENTAL ISSUES BELOW 150 KILOTON

☛ LATERAL VARIATIONS IN MATERIAL PROPERTIES

**wave propagation
source coupling**

☛ ANISOTROPY

☛ NOISE FIELD QUANTIFICATION

☛ SOURCE PHENOMENOLOGY

**material effects/coupling
free surface effects
tectonic release**

☛ CHEMICAL EXPLOSIONS

**single burst
spatial/temporal arrays**

EFFECTS OF REDUCED YIELD EXPLOSIONS

- **DECREASED COUPLING**
- **SMALLER CAVITY**
- **SMALLER ELASTIC RADIUS**
- **HIGHER CORNER FREQUENCY**
- **POSSIBLE SHALLOWER BURIAL DEPTH**

SCALE LENGTHS IN SATURATED TUFF/RHYOLITE

$$r_{el} = 1490 \frac{W^{1/3}}{h^{0.42}}$$

$$h = 122 W^{1/3}$$

150 KILOTON

$$h = 648 \text{ m}$$

$$r_{el} = 522 \text{ m}$$

50 KILOTON

$$h = 449 \text{ m}$$

$$r_{el} = 422 \text{ m}$$

10 KILOTON

$$h = 263 \text{ m}$$

$$r_{el} = 309 \text{ m}$$

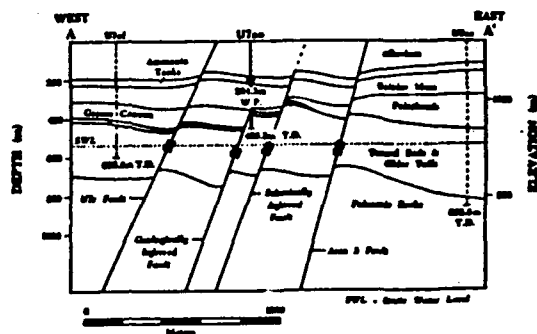
1 KILOTON

$$h = 122 \text{ m}$$

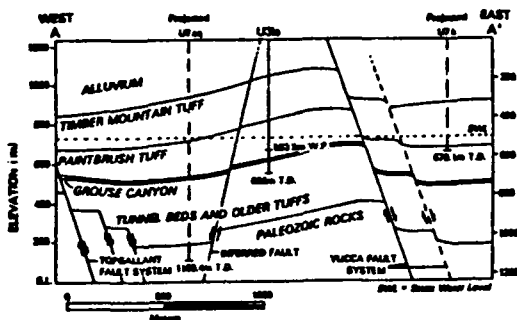
$$r_{el} = 198 \text{ m}$$

SPATIAL VARIATION OF GEOLOGICAL STRUCTURE IN CENTRAL YUCCA

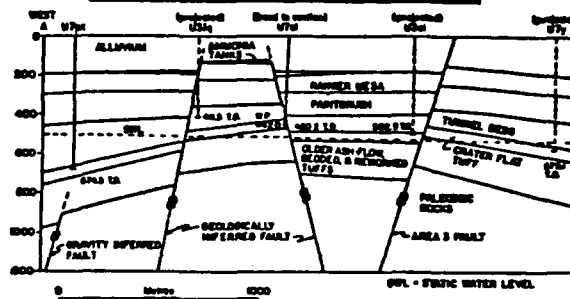
EAST-WEST GEOLOGIC CROSS-SECTION THRU U7a0



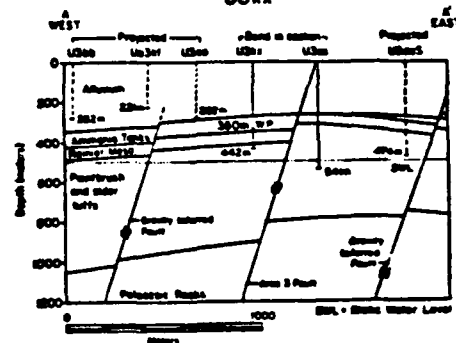
U31a EAST-WEST CROSS SECTION



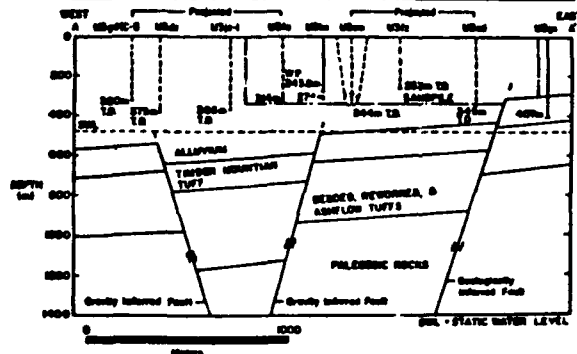
U701 EAST-WEST CROSS-SECTION



CROSS SECTION AND SURFACE EFFECTS U3kx



U31a EAST-WEST CROSS SECTION



ANISOTROPY

EVIDENCE

- ✎ **IMPORTANT IN INTERPRETING SURFACE SEISMIC SHEAR WAVE DATA**
- ✎ **VSP EFFECTS IDENTIFIED**
- ✎ **FRACTURE INDUCED - VERTICALLY ORIENTED**

EXPLOSION IMPLICATIONS

- ✎ **WAVE PROPAGATION EFFECTS**
- ✎ **SOURCE COUPLING**
- ✎ **MATERIAL CHARACTERIZATION**

NOISE ISSUES

- ✎ **COHERENT/INCOHERENT**
- ✎ **SPATIAL VARIABILITY**
- ✎ **VARIATION WITH DEPTH**
- ✎ **SEPARATION OF SYSTEM/BACKGROUND NOISE**
- ✎ **DEVELOPMENT OF NOISE CATALOG**

NOISE FIELD VARIABILITY

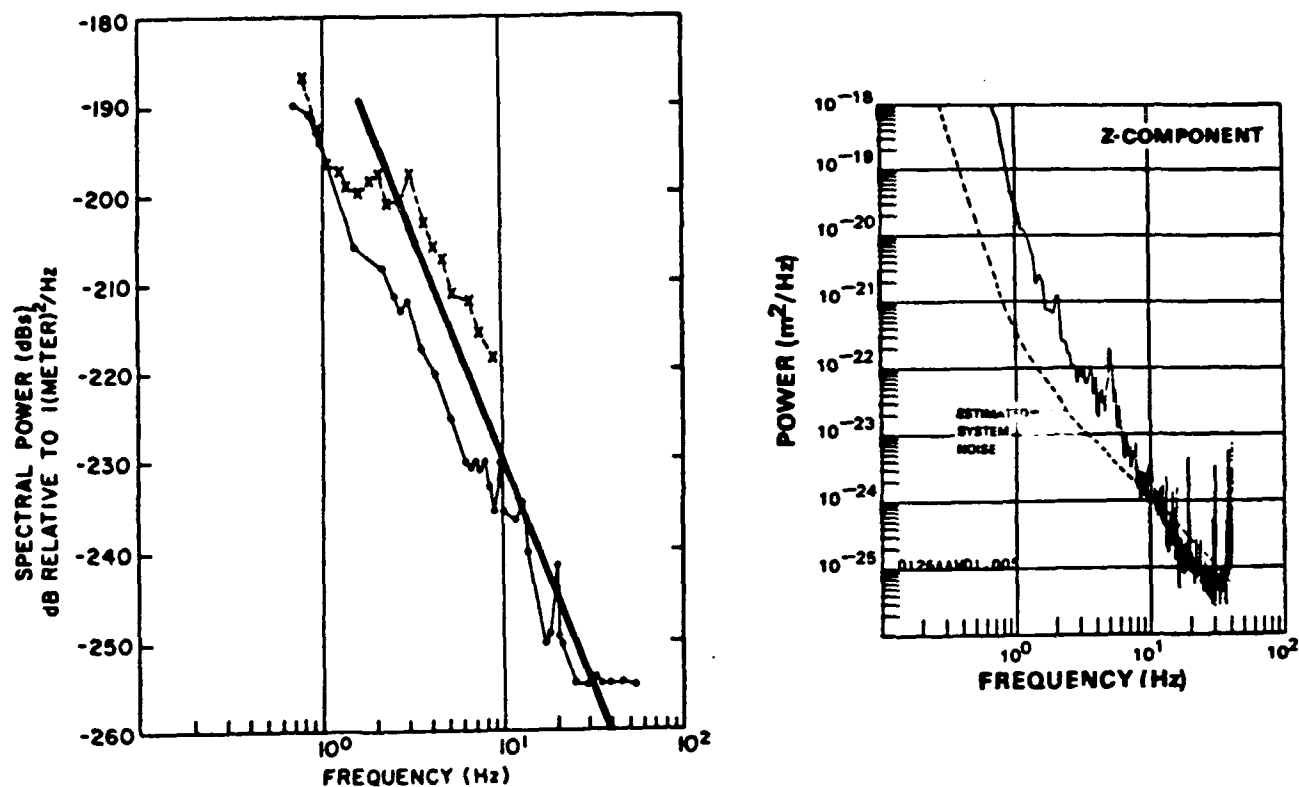


FIG. 8. Noise power spectra for (1) Lajitas (dots), and for (2) Queen Creek (X's) together with (3) a low-noise model for southeastern Norway (heavy line). (1) and (2) are taken from Herrin (1982), while (3) is from this study.

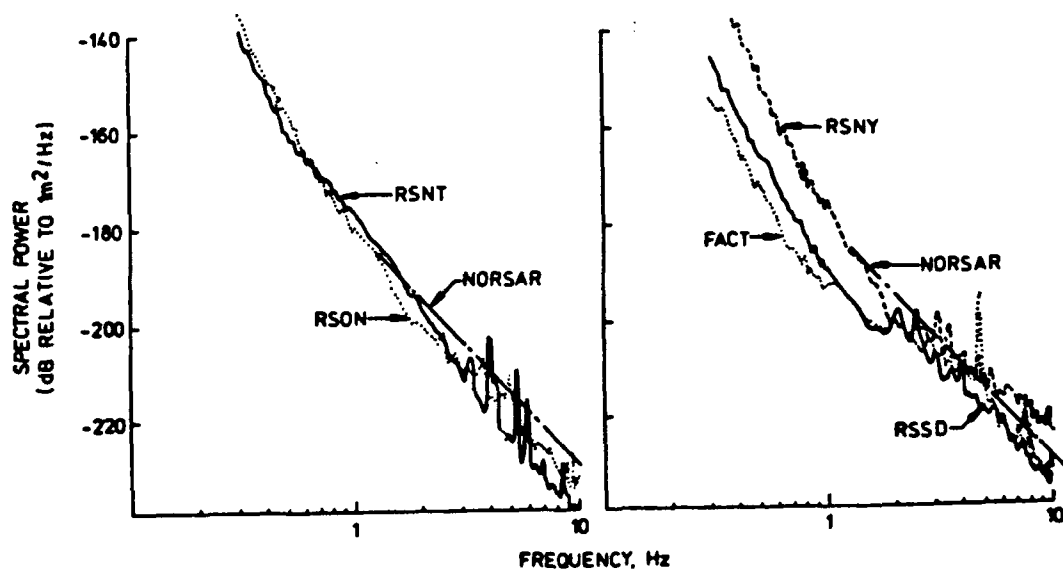
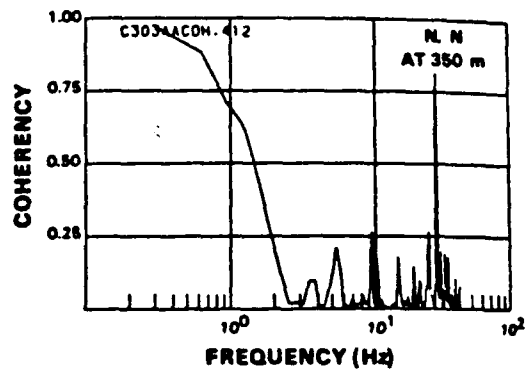
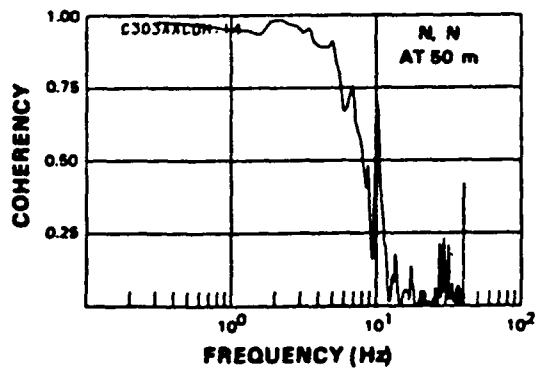
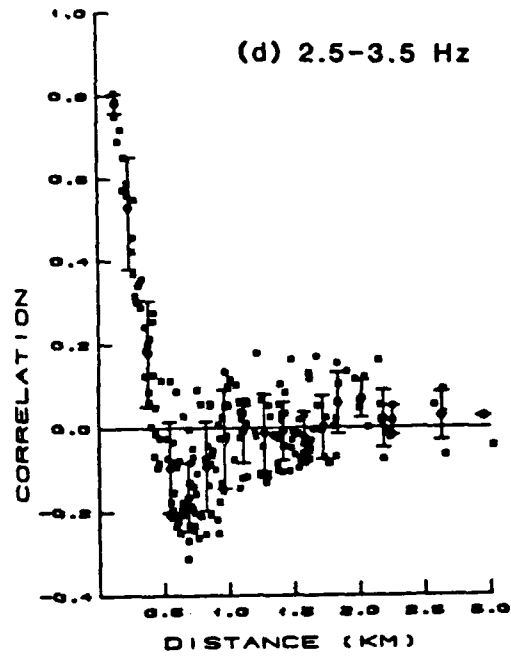
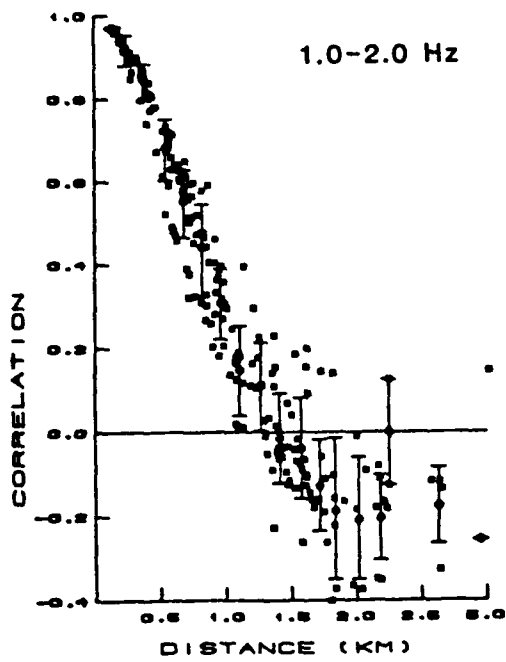


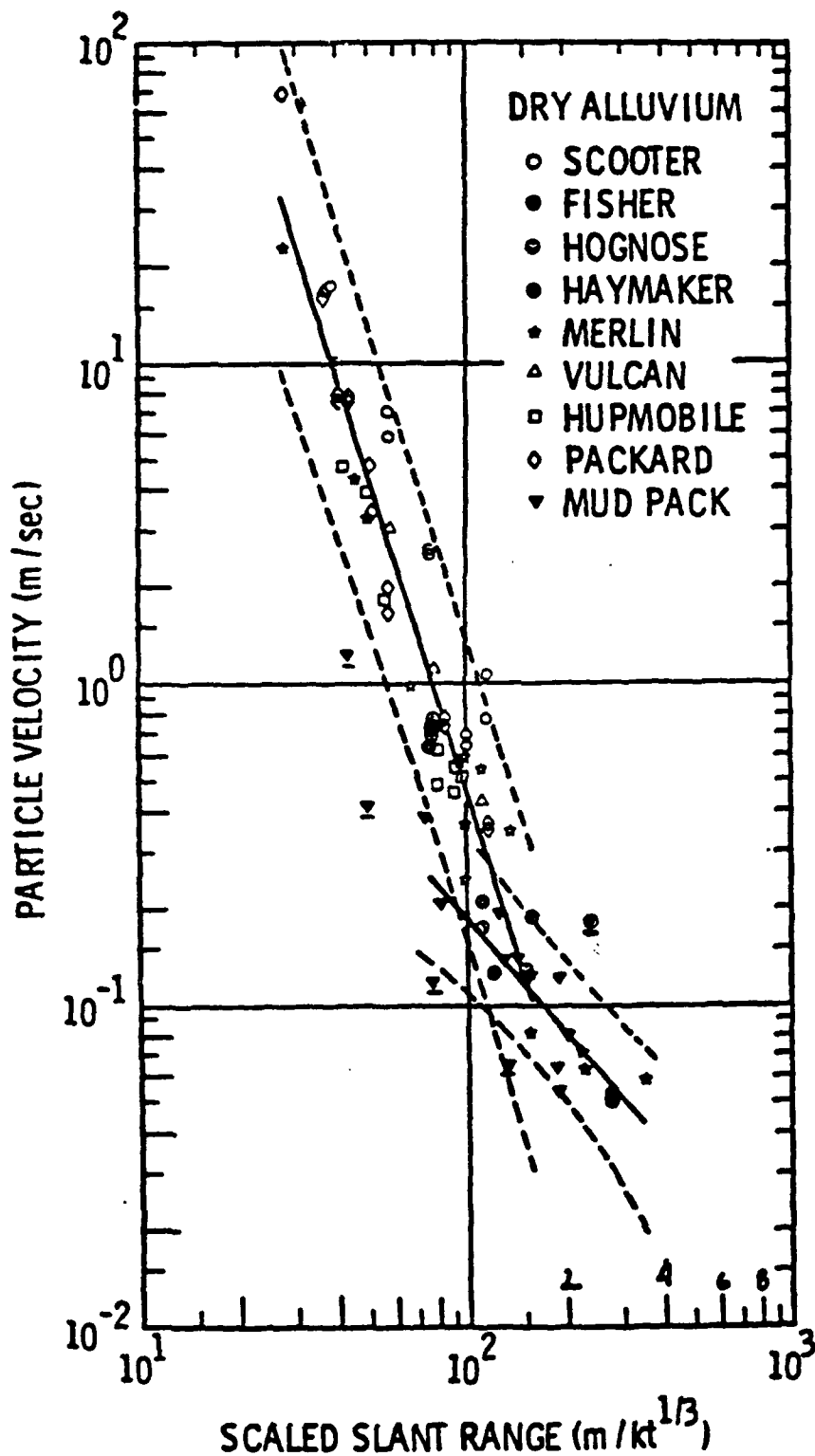
FIG. 3. The quiet-day noise power spectrum for NORSEAR is compared to typical background noise spectra for moderately quiet conditions at the RSTN sites (H. B. Durham, personal communication). The station locations are RSNT (Yellowknife, Northwest Territories) and RSON (Red Lake, Ontario) in Canada and RSNY (New York), RSSD (South Dakota) and FACT (Albuquerque, New Mexico) in the U.S. Spectral peaks at the RSTN sites are probably caused by vibrating surface equipment (S. Taylor, personal communication).

NOISE COHERENCE

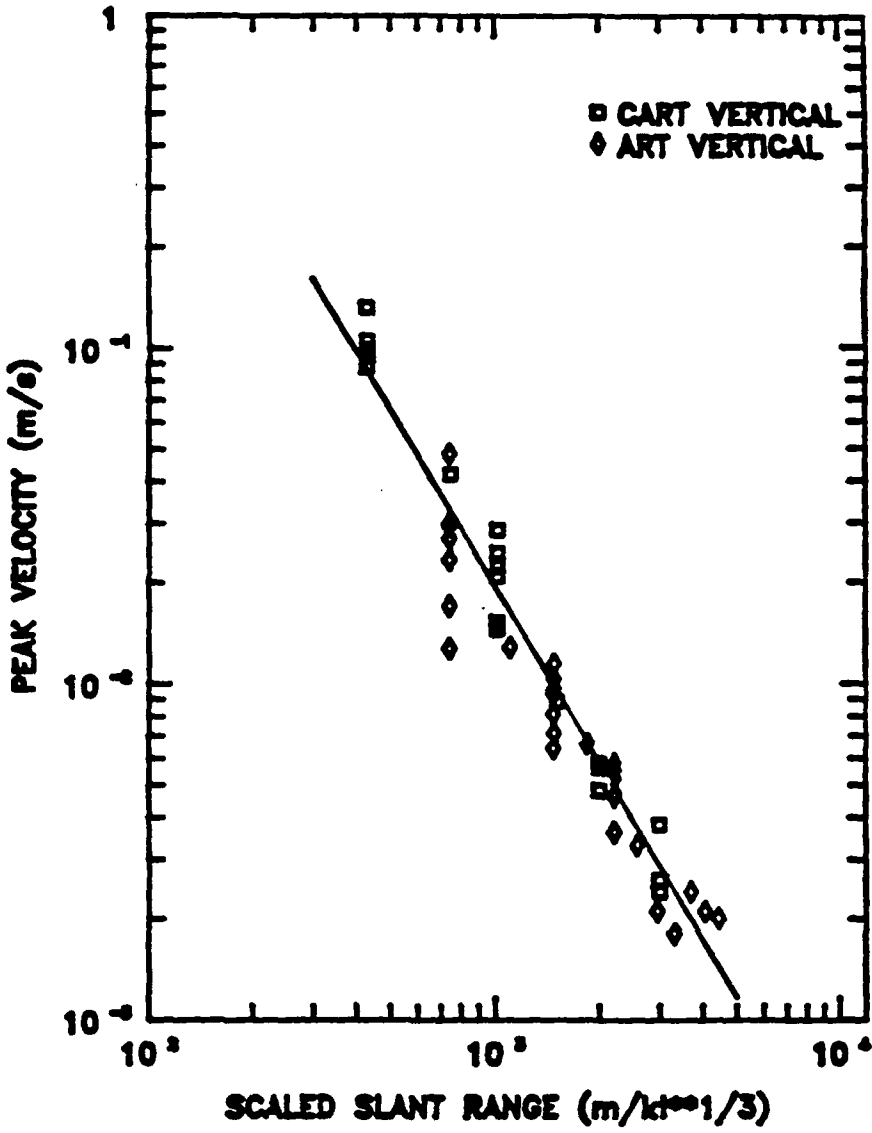


EFFECTS OF MATERIAL PROPERTIES

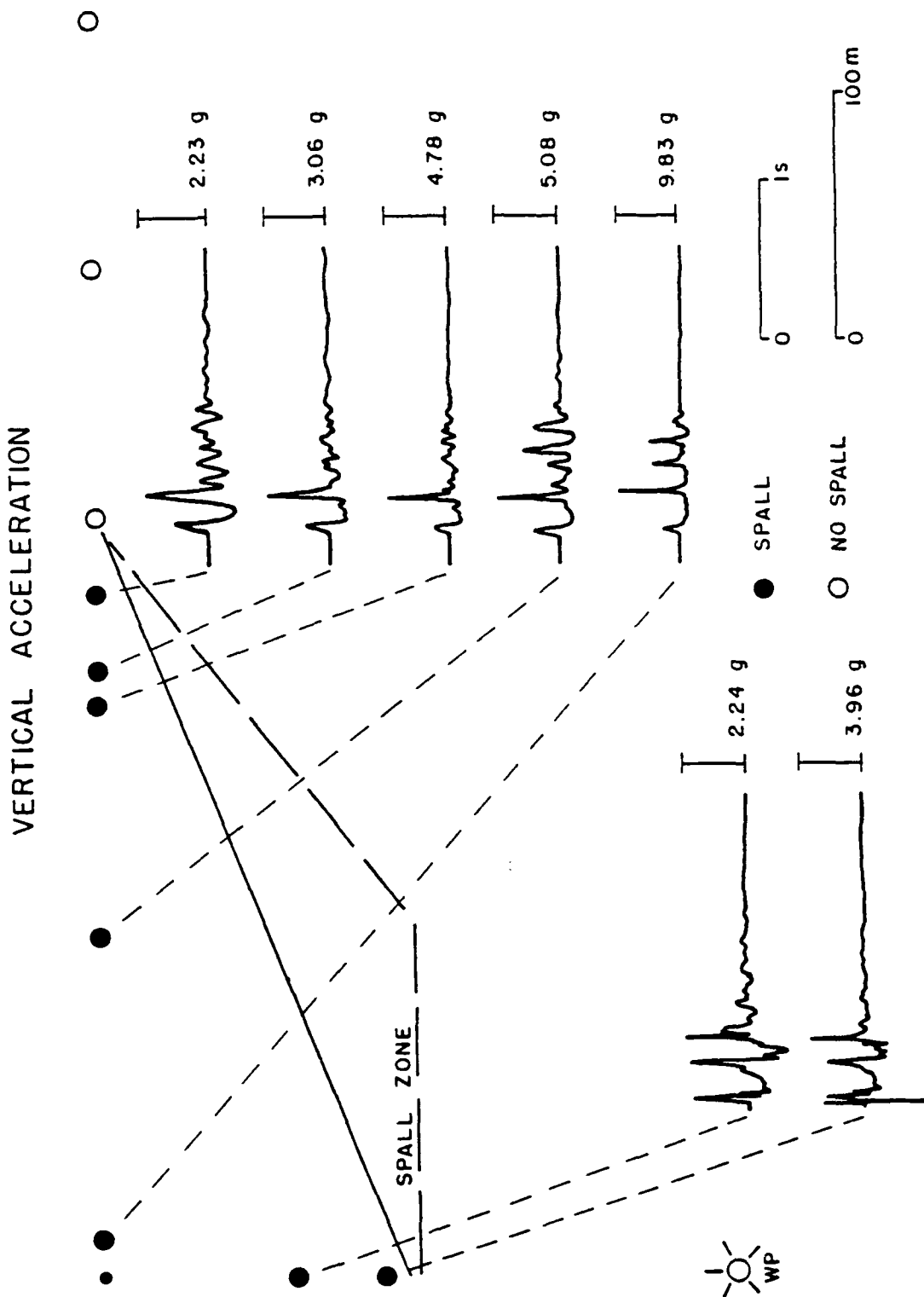
NUCLEAR



CHEMICAL



SPALL DELINEATION WITH EXPERIMENTAL DATA



ENGINEERING EXPLOSION TYPES

SHOT 3 SAN VEL QUARRY

7/29/87

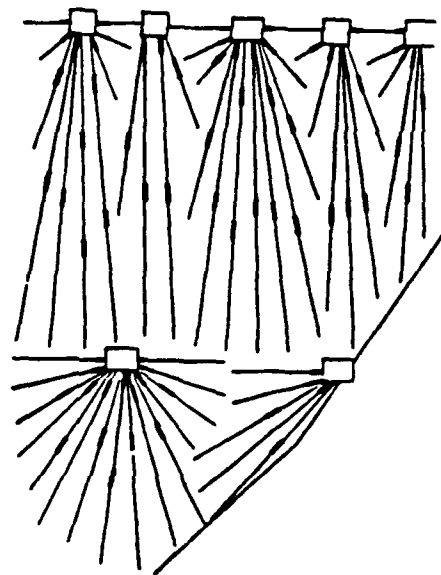
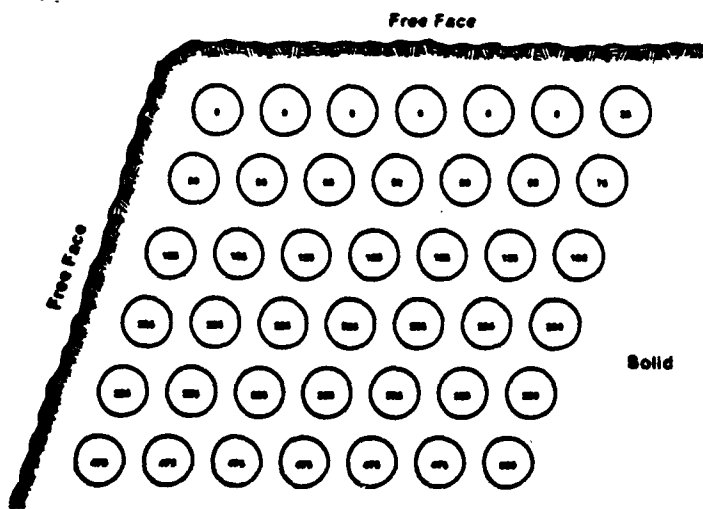
ms delay time

1-9-4



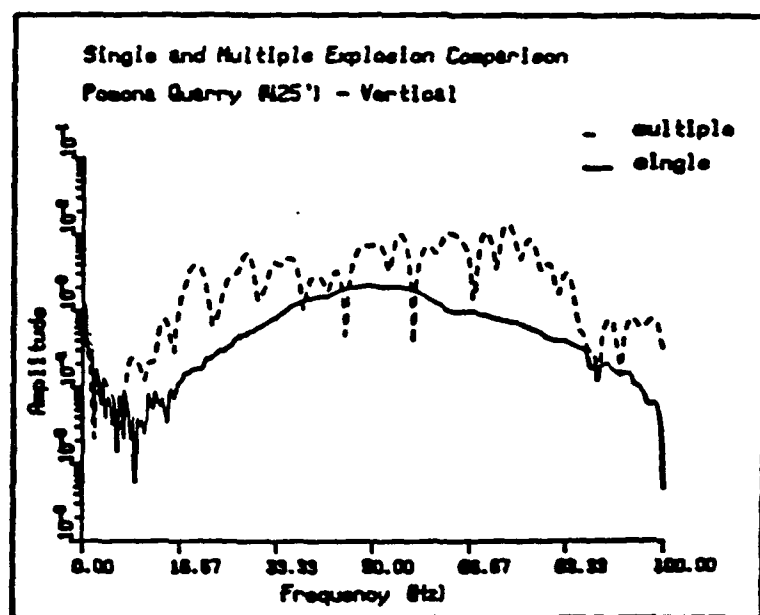
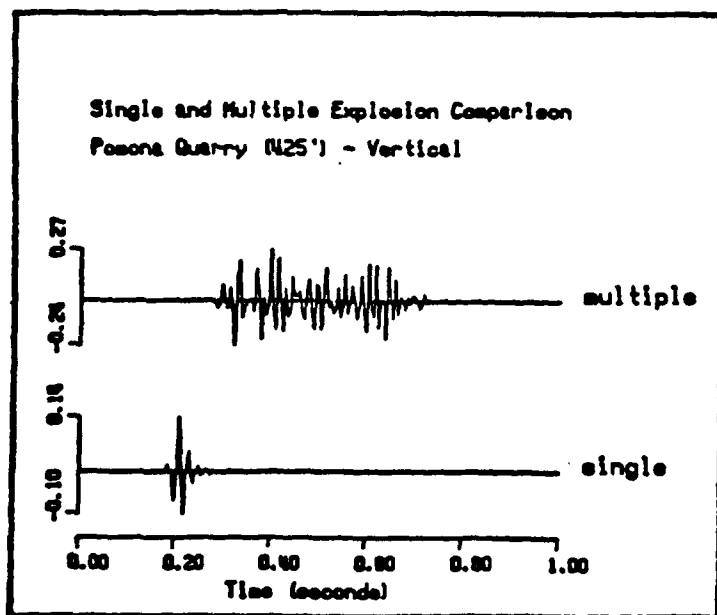
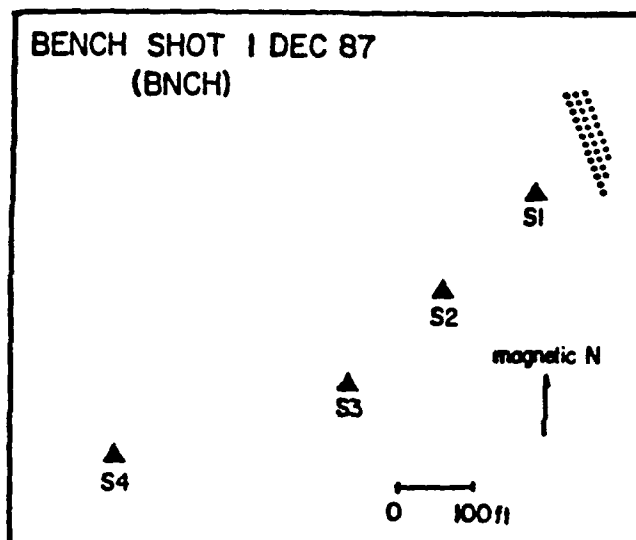
TOTAL LBS: 24350
MAX HOLES/DELAY: 2
MAX LBS/DELAY: 696
HOLE DEPTH: 58'-60'
STEMMING: 4'-8.5'

QUARRY
FACE



TOTAL CHARGE WEIGHT = 22,322 KG
% DRILL HOLE CHARGED = 70%

MULTIPLE CHEMICAL EXPLOSIONS IN TIME AND SPACE



CONCLUSIONS/RECOMMENDATIONS

- ✎ **SEPARATION OF DETERMINISTIC/STOCHASTIC WAVE PROPAGATION EFFECTS**
- ✎ **NEED FOR LIMITED/CALIBRATED TEST SITE**
- ✎ **DEVELOPMENT OF MODERN DIGITAL NOISE CATALOG**
- ✎ **QUANTIFICATION OF ANISOTROPIC EFFECTS**
- ✎ **USE OF AUXILLIARY SOURCE INFORMATION IN DEVELOPING MODELS**
- ✎ **SCALING OF SECONDARY SOURCES**
 - Tectonic**
 - Free Surface Interaction**
- ✎ **INTEGRATED EXPERIMENTAL TESTS DRIVEN BY THEORETICAL MODELS**
- ✎ **QUANTIFICATION OF CHEMICAL EXPLOSIONS**



S-CUBED

A Division of Maxwell Laboratories, Inc.

CURRENT RESEARCH ISSUES IN NUCLEAR TEST LIMITATION TREATY MONITORING

- 150 KT TTBT
- LOWER YIELD TTBT
- 1 KT "CTB"

150 KT TTBT

- SEISMIC YIELD ESTIMATION AT 150 KT AT SHAGAN HAS BEEN EXTENSIVELY (EXHAUSTIVELY?) INVESTIGATED. WITH SOME CORRTEX CALIBRATION, A COMBINATION OF SEISMIC TECHNIQUES (I.E., M_B , L_G , M_0 ETC.) CAN BE EXPECTED TO GIVE A YIELD ESTIMATION ACCURACY (2σ) TO WITHIN A FACTOR OF ABOUT 1.5. WITH EXTENSIVE CALIBRATION AND RIGID CONTROLS ON TEST PRACTICES, SEISMIC YIELD ESTIMATION MAY APPROACH THE NOMINAL FACTOR OF 1.3 QUOTED FOR CORRTEX IN THIS YIELD RANGE.
- YIELD ESTIMATION AT 150 KT AT OTHER SOVIET TEST AREAS (DEGELEN, NOVAYA ZEMLYA) HAS BEEN LESS WELL STUDIED. HOWEVER, MANY OF THE APPROACHES WHICH WERE SUCCESSFUL AT SHAGAN (E.G., SURFACE WAVE MOMENT TENSOR INVERSION, L_G YIELD ESTIMATION, NETWORK-AVERAGED P WAVE SPECTRA) ARE CURRENTLY BEING APPLIED AT THESE OTHER TEST SITES. THIS SHOULD RESULT IN YIELD ESTIMATION CAPABILITY FOR THESE SITES COMPARABLE TO THAT AT SHAGAN.
- IN SUMMARY, MOST OF THE REMAINING ISSUES AT 150 KT AT DESIGNATED SOVIET TEST AREAS ARE PREDOMINANTLY STATISTICAL RATHER THAN SEISMOLOGICAL IN NATURE. ADDITIONAL RESEARCH IS NEEDED TO DEVELOP OPTIMUM METHODS TO:
 - (I) INCORPORATE YIELD CALIBRATION INFORMATION
 - (II) COMBINE VARIOUS SEISMIC YIELD ESTIMATION PROCEDURES
 - (III) QUANTIFY UNCERTAINTY IN SEISMIC YIELD ESTIMATES
 - (IV) ASSESS COMPLIANCE OF A SINGLE EVENT OR TEST SERIES WITH SPECIFIED THRESHOLD
 - (V) COMMUNICATE THE RESULTS OF (III) AND (IV) TO POLICY-MAKERS

LOWER YIELD TTBT

- UNDER THE ASSUMPTION THAT CAVITY DECOUPLING IS NOT FEASIBLE ABOVE 10-20 KT, DETECTION AND IDENTIFICATION OF NUCLEAR EXPLOSIONS IN THE SOVIET UNION TO THAT YIELD LEVEL CAN BE ACCOMPLISHED USING EXTERNAL STATIONS ALONE.
- HOWEVER, YIELD ESTIMATION CAPABILITY DECREASES AS YIELD DECREASES. WITH EXTERNAL STATIONS ALONE, L_G AND SURFACE WAVE DETECTION BECOMES PROBLEMATICAL BELOW ABOUT 50 KT. THE SUBSEQUENT DECREASE IN THE NUMBER OF INDEPENDENT YIELD ESTIMATES RESULTS IN REDUCED PRECISION.
- MORE FUNDAMENTALLY, LITTLE WORK HAS YET BEEN DONE TO PIN DOWN THE ABSOLUTE LEVEL OF THE SEISMIC SIGNALS AT THESE LOWER YIELD LEVELS. FOR EXAMPLE, WHAT IS THE M_B VALUE CORRESPONDING TO A 10 KT COUPLED EXPLOSION IN SOVIET SALT? OUTSTANDING ISSUES AFFECTING YIELD ESTIMATION BELOW ABOUT 75 KT INCLUDE:
 - (I) SLOPE OF THE M_B /YIELD CURVE
 - (II) YIELD (FREQUENCY) AND GEOGRAPHICAL DEPENDENCE OF THE ATTENUATION BIAS CORRECTION
 - (III) SOURCE MEDIUM DEPENDENCE OF THE SEISMIC COUPLING

- BELOW 10-20 KT CAVITY DECOUPLING BECOMES AN ISSUE. IT IS GENERALLY BELIEVED THAT CAVITIES LARGE ENOUGH TO FULLY DECOUPLE 10 KT COULD ONLY BE MADE IN SALT. EVEN SO, POTENTIAL SOURCE REGIONS ENCOMPASS LARGE AREAS OF THE SOVIET UNION. SINCE THE m_B VALUE CORRESPONDING TO 10 KT FULLY DECOUPLED IS ABOUT 3.0 ± 0.25 , INTERNAL STATIONS WILL BE REQUIRED TO MONITOR TO THIS YIELD LEVEL.
- EXTRAPOLATIONS OF OBSERVED SOVIET SEISMICITY SUGGEST THAT THERE WILL BE MORE THAN 1000 EARTHQUAKES/YEAR ON SOVIET LAND AREAS WITH $m_B > 3.0$. THE MAJORITY OF THESE OCCUR WHERE 10 KT DECOUPLING IS NOT POSSIBLE. ON THE OTHER HAND, THIS TOTAL IGNORES CHEMICAL EXPLOSIONS (CE), ROCKBURSTS AND LOW LEVEL NATURAL SEISMICITY IN AREAS WHICH APPEAR TO BE ESSENTIALLY ASEISMIC ABOVE $m_B = 5.0$.
- AN m_B VALUE OF 3.0 IN THE EUS CORRESPONDS TO 20 TO 40 TONS OF CE. MCGARR REPORTS THAT IN THE DEEP GOLD MINING DISTRICTS OF SOUTH AFRICA, HE IS DETECTING 20 ROCKBURST EVENTS/MONTH WITH $M > 3$, INCLUDING EVENTS AS LARGE AS $M = 4.6$. THESE OBSERVATIONS SUGGEST THE FOLLOWING QUESTIONS:
 - (I) WHAT IS THE RATE OF OCCURRENCE AND SPATIAL DISTRIBUTION OF CE WITH YIELDS GREATER THAN 20 TONS IN THE SOVIET UNION?
 - (II) WHAT IS THE RATE OF OCCURRENCE AND SPATIAL DISTRIBUTION OF ROCKBURSTS AND LOW LEVEL NATURAL SEISMICITY ABOVE $m_B = 3.0$ IN THE SOVIET UNION?

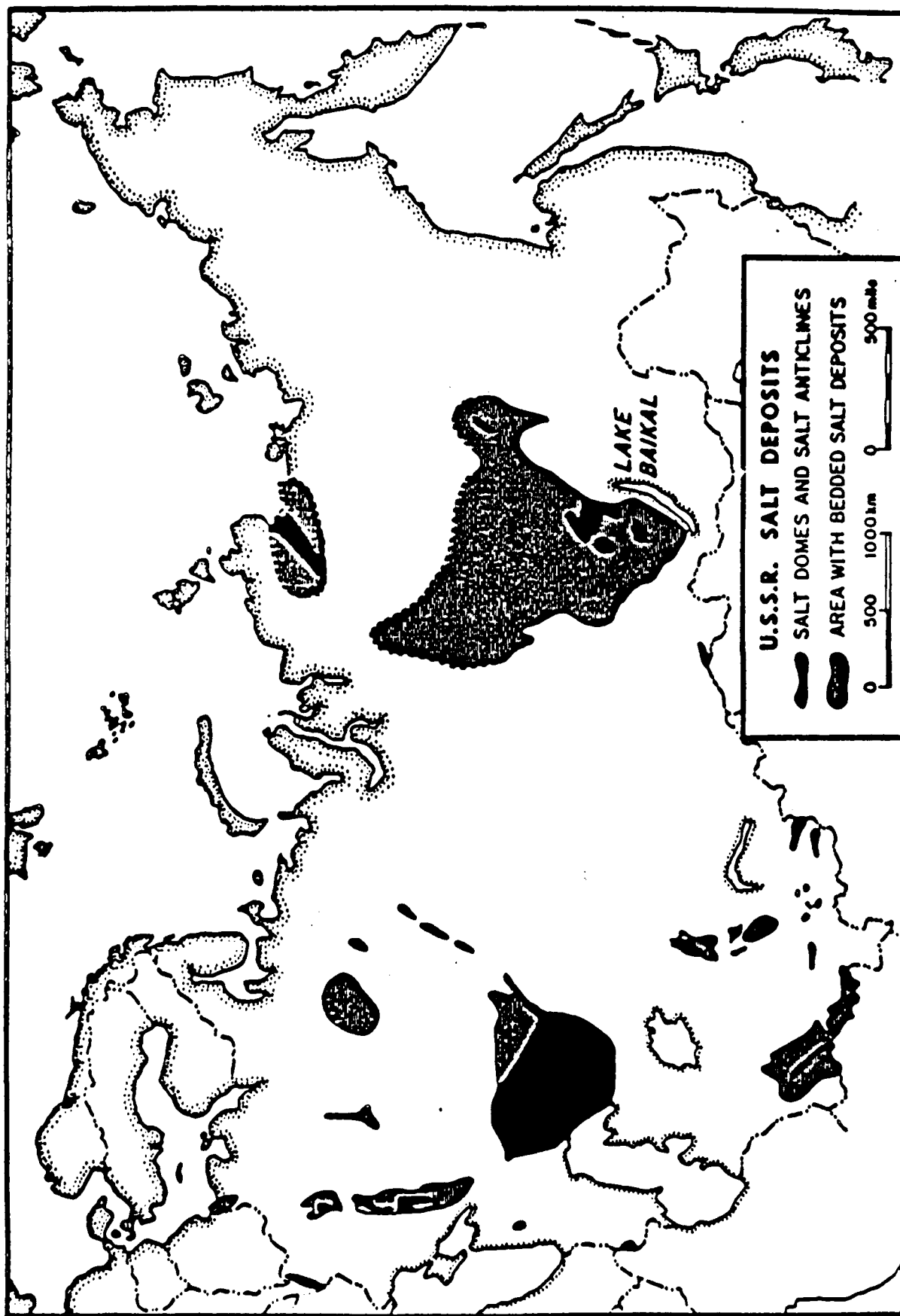


Figure 2. General distribution of salt deposits in USSR.

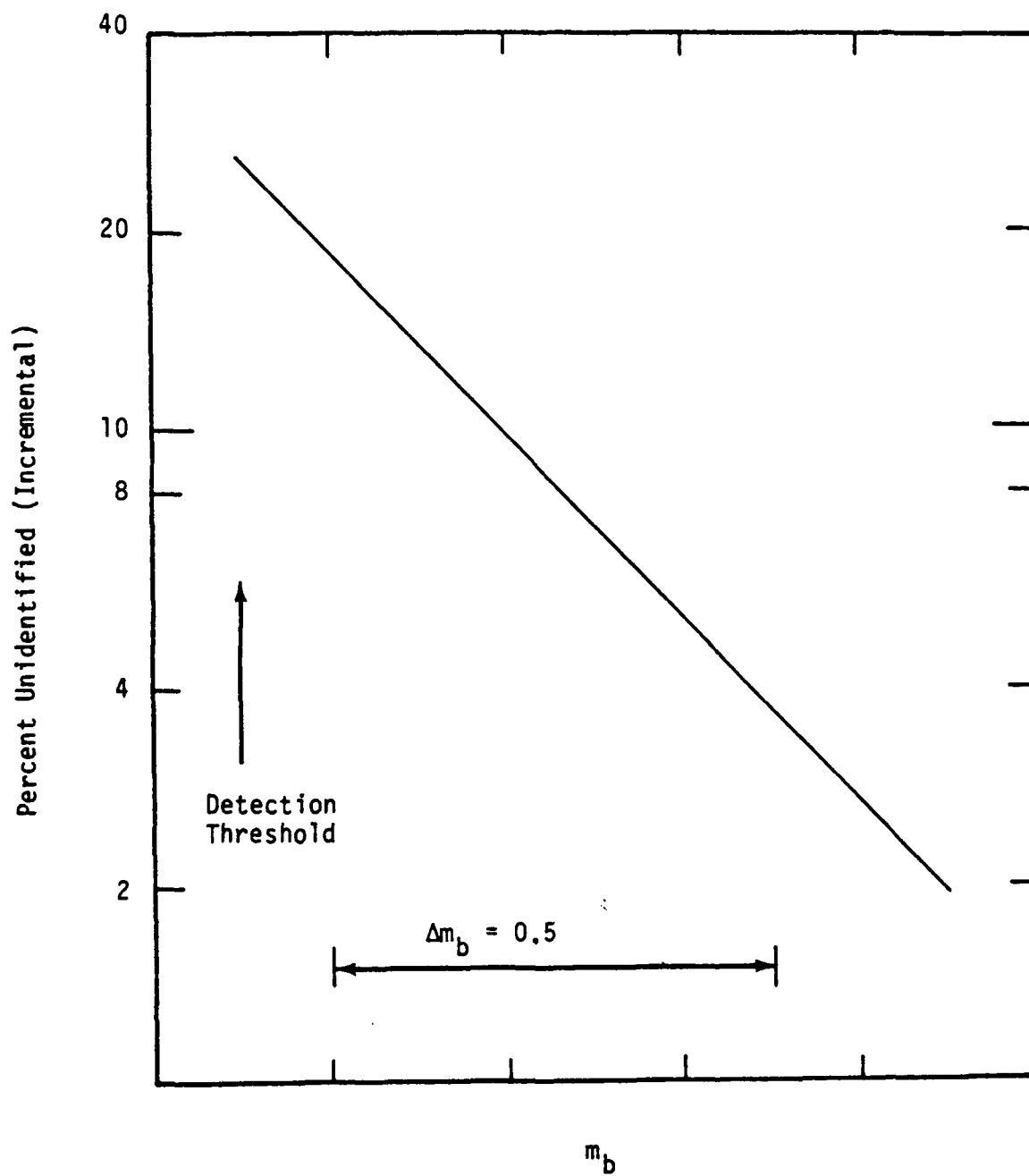
- CAPABILITY TO DISCRIMINATE AT $M_B = 3.0$ IS CURRENTLY UNKNOWN. IN THE ABSENCE OF A BETTER THEORETICAL UNDERSTANDING OF THE CHARACTERISTICS OF THE VARIOUS SEISMIC SOURCES OF INTEREST, DEMONSTRATION OF IDENTIFICATION CAPABILITY AT LEVELS APPROACHING $M_B 3.0$ WILL REQUIRE PRACTICAL EXPERIENCE WITH SOVIET REGIONAL SEISMIC DATA. OUTSTANDING ISSUES REQUIRING FURTHER RESEARCH INCLUDE:

- (I) SOURCE CHARACTERISTICS OF DECOUPLED EXPLOSIONS, CE, ROCKBURSTS AND SMALL TECTONIC EVENTS, PARTICULARLY AT HIGH FREQUENCY
- (II) THEORETICAL FOUNDATION FOR EMPIRICALLY-BASED REGIONAL DISCRIMINANTS (DEPTH DETERMINATION, PHASE EXCITATION AS A FUNCTION OF FREQUENCY ETC.)
- (III) IMPROVED CAPABILITY TO THEORETICALLY SYNTHESIZE ACCURATE, BROADBAND REGIONAL SEISMOGRAMS FOR AREAS OF LOW NATURAL SEISMICITY (I.E., TRANSPORTABILITY)

1 KT "CTB"

- WELL COUPLED NUCLEAR EXPLOSIONS IN THE SOVIET UNION WITH YIELDS AS LOW AS A FEW KT CAN BE WELL MONITORED (I.E., IDENTIFIED, YIELD ESTIMATED) USING EXTERNAL STATIONS ALONE. ACCURATE YIELD ESTIMATION WOULD, HOWEVER, REQUIRE INTERNAL STATIONS AND CALIBRATION.
- 1 KT FULLY DECOUPLED IN A CAVITY CORRESPONDS TO m_B VALUES IN THE RANGE OF ABOUT 2.0 TO 2.5. CAVITIES LARGE ENOUGH TO FULLY DECOUPLE 1 KT CAN PROBABLY BE CONSTRUCTED IN A VARIETY OF MEDIA (E.G., GRANITE AND TUFF AS WELL AS SALT) AND IS, THEREFORE, POSSIBLE THROUGHOUT MUCH OF THE SOVIET UNION.
- SIMULATION RESULTS SUGGEST THAT A 50 STATION INTERNAL NETWORK MIGHT PROVIDE A DETECTION THRESHOLD BETWEEN m_B 2.0 TO 2.5 THROUGHOUT THE SOVIET UNION. AS A POINT OF REFERENCE, HOWEVER, IT IS WORTH NOTING THAT MASSÉ ESTIMATES THAT MORE THAN 100 STATIONS WILL BE NEEDED TO ACHIEVE A DETECTION THRESHOLD OF m_B 2.5 IN THE CONTINENTAL U.S. MOREOVER, BACHE ARGUES THAT "...THE DETECTION THRESHOLD (IN THE SOVIET UNION) IS NO BETTER THAN m_B 2.5 WITH ANY CONCEIVABLE NETWORK." ON THE OTHER HAND, EVERNDEN ET AL. ARGUE THAT THRESHOLDS AS LOW AS m_B 1.5 MAY BE ACHIEVABLE USING HIGH FREQUENCY DATA. MORE SOVIET REGIONAL DATA WILL BE REQUIRED TO RESOLVE THIS ISSUE.

- IN ANY CASE, THE SIGNALS FROM A 1 KT CAVITY DECOUPLED EXPLOSION WILL BE NEAR THE DETECTION THRESHOLD OF EVEN AMBITIOUS INTERNAL NETWORKS. DETECTION DOES NOT EQUAL IDENTIFICATION. EXPERIENCE INDICATES THAT THE IDENTIFICATION THRESHOLD LIES AT LEAST 0.5 UNITS M_B ABOVE THE DETECTION THRESHOLD.
- EXTRAPOLATIONS OF EXISTING DATA SUGGEST THAT ON THE ORDER OF 10,000 EARTHQUAKES WITH $M_B > 2.0$ OCCUR BENEATH THE SOVIET LAND-MASS EVERY YEAR. JUDGING BY PAST EXPERIENCE, A SIGNIFICANT NUMBER OF THESE WILL BE AMBIGUOUS, EVEN GRANTED A DETECTION THRESHOLD OF M_B 2.0. MOREOVER, M_B 2.0 CORRESPONDS TO CE OF LESS THAN 10 TONS. THERE ARE HUNDREDS OF CE WITH YIELDS OF 100 TONS OR MORE IN THE U.S. EVERY YEAR. IT HAS YET TO BE DEMONSTRATED THAT CAVITY DECOUPLED EXPLOSIONS CAN BE DIFFERENTIATED FROM CE OF COMPARABLE M_B WITH A HIGH DEGREE OF CONFIDENCE.
- A MAJOR BREAKTHROUGH IN IDENTIFICATION CAPABILITY WILL BE REQUIRED BEFORE CAVITY DECOUPLED EXPLOSIONS WITH YIELDS OF 1 TO 2 KT CAN BE RELIABLY DIFFERENTIATED FROM THE BACKGROUND OF MANY SMALL EARTHQUAKES AND ROUTINE CE OF COMPARABLE MAGNITUDE.
- THEORETICAL AND EMPIRICAL ANALYSES OF THE HIGH FREQUENCY SEISMIC CHARACTERISTICS OF THE VARIOUS SOURCE TYPES WOULD APPEAR TO OFFER THE BEST PROSPECTS FOR PROGRESS IN THIS AREA.



ENGINEERING PERSPECTIVES
on
SEISMIC MONITORING
of the
SOVIET UNION

W. E. Farrell

Science Applications International Corporation

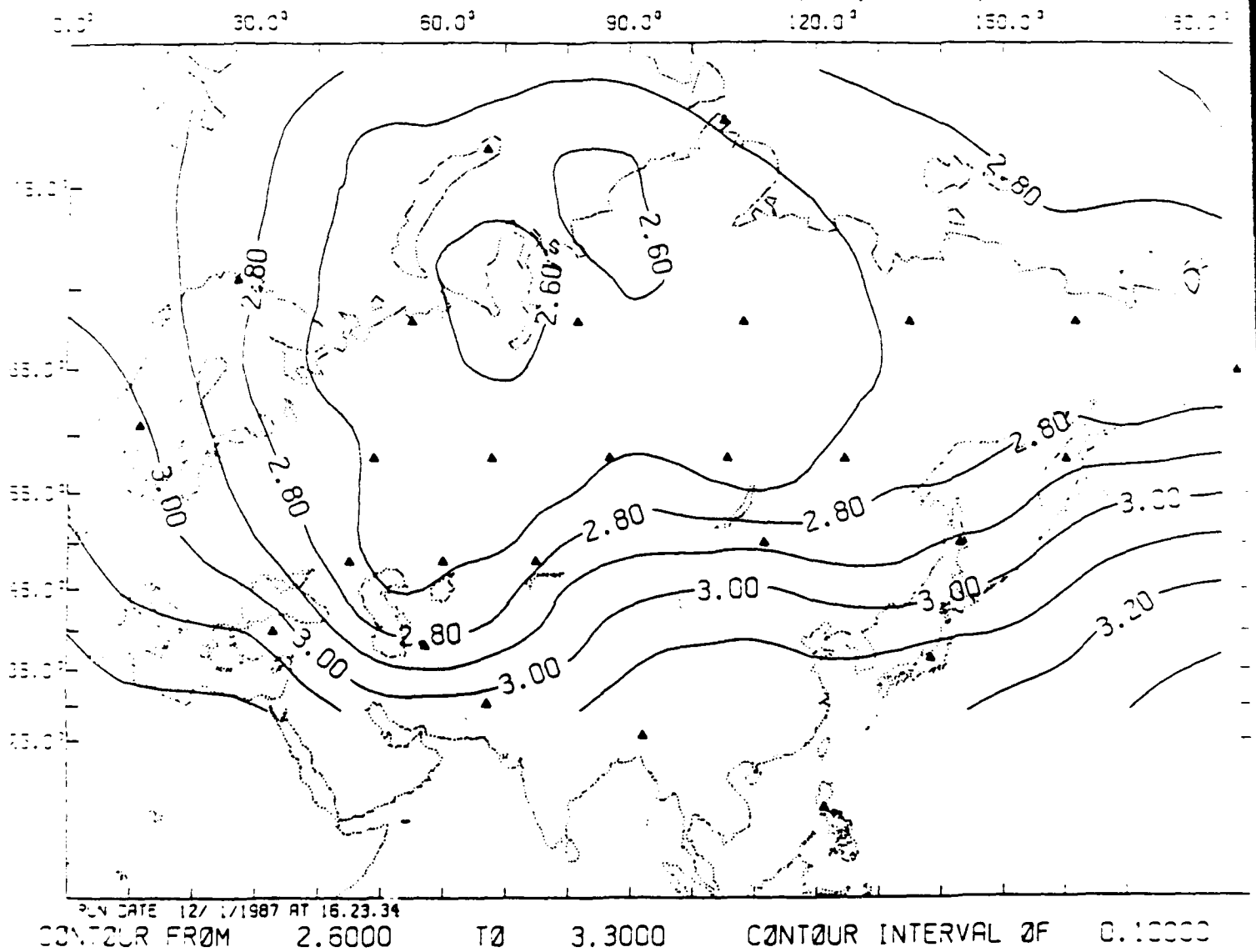
San Diego, Ca

Presented to

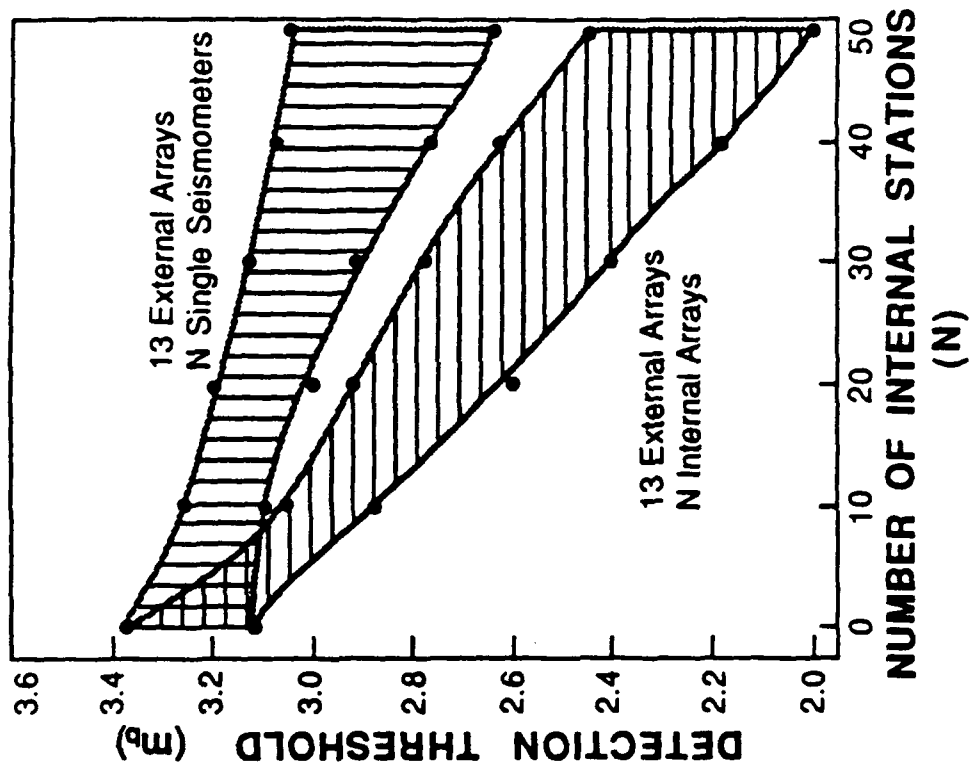
AFGL/DARPA Seismic Research Symposium

4 May, 1988.

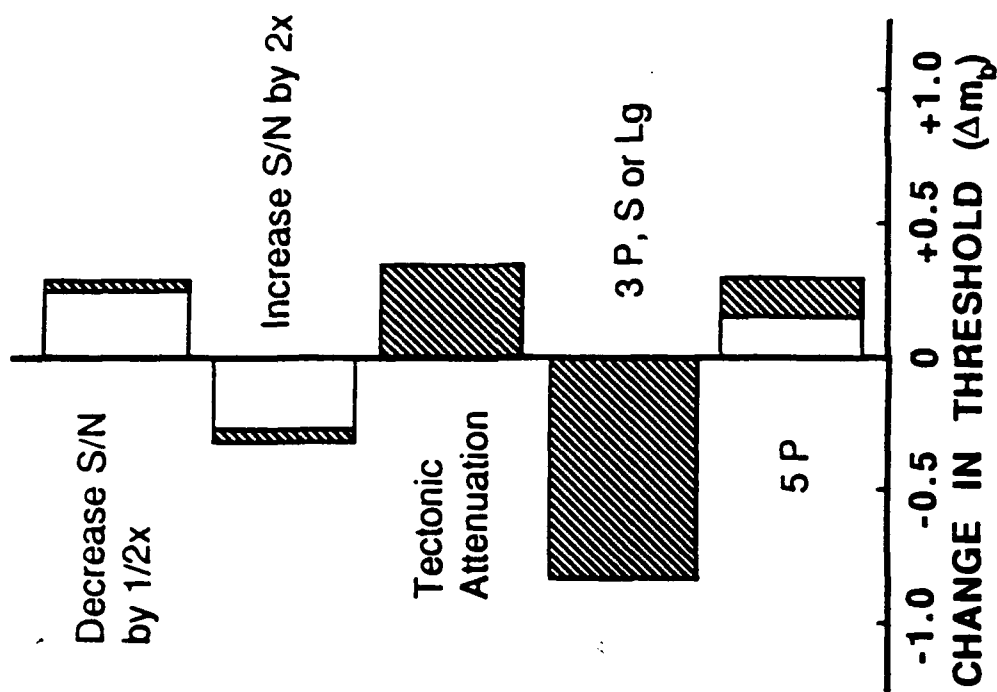
13EX 20INT ARRAYS, NOR D, P/3 (D20A02)



USSR HYPOTHETICAL DETECTION THRESHOLDS (90% Probability of 3 P-waves)



PARAMETER SENSITIVITY



Chemical Explosions

(1/86 through 6/86)

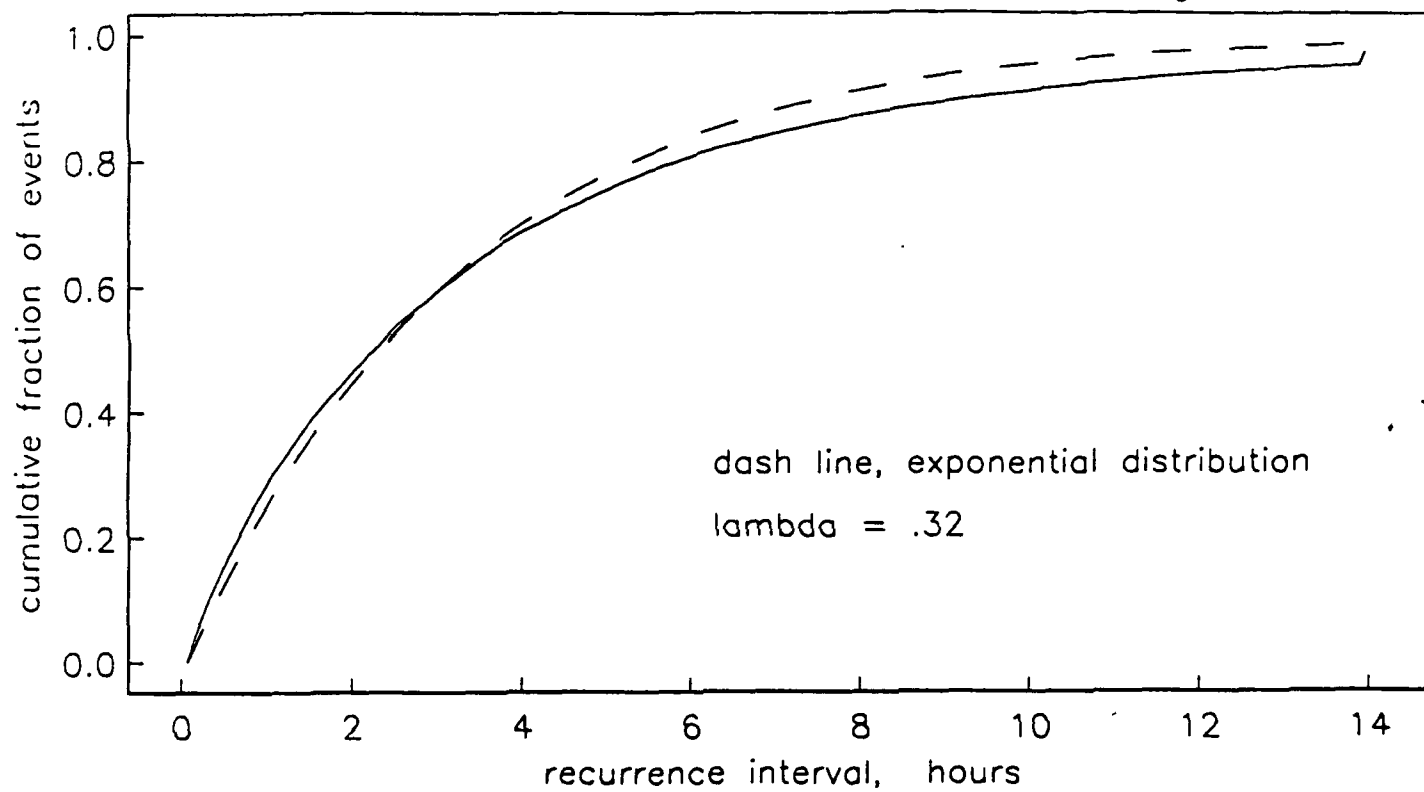
N.W. USSR

m_b	Number.
>3.0	3
>2.5	72
>2.0	490

SEISMICITY

m_b	Earthquakes per Year		
	Worldwide	USSR	
		All	Continental
4.5	2,500	200	70
4.0	7,000	650	225
3.5	20,000	2,000	700
3.0	60,000	6,000	2,000
2.5		18,000	6,000

Earthquake Recurrence Distribution Function, ISC $m_b \geq 5$



DATA RATES

	Sampling Rate	FOR EACH STATION	
		Channels	kilobits/second
EXTERNAL			
13 Arrays	20	15 (+6)	4.8
INTERNAL			
20 Stations [†]	100	3 (+6)	6.0
or			
20 Arrays [‡]	40	25 (+10)	16.0

- N kilobits/second is nearly 10N megabytes/day

† eg. DOE/Sandia Deployable Seismic Verification System (DSVS)

‡ eg. NORESS

LESSON: 20 kilobits/second from 33 stations yields 6 gigabytes/day of time-series data.

SEISMIC MONITORING: OPPORTUNITIES

- Quasi-operational processing systems are now emerging
- New data of higher bandwidth is being obtained to feed them
- Mass storage devices will make raw and *partially processed* data easily available
- Research concepts susceptible to automation should be turned into algorithms and joined to the automatic systems.

SEISMIC MONITORING:

CONCLUSIONS

- A HIGH DEGREE OF AUTOMATION WILL BE NEEDED
- MANY OF THE NECESSARY SUBSYSTEMS HAVE BEEN DEMONSTRATED
- A COMPLETELY AUTOMATIC SYSTEM EVEN A TENTH THE REQUISITE SIZE REMAINS TO BE SHOWN

ATTENUATION AND MODULI FROM HYSTERESIS LOOPS AT 0.1 Hz

Karl B. Coyner and Randolph J. Martin III
New England Research, Inc., P.O. Box 857
Norwich, Vermont 05055

INTRODUCTION

In order to clarify the frequency dependence of attenuation between 0.1 and 100 Hz, there is a useful role for laboratory investigations of frequency, strain amplitude, pressure, saturation, and lithology effects. If the laboratory properties of rock can match seismic observations of both the value of Q and its frequency dependence, particularly in the 1 to 20 Hz band, then seismic observations can be interpreted by physical mechanisms quantified through a series of additional experiments. If not, appropriate explanations must rely on other physical realities, such as contrasts in lithology, anisotropy, the presence of fractures, or scattering due to other inhomogeneities.

The frequency range of interest spans from approximately 0.01 to 100 Hz over the strain amplitude range from 10^{-9} to 10^{-2} . Unfortunately, seismic velocities are too high for true pulse propagation experiments to be possible in the laboratory at these frequencies. Instead, stress-strain data can be directly measured on samples subjected to cyclic stress. Attenuation is computed either from the phase angle between stress and strain or else from the fractional energy loss per cycle recorded in the hysteresis loop. Previous experimental studies with this technique include Gordon and Davis (1968), Walsh et al. (1970), McKavanagh and Stacey (1974), Spencer (1981), Brennan (1981), and Liu and Peselnick (1983). Although seismic frequencies and large strain amplitudes are easily attained, far-field strain amplitudes less than 10^{-6} are experimentally difficult.

The experimental results described in this report are for room dry samples of Sierra White granite and Cedar City quartz diorite. Hysteresis loops were recorded during sinusoidal, 0.1 Hz uniaxial loadings at strain amplitudes between 10^{-3} and 10^{-6} . At high strain amplitudes the hysteresis loops were cusped, a feature indicative of nonlinear attenuation, and which is probably due to a frictional attenuation mechanism. Attenuation factors are similar to those calculated from ultrasonic spectral

ratio measurements, but much higher than those measured with the resonant bar technique. For Cedar City quartz diorite, preliminary results indicate a transition from cusped to elliptical loops below 10^{-5} strain and a corresponding dramatic decrease in attenuation.

EXPERIMENTAL PROCEDURES

Hysteresis loop measurements were made on a precisely ground cylinder of Sierra White granite 0.0254 meters in diameter and 0.0508 meters long. The sample was instrumented with two 0.0127 meter axial strain gages and placed in series with a precision load cell in a hydraulic servo-controlled loading frame. The sample was exposed to the atmosphere at room temperature and preloaded to 0.1 MPa axial stress. A 0.1 Hz sinusoidal axial force was applied to the sample end with the servo-controller operating in a force-feedback mode. Axial force and strain data were recorded for about 20 repeatable cycles with a PC-based A/D converter. Measurements were made at 9 different strain amplitudes between 10^{-5} and 10^{-3} strain by varying the voltage of the sinusoidal signal driving the axial ram. The cycle minima were near zero stress and strain. Axial strain was averaged between the two strain gages and axial stress was calculated from the measured load and sample diameter.

The procedure for measurements on Cedar City quartz diorite were similar to those described above except that the sample size was 0.152 m in diameter by 0.286 m long. The larger sample size allowed for greater resolution of force and strain. Axial and radial displacements were measured with LVDT's mounted on rings encircling the sample. Axial force was generated from an amplified D/A sinusoidal voltage and up to 1000 cycles were averaged at the lower strain amplitudes.

The fractional energy loss per cycle was calculated from the stress-strain data by dividing the area enclosed within the hysteresis loop, which is the energy dissipated during one cycle, by the integrated area beneath the loading section of the cycle, which is the energy introduced into the rock volume. The ratio, divided by two times pi, is the attenuation factor, or Q^{-1} . For comparison, attenuation factors were also calculated from the phase angle between stress and strain taken from phase spectra for the respective signals.

RESULTS AND DISCUSSION

Table 1 contains the results of attenuation measurements from observations of hysteresis loops in Sierra White granite. Across the table are the maximum strain amplitude and stress of the hysteresis loop, the average Young's modulus, and the attenuation factor expressed as $1000/Q$. Since the stress-strain relationship is nonlinear the Young's modulus calculations are averages. Results are tabulated for successively larger strain amplitudes and loads, up to the maximum, about 28 MPa load and 780 microstrain. The errors in the hysteresis loop measurements are quite small except at low attenuations for Cedar City quartz diorite. Load and strain were observed to within 1%, the integration of the hysteresis loop is accurate to within 0.5%, and the precision of these measurements is approximately 1%.

Figure 1 shows the hysteresis loop for Sierra White granite recorded at the maximum strain amplitude. The nonlinearity is evident in the nonellipticity of the loop and the cusped ends. Since the cycling was sinusoidal, this feature indicates that attenuation was nonlinear. In contrast to the Sierra White granite data, preliminary results for the Cedar City quartz diorite sample indicate that the transition from nonlinear to linear attenuation was bridged at low strain amplitudes. In Figure 2 a selection of hysteresis loops are shown from high to low strain amplitudes (left to right, top and bottom). The shrinking size of the loop is easily seen, and there is a transition from cusped loops to elliptical loops at the lower strain amplitudes (although not easily discernable in these plots). The attenuation factors decrease dramatically at the low strain amplitudes (Q 's increase to around 500).

Figure 3 contains a summary of resonant bar, hysteresis loop, and ultrasonic extensional attenuation factors for Sierra White granite plotted as a function of log strain amplitude. In addition, the preliminary Cedar City data are plotted with x's. Hysteresis loop attenuation at high strain amplitudes is of the same magnitude as for the ultrasonic pulse (Q 's from 30 to 40). Resonant bar attenuation at 10-40 kHz is constant as a function of frequency and strain amplitude and corresponds to a Q factor of around 130.

The truly interesting feature of Figure 3 is the decrease of hysteresis loop attenuation in the direction of lower strain amplitude. This is evident for both Sierra White granite and, particularly, for the Cedar City data. Quality factors (inverse

attenuation) increase from approximately 35 to 500 between strain amplitudes from 8×10^{-4} to 3×10^{-6} , and then apparently remain constant at lower strain amplitudes. This defines the threshold from a nonlinear to linear attenuation mechanism, accompanied by a transition of hysteresis loop shape from cusped to elliptical. Although the ultrasonic pulse data indicate a higher threshold, around 1×10^{-5} , the ultrasonic pulse strain amplitudes were calculated from the voltage amplitude placed across the source crystals and represent maximums.

The threshold and portions of the strain amplitude dependence have been previously observed (Gordon and Davis, 1968; Brennan and Stacey, 1977; Winkler et al., 1979; Johnston and Toksoz, 1980; Stewart et al., 1983; Tittmann, 1984), but remain largely unexplored in terms of functional shape and pressure, saturation, and lithological dependence. The presence of microcracks or pore geometry influences the strain amplitude dependence, and nonlinearity is consistent with frictional models of attenuation (Walsh, 1966; Mavko, 1979; Stewart et al., 1983). Hence, at strains above approximately 1×10^{-6} , the increase in attenuation can be interpreted as frictional loss at grain and crack surfaces in contact.

In Figure 4 the results of these attenuation experiments and others are plotted as a function of log frequency from 100 Hz to 1 MHz. The data along the axis at the left, identified by dashed lines, indicate lower frequencies offscale. Other hysteresis loop measurements are by Gordon and Davis (1968), Walsh et al. (1970), Spencer (1981), and Liu and Peselnick (1983). The lowest attenuation factors are from the low strain amplitude ($<10^{-6}$), low frequency, direct stress-strain measurements. Some of the highest attenuation factors are from similar experiments at high strain amplitude and ultrasonic attenuation measurements. For room dry rocks, at low strain amplitude, there appears to be a monotonic increase in attenuation with frequency, although three different experimental techniques were used. At low strain amplitudes and seismic frequencies there is a reasonable indication that hysteresis loop attenuation measurements for room dry and vacuum dry intact rocks will consistently result in high Q values.

CONCLUSIONS

A comparison of the three different experimental techniques applied to room dry Sierra White granite and Cedar City quartz

diorite indicates the importance of frequency and strain amplitude. At low strain amplitudes, within the linear regime of attenuation, attenuation increases with frequency for room dry rock with a Q factor of about 500 at 0.1 Hz from the hysteresis loops, 130 at 10-40 kHz from the resonant bar, to 40 at 100-1000 kHz from ultrasonic spectral ratios. An extrapolation of ultrasonic results to lower frequencies and resonant bar results to higher frequencies indicates that ultrasonic pulse attenuation will probably be higher than resonant bar at the same frequency. The threshold of linear to nonlinear attenuation is between 1×10^{-6} and 1×10^{-5} strain, and is clearly evident in the behavior of hysteresis loops. Strain amplitude dependence is probably due to frictional attenuation. Finally, at low strain amplitudes ($<10^{-6}$) and frequencies below 40 kHz the available experimental evidence indicates that attenuation factors (1000/Q) in room dry intact granite are lower than 10.

REFERENCES

Brennan, B.J., and F.D. Stacey, Frequency dependence of elasticity of rock-test of seismic velocity dispersion, Nature, 268, 220-222, 1977.

Brennan, B.J., Linear viscoelastic behavior in rocks, in Anelasticity in the Earth, Geodyn. Ser., vol. 4, edited by F.D. Stacey, M.S. Paterson, and A. Nicolas, pp. 13-22, AGU, Washington, D.C., 1981.

Coyner, K.B., 1987, Attenuation measurements on dry Sierra White granite, dome salt, and Berea sandstone, final report to Lawrence Livermore National Laboratory, Contract #9092405.

Gordon, R.B., and L.A. Davis, Velocity and attenuation of seismic waves in imperfectly elastic rock, J. Geophys. Res., 73, 3917-3935, 1968.

Liu, H.-P., and L. Peselnick, Investigation of internal friction in fused quartz, steel, plexiglass, and Westerly granite from 0.01 to 1.00 Hertz at 10^{-8} to 10^{-7} strain amplitude, J. Geophys. Res., 88, 2367-2379, 1983.

Mavko, G.M., Frictional attenuation: An inherent amplitude dependence, J. Geophys. Res., 84, 4769-4775, 1979.

Spencer, J.W., Stress relaxations at low frequencies in fluid-saturated rocks: Attenuation and modulus dispersion, J. Geophys. Res., 86, 1803-1812, 1981.

Stewart, R.R., M.N. Toksoz, and A. Timur, Strain dependent attenuation: Observations and a proposed mechanism, J. Geophys. Res., 88, 546-554, 1983.

Tittmann, B.R., Nonlinear wave propagation study, semi-annual technical report No. 2 for the period December 1, 1983 through May 31, 1984, SC5361.6SAR, Rockwell International Science Center, 1984.

Walsh, J.B., Seismic wave attenuation in rock due to friction, J. Geophys. Res., 71, 2591-2599, 1966.

Walsh, J.B., W.F. Brace, and W.R. Wawersik, Attenuation of stress waves in Cedar City quartz diorite, Technical Report No. AFWL-TR-70-8, M.I.T., 1970.

Winkler, K.W., A. Nur, and M. Gladwin, Friction and seismic attenuation in rocks, Nature, 277, 528-531, 1979.

TABLE 1. Maximum strain amplitude, maximum load, Young's modulus, and attenuation calculated from the hysteresis loops of a Sierra White granite sample sinusoidally loaded at 0.1 Hz.

STRAIN AMPLITUDE (microstrain)	LOAD (MPa)	YOUNG'S MODULUS (* 1.e+05 MPa)	ATTENUATION (1000/Q)
17	0.55	0.032	20.2
30	0.95	0.032	21.0
77	2.30	0.030	23.4
140	4.20	0.030	24.2
220	6.80	0.031	26.6
350	11.0	0.031	27.5
480	16.0	0.033	28.3
610	21.0	0.034	27.8
780	28.0	0.036	28.1

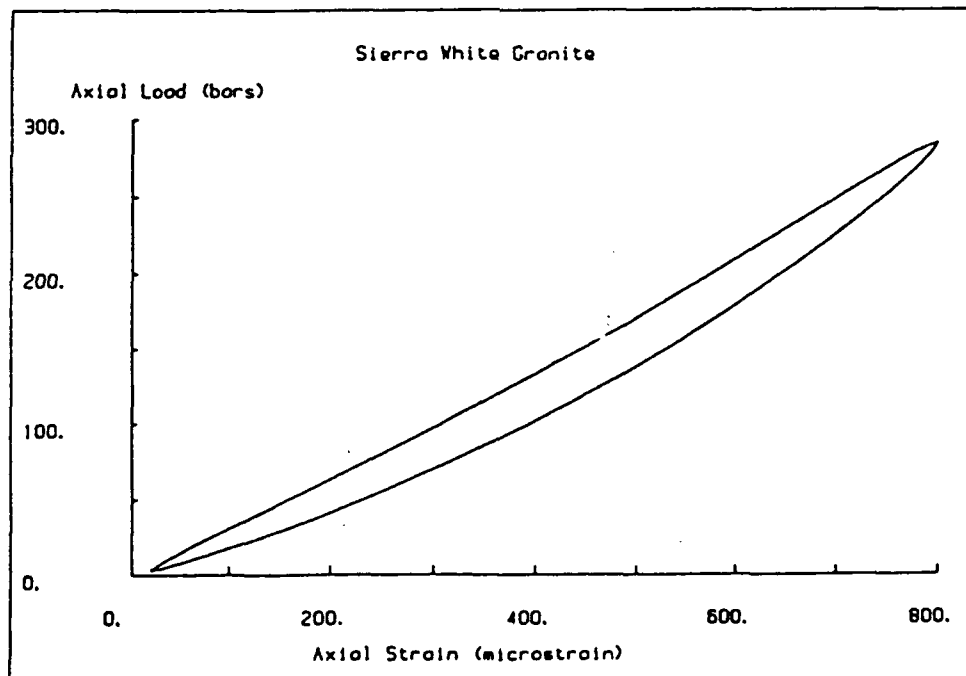


Figure 1. A stress-strain hysteresis loop measured on a 0.0508 meter long sample of Sierra White granite. The maximum strain amplitude and load are 780 microstrain and 28 MPa. The calculated attenuation factor (1000/Q) was 28.1 (Q=36).

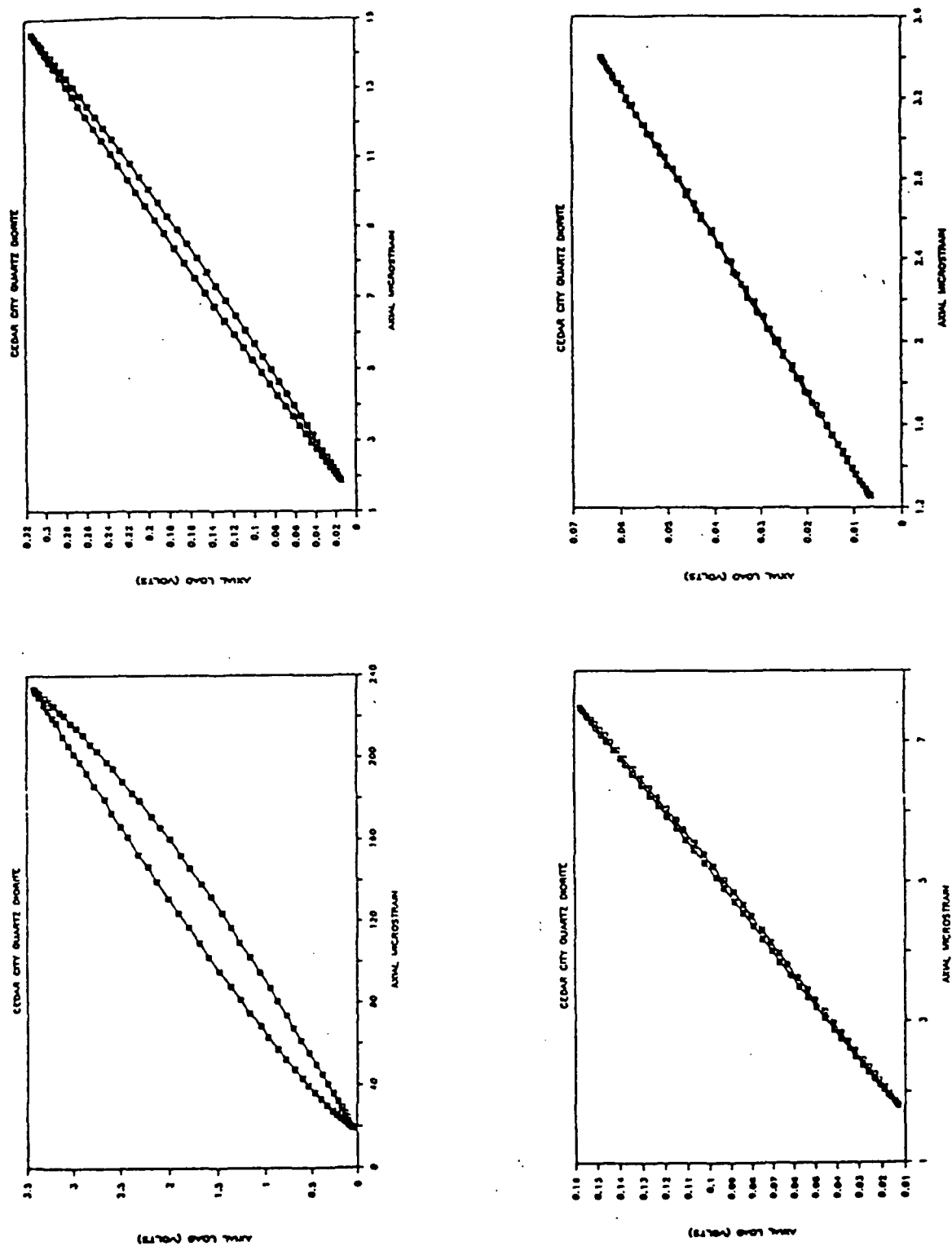


Figure 2. Hysteresis loops for Cedar City quartz diorite as a function of strain amplitude. Highest strain amplitude (215 microstrain) is in the upper left; lowest strain (1.43 microstrain) in the lower right.

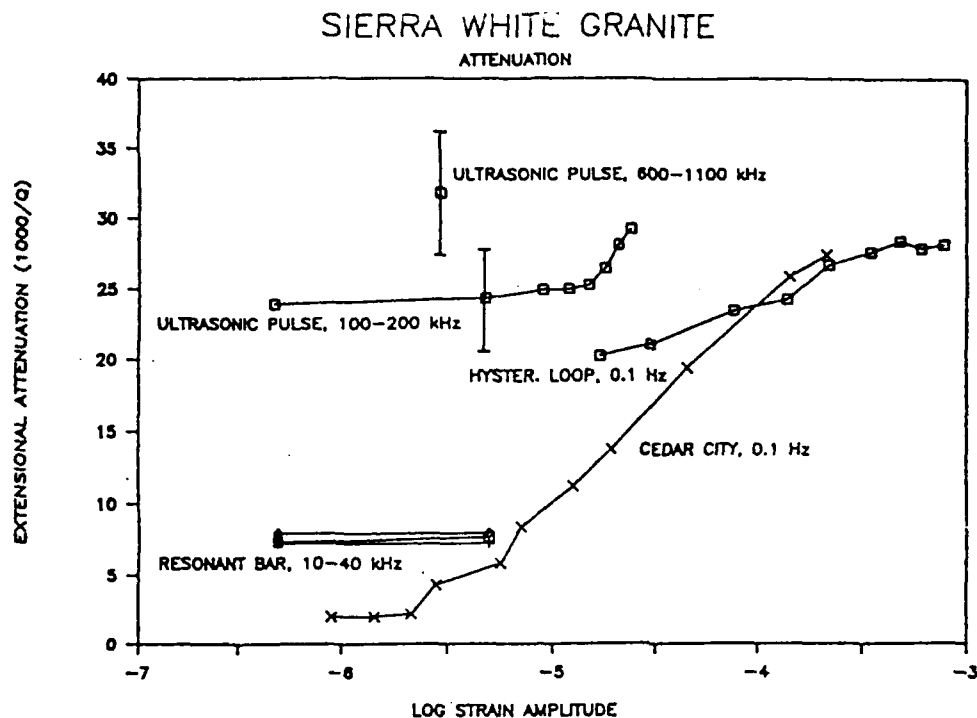


Figure 3. Summary plot of extensional attenuation factors versus log strain amplitude for room dry Sierra White granite.

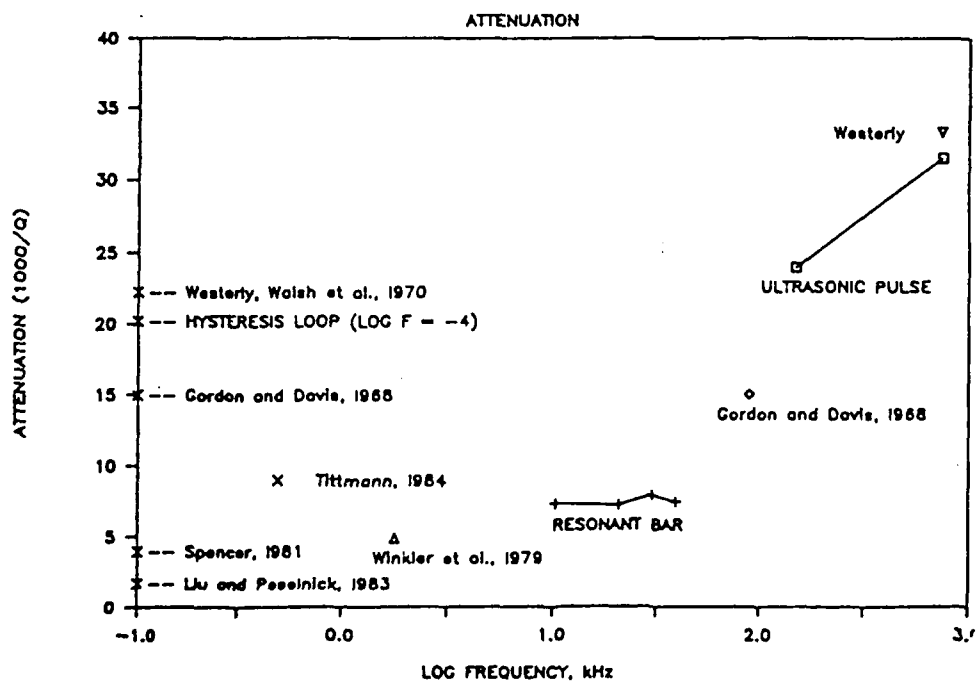
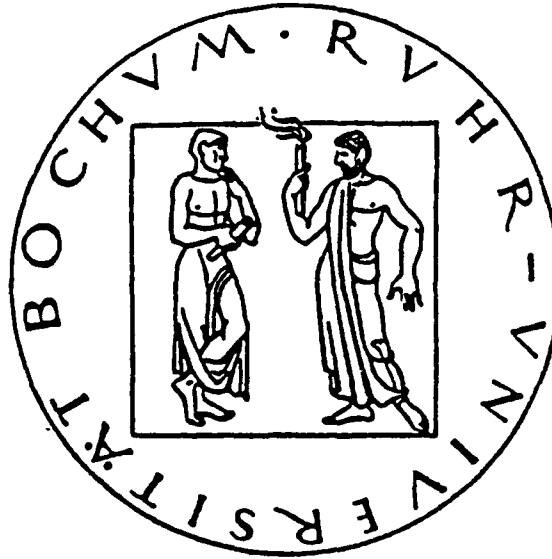


Figure 4. Summary plot of attenuation factors versus log frequency (kHz) for Sierra White granite together with other sources of attenuation data for dry granite at low pressures.



Pattern Recognition for Earthquake Detection

*Manfred Joswig, Institute of Geophysics, Ruhr-University Bochum
D 4630 Bochum, F.R.Germany*

I. Introduction

For more than 25 years automatic detection of earthquakes in environmental noise has been the goal of research efforts. Originally motivated by the large amount of on-line data provided by seismic arrays and regional networks, standard detectors like STA/LTA are currently well known in all fields of geophysical data acquisition.

Despite improvements in detail, automatic processing in seismology is usually limited to the low level task of data collection. The simple *Expert Systems* or *Knowledge Based Systems* of today are the beginning of a new era in the short history of automatic data processing. The formal techniques of Artificial Intelligence research, i.e. the inference machine, probabilistic reasoning and knowledge bases, promise to improve the performance of automated seismological processing systems. Eventually such systems will supplant the seismologist at the routine work. In addition to the details of knowledge representation and reasoning within the expert system one important problem must be solved before these techniques can successfully be applied to earthquake detection:

How should the seismic data be preprocessed for the expert system ?

or from the human point of view:

What are our initial impressions, where all reasoning starts off ?

For the application of expert systems in seismology there are 3 possible preprocessing methods:

- The initial parameters like phase onset times, quality of picking, amplitudes and obvious anomalies are extracted by the human observer. The expert system then acts more like a seismological assistant rather than an independent automatic system.
- We use one of the traditional detector approaches. They all describe the stationary noise level by some kind of median and deviation, which in turn determines the detection threshold [1],[2],[3] (table 1).

Each pulse with energy above this threshold will trigger a detection. The main disadvantage of these detectors is their high false alarm rate. They are not able to distinguish between small earthquakes and instationary noise with the same or even higher amplitude. They inherently follow negative logic:

The defined state is the *non-detection*, every change must be assumed to be caused by an earthquake, since it is indistinctable from a noise burst.

The consequence was to include a separate block of *postdetection* in the detector design, to reduce the false alarm rate [4].

In our application expert systems turn out to be sophisticated post-detectors for the rejection of unwanted noise detections most of the time.

- The third method uses the techniques of knowledge based reasoning for preprocessing to detect and extract waveform parameters. The general approach is that of pattern recognition which implements a decision logic of positive kind:

The defined states are wanted (earthquakes) or unwanted (temporary noise) signals, only a sufficient similarity with one of these patterns will trigger a detection.

The identified pattern and phase picking of onset times are the input for further reasoning in the expert system.

II. Pattern Recognition

Reflection on human thinking led philosophy to state that there are two main ways of reacting to environmental situations [5]:

- Thinking as a kind of internal talking or *mental discurs*. This linguistic approach is mainly used for knowledge reasoning in theses and inferences (*'knowing that'*).
- Thinking as a kind of internal vision in *mental pictures*. This visual approach dominates knowledge acquisition and knowledge application (*'knowing how'*).

In Artificial Intelligence the linguistic approach is adequate for expert systems, while pattern recognition is an example for the visual approach.

Since earthquake detection and parameter extraction is usually accomplished through pattern recognition, it is reasonable to use some pictorial representation of the seismograms rather a syntactic pattern representation [6], which is too close to the linguistic way of problem treatment.

But Computer Vision in its original application is also not applicable. The definition of selected seismograms as knowledge patterns is equivalent to a *matched filter* design. This approach must fail because of the variety of individual seismograms, which are hard to predict or even to catalogue.

Nevertheless the human observer is able to detect and distinguish typical and simple forms of earthquakes even in high and varying noise. To copy this behaviour in AI, mental pictures are postulated as the key processing step between sensed impressions and the knowledge based identification [7]. The main goal of these pictures is simplification of the recognition problem by robust parameter extraction and signal to noise enhancement. According to neurophysiological principles the resulting mental picture will be highly nonlinearly scaled.

For earthquake detection these mental pictures by convenience are based on any representation of spectral energy versus time. This can be a sonogram for one component stations, a vespagram or ω -k filter for arrays or an eigenvalue representation of the polarisation matrix for three component stations.

So the general pattern recognition detector consists of:

- The transformation of seismograms into mental pictures
(for the SONOGRAM-Detector see fig. 1)
- The knowledge base of typical earthquakes and noise bursts as a set of mental pictures
- The pattern recognition process for mental pictures as the inference machine of the detector (fig. 2)

- The optional definition of some numerical similarity measure between mental pictures. This will speed up the consistency check of the knowledge base for the interactive pattern acquisition and is a prerequisite for a later detector version with automatic pattern creation.

The pattern recognition process for mental pictures may be any algorithm, that is applicable to pattern recognition problems of 'optical' pictures like photo or tv.

III. SONOGRAM-Detector

The general principle of the pattern recognition detector was first realized for the detection of local earthquakes on single traces. The mental pictures are nonlinearly scaled sonograms, i.e. spectral energy versus time.

Although designed for on-line processing and of special advantage in seismic networks with loosely coupled remote stations like the BOCHUM UNIVERSITY GERMANY network [8], the first tests were performed off-line as a postdetector behind the WALSH-detector [9]. The results for 25 days on-line detection of the WALSH-algorithm agree in number of missed events (half of them missed by network downtime), false alarm rate and inaccurate phase picking with those of other reported applications, when the high cultural noise level of the BUG-network is taken into account (table 2).

The preselected data set for postdetection consists of 2 minute time windows, 109 of them earthquakes and 124 noise bursts. Except for a few very small earthquakes they are representative of the seismicity in our network.

The knowledge base of mental pictures for the SONOGRAM-detector included only five event-types, distinguished by epicentral distance (fig. 3). The edge conversion (crossed) requires *no* energy around the earthquake (striped) for signal to noise enhancement of the pattern fit (fig. 2). The detection depends on the whole seismogram of an earthquake instead of the single phase picking of traditional detectors.

The results of the detection run (table 3) show a better detection rate, an extremely low false alarm rate and better timing accuracy than those of the WALSH-detector. All missed events have a maximal amplitude of less than 6 dB above noise.

In contrast to other detector principles pattern recognition detectors can be improved by updating the knowledge base rather than changing the algorithm.

- The definition of noise patterns allows a lower detection threshold without false alarm increase, since only the most similar pattern is picked (i.e. a recognized noise pattern inhibits detection).
- A comparison of the identified pattern type with the epicentral distance determined by using the whole network still shows significant uncertainty (table 4). This is due to azimuthal differences in the events neglected in the initial set of patterns. A detailed analysis has shown that inaccuracies in both the determination of distance and onset time are associated with earthquakes from selected azimuths.

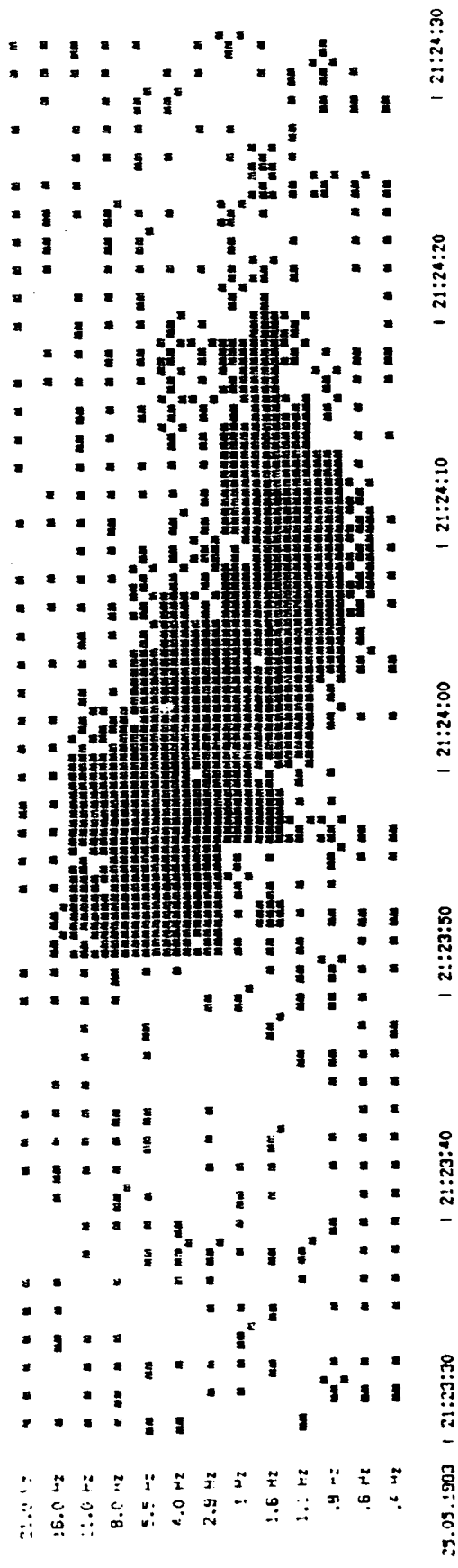
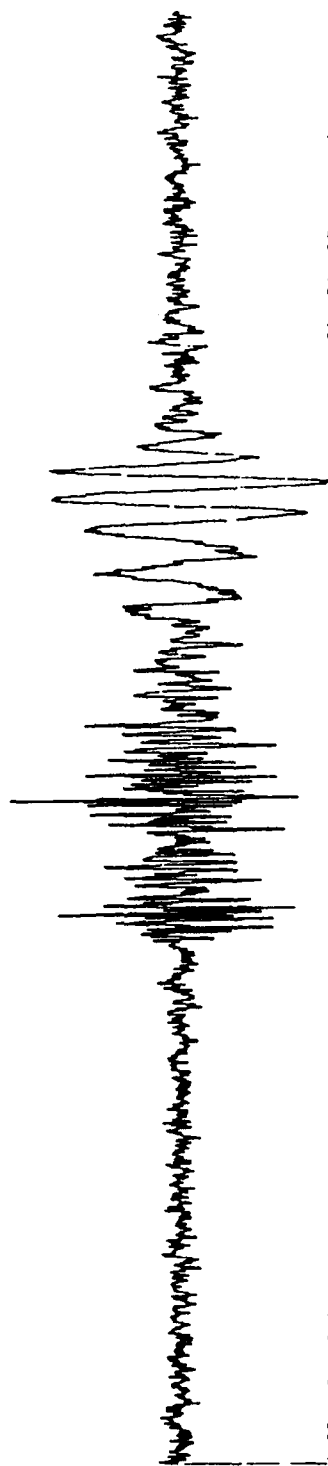
Thus detector performance depends crucially on the definition of an appropriate knowledge base. Starting with a rough estimate, further refinement promises detector performance equal to that of a skilled human observer. Besides the onset time the SONOGRAM-detector delivers the additional information of identified pattern type and quality of fit. Its detection reports are therefore a competent base for the further automatic event processing by an expert system.

- [1] Freiberger, W. F., "An Approximate Method in Signal Detection", *Quarterly App. Math.*, vol. 20, pp. 373-378, 1963
- [2] Blandford, Robert R., "Seismic Event Discrimination", *Bull. Seism. Soc. Am.*, vol. 72, pp. S69-S87, 1982
- [3] Joswig, Manfred, "Methoden zur automatischen Erfassung und Auswertung von Erdbeben in seismischen Netzen und ihre Realisierung bei Aufbau des lokalen 'BOCHUM UNIVERSITY GERMANY'-Netzes", Dissertation, Ruhr-Universität Bochum, 1987
- [4] Allen, Rex, "Automatic Phase Pickers: Their Present Use and Future Prospects", *Bull. Seism. Soc. Am.*, vol. 72, pp. S225-S242, 1982
- [5] Haugeland, J., *Artificial Intelligence: The Very Idea*, MIT Press, Cambridge Mass., 1985
- [6] Liu, Hsi-Ho and King-Sun Fu, "An Application of Syntactic Pattern Recognition to Seismic Discrimination", *IEEE Trans. Geosc. Rem. Sens.*, vol. GE-21, pp. 125-132, 1983
- [7] Joswig, Manfred, "Pattern Recognition Detector and Remote Station Dialog in a Local Seismic Network", *AGU-Fall Meeting*, San Francisco 1985
- [8] Joswig, Manfred and Hans-Peter Harjes, "A Seismic Network with Loosely Coupled Remote Stations", *ESC-Proceedings, Kiel 1986*, ed. D. Mayer-Rosa, J.M. Van Gils, H. Stiller, Zürich 1987
- [9] Goforth, Tom and Eugene Herrin, "An Automatic Seismic Signal Detection Algorithm Based on the Walsh Transform", *Bull. Seism. Soc. Am.*, vol. 71, pp. 1351-1360, 1981

	processing of seismogram			statistics of seismic noise		decision	postdetection
	filter $x \rightarrow y$	characteristic function	energy during length of signal	median	deviation		
Freiberger	$\sqrt{\frac{S}{N(S+N)}}$		$STA = \frac{1}{n} \sum_{i=1}^n y_i^2$			$STA > \beta$	
STA/LTA	$\frac{BP}{\sqrt{N}}$		$STA = \frac{1}{n} \sum_{i=1}^n y_i $	$LTA_i = \alpha STA_i + (1-\alpha) LTA_{i-1}$		$STA > \beta LTA$	window
Z-Detector	BP		$STA = \frac{1}{n} \sum_{i=1}^n y_i^2$	$LTA_i = \alpha STA_i + (1-\alpha) LTA_{i-1}$	$\sigma_i^2 = \alpha (STA_i - LTA_i)^2 + (1-\alpha) \sigma_{i-1}^2$	$STA > LTA + \beta \sigma$	3 windows
Walsh	$\frac{BP}{\sqrt{N}}$		$M = \sum_{Seq} Y_S $	M_{50}	$V = M_{75} - M_{50}$	$M > M_{50} + \beta V$	window
Allen		$CF = x^2 + \gamma x^2$	$STA_i = \delta CF_i + (1-\delta) STA_{i-1}$	$LTA_i = \alpha STA_i + (1-\alpha) LTA_{i-1}$		$STA > \beta LTA$	analysis of min-max-fct. by adaptive window
SRO	BP	$PT = \Delta ptf(y) $			$s' \approx 2 \sigma(PT)$	$PT > \beta s'$	window
ARMA	BP	$d = \ \hat{\Theta}_i - \hat{\Theta}_{i-1}\ ^2$				$d > d_{99.5}^*$	

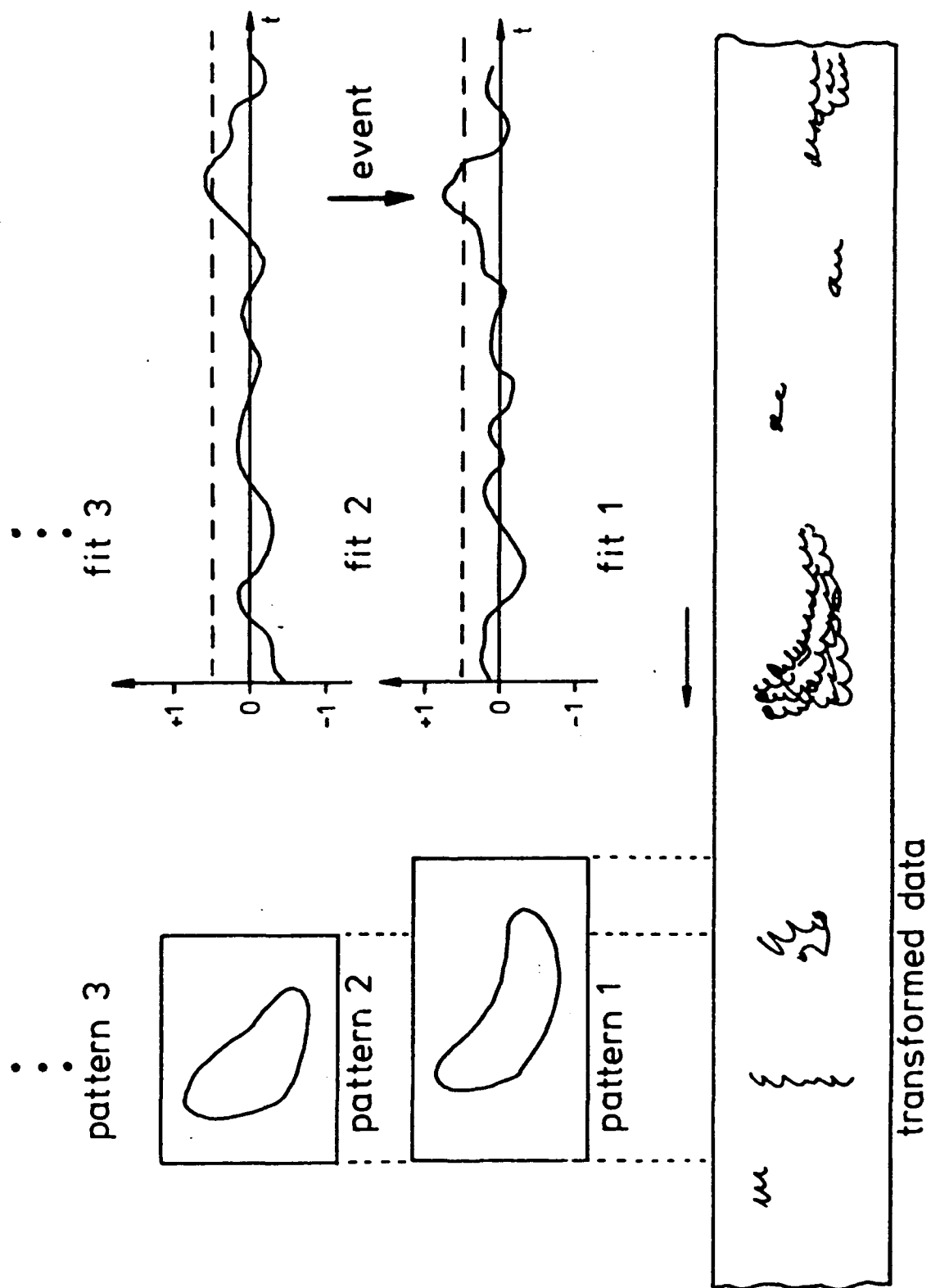
* as off-line phase-picker (at least 1 detection in 10^4 samples)

table 1: Elements of Single Trace Detectors



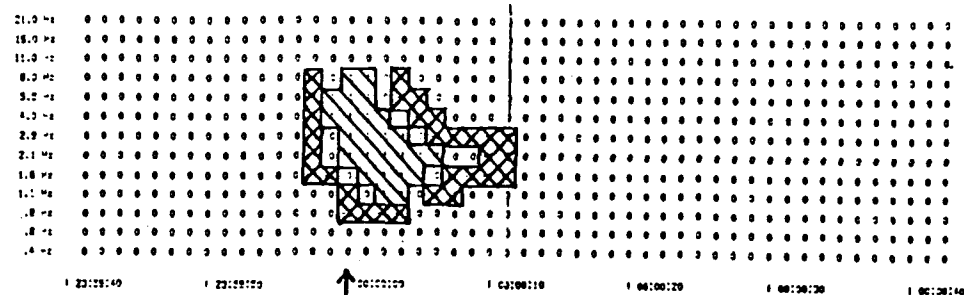
(Normalisierungsfaktor: .11E-03 Skalierung: lin dargestellte Intensitätslevel: 0-9 Pre-whitenig: ein max Noise-level (= 4)

fig. 1



Pattern Recognition and Decision Process

fig. 2

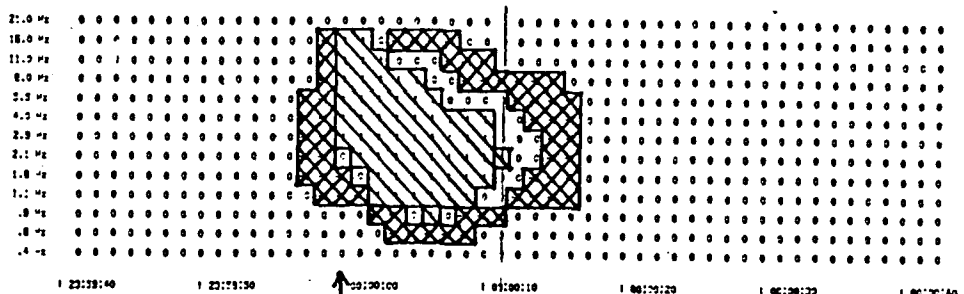


Maske 9km

$$\sum |m_{ij}| = 55$$

$$\sum m_{ij} = -5$$

$$\text{level}_{\text{fit}} = 0.5$$

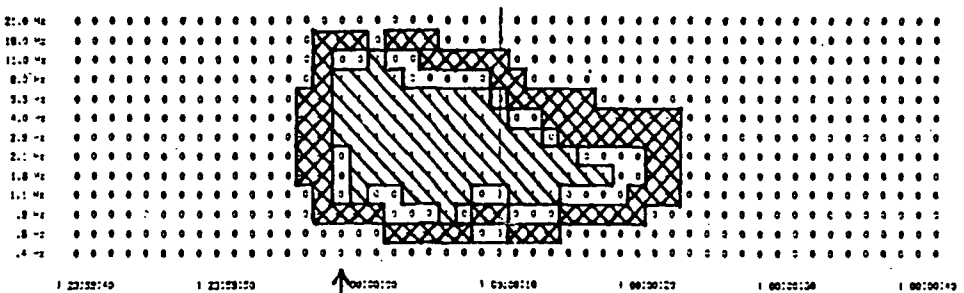


Maske 12km

$$\sum |m_{ij}| = 115$$

$$\sum m_{ij} = -1$$

$$\text{level}_{\text{fit}} = 0.45$$

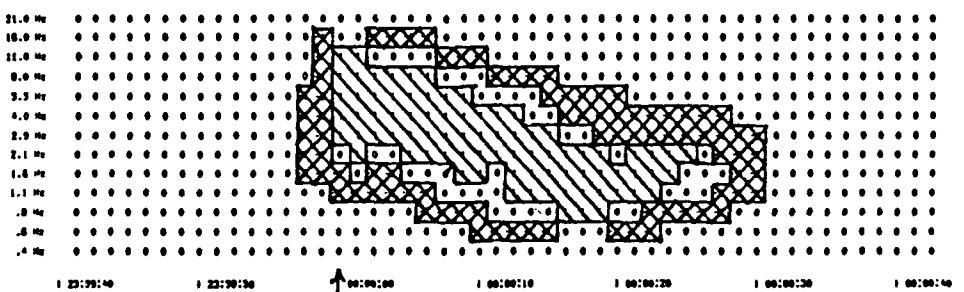


Maske 18km

$$\sum |m_{ij}| = 145$$

$$\sum m_{ij} = -2$$

$$\text{level}_{\text{fit}} = 0.45$$

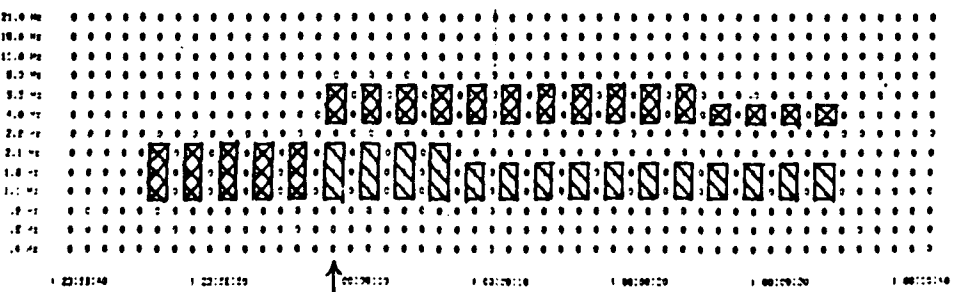


Maske 35km

$$\sum |m_{ij}| = 164$$

$$\sum m_{ij} = -2$$

$$\text{level}_{\text{fit}} = 0.45$$



Maske
Telesism. Einsat

$$\sum |m_{ij}| = 75$$

$$\sum m_{ij} = -7$$

$$\text{level}_{\text{fit}} = 0.4$$

fig. 3

162 events	118 e. detected	28 with ± 1 sec
		14 more with ± 2 sec
		27 more with ± 4 sec
		49 more with ± 8 sec
	44 events missed	
25 days with noise	125 false alarms	

table 2: Performance of the WALSH-Detector

109 seismograms with events	105 e. detected	68 with ± 1 sec
		14 more with ± 2 sec
		5 more with ± 4 sec
		18 more with ± 8 sec
	4 events missed	
124 seismograms with false alarms of WALSH-Detector	118 noise bursts rejected	
	6 false alarms	

table 3: Performance of the SONOGRAM-Detector

pattern distance	9 km	12 km	18 km	35 km	teleseis
0-10 km	1				
11-14 km	2	3	1		
15-25 km	2	3	3		
26-50 km		1	6	7	1
50-100 km					
100-1000 km					
>1000 km					13

table 4: **BUG-Patterns and Epicentral Distance**

Nonlinear Constitutive Relations at Moderate Strain - 10^{-3} to 10^{-6} in Salt

G. D. McCartor and W. R. Wortman, MRC

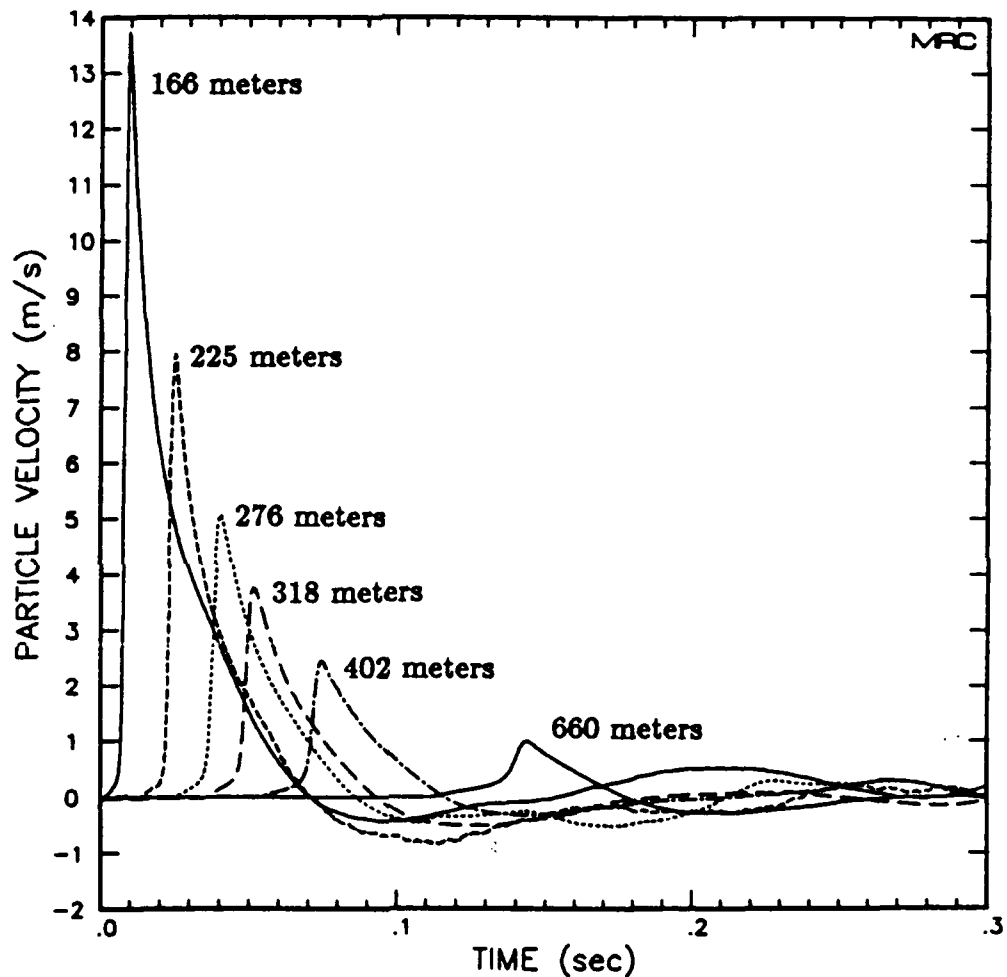
ABSTRACT

Nonlinear constitutive relations are being developed for the mildly nonlinear attenuation in the moderate strain regime (scaled ranges of 10^3 m/kt^{1/3} to 10^4 m/kt^{1/3}) for explosively generated seismic pulses. The relations are to determine the shape and amplitude of seismic pulses in the linear low strain regime (beyond 10^4 m/kt^{1/3}) to serve as source functions for regional or teleseismic propagation. Experimental data provide restrictions on candidate constitutive relations. Attenuation in salt from Salmon, Cowboy, Livermore and Rockwell are fairly consistent internally. The first two provide a detailed indication of the change of amplitude and shape of explosively driven pulses. Proposed constitutive relations must reproduce these data. The data from the wide range of yields in salt indicate that yield^{1/3} scaling applies with a remarkable precision; if all times and distances are scaled by yield^{1/3}, the scaled amplitudes and shapes of pulses from all experiments are nearly the same. Thus the initial pulse on entering the moderate strain regime must scale at some small scaled range and the subsequent attenuation must result from constitutive relations which have no scales. This provides a significant reduction in the domain of allowable nonlinear behavior. In order to investigate nonlinear constitutive relations, a standard numerical time stepping method is used. Pulses are propagated using, as a source, the observed Salmon initial velocity pulse at small ranges. The results are compared with observed signals at larger ranges. The Salmon data have a feature which may be a clue to understanding some nonlinear effects of the attenuation. Each of the pulses from 166 meters to 660 meters exhibit a discontinuity in the slope upon the initial steep rise in pulse velocity. This appears as a toe-like precursor behavior in the leading edge of the velocity profile. The absolute amplitude of the toe remains nearly constant with range while its amplitude relative to the peak increases with range. The leading edges of the pulses propagate at a speed of 4.7 km/sec while the pulse peaks, always after the toe, propagate at a speed of 3.7 km/sec. The toe amplitude corresponds to a constant strain level, $\epsilon = 10^{-4}$. This suggests a model for the material behavior for which the elastic modulus decreases permanently upon having a critical ϵ exceeded. The modulus before and after exceeding the critical ϵ reflect the compressional speeds at the beginning and peak of the Salmon pulses. Initial work suggests that the precursor is reproduced rather well with this hypothesis. However, the overall attenuation produced is not adequate to account for that seen in the data.

#1

SALMON DATA

Salmon was a 5.3 kT nuclear test in a salt dome which was well instrumented for free field motion for ranges of 100 to 1000 meters.



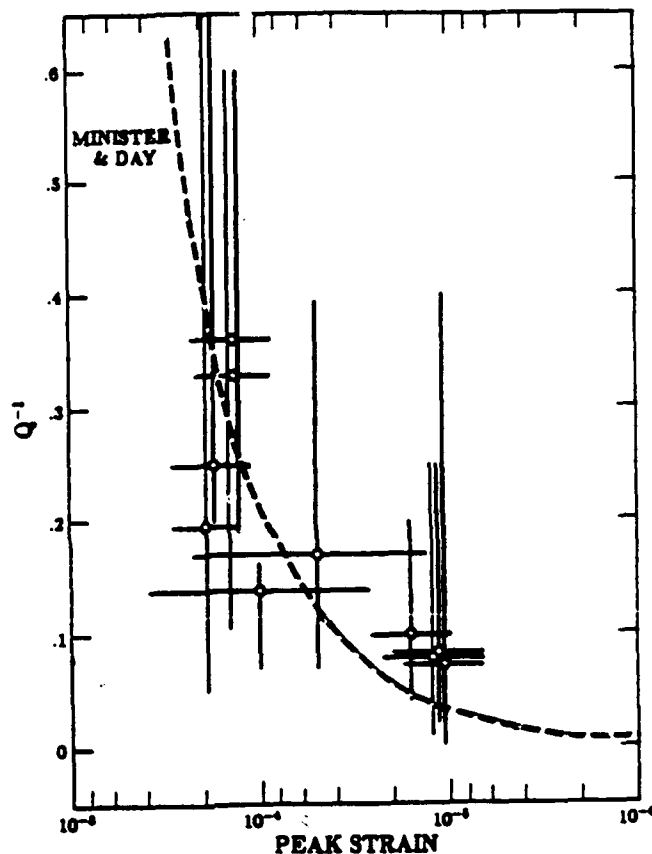
- Effective $Q \approx 5$ Approximately constant for
- Strains of $4 \times 10^{-3} > \epsilon > 3 \times 10^{-4}$

The Salmon data indicate a large degree of attenuation for explosively driven pulses in salt at moderate strains. Within these data alone there is not strong evidence for nonlinear effects. However, in the context of a larger array of salt data, it appears that the effective Q must be strain dependent.

#2

COWBOY DATA

Cowboy was a series of smaller scale, 100 to 2000 pounds, chemical explosions in a salt dome. Each shot was instrumented by several free field motion sensors. Taking data records in pairs, effective Q estimates can be made and the dependence on strains estimated.



Circles with Error Bars Give Q Estimates from Pairs

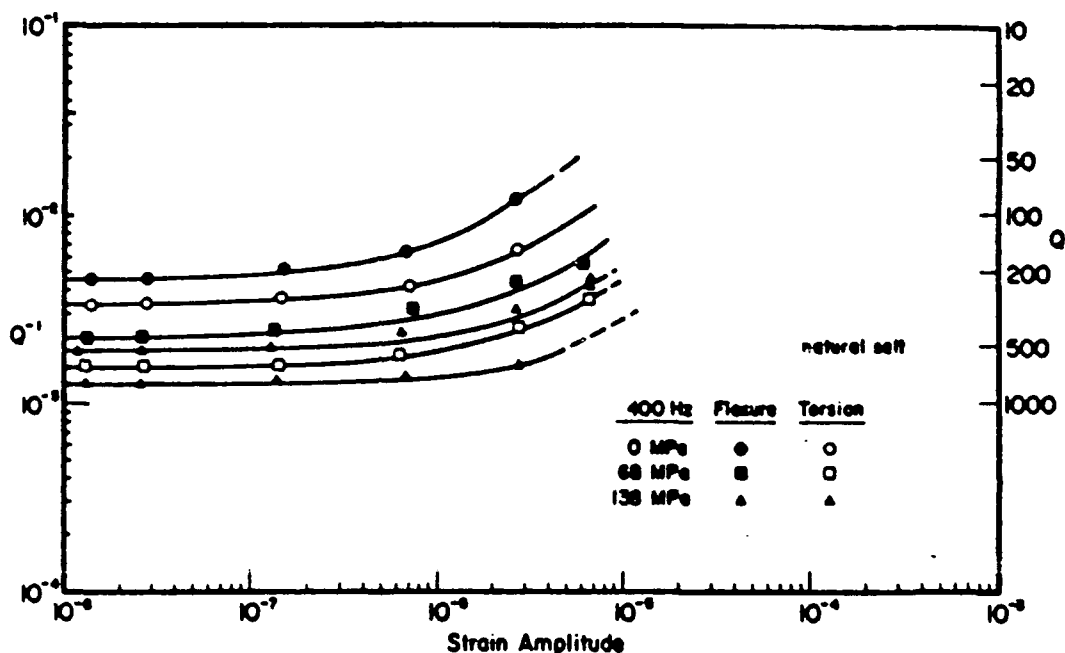
Dashed Line Minster and Day Fit by Strain Dependent Q for Data as Whole

- Effective Q Distinctly Strain Dependent for
- Strains for Useful Pairs $2 \times 10^{-4} > \epsilon > 10^{-5}$

Attenuation at larger strains, which are comparable with those in Salmon, are similar to the Salmon results. Attenuation diminishes quickly for strains approaching 10^{-5} . Minster and Day used a fit with Q^{-1} as a constant plus a term linear in strain which was consistent with the data from Rockwell.

ROCKWELL SALT DATA

Attenuation in salt samples has been estimated at Rockwell by observing the damped harmonic oscillations at about 400 Hz, in both flexure and torsion. For strains less than about 10^{-6} , Q is approximately constant for confining pressures of interest. Attenuation increases noticeably as the peak strain increases.



The Rockwell experiments suggest that the behavior at small strains may be described by

- $Q \approx 200$ for Small Strains
- Attenuation Increases for $\epsilon > 10^{-6}$

Thus, the combination of Salmon, Cowboy and Rockwell data for salt span a strain range from 4×10^{-3} to less than 10^{-7} . The trends are for a $Q \approx 5$ and not changing too rapidly for larger strains, Q increasing substantially near 10^{-4} , and Q stabilizing at a few hundred for small strains.

- THIS CLEARLY REQUIRES A NONLINEAR CHARACTERIZATION OF ATTENUATION BUT DOES NOT DIRECTLY SUGGEST A PHYSICAL MECHANISM OR RHEOLOGY.

SCALING OF SALT DATA

Data from the above explosive tests as well as from smaller scale at LLL can be combined to yield a remarkable result. This is that the peak particle velocities in the pulses are compared at the same scaled range, physical range/(yield)^{1/3}, it is found that all the data lie nearly on the same curve. More generally, if any other dynamic variables such as displacement are scaled in time using scaled time, physical yield/(yield)^{1/3}, the waveforms all tend to follow a universal form independent of the yield. This simple scaling with yield does not depend upon linear behavior of the medium since it applies in the moderate strain regime which appears nonlinear.

- Simple Scaling Indicates that Medium Cannot Have Any Inherent Time or Length Scales or
- The Constitutive Relation Describing the Medium Can Depend on the Strain but Not on the Strain Rate
- The Initial Pulse Upon Entering the Moderate Strain Region Must Scale

NEED FOR NONLINEAR CONSTITUTIVE RELATION

It appears that the moderate strain regime, which in scaled range extends from about one hundred meters/ $kt^{1/3}$ to several thousand meters/ $kt^{1/3}$, may provide attenuation which is different in both magnitude and character from the linear attenuation at seismic ranges. Yet source functions are often defined inside this region with the assumption that the attenuation which follows is strictly linear. This may lead to errors in estimates in yield.

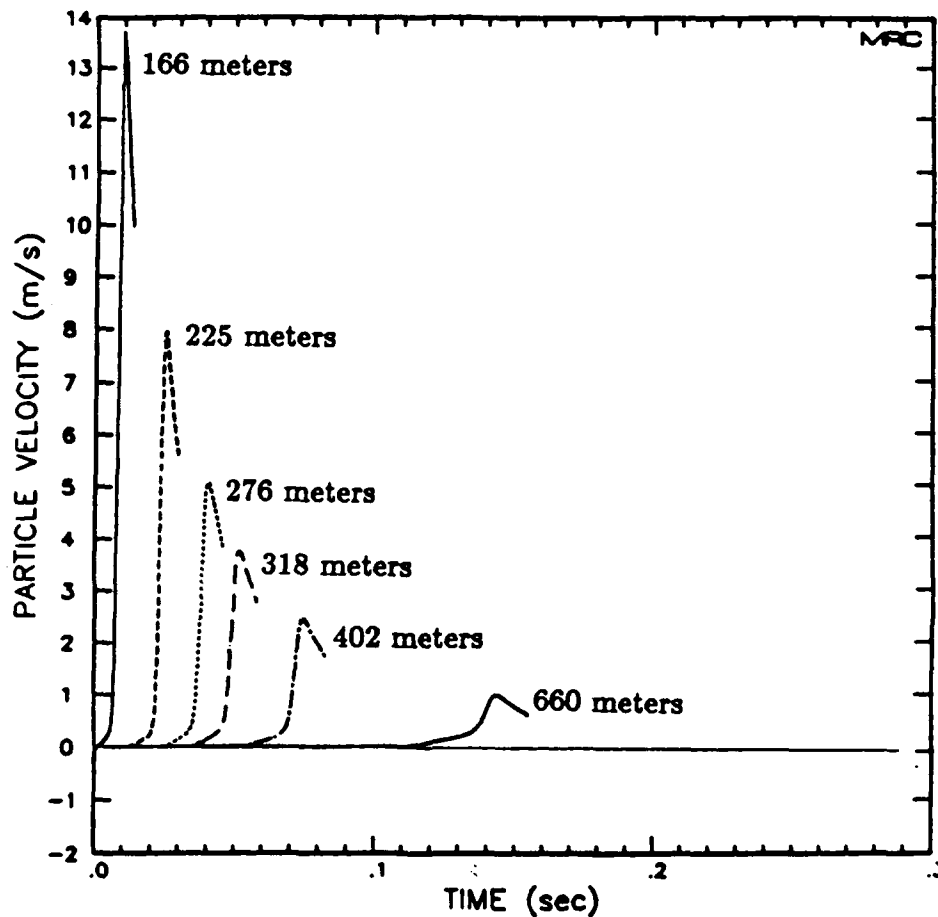
Mild nonlinear attenuation cannot be properly described by a Q function since the Q formalism is inherently linear. While it may be possible to describe the nonlinear attenuation for a particular situation by an equivalent Q , the generalization to other conditions is not possible.

It is then of great interest to construct an attenuation formulation which has a physical basis, which can generate nonlinear effects and which reproduces the moderate strain data given above. Ideally, one would also like to be able to apply the result to media other than salt.

#6

SALMON 'ELASTIC PRECURSOR' CLUE

The Salmon pulses from ranges of 166 to 660 meters show a precursor growing with range. The leading edge of the pulse at six stations are shown.



Perret refers to this structure as an 'elastic precursor' which has the properties that it lengthens with range while the peak amplitude at the base of the main pulse remains nearly constant at about 0.5 m/sec.

- Leading Edge of Precursor Propagates at 4.7 km/sec
- Main Pulse Propagates at About 3.7 km/sec
- Perret Attributes This Difference as Being Due to Shear Failure of the Salt Medium

SHEAR FAILURE

Consider an initial elastic medium with Lamé constants λ and μ where $\lambda \approx 2\mu$. The compression velocity, α , is proportional to $(\lambda + 1\mu)^{1/2}$. If the medium suffers a partial shear failure, that is reducing μ , α will be reduced.

- Change of α from 4.7 to 3.7 requires reducing μ about 70%

When partial shear failure occurs, energy residing in this mode will be reduced as the supported shear stress decreases instantaneously while the shear strain is unaltered. The total energy in the pulse is approximately proportional to α^2 . On this basis, the rate of energy loss can be estimated. When the entire pulse is subject to partial shear failure, the fractional loss over a cycle will be

$$\Delta E/E \approx \Delta \alpha^2 / \alpha^2$$

but over a cycle

$$\Delta E/E = \exp(-2\pi/Q) \quad \text{defines a mean } Q$$

- FOR 4.7 TO 3.7 km/sec CHANGE IN α : $Q \approx 13$

Thus partial shear failure can be expected to produce an attenuation comparable to that seen in Salmon data.

Can this failure produce the elastic precursor?

#8

FINITE DIFFERENCE FAILURE TEST

Partial shear failure which has its onset at some fixed but arbitrary critical strain level, ϵ_{crit} , will have the following properties:

- Will Be Consistent With Simple Scaling
- Will Be A Nonlinear Mechanism
- Attenuation Will Cease Once the Peak Amplitude of the Pulse Goes Below Onset Level
- Easily Treated in a Finite Difference Calculation
- Salmon Data Suggests ϵ_{crit} Should Be About 10^{-4}

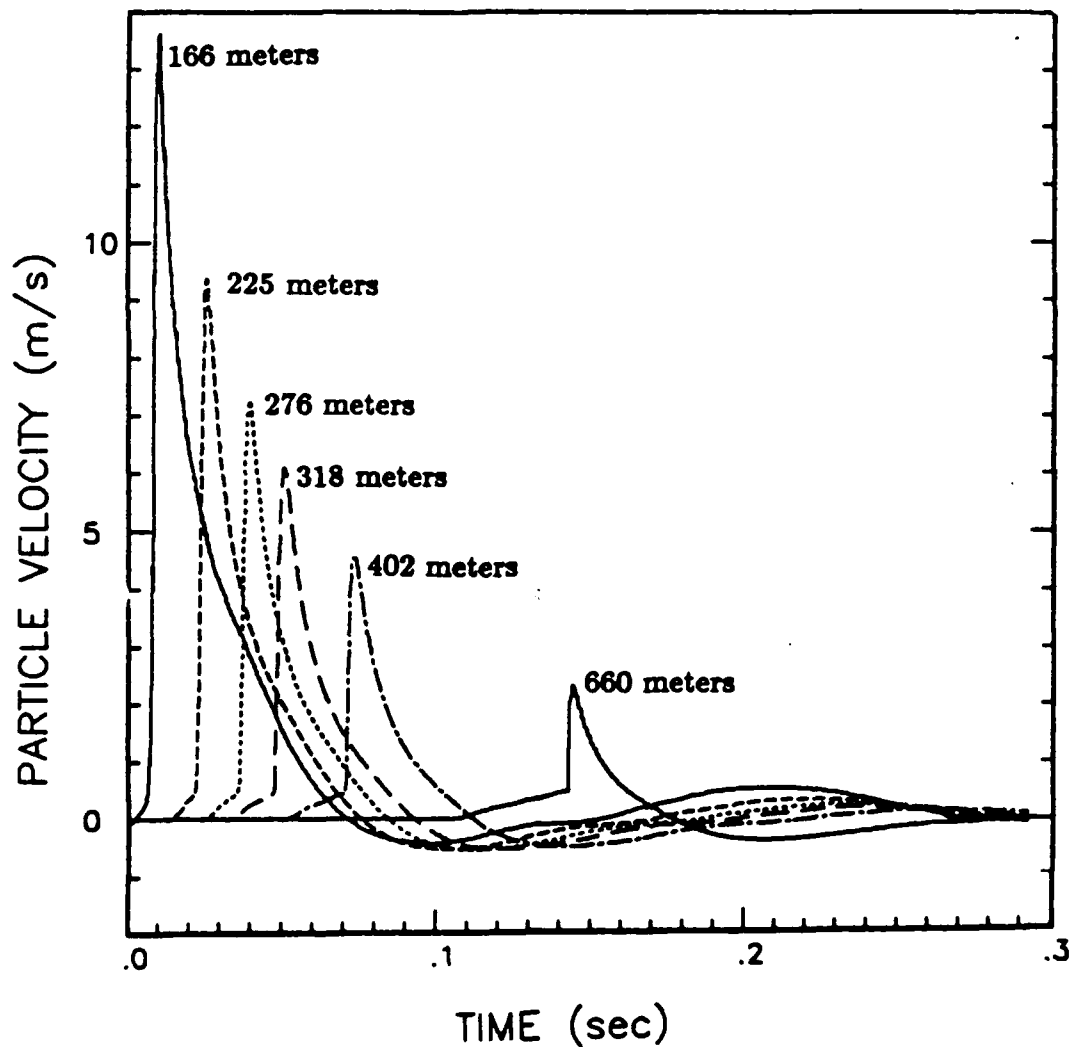
#9

SALMON TEST OF PARTIAL SHEAR FAILURE

Using a standard finite difference method as given by Wilkins and employing a linear two-sided viscous pressure as demonstrated by Viecelli, a constitutive relation for each grid cell is defined by the following:

- If $\epsilon > 10^{-4}$, Reduce μ by 70% For This Cell Permanently

The result is that a fast moving, 4.7 km/sec, elastic portion of the pulse will propagate ahead of the main pulse which will have an effective propagation speed of 3.7 km/sec



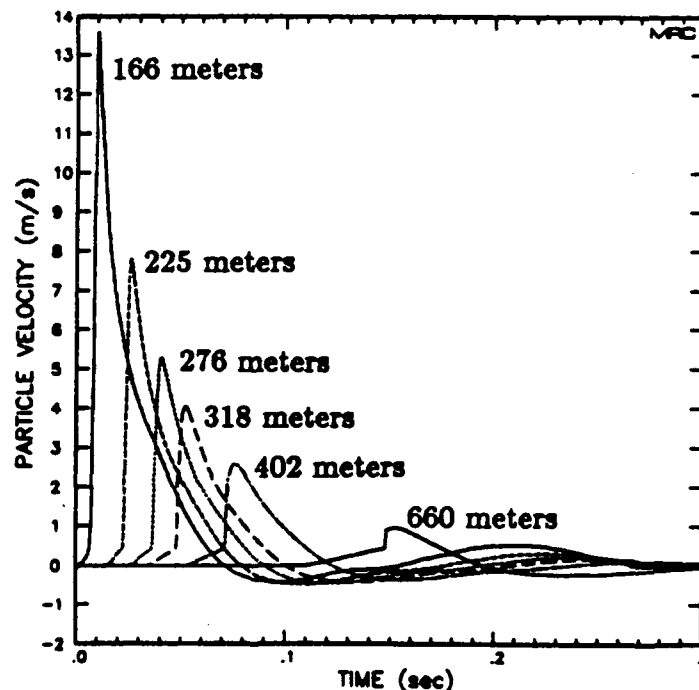
#10

PARTIAL SHEAR FAILURE DATA COMPARISON

Calculations with simple partial shear failure

- Shear Failure Model Produces a Precursor Which Resembles That for Salmon
- Attenuation Associated with Shear Failure Substantial
- Shear Failure Attenuation Still Not Adequate to Account for Salmon Attenuation
- ABSORPTION BAND LINEAR Q ADDED TO CALCULATION

For an absorption band from 1 to 100 Hz with a minimum Q of 20 along with partial shear failure, the pulse propagation produced is:



- Magnitude and Precursors in Approximate Accord with Data
- Waveforms not a Great Match Due Chiefly to the Sharp Leading Edge of the Calculated Main Pulse

SUMMARY

- Salt Data Indicate Nonlinear Attenuation Which Decreases for Strains Less than 10^{-5}
- Need Nonlinear Constitutive Relation Applicable in Moderate Strain Regime Which Is Consistent with Scaling
- Elastic Precursor in Salmon Data Suggests Shear Failure
- Partial Shear Failure Produces Substantial Attenuation but Not as Much as in the Data
- Partial Shear Failure Reproduces Elastic Precursor and Is Consistent With Scaling
- Shear Failure Model Which Has Onset at Some Critical Strain Will Cause Rapid Decrease in Attenuation with Range
- Necessary to Determine Nonlinear Constitutive Relations Which Can be Generalized to Other Media

INTELESEIS

DEVELOPMENT OF AN INTELLIGENT SEISMIC FACILITY

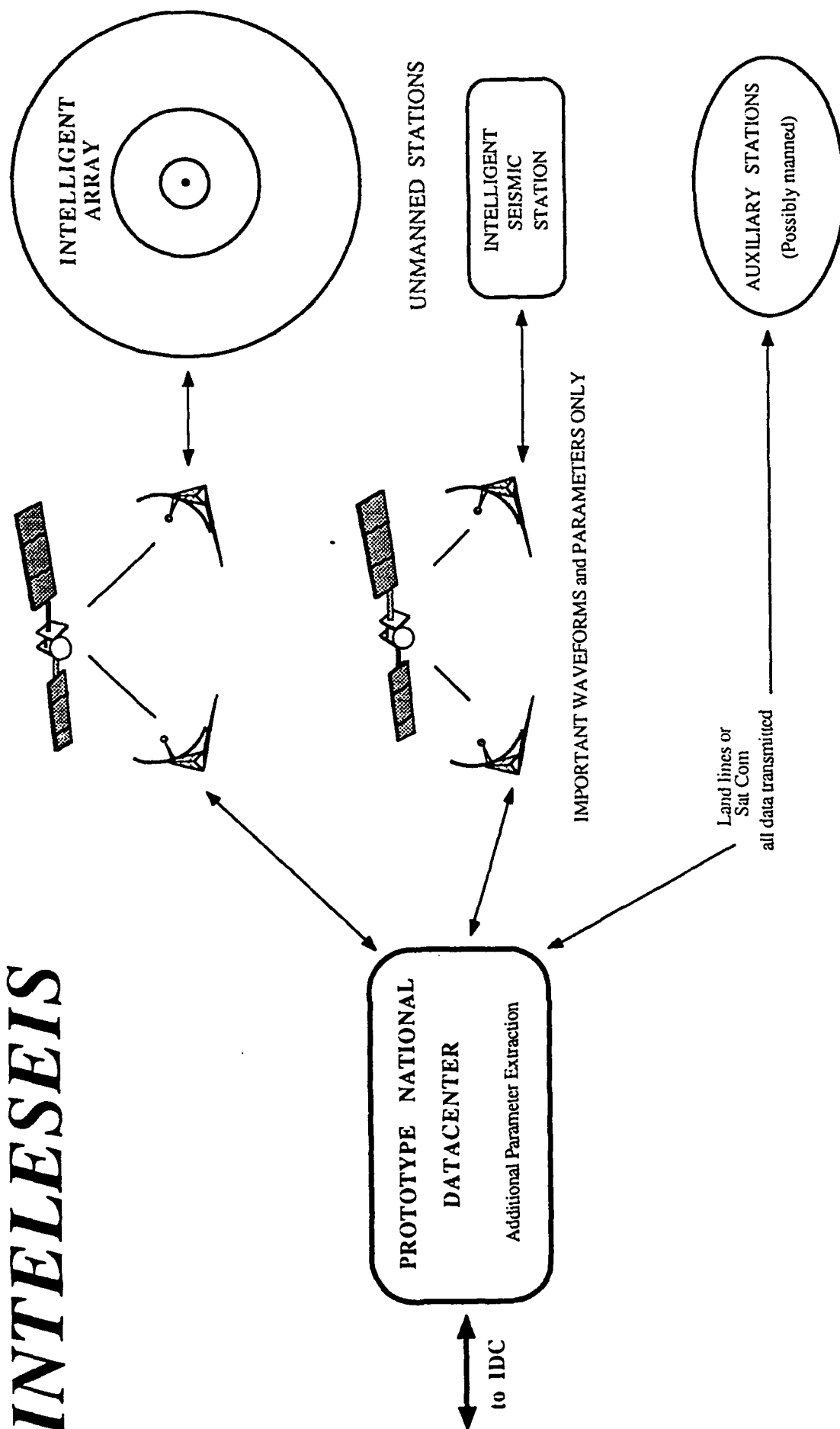
DARPA SMU TFS TELEDYNE SHI

DEVELOPMENT OF AN INTELLIGENT SEISMIC FACILITY

Eugene Herrin

The intelligent seismic facility is a new concept in seismic data acquisition and processing in that the seismic station itself will, without human intervention, determine what data, including waveform segments and parameters, are important enough to be transmitted to the datacenter. This capability will result in a considerable savings in communication costs and a redistribution of the computing load for an international network. The program at SOUTHERN METHODIST UNIVERSITY sponsored by DARPA will provide for the construction of a prototype intelligent field station at the Lajitas site and a prototype National Datacenter (NDC), which will communicate with the field station. The prototype National Datacenter at SMU will ultimately transmit seismic information from Lajitas and several other intelligent seismic field stations to the DARPA Center for Seismic Studies in Washington, and during the next global GSE experiment, to prototype International Datacenters in Washington, Moscow, Stockholm, and Canberra. The prototypes developed in the SMU-DARPA program will be based on the DARPA scientific work station systems developed to support research in the monitoring of international treaties. The intelligent seismic facility concept draws upon recent advances in experimental seismology, seismic sensors, array technology, artificial intelligence, advanced data processing techniques, interactive data analysis systems, and other related technologies.

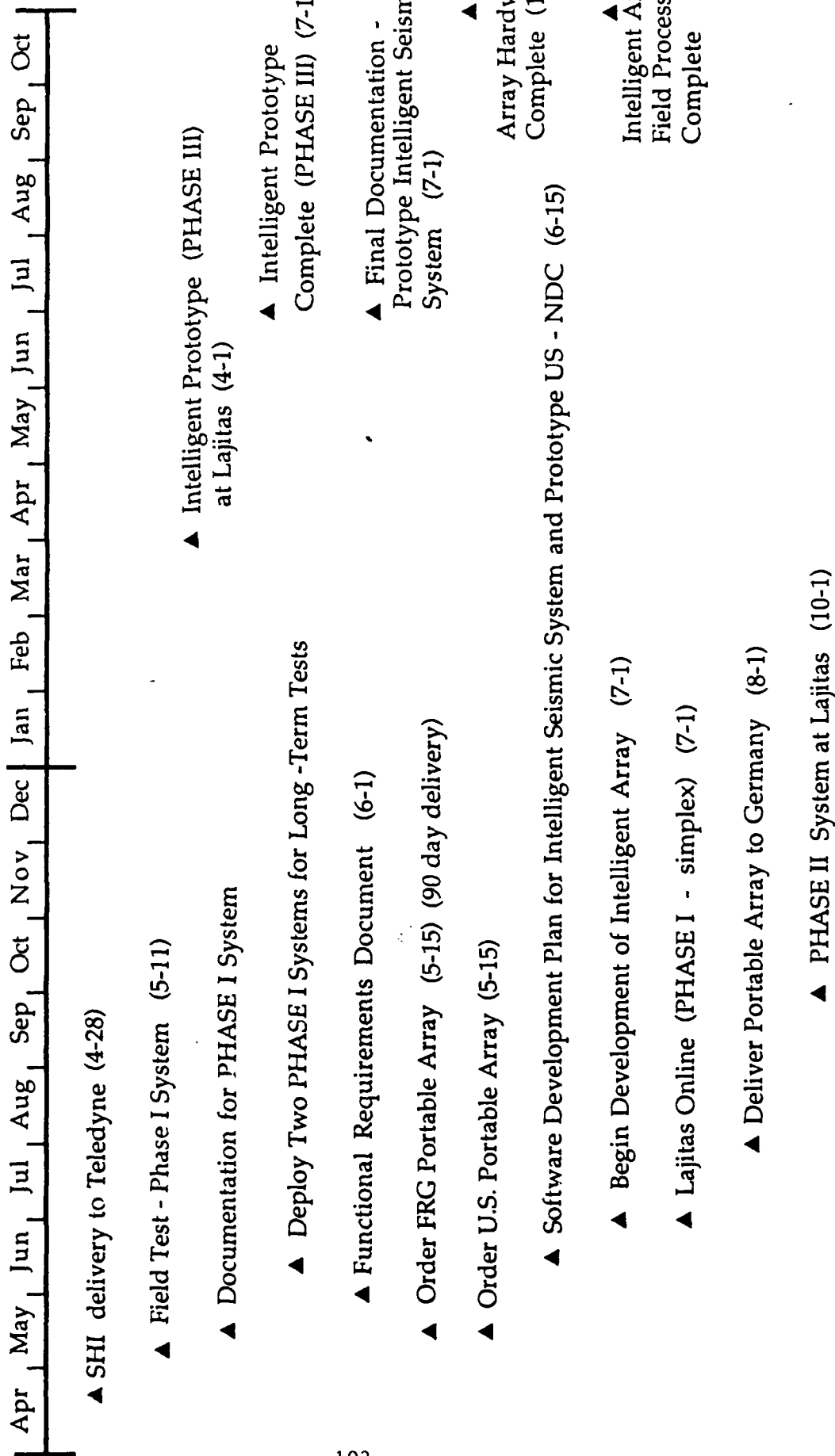
INTELLESEIS



PROGRAM MILESTONES

1989

1988



THREE-PHASE DEVELOPMENT PLAN

PHASE I COMPLETED SYSTEM

REMOTE DATA ACQUISITION SYSTEM (RDAS) DEVELOPMENT

Rugged, low-power design

Wide dynamic range, 24 bit A/D converter

Precisely time tags digital data

12 Mbytes of nonvolatile, CMOS static memory

Transmits all data to workstation via simplex SDLC port

Accepts commands from controller

WORKSTATION / DATA RECORDER DEVELOPMENT

'Ruggedized' workstation for field deployment developed

Acquires data from RDAS via simplex SDLC port

Records all data in CSS database version 2.8 in near real time

Archives all data on disk

Data quality assurance software

Spectral analysis software

System calibration analysis software

PHASE II PROTOTYPE NDC

SEISMIC STATION DEVELOPMENT

CMOS static memory will increase to 48 Mbytes

Data will include wind velocity and direction

Full duplex SDLC protocol will be implemented

Workstation will control RDAS through SDLC port

Ability to auto calibrate and change parameters remotely

Simple event detection capability in field

NATIONAL DATACENTER DEVELOPMENT

Complete seismic analysis system

Fully automated parameter extraction (analyst approved)

Fully automated bulletin transmission to International Data Center

Fully automated responses to IDC requests

PHASE III INTELLIGENT SYSTEM

AUTOMATIC DIAGNOSTIC FUNCTIONS for SYSTEM STATE-of-HEALTH

Analysis and control of calibration signals

Analysis and reporting of unusual ambient noise conditions that could indicate failure or could affect signal detection capability.

Graceful degradation of system performance in the event of failure

AUTOMATIC SIGNAL DETECTION

Detection algorithm and parameters automatically varied as noise conditions change

Initial signal classification based on simple attributes

Characterization of ambient noise during any signal segment

DATA MANAGEMENT

Archiving of all signal detections for later transmission

Archiving station state for each time sample

Intelligent lossless compression

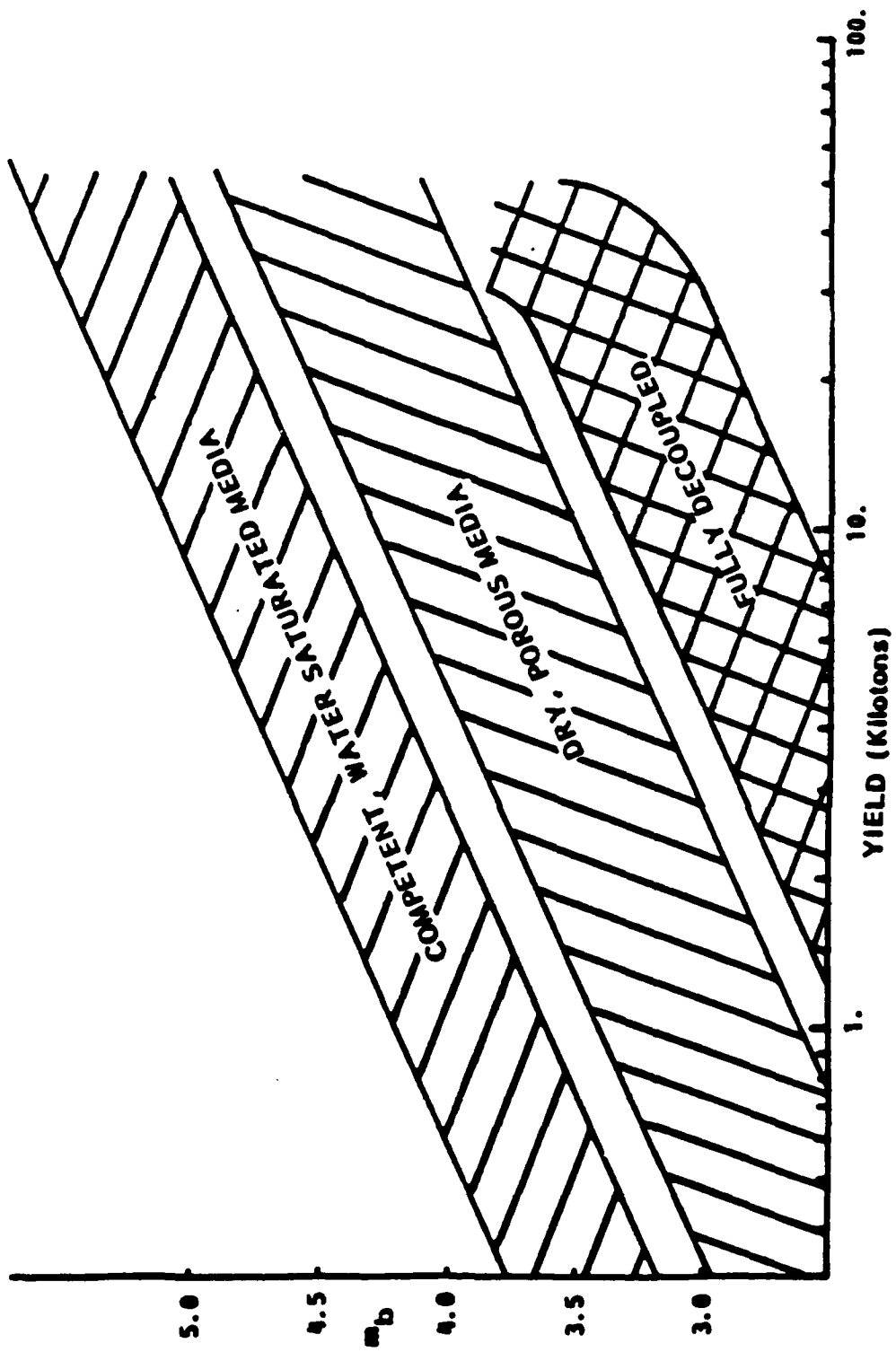
COMMUNICATIONS BANDWIDTH MANAGEMENT

Response to data requests

Additional lossy compression for less important segments

ENGINEERING ISSUES

- Sensors and Installations
 - Communications
-
- Data Processing
 - Data Management
 - Seismologist Staff
 - On-site Inspection Teams



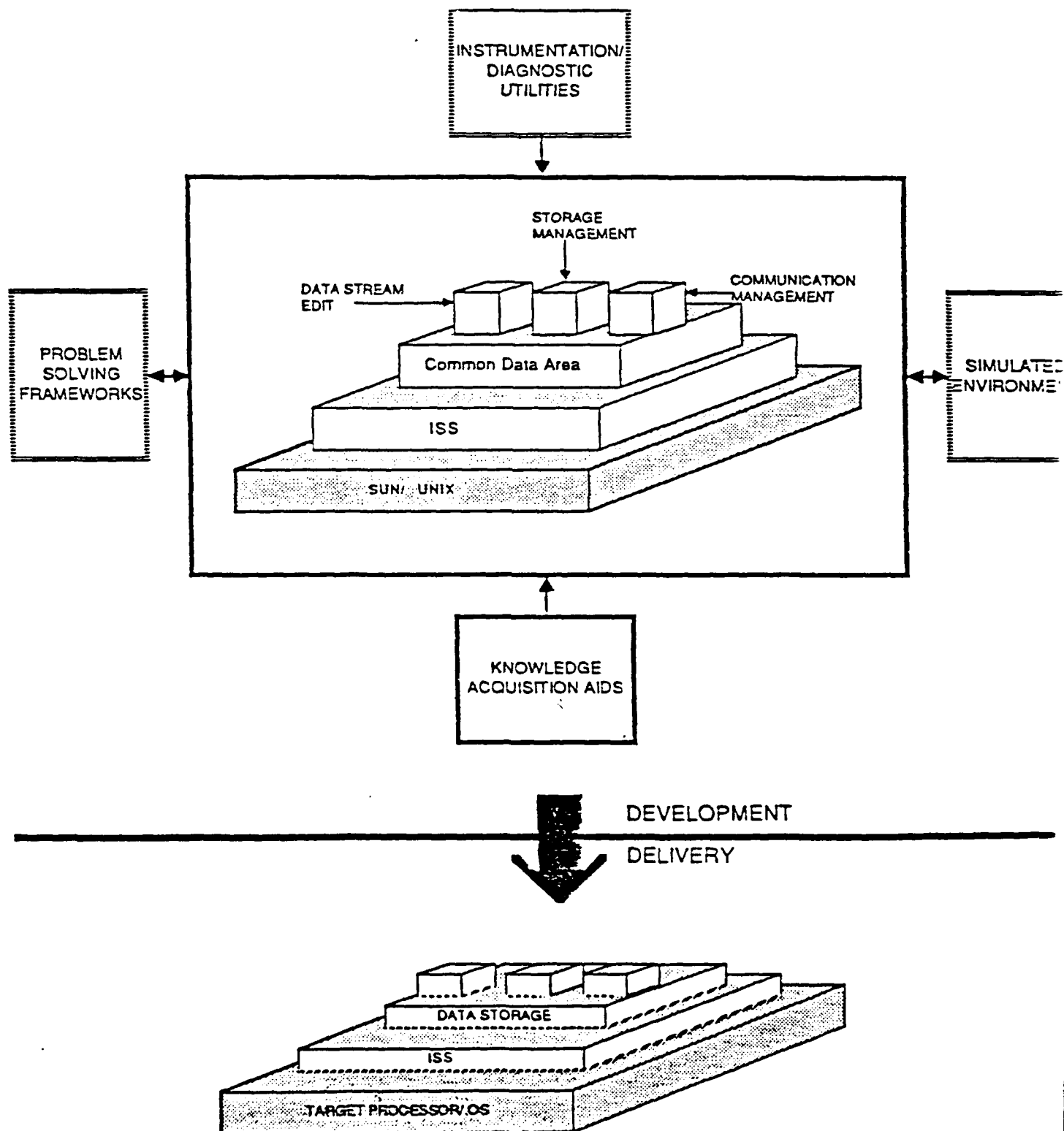
USSR DETECTION SIMULATIONS

Study	External Stations	Internal Stations	Thresholds (m_b)	f
Ringdal (1986)		115	3.9 - 4.3	~1 Hz
Evernden/Sykes (1976,1982)	15 SS	0	3.6 - 3.9	~1 Hz
	15 SS	15 SS	3.2 - 3.6	~1 Hz
Hannon (1985)	15 SS	15 AR	2.4 - 3.3	~1 Hz
Evernden et al. (1986)	25 AR	0	3.4 - 3.5	1 Hz
	15 SS	25 SS	1.6 - 2.0	5 Hz
	15 SS	25 SS	0.9 - 1.2	15 Hz
	15 SS	25 SS	0.5 - 0.8	30 Hz
Bratt et al. (1987)	13 AR	20 AR	2.6-2.9	1-15

- Discrimination Threshold is perhaps .5 m_b higher than the Detection Threshold

INTELLIGENT PROCESSOR ARCHITECTURE

TFS

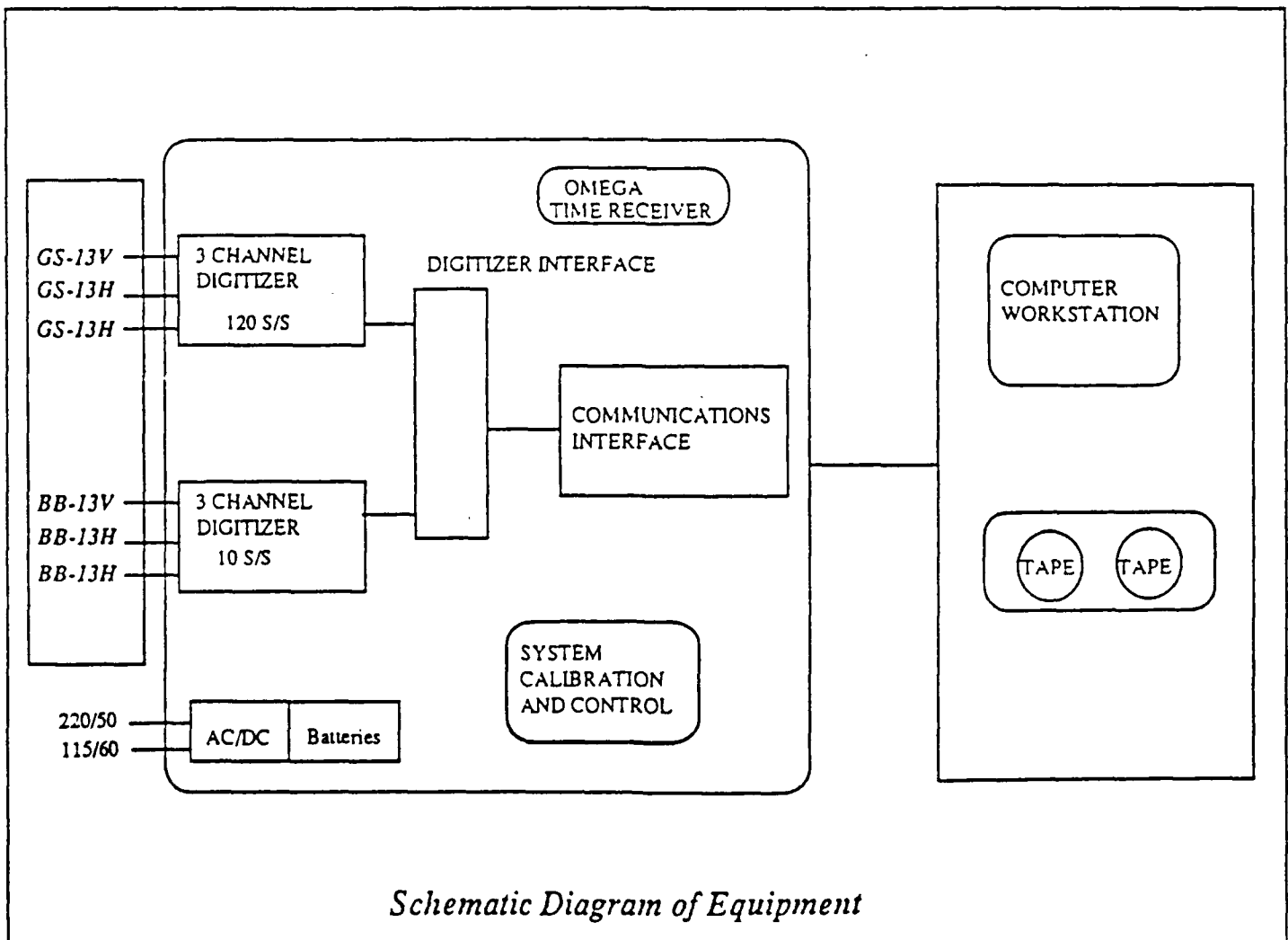


PORTABLE SEISMIC EQUIPMENT FOR FIELD APPLICATIONS

The seismic equipment for field applications is a rugged portable seismic system easily installed and operated in remote field environments. Seismic signals are recorded over a large dynamic range (minimum resolution 5×10^5) to insure against loss of signal resolution due to clipping or gain ranging. Capabilities are provided to modify system gains, perform quality control and record high quality digital data on standard media in temporary field emplacements.

THE EQUIPMENT INCLUDES FOUR MAIN MODULES :

• SENSORS • DATA ACQUISITION • QUALITY CONTROL • DATA RECORDING



SEISMOMETERS

THREE COMPONENT SHORT PERIOD

The Portable Short-Period Model GS-13 Seismometer is an instrument designed for the portability, environmental and operational requirements of seismic field operations, where a small light-weight instrument is desired.

The seismometer period is adjustable from 0.75 to 1.1 Hz, which is optimal for the recording of teleseismic body waves. The design of the GS-13 offers an unusually stable natural period over a wide range of operating temperatures and places the first significant spurious mode beyond 100 Hz.

THREE COMPONENT BROADBAND

The Model BB-13 seismometer is designed for recording teleseismic body and surface waves. The instrument response can be modified in the field to selectable frequency bands through the use of filters.

The BB-13 is an enhancement of the industry standard S-13 short period seismometer. It has a frequency response flat to acceleration from DC to 20 Hz. The BB-13 has an additional gain of approximately 10 dB over system noise when compared with the standard S-13.

COMPONENTS OF EQUIPMENT IN EACH SYSTEM

SENSORS

3 Teledyne Geotech GS-13

3 Teledyne Geotech BB-13

DATA ACQUISITION MODEL

1 Digitizer Module

1 System Calibrator and Controller

1 Communications Interface

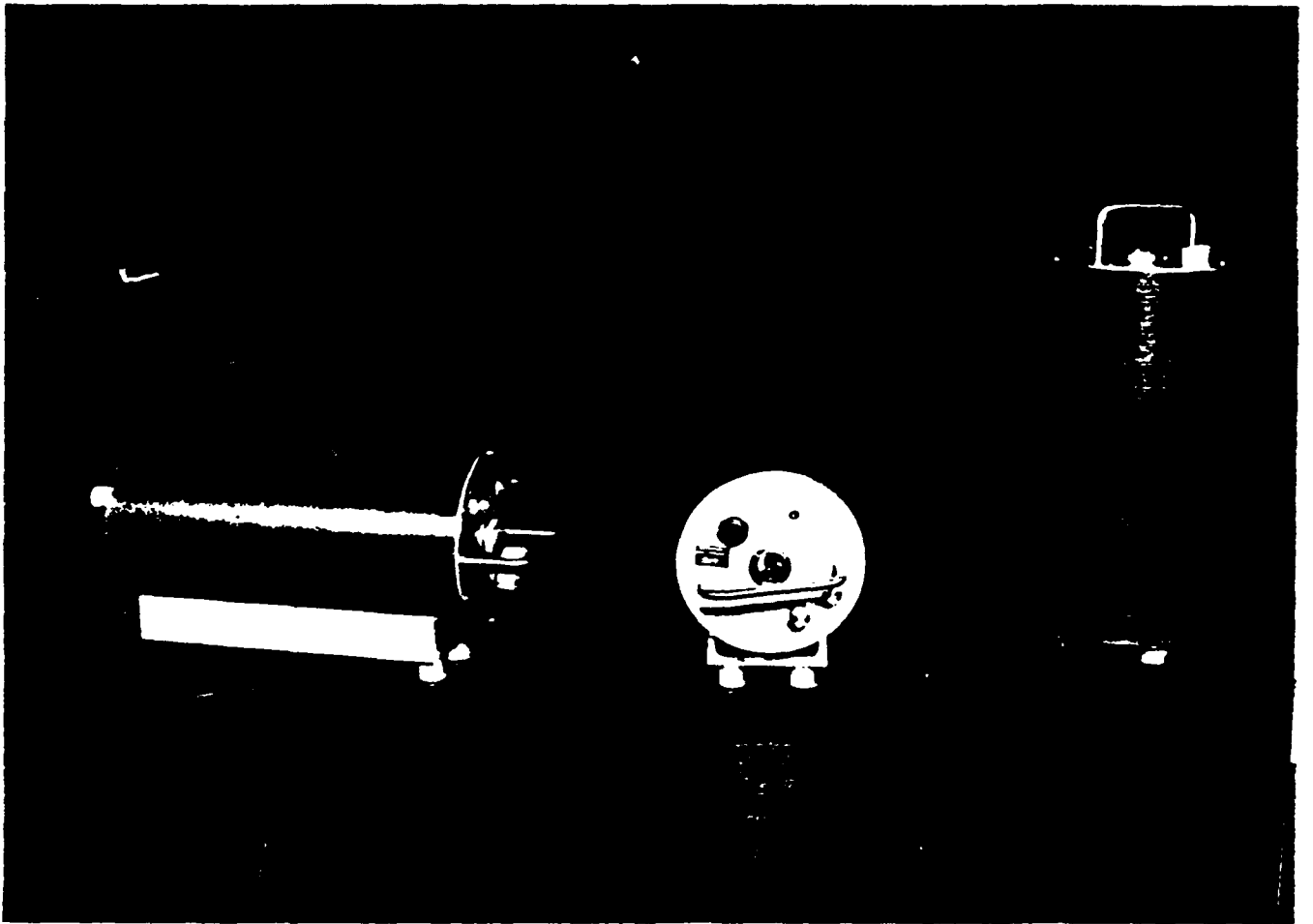
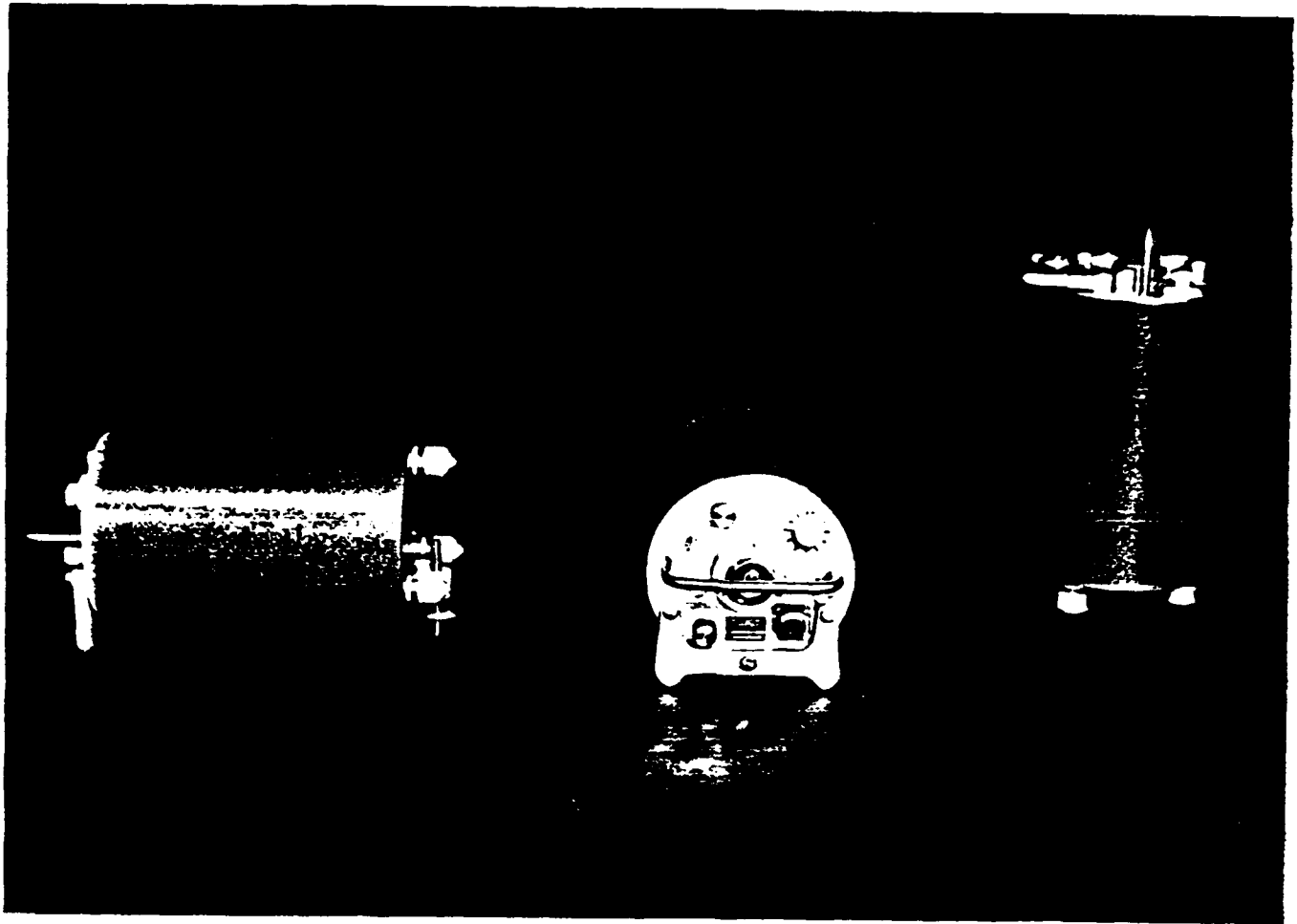
1 Omega Time Receiver

QUALITY CONTROL

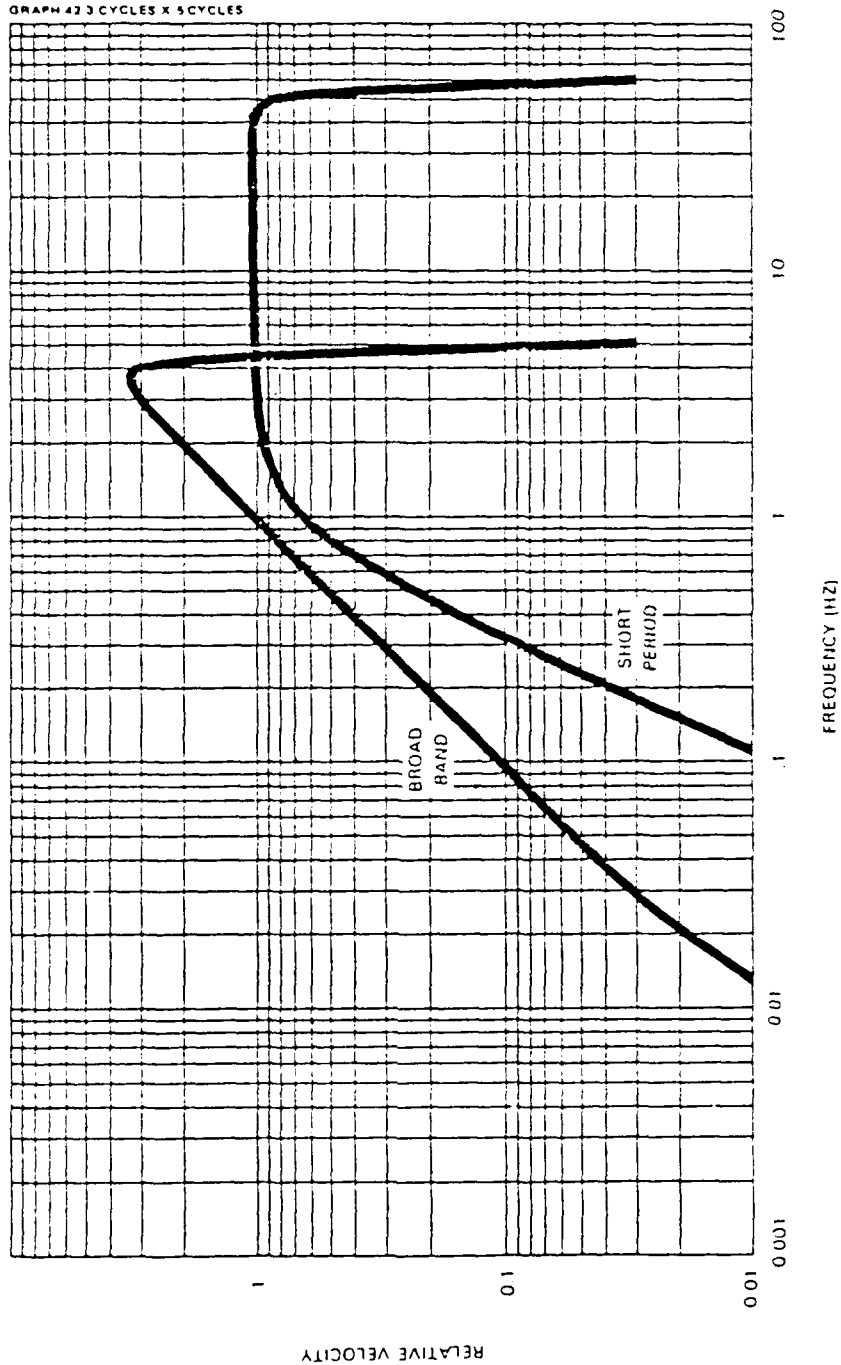
1 Computer Workstation

DATA RECORDING

2 1600 bpi Magnetic Tape Drives



GRAPH 42 3 CYCLES X 5 CYCLES



System Response

DATA ACQUISITION

The data acquisition module has several components for data digitization, timing, calibration, and formatting.

WIDE DYNAMIC RANGE DATA DIGITIZATION

The digitizers provide the capability to record signals over the widest dynamic range. Minimum resolution (19 bits or $5 \cdot 10^5$) insures no loss of signal due to clipping or gain ranging problems.

Two digitizer subassemblies are included. One accepts three channels of short-period and the other accepts three channels of broadband data.

Each subassembly provides all the conditioning and processing needed for the wide-range digitizing for its passband.

TIMING THE DATA

The system times the data and sets standard sample frequencies by obtaining Universal Time (U.T.) through a low frequency navigation system (Omega). Sample rates are 120 samples per second for short period and 10 samples per second for long period data.

SYSTEM CALIBRATION AND CONTROLLER

The system provides the capability for on-site personnel to calibrate the sensors and change the system parameters. In the event of temporary failure, the controller can act as a backup device to record up to two hours of data.

BATTERY BACKUP POWER

The system protects against transients and temporary loss of power. DC power is used to charge the batteries. In the event of primary power failure, the batteries provide power to the system, permitting uninterrupted operation during the outage.

POWERFUL MULTI-PURPOSE SEISMIC WORKSTATION

Science Horizons is providing a powerful, flexible seismic workstation which is based on the Sun-3E Eurocard CPU, Ethernet, and Video board set. This seismic workstation is configured for real-time data acquisition and display, near-real-time data processing, and video interactive data analysis. It provides 3 MIPS performance to the analyst, high resolution color graphics, and is compatible with Sun Operating System releases 3.4 and above.

STANDARD FEATURES

- 20 Mhz MC68020 Processor*
- 20 Mhz MC68881 Floating Point Coprocessor*
- Sun's Proprietary Sun 3 MMU*
- 4 MByte On-Board Memory*
- 2 RS-423 TTY ports*
- 2 TTL serial ports for keyboard/mouse*
- 32 bit VMEbus, 233X160mm Eurocard Form Factor*
- Seven slot chassis, 19 inch rack mount or stand-alone, 7.0 inches high*
- 10 Mbit Ethernet With on-board Transceiver*
- 1.5 Mb/Sec Asynchronous SCSI Bus*
- UNIX and C right to use license*

HARDWARE

- 4 or 12 MByte Expansion Memory Boards*
- Monochrome or Color Video, Monitor, Keyboard, and Mouse*
- 19-inch Rack-Mount Removable Disk Subsystem (760 MByte Total Capacity)*
- 8mm Cartridge Tape Subsystem (Mounts in System Chassis)*
- 60 MByte, 1/4 inch Cartridge Tape Subsystem (Mounts in System Chassis)*
- Rackmount 1/2 inch 1600/6250 bpi Magnetic Tape Subsystem*
- Synchronous Serial Communications Processor Subsystem*
- Shock Mounted, Ruggedized Transport Cases*

SOFTWARE

- Real-time Data Acquisition Software*
- Near Real-time Processing, Display and Archiving Software*
- Off-line Interactive Analysis Software*
- Data Quality Assurance Software*

DATA QUALITY ASSURANCE MONITOR

The purpose of the DQAM is to verify proper operation of the system in near real time so that any problems can be detected and corrected as quickly as possible.

The DQAM consists of 3 components:

A continuous trace display of all channels at a selected gain and time scale.

A recorder monitor/status reporting:

*tape footage
current recording time
time since start
Trace RMS amp
Trace Peak abs amp*

An alarm panel that brings any unusual conditions to the attention of the operator.

RECORDING ALARM

The purpose of the recording alarm is to bring unusual conditions to the immediate attention of the operator. As such, if it presents a window, when a new alarm condition occurs, the alarm panel will flash to the front of all other views and present an audible alarm.

There are 5 alarms associated with the field recording.

Omega Clock Problems

*Clock not in sync (from state-of-health)
Clock time does not agree with calculated time.*

No Real Time Data

RDAS not transmitting at all - ought to be obvious from the trace display unless the gain is set too low or you haven't accumulated enough data to display.

RDAS retransmitting

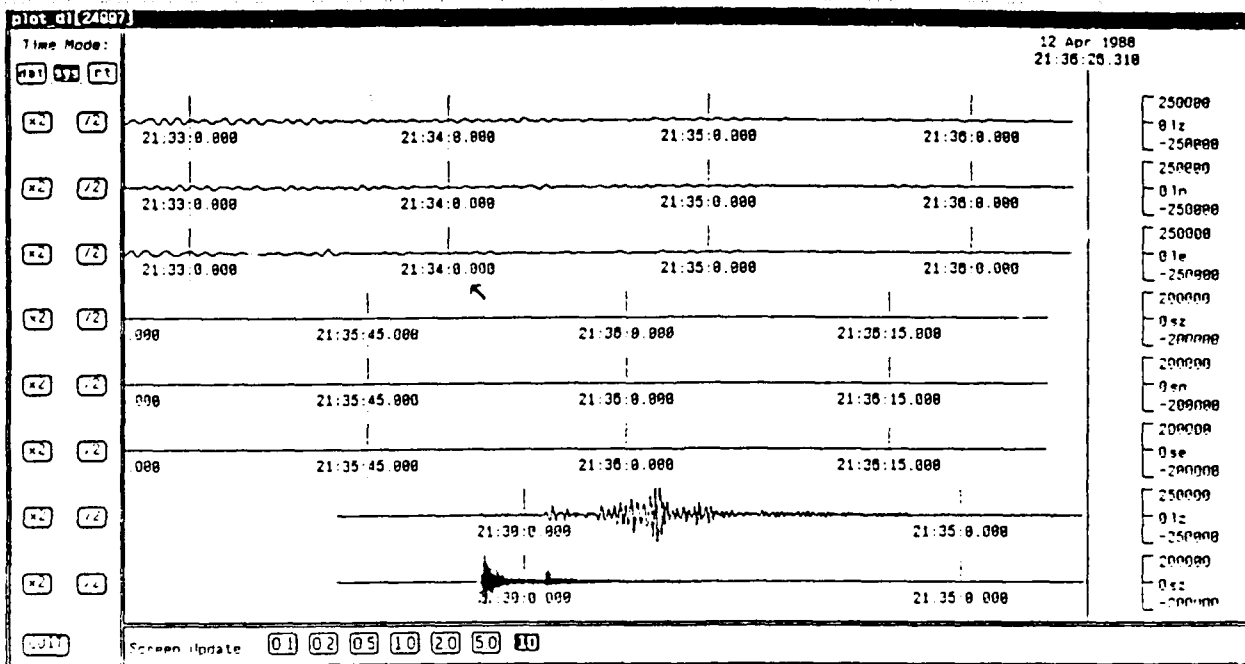
Available from state-of-health bits in header.

Clipped Data

Number Samples clipped in nnn seconds and mmm samples. The clipping level will be specified by the operator.

Dead Channel

Number RMS windows below threshold, (Channel nn). The window length and RMS threshold will be determined by the operator.



RECORDING MONITOR

CURRENT TIME: 14:06:17.0001

From OMEGA time tag

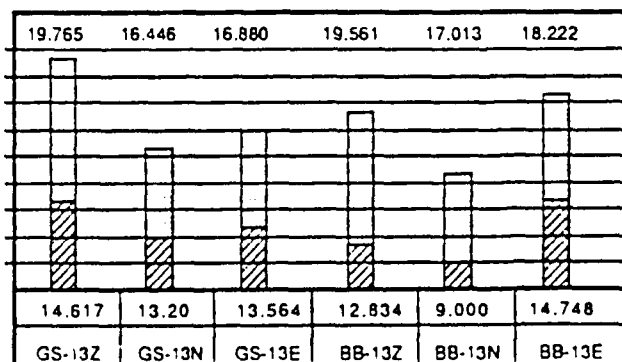
CURRENT TAPE FOOTAGE: 1267 ft.

Calculated from standard IRG, TM, & record length (approx.)

TIME SINCE RECORDING START: 2:26:03

TIME SINCE MARK: -1:07:03.1

The mark time may be entered at any time, hence this could be + or -



TRACE RMS AMPLITUDE --

TRACE PEAK AMPLITUDE --

RMS amplitude and peak amplitude are calculated over a specified window which is different for GS-13 and BB-13 channels. These are moving windows of operator specified length.

THE FINE STRUCTURE OF P_N AND P_G

BY L J BURDICK

The high frequency P_g phase for shallow events typically appears as a complex arrival with a duration of several tens of seconds, much longer than the possible duration of the source. If model responses for a layer over a half space are computed by progressively adding in rays with one reverberation in the crust, then two and so on, it is observed that a sequence of high frequency arrivals develops spanning the typical range of P_g . We have defined these arrivals as crustal resonance phases (FIGURE 1). If a typical amount of scatter is associated with each resonance phase, the duration and complexity of P_g is simple to understand. We have investigated the composition of the first two resonance phases in detail. At the top of FIGURE 2, we compare the four fundamental Green's functions generated from all 254 rays in the first three crustal reverberations to responses generated from those 6 rays which contribute most strongly to the first crustal resonance phase. Interestingly, the second resonance phase is not dominated by rays with a complete extra reverberation in the crust but by 8 rays which have at least one converted leg. The response to just these rays is compared to the complete Green's function at the bottom of Figure 2. To investigate the character and stability of the crustal resonance phases, we assembled long period record sections from the 8/16/66 Caliente earthquake which occurred near NTS and from several nuclear explosions (FIGURE 3 AND FIGURE 4). A comparison between the earthquake data and synthetics for 4 different stations is shown in FIGURE 5. The match of the double-peaked structure at the arrival time of the first crustal resonance is quite remarkable. Features specifically associated with the arrival of the second crustal resonance are also apparent. A similar comparison between synthetics and data for the explosion observations is shown in FIGURE 6. The synthetic predictions are a relative failure given the high success at predicting fine details and general complexity and period of the resonance phases in the earthquake records. The synthetics are much too simple in character and in most cases too low in frequency content to explain the observations. In FIGURE 7, we compare the crust model used to a realistic crustal model for NTS. The simple model does not contain the strong drop in velocity which is known to exist at the earth's surface. It is clear that the long period response of the two models should be just about the same, but at short periods, the waves will react to the strong gradient. The physical effect of the strong near surface velocity gradient will be to cause the depth phases to develop more strongly at shorter ranges than in the layer over a half space model. This suggests that we might wish to use an appropriate observed record from regional ranges as an effective source. Likely candidate records are found at regional distances where the first arrival has penetrated the low velocity zone and begun to turn against the upper mantle gradient. Two such observed first arrivals are shown at the top of FIGURE 8. In the second row of the figure are shown P waves from beyond 30° for the two events. In the bottom row are synthetic traces appropriate for 30° computed using simple plane wave theory. The P and sP arrivals typical of a shallow strike slip earthquake are indicated on the left. It seems clear that the free surface phases are almost completely developed in the LON record from Caliente. The synthetic for COLBY was computed using the structure shown in Figure 8. The P and pP phases are identified. It seems clear that the LUB P wave should make a reasonable effective source. Most of the phenomena usually represented by operators are present in the effective source time history. Making this assumption, we repeat the calculation of explosion P_{n1} 's as shown in FIGURE 9. The synthetics now have the appropriate frequency content and the general complexity of the P_g is matched to a much higher degree.

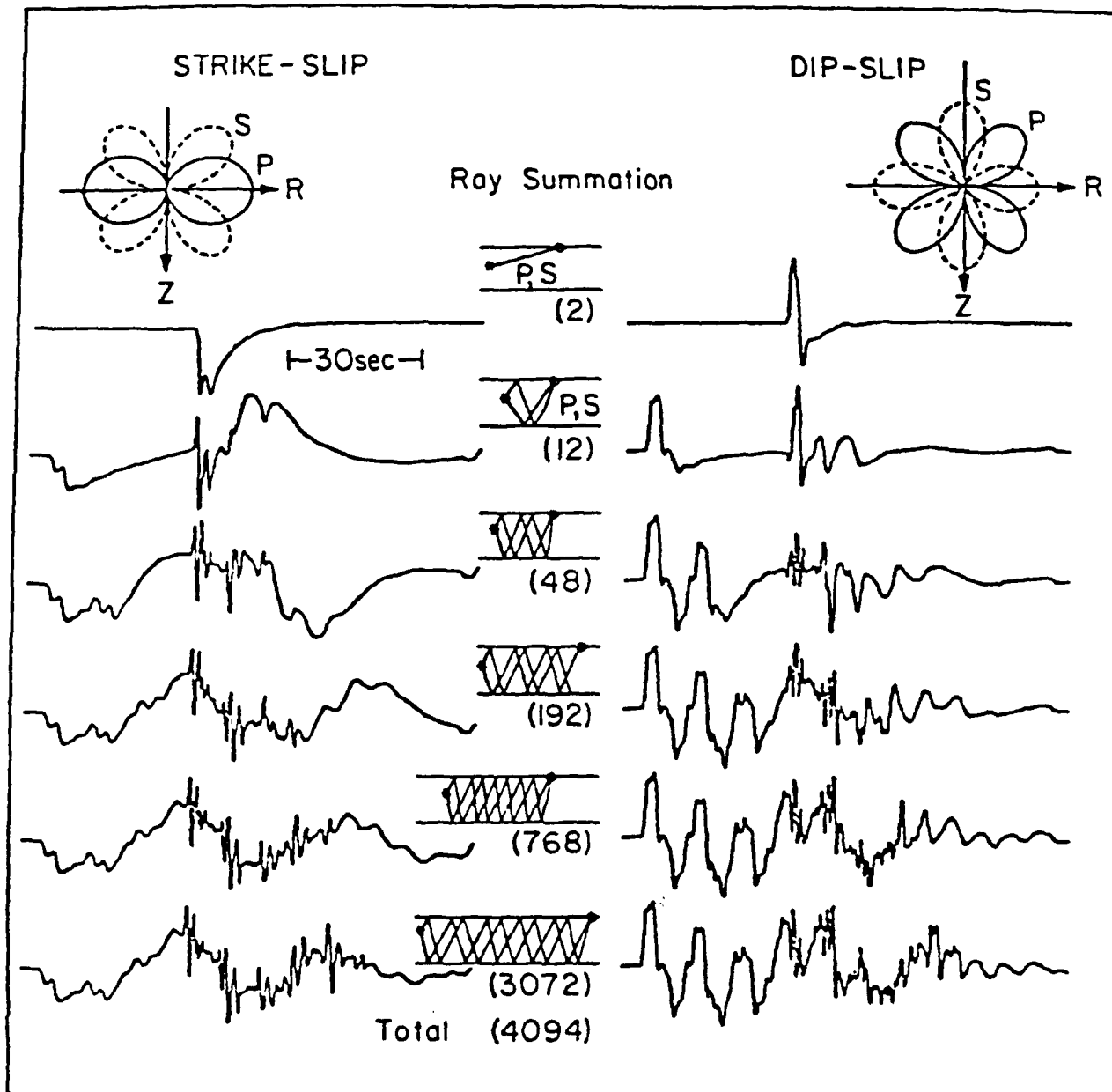


Figure 1.

Green's functions for a layer over a half space computed using generalized rays. Successive rows are computed by adding in more crustal reverberations as indicated. The strike slip and dip slip results vary substantially because of the difference in vertical radiation pattern. The phases we have defined as "CRUSTAL RESONANCE PHASES" are the rhythmic high frequency pulses which begin to arrive at PmP time and develop progressively as more rays are added in.

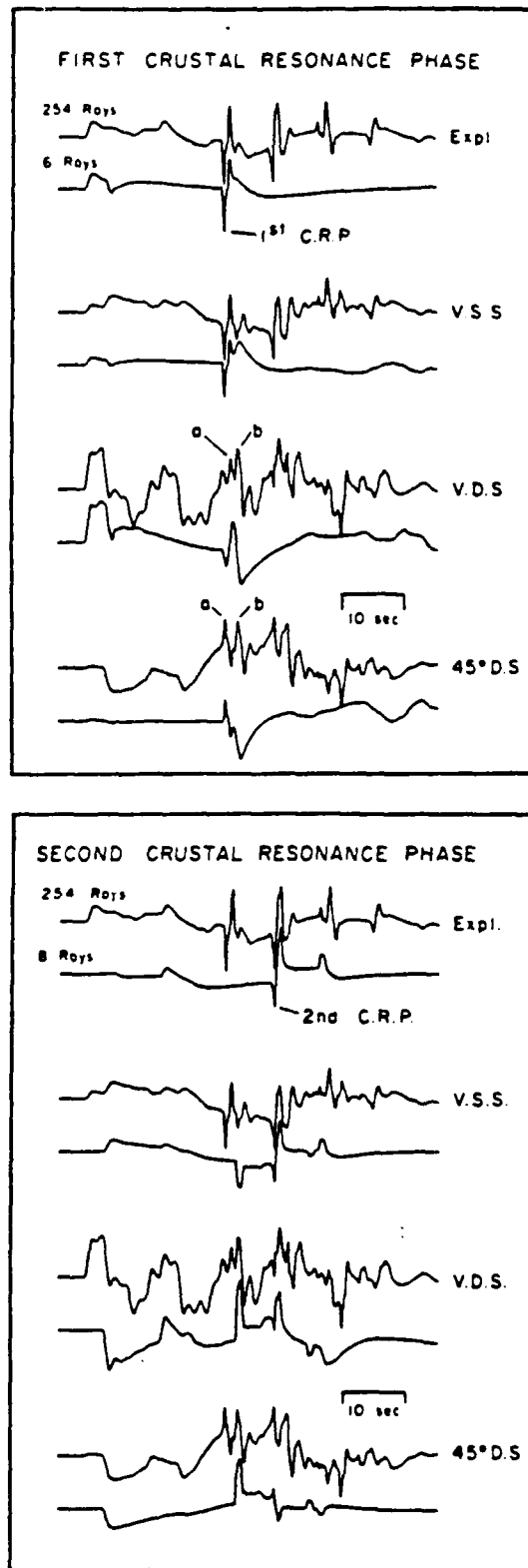


Figure 2.

Analysis of the composition of the first two crustal resonance phases. The lower traces in the upper figure which contain most of the energy in the first C.R.P. were computed with only the 6 rays P, S, PmP, SmS, pPmP and sSmS. The lower traces in the lower figure were computed from the 8 rays PmS, SmP, pSmS, sPmP, PmPSmS, SmSPmP, PmPSmP and PmSPmP. The upper traces were computed from a much more complete ray set. The arrival labeled "b" is associated with sPmP and is therefore more appropriately grouped with the second resonance phase.

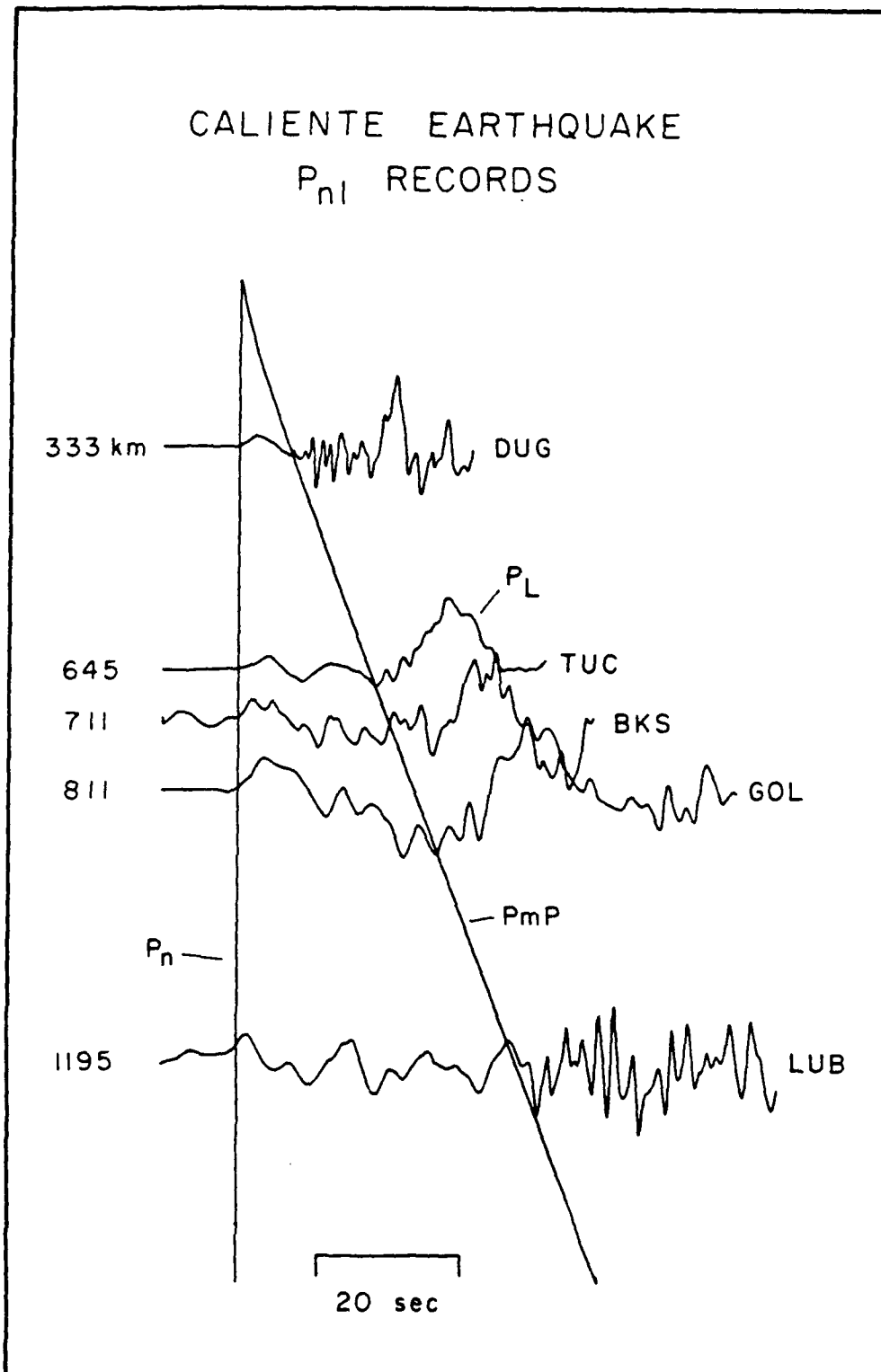


Figure 3.

Long period WSSN records of the Caliente earthquake at regional ranges displayed as a seismic section. The long period P_g commences with P_mP time which also signals the onset of the crustal resonance phases.

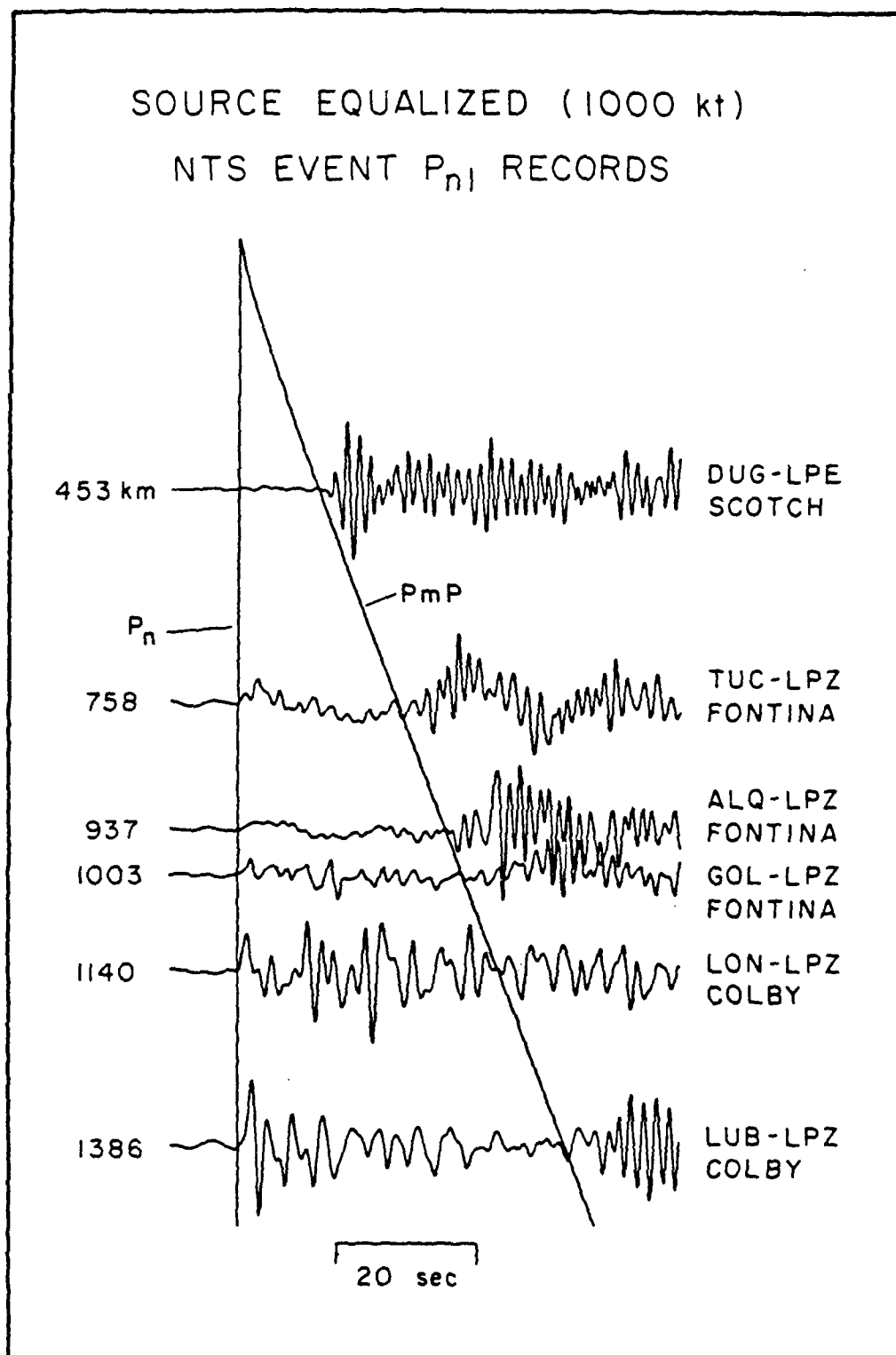


Figure 4.

An NTS regional seismic section corrected to a common explosion source time history. The explosion P_n is much higher in frequency content than the earthquake's even though their source time histories are roughly equal in duration.

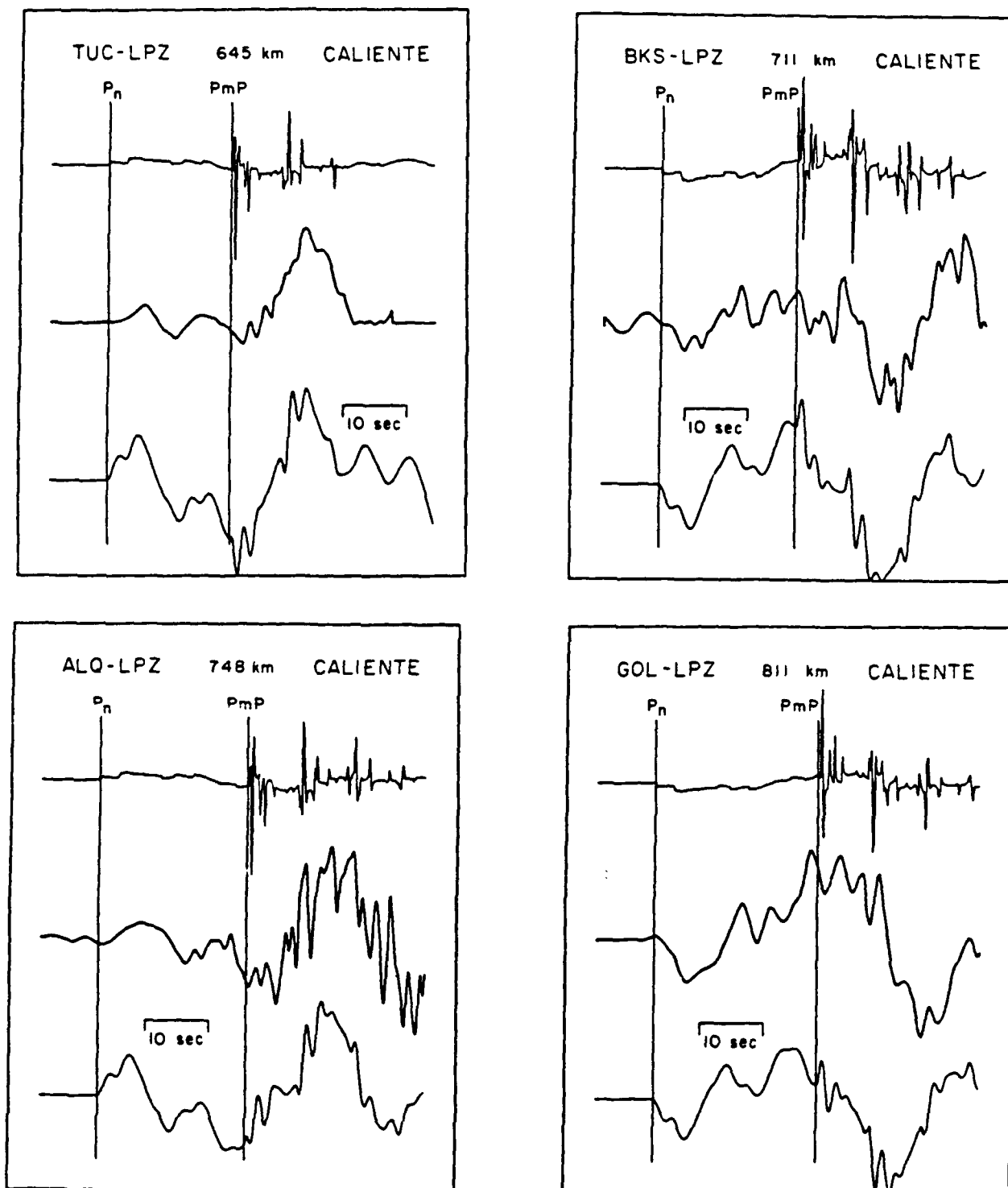


Figure 5.

A comparison between observed and synthetic P_{n1} records of the Caliente earthquake. The Green's function is shown at the top, the data in the center and the synthetic at the bottom.

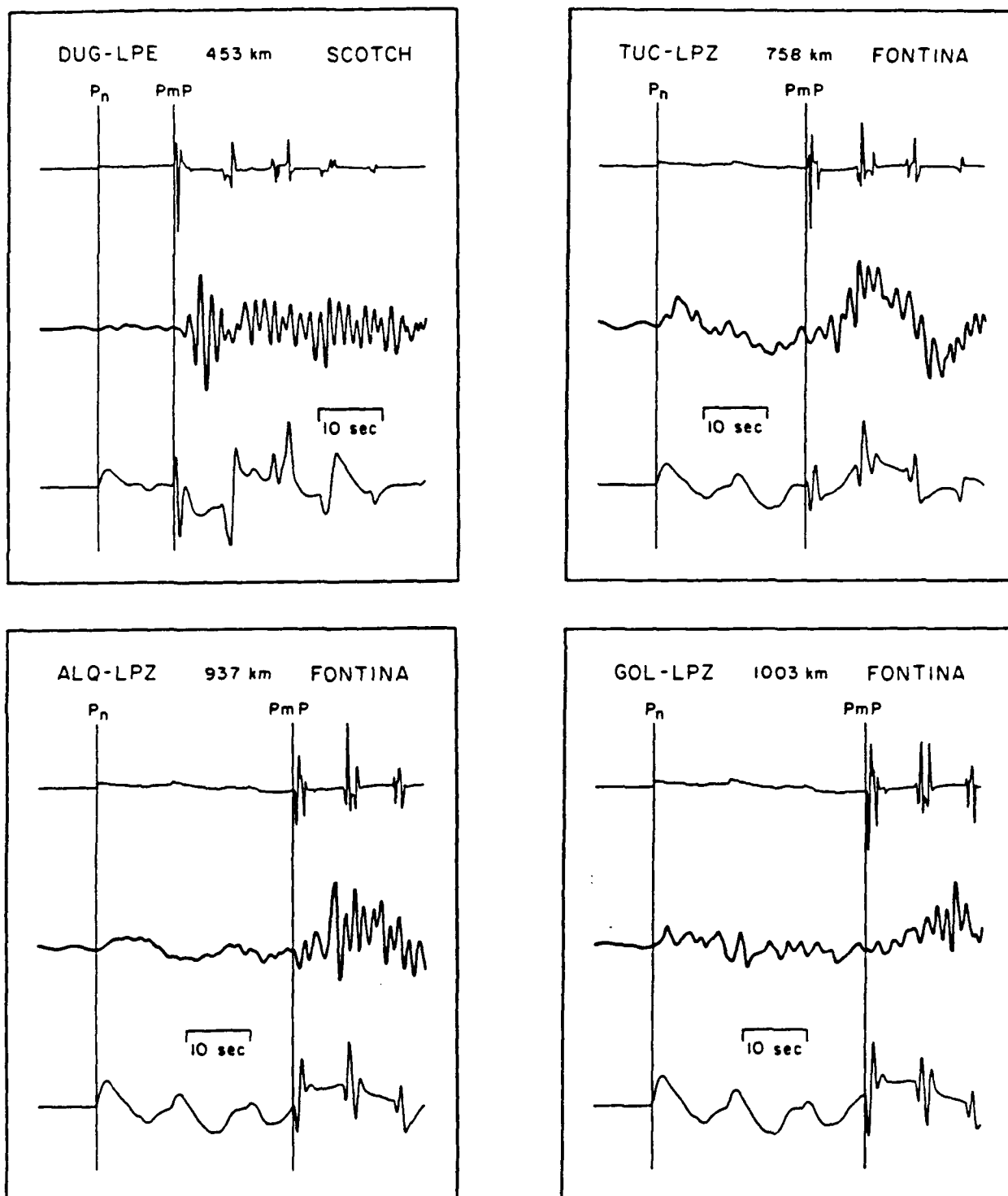


Figure 6.

A comparison between observed and synthetic P_{n1} records of the NTS events. The synthetics are too simple in character to match the data.

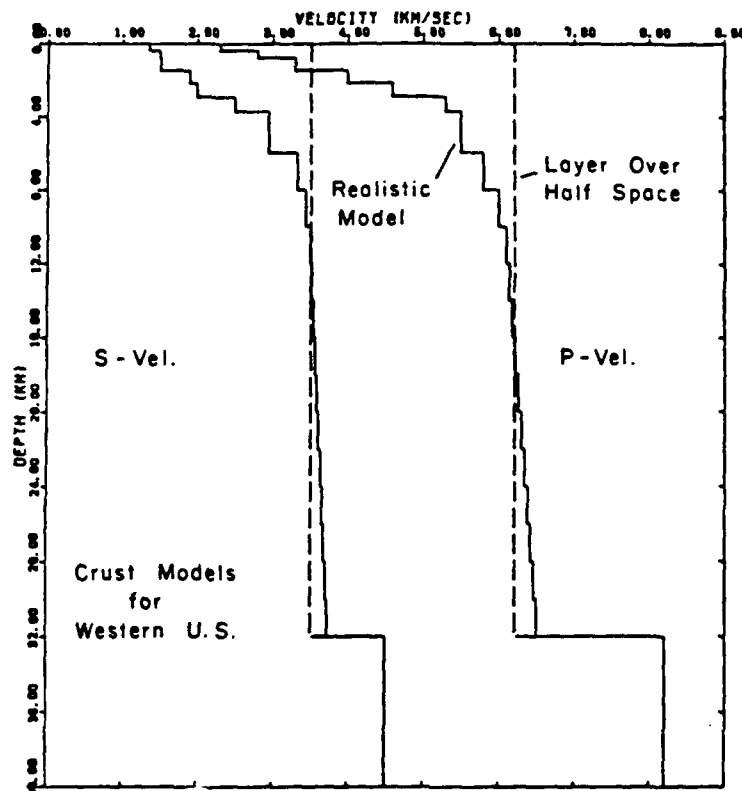


Figure 7.

A comparison between a realistic and a layer over a half space crust model for the western U.S. The major difference is that the realistic model has a strong gradient at the surface which amplifies depth effects.

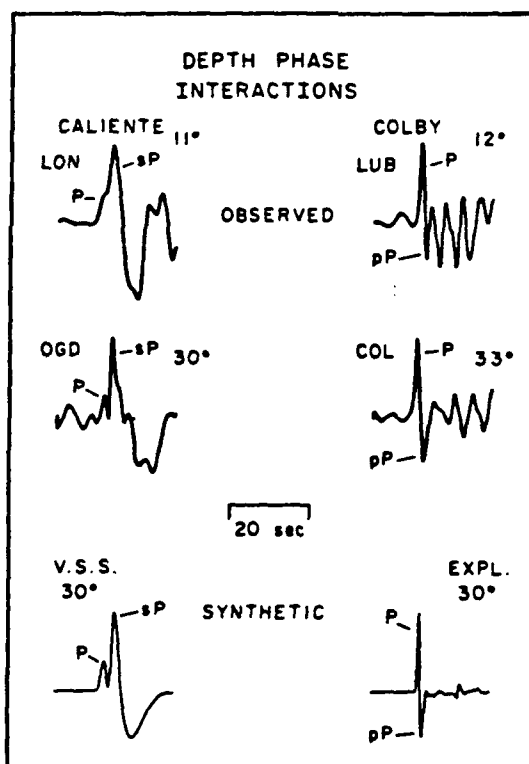


Figure 8.

Observed records for the Caliente earthquake and Colby explosion at regional (top) and teleseismic (center) ranges compared to teleseismic synthetics (bottom). The regional records have developed depth phases comparable to those at teleseismic distance. We use the Colby-LUB record to recompute the explosion synthetics.

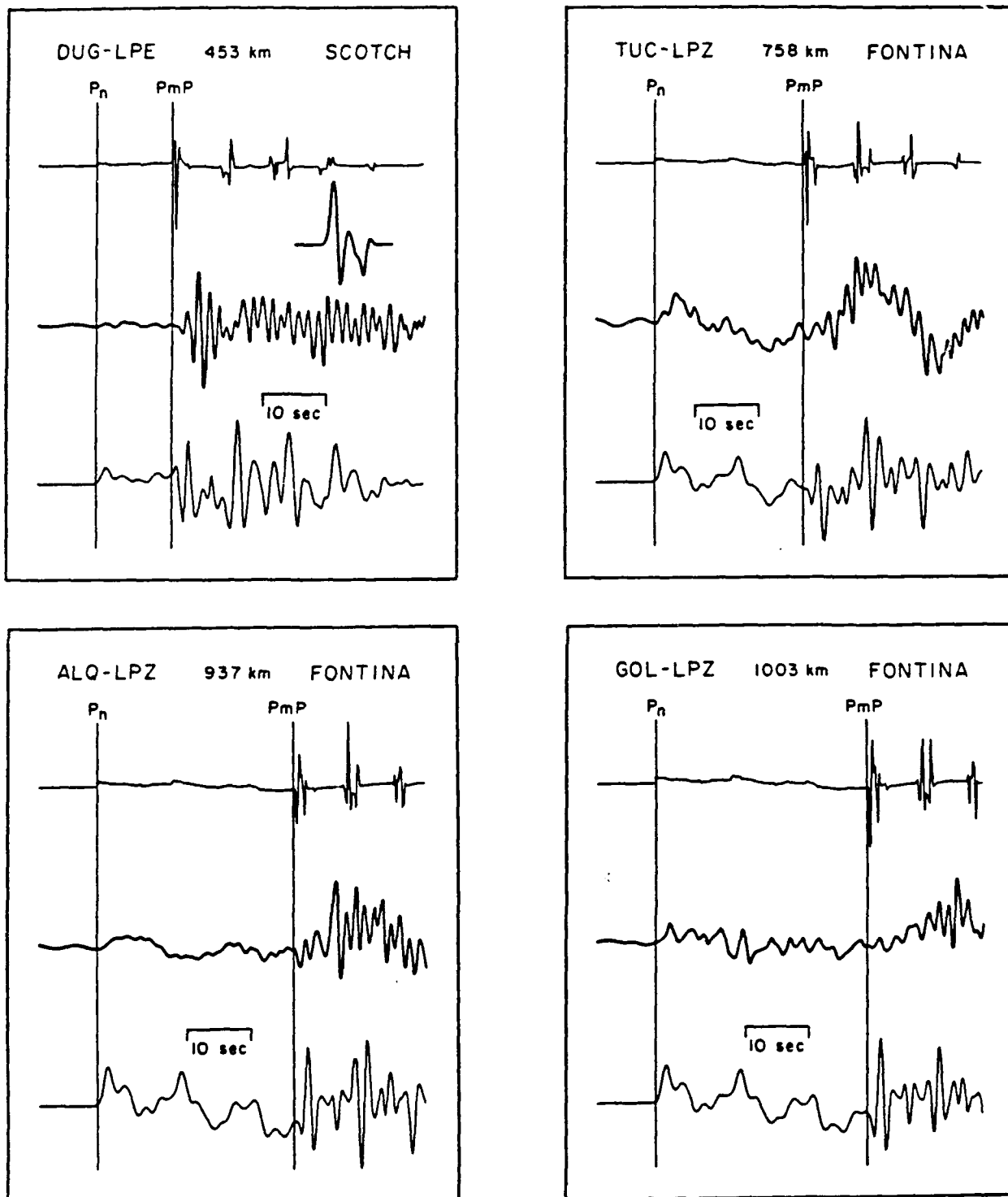


Figure 9.

A comparison between observed and synthetic explosion P_{n1} records. The synthetics are now computed using the effective source approach and have a complexity comparable to the observed. The P_{n1} records contain more depth phase information than would be inferred from a layer over a half space calculation. The effective source is shown next to the DUG record.

In the investigation of long period crustal resonance phases shown on the adjoining board, we present evidence that there are coherent resonance arrivals at periods at least as short as 2 s. There remains, however, some question as to whether these organized crustal reverberations remain coherent in the short period body wave band. Digital recordings of a series of nuclear events at a single test site offer a unique opportunity to suppress incoherent effects and test for the presence of crustal resonance phases at high frequency. To perform this test, we collected a large data base of digital recordings of Pahute and Yucca events at the digital stations ALQ and ANMO. Samples of the observed $P_n - P_g$ sections of the records are shown in FIGURE 1 and FIGURE 2. Though there are some indications of a series of arrivals pumping energy into the P_g codas (event Jornada from Yucca), the effects of scattering and other variations between events seems to dominate. To suppress these effects, we aligned the signals from sets of events very carefully in time and summed. The results are shown in FIGURE 3 and Figure 4 where we show progressive sums of records. That is each subsequent line shows the result of adding in an additional record. The results show that there are coherent crustal resonance phases at frequencies of several hz. There are 10 traces summed in the stack of Yucca events. The first two crustal resonance phases develop almost immediately showing that they are very coherent. A third appears by the time 4 traces are added in and the sum has stabilized by the time 8 are added in. Actually, this is a relatively rapid rate of stabilization indicating that the resonance phases are very coherent for this path. In the Pahute record stack, the first and third resonance phase stabilize first, while the second does not really emerge clearly until 11 traces are added. The sum ceases evolving after 13 traces are added. At the bottom, we show a synthetic for the simple layer over a half space model just to show that the resonance phases have approximately the character we expect. The relative change in timing of the P_n and resonance phases is not well matched because the true speed of P_n at ALQ is 8.6 km/sec while in the half space model it is only 8.2 km/sec. A multiply refracted P_n can be observed pulling ahead of P_g between the Pahute and Yucca stacks.

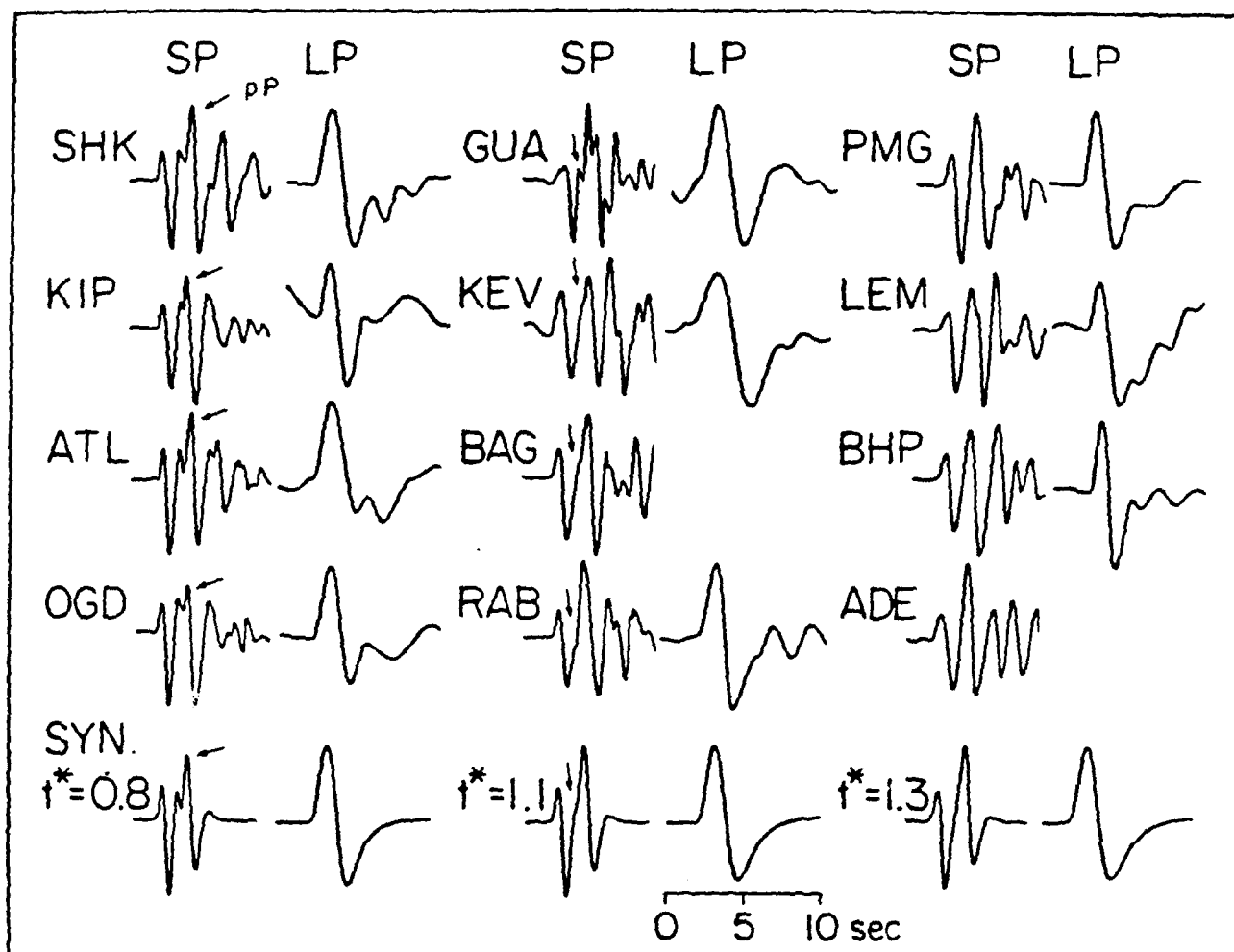


Figure 1.

The teleseismic pP arrival can be observed as a distinctive double peak in the "c" swing of some short period records from CANNIKIN. This is a comparison of observed short and long period P waves with synthetics for a range of t^* values. As t^* increases, the interference in the second upswing produced by pP becomes less apparent. The synthetics were computed with an artificially delayed pP.

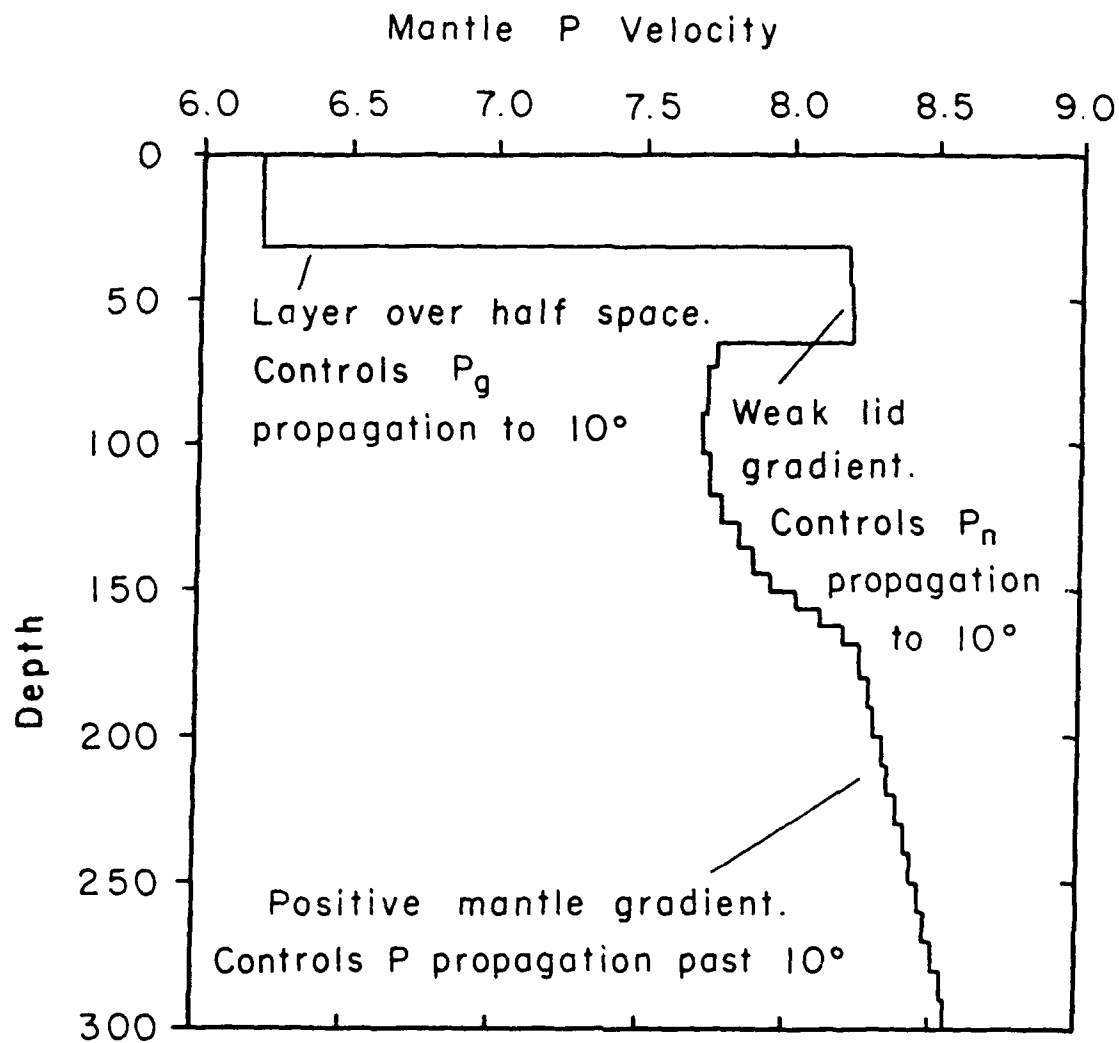


Figure 2.

Our conception of the P velocity structure of the crust and uppermost mantle of the western U. S. The significant point here is that we believe that high frequency P_n is not a true head wave but a turning ray in the weak lid gradient.

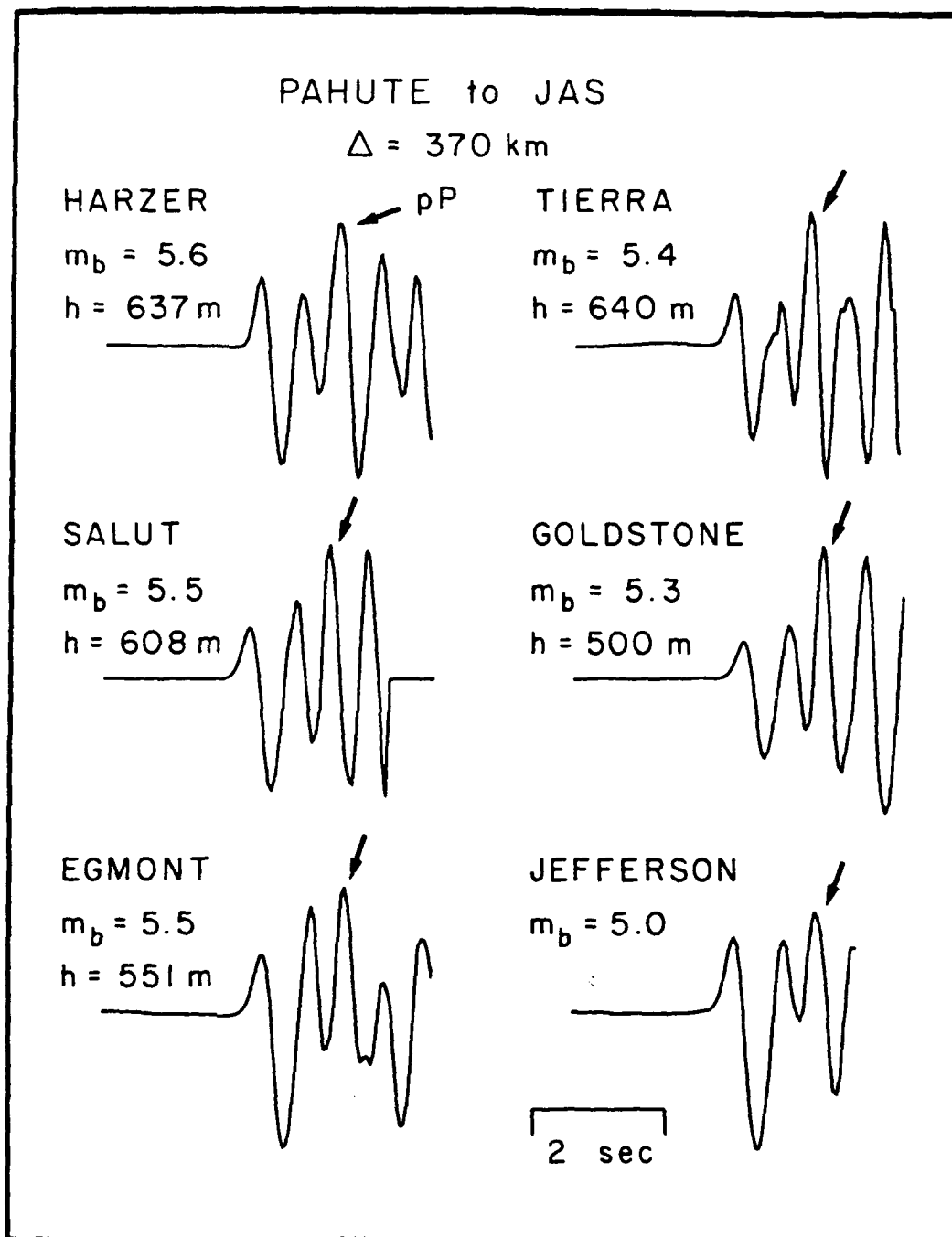


Figure 3.

Observed P_n signals from Pahute events at DWWSSN station JAS. The "c" swing is strongly split which we interpret as the arrival of effective pP_n .

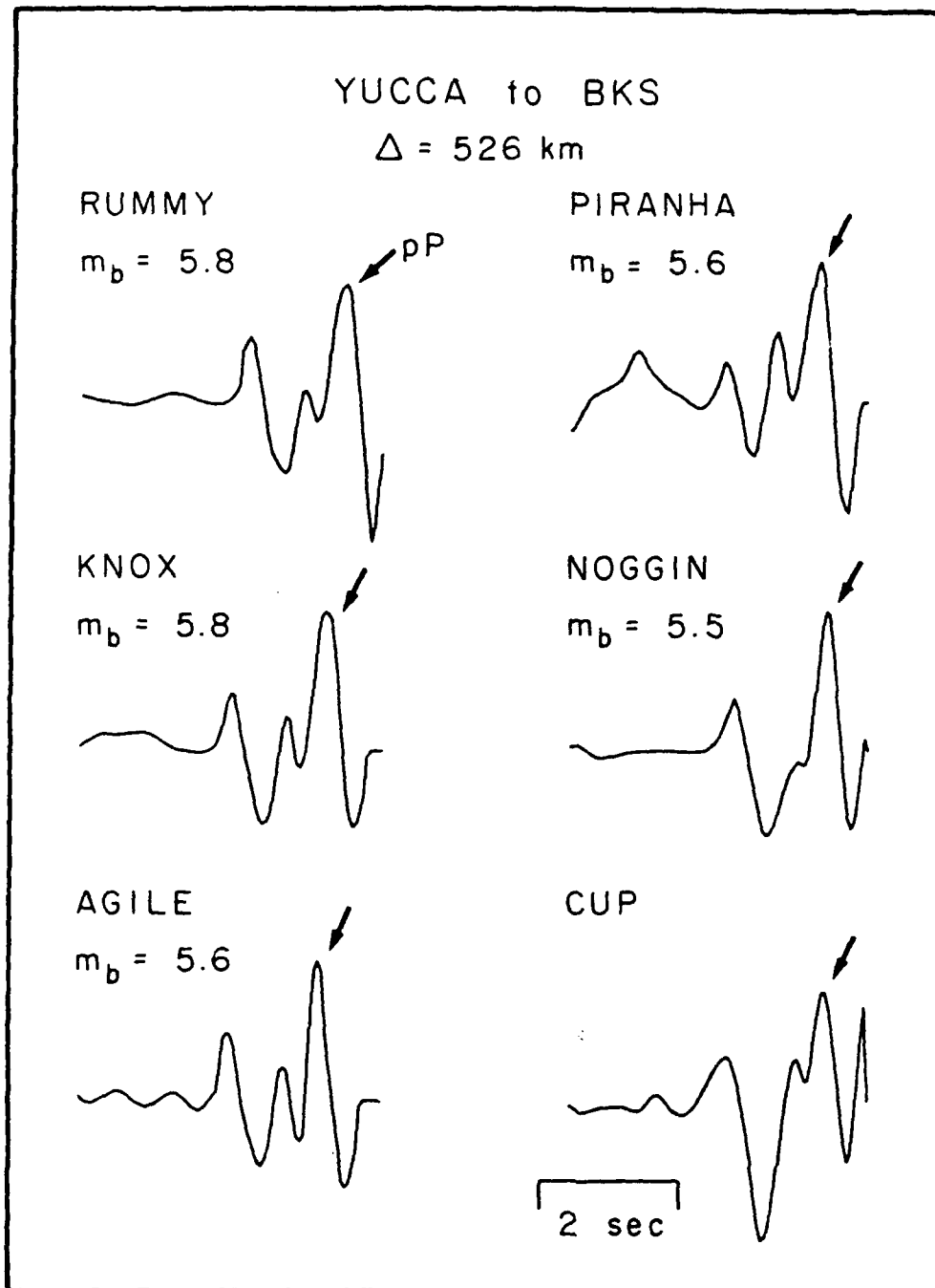


Figure 4.

Hand digitized P_n signals from Yucca events at WWSSN station BKS. The split "c" swing is interpreted as the effect of pP_n . Note that the pP arrival is somewhat closer to P than at JAS.

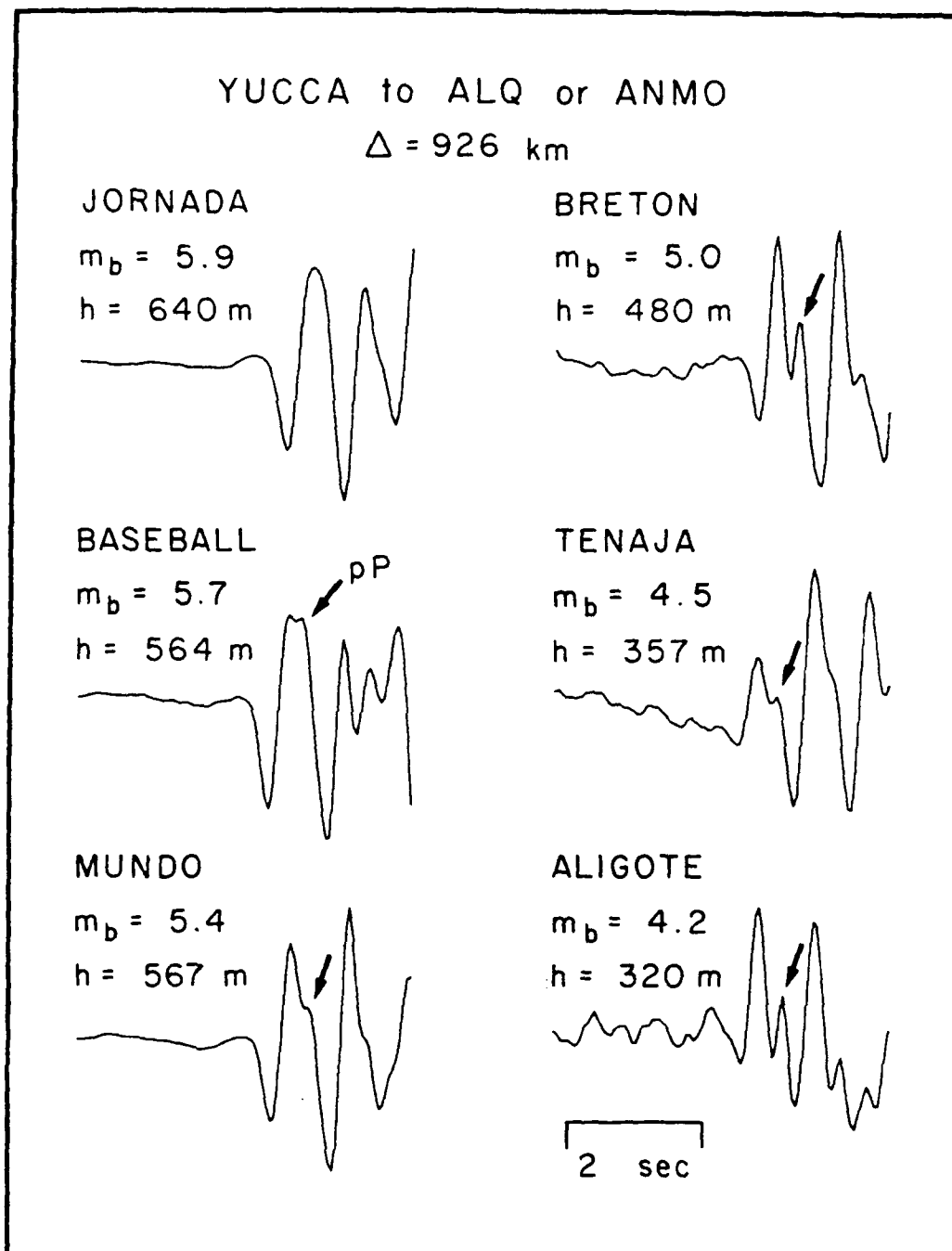


Figure 5.

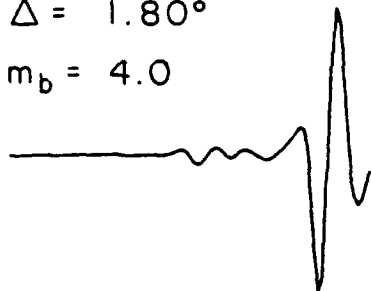
Observed P_n signals from Yucca events at DWSSN station ALQ. The split "c" swing is interpreted as the effect of pP_n . The differential P to pP time is again reduced. As events get larger, the increase in the duration of the source function washes out the pP effect.

RANDOMLY SELECTED EARTHQUAKE P_n ARRIVALS AT JAS

Oct. 1, 1982

$\Delta = 1.80^\circ$

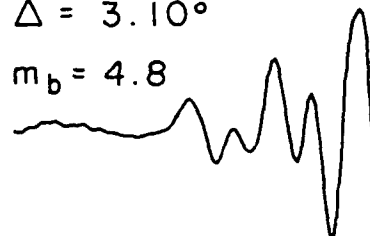
$m_b = 4.0$



Oct. 1, 1982

$\Delta = 3.10^\circ$

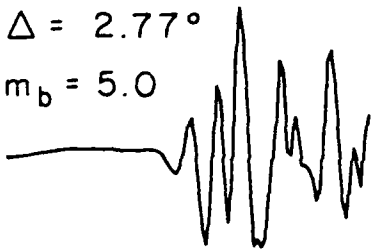
$m_b = 4.8$



Feb. 8, 1985

$\Delta = 2.77^\circ$

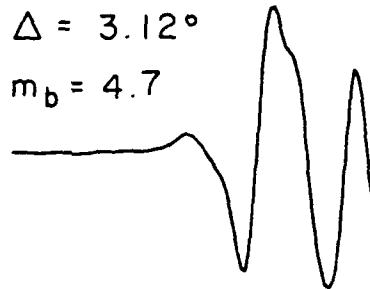
$m_b = 5.0$



Nov. 10, 1981

$\Delta = 3.12^\circ$

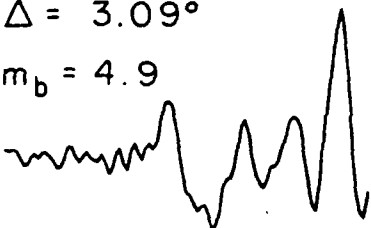
$m_b = 4.7$



Oct. 1, 1982

$\Delta = 3.09^\circ$

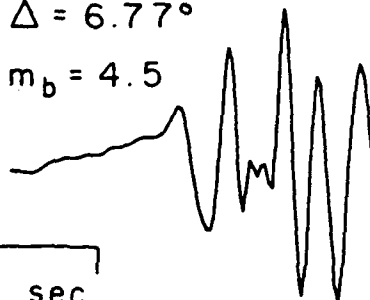
$m_b = 4.9$



July 24, 1981

$\Delta = 6.77^\circ$

$m_b = 4.5$



2 sec

Figure 6.

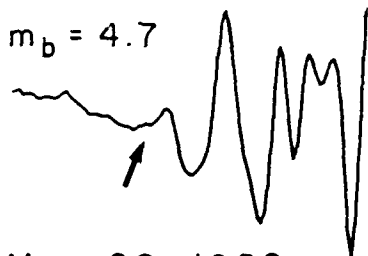
A data base of P_n signals from small earthquakes near NTS is being collected. These are the first 6 records collected from JAS.

RANDOMLY SELECTED EARTHQUAKE P_n ARRIVALS AT ALQ AND ANMO

May 24, 1982

$\Delta = 5.84^\circ$

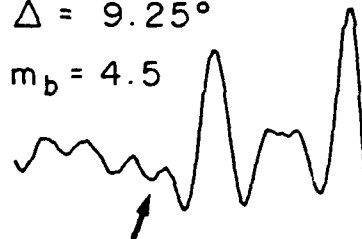
$m_b = 4.7$



Apr. 19, 1981

$\Delta = 9.25^\circ$

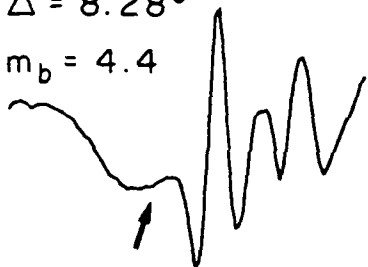
$m_b = 4.5$



Mar. 22, 1982

$\Delta = 8.28^\circ$

$m_b = 4.4$



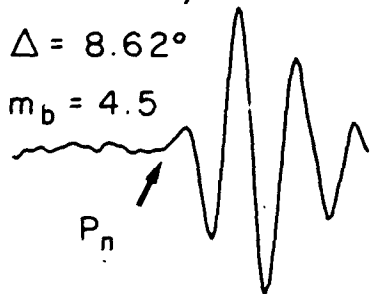
Oct. 1, 1982



JUNE 15, 1982

$\Delta = 8.62^\circ$

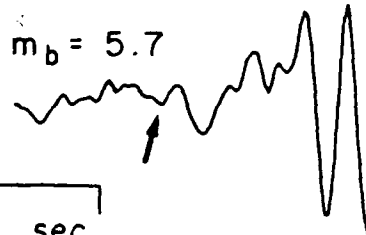
$m_b = 4.5$



Nov. 23, 1984

$\Delta = 10.01^\circ$

$m_b = 5.7$



2 sec

Figure 7.

A data base of P_n signals from small earthquakes near NTS is being collected. These are the first 6 records collected from ALQ.

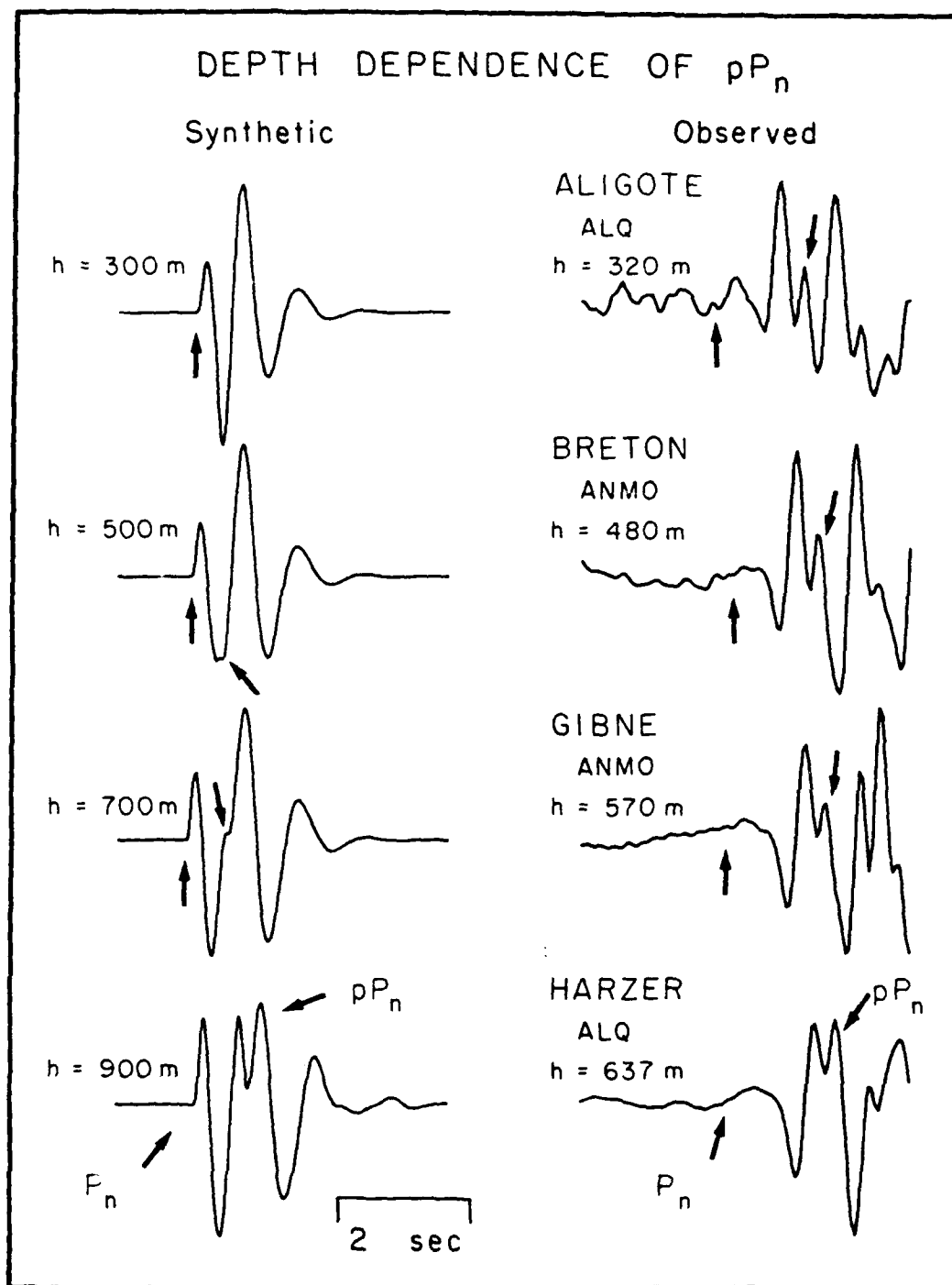


Figure 8.

A comparison of synthetic to observed ALQ records from NTS explosions. We assume that P_n is a simple turning ray in the lid, and perform a plane wave calculation using a structure for Pahute Mesa. The effective pP is obviously late.

EFFECTS OF DEPTH OF BURIAL AND TECTONIC RELEASE ON EXPLOSION AND EARTHQUAKE REGIONAL SEISMOGRAMS

K. McLaughlin, T. Barker, S. Day, J. Stevens, B. Shkoller
S-CUBED, P.O. Box 1620, La Jolla, CA. 92038-1620.

ABSTRACT

We have initiated a study of WUS velocity and attenuation models to compute synthetic regional phases. Wavenumber integration synthetics are used in an attempt to model the frequency dependent nature of explosion and earthquake regional phase amplitude-distance curves and spectral attenuation for regional phases in the basin and range. LRSM, VELA array, and LLNL regional data for NTS explosions and neighboring earthquakes are being examined for comparison with the synthetics. Focus has been placed on proposed spectral discriminants between shallow explosion sources and deeper earthquake sources.

Results from comparison of synthetics with observations suggest that frequency dependent crustal Q models will be needed to model Lg and Pg spectra. We find that synthetic Pg and Lg spatial attenuation is a good measure of the vertically averaged attenuation of the crust and is relatively insensitive to the depth dependence of the attenuation within the crust. The distance decay of the maximum Lg amplitudes are consistent with published rates of decay for the WUS. Consistent with other synthetic studies, the shallow explosion point source produces insufficient Lg motion at regional distances. Layering near the source is an inefficient mechanism for P-SV conversion at the proper phase velocities to contribute to Lg. The underestimate of Lg amplitudes relative to Pg amplitudes from shallow point explosions is particularly exacerbated when crustal attenuation is introduced into the synthetic models.

An interface between finite difference calculations and regional synthetic seismogram codes has been developed. A complete and accurate interface has been implemented for a wavenumber integration code to compute full waveform synthetics at regional distances. Tests are being made to examine non-linear processes as possible mechanisms for observed differences between explosion and earthquake regional seismograms. Analysis of synthetic P-waves from three non-linear finite difference calculations for a 125 Kt explosion at depths of 200, 680, and 980 m in a Pahute Mesa structure indicate that the P-waves from the overburied shot are relatively enriched in high frequencies w.r.t. the normal burial depth and the underburied shot. A study of synthetic teleseismic P-waves has been made to compare predicted waveform statistics to observed teleseismic $\log(P_{\max}/P_a)$ and $\log(P_b/P_a)$ statistics for events of several scale depths of burial in the Pahute Mesa and Shagan structures. Results indicate that although ratio of the "b" phase amplitude to the "a" phase amplitude is accurately predicted, the absolute P_{\max}/P_a ratio is under predicted.

As part of a general process of program validation, comparison was made between two approaches for computation of regional synthetic seismograms. The locked-mode modal summation was compared to results from a wavenumber integration code. Considerable differences have been found between the two approaches for realistic crustal and mantle Q structures for the WUS. Failure of the perturbation approximation for modal summation techniques can introduce significant errors when attenuation is introduced into the velocity model.

A COMPARISON OF LOCKED MODE AND WAVENUMBER INTEGRATION SYNTHETICS

Figure 1.1 and 1.2 show a comparison of regional synthetics computed using the locked mode approach and a wavenumber integration algorithm. For weak attenuation, it is found that the two methods give comparable results. However, when significant attenuation is introduced into the model, the locked mode approach can give unreliable results. In particular, those phases most affected by the attenuation may not be intuitively obvious.

FIGURE 1.1

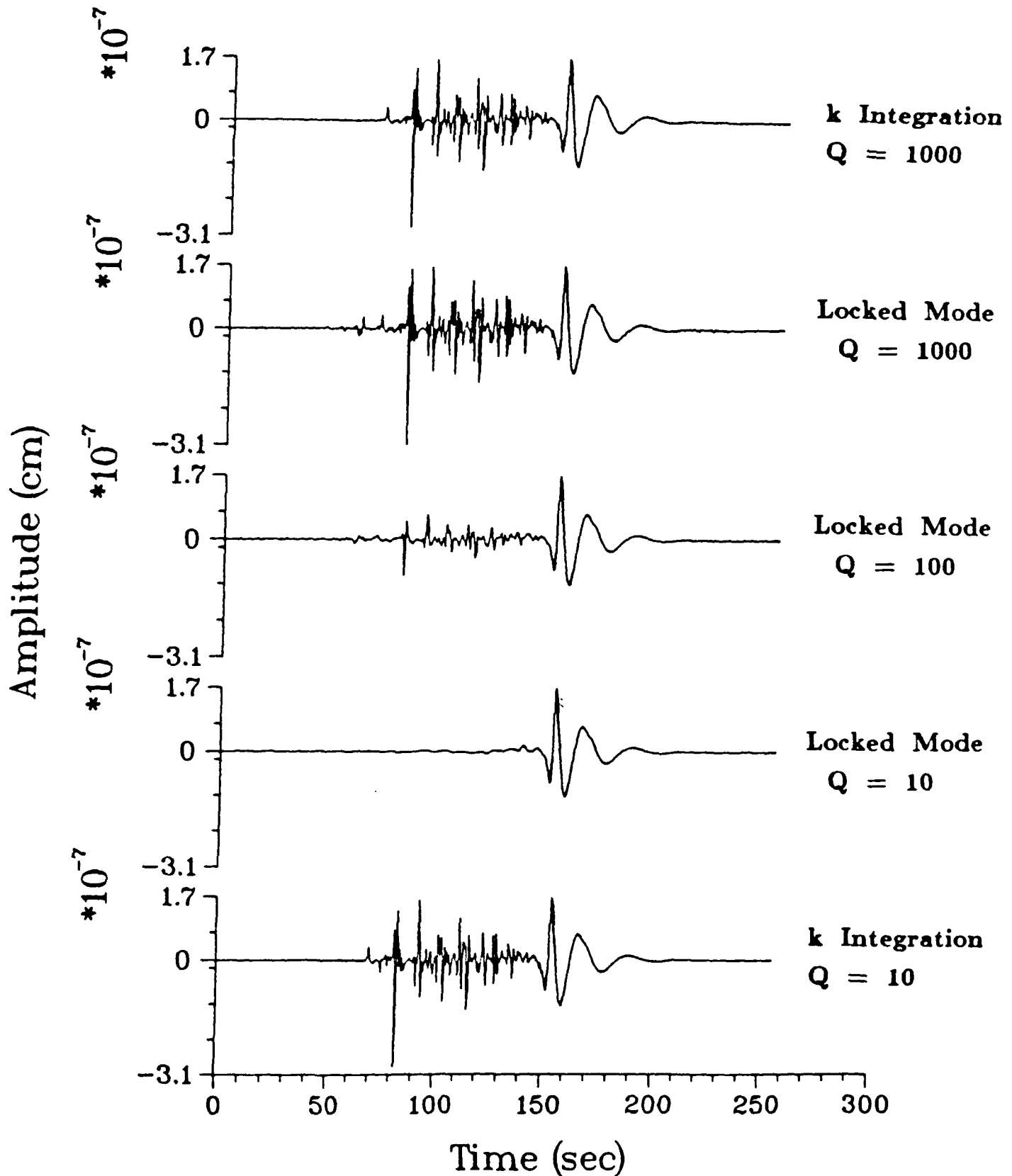
To illustrate this the first case, we have used a simple 1-layer crustal model over a half-space mantle (see Herrmann, 1985). We have introduced significant attenuation only into the mantle half-space. For shear wave Q 's greater than 1000, the differences are not noticeable, however, when shear Q 's of 100 to 300 are introduced into the mantle, the P_g phase is significantly attenuated in the locked mode synthetics. The L_g wavetrain is also affected to a lesser degree. The apparent explanation for the error in the locked mode synthetic is due to a break down in first order perturbation theory. The P-SV modes in the crust are coupled to the SV modes in the mantle and first order perturbation theory attributes attenuation to a wave group from all coupled modes.

FIGURE 1.2

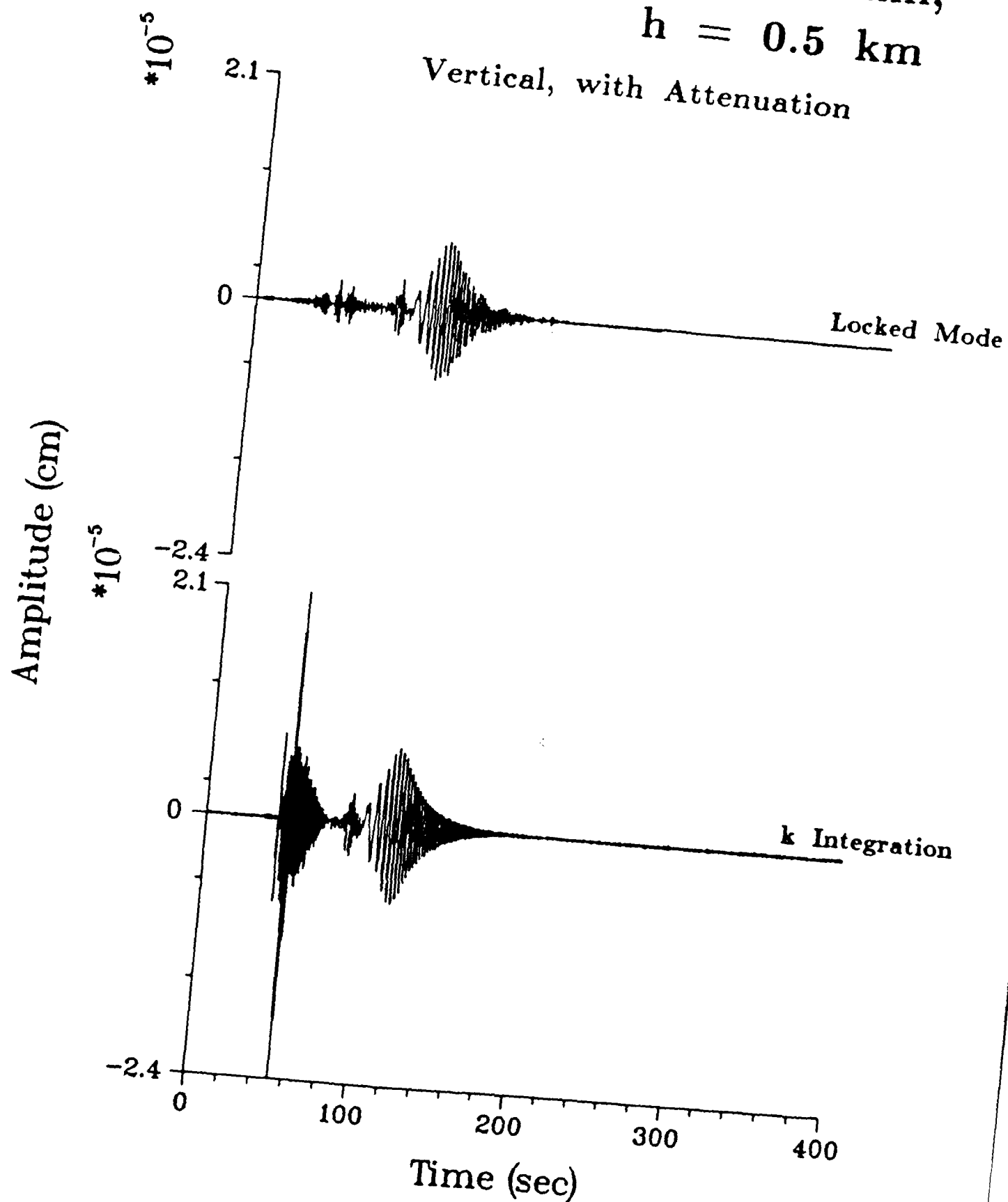
In the second case, a more realistic basin and range model has been used with a crustal shear Q of about 150 and a mantle low-velocity zone with low Q . The locked mode synthetic significantly underestimates the P_n and P_g amplitudes. The L_g wavetrain is also in error to a lesser degree.

Crustal Model

Vertical, Dist = 500 km, Depth = 10 km



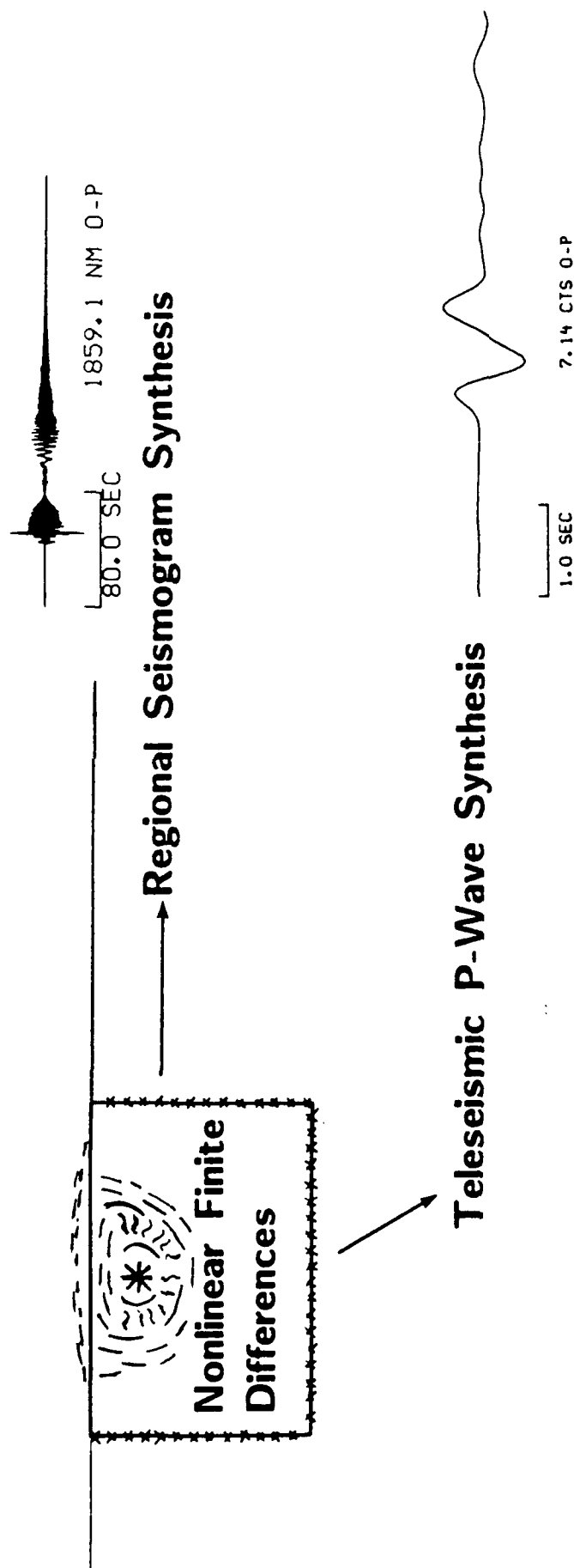
Explosion Source $\Delta = 300$ km,
 $h = 0.5$ km



DEPTH OF BURIAL AND P-WAVE SPECTRA

We have computed synthetic teleseismic P wave forms from 2-D non-linear finite difference calculations for 125 kt explosions in a Pahute Mesa structure at normal depth of burial (680 m), 44% over burial (980 m), and optimum cratering depth (200 m). Spectra for a take off angle of 10° are shown in Figure 2.3. The far-field P-waves for the two contained cases show a slight systematic enhancement of high frequencies for the over-buried case (see Figure 2.4). The spectral ratios of 680/980 burial depths have been log-averaged for take off angles of 10° , 20° , and 30° over selected frequency bands. The relative enhancement is in agreement with predictions of Murphy (1977) for explosions in saturated tuff (solid line in Figure 2.4).

For comparison, the predicted spectral ratio of a normally buried explosion at 200 m versus the same yield at 500 m is shown in Figure 2.5. Enhancement of high frequencies by a factor of 3 is predicted for 5 Kt shots over buried 100% based on empirical scaling laws for saturated tuff and a published velocity model for Pahute Mesa. However, NTS tuffs at such depths are generally unsaturated and no reliable scaling laws have been derived for explosions under such conditions.



OBJECTIVE:

Formulate a physical basis for discriminants between explosions and earthquakes.

METHODOLOGY:

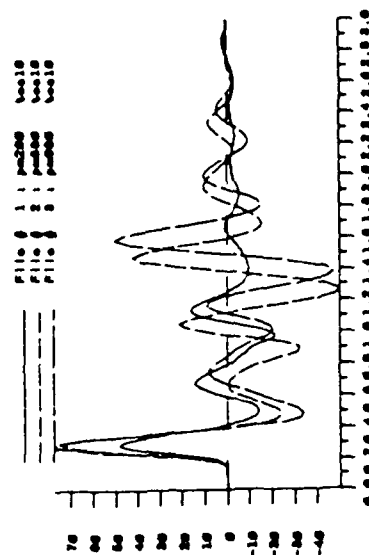
Using physical models for explosions and numerical wave propagation theory model teleseismic and regional synthetics.

FIGURE 2.1

NONLINEAR FINITE DIFFERENCE MODEL FOR 125 KT EXPLOSION

- 200 m Crater
- 680 m Normal depth
- 980 m Overburied

Pahute Mesa Tuff Model



Teleseismic P-Waves
10° Takeoff Angle

Conclusion: 980 m depth has relative enrichment in H.F. w.r.t. 680 m for all takeoff angles.

FIGURE 2.2

SYNTHETIC TELESEISMIC P-WAVE SPECTRA
PAHUTE MESA TUFF MODEL, 125 KI, TAKEOFF ANGLE 10°

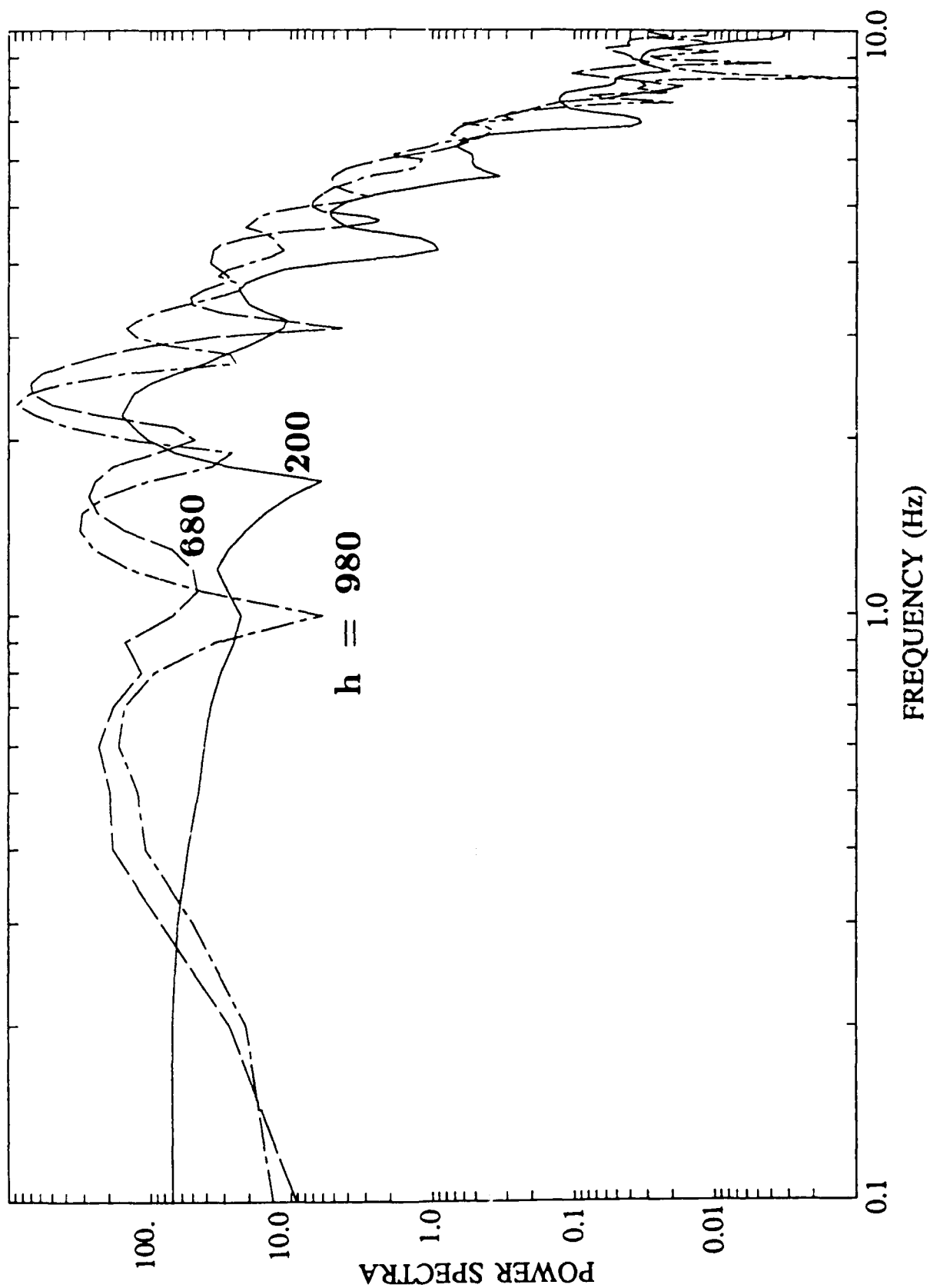


FIGURE 2.3

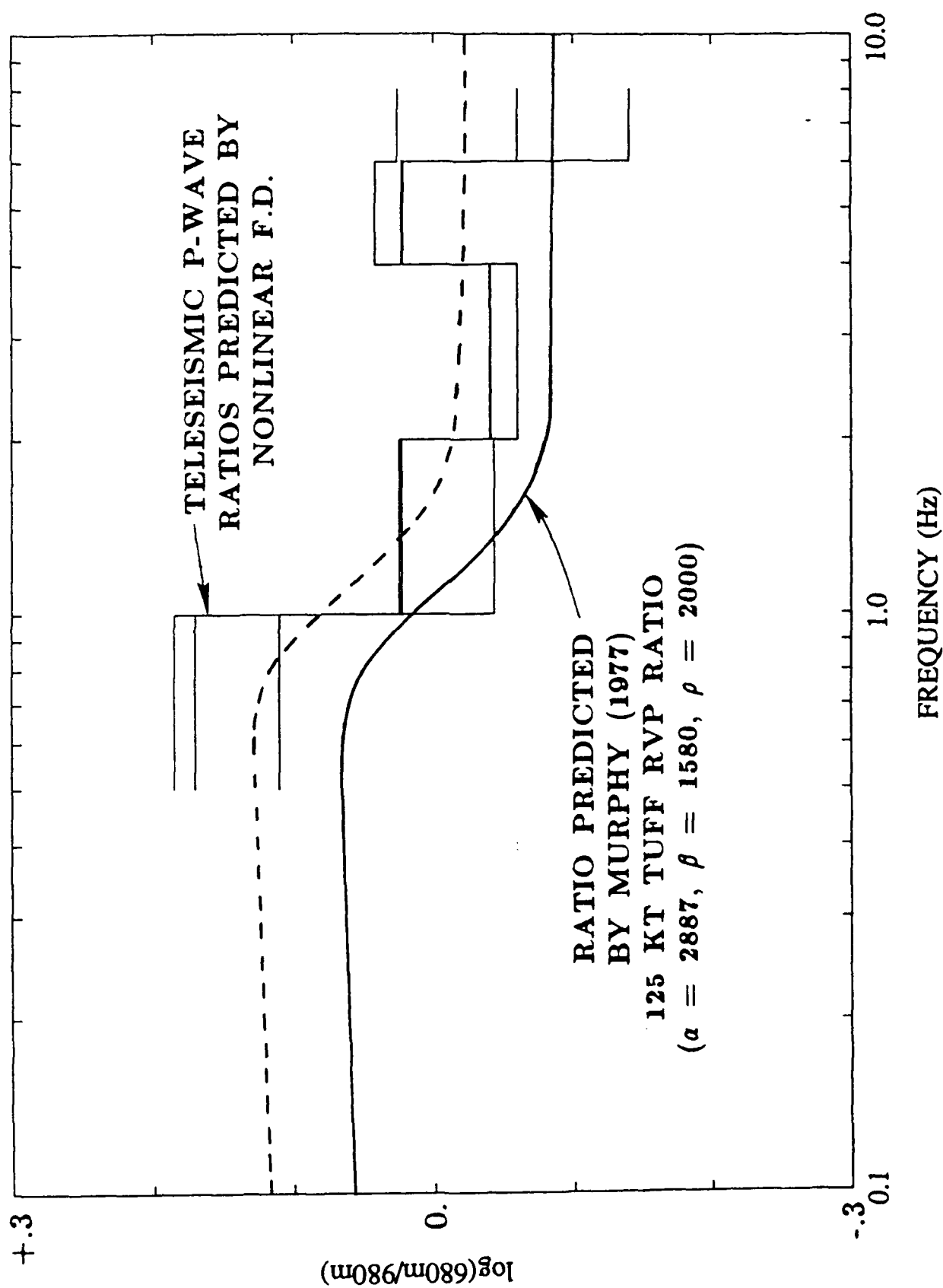
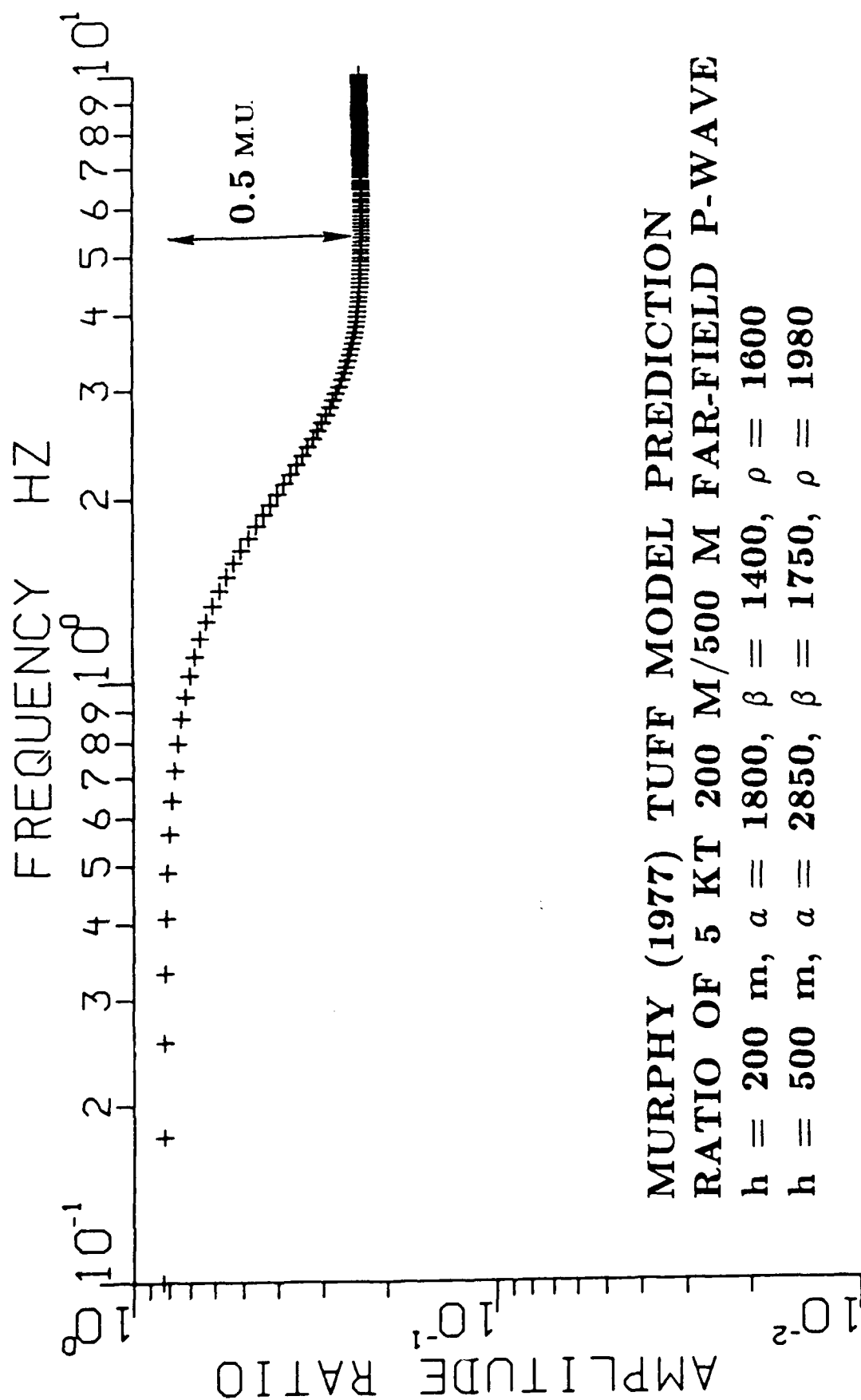


FIGURE 2.4



MURPHY (1977) TUFF MODEL PREDICTION
 RATIO OF 5 KT 200 M/500 M FAR-FIELD P-WAVE

$h = 200$ m, $a = 1800$, $\beta = 1400$, $\rho = 1600$

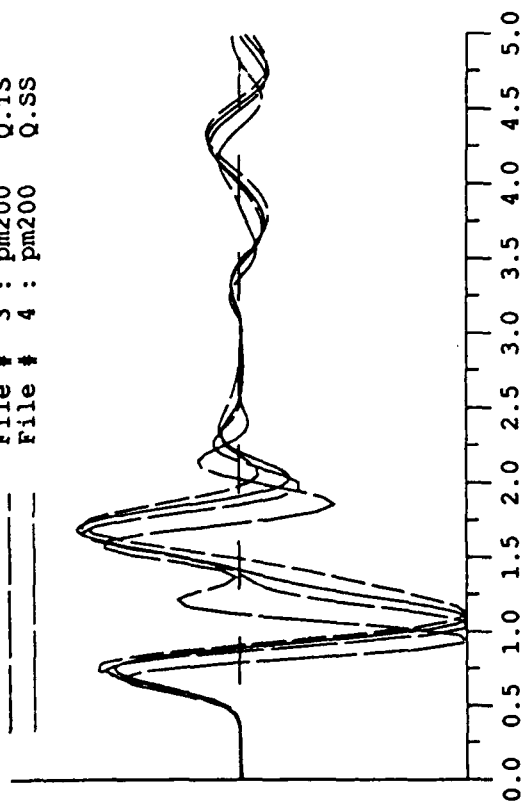
$h = 500$ m, $a = 2850$, $\beta = 1750$, $\rho = 1980$

FIGURE 2.5

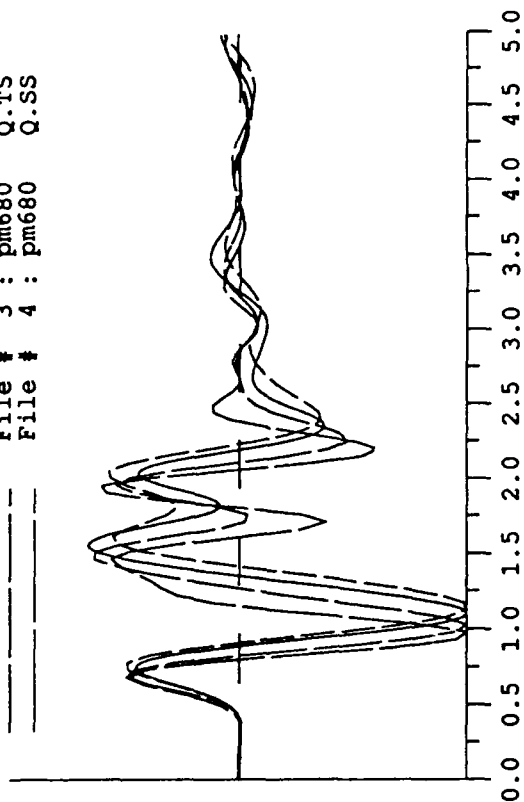
DEPTH OF BURIAL AND TELESEISMIC WAVEFORMS

Predicted waveforms from 2-D non-linear finite difference simulations are compared with observed statistics for WWSSN waveforms from NTS (Figure 3.1 and 3.2) and Shagan River. It is found that the predicted relative amplitude of the "Pa" phase to the "Pb" phase ($\text{Log}(\text{Pb}/\text{Pa}) = 0.2$ to 0.3) is in agreement with observations, while the relative motion of the maximum P motion, "Pmax", is generally underestimated ($\text{Log}(\text{Pc}/\text{Pa}) = 0.2$ to 0.3 versus 0.4 to 0.6). Observations and predictions for contained as well as cratering shots in the 100 Kt range are shown in Figure 3.3. This may indicate that non-linear models over estimate the effects of non-linearities above the shot that attenuate and delay the "pP" phase. Figure 3.4 shows comparison of deconvolved Shagan River events recorded at EKA compared to predictions from non-linear finite differences. The agreement in general waveform shape is good for the cratering event (19650115) but the contained shots show a larger "pP" than predicted.

File # 1 : pm200 tstar.5
 File # 2 : pm200 Q.TT
 File # 3 : pm200 Q.TS
 File # 4 : pm200 Q.SS



File # 1 : pm680 tstar.5
 File # 2 : pm680 Q.TT
 File # 3 : pm680 Q.TS
 File # 4 : pm680 Q.SS



File # 1 : pm980 tstar.5
 File # 2 : pm980 Q.TT
 File # 3 : pm980 Q.TS
 File # 4 : pm980 Q.SS

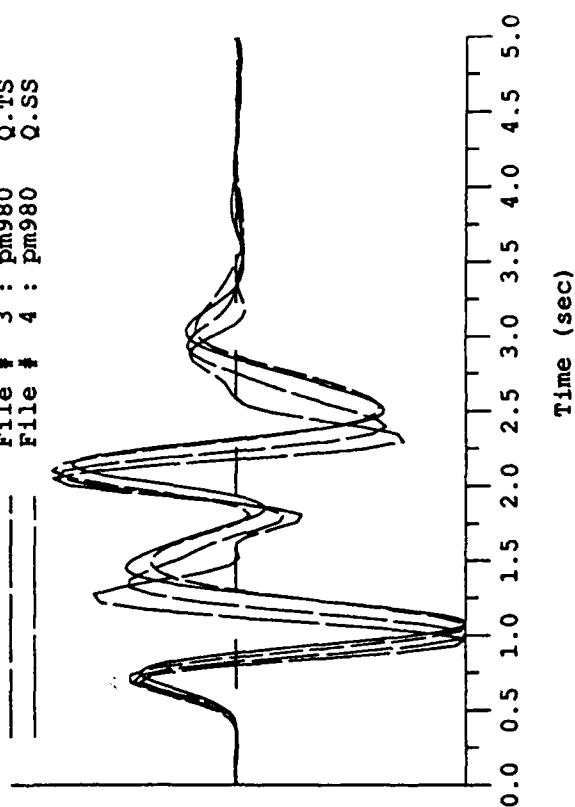


FIGURE 3.1 WWSSN far-field P-wave synthetics (125Kt) for Pahute Mesa model sources at three scale depths (200, 680, 980 m), take-off angle 10 degrees, and several different t^* models.

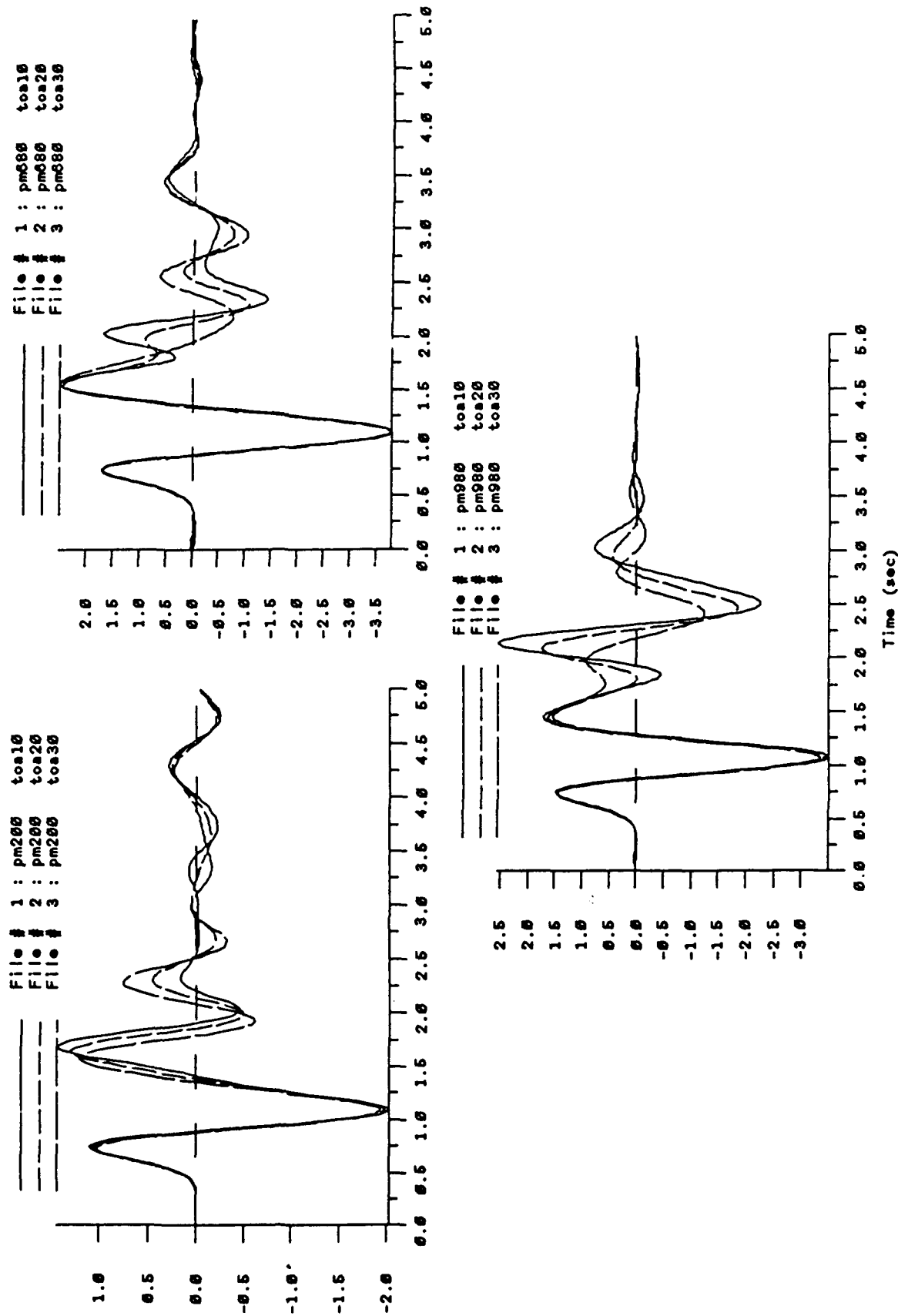


FIGURE 3.2 WWSSN far-field P-wave synthetics (125 Kt) for Pahute Mesa model sources at three scale depths (200, 680, and 980 m), $t^* = 0.5$ s, and different take-off angles of 10, 20 and 30 degrees.

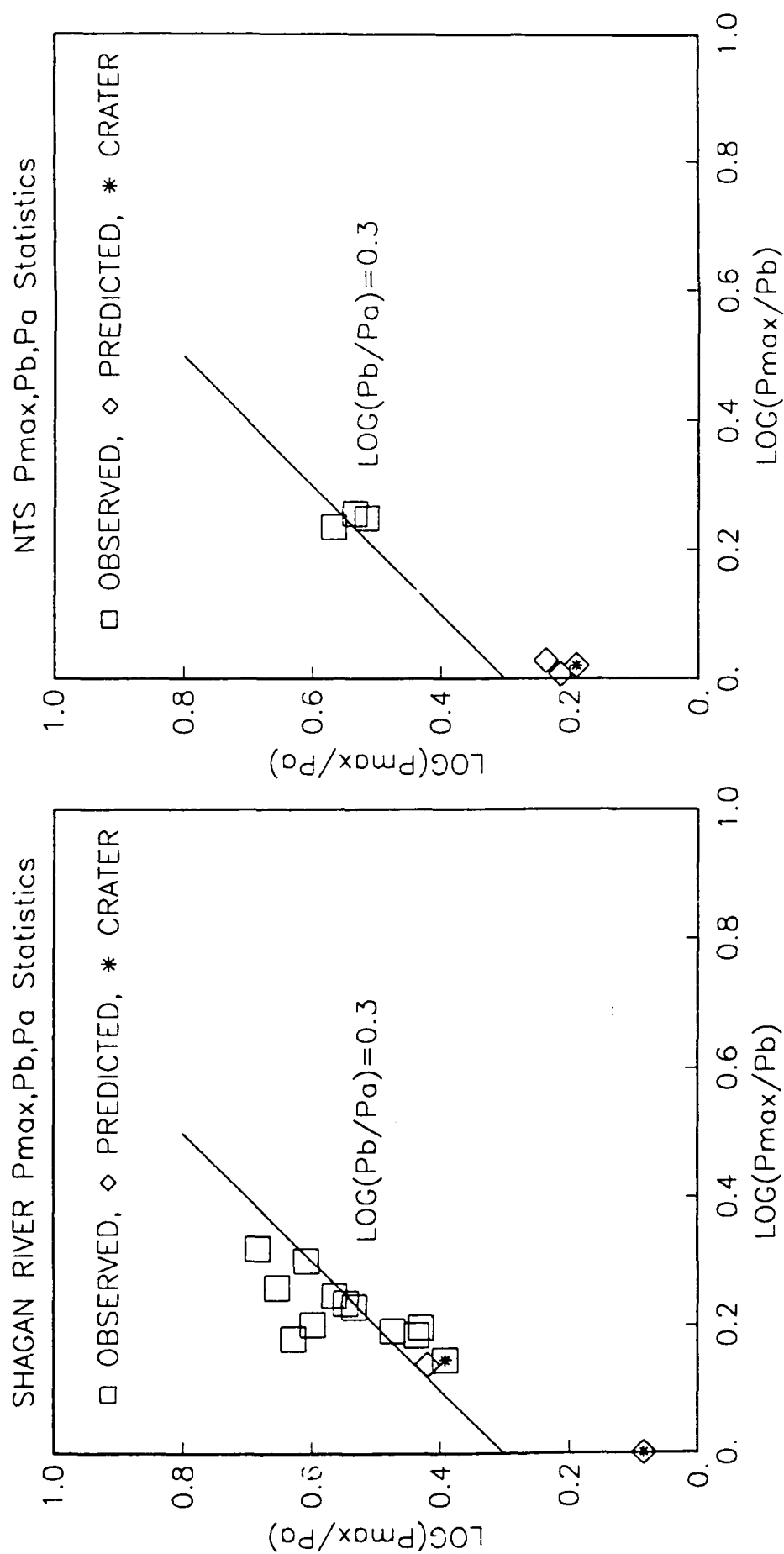
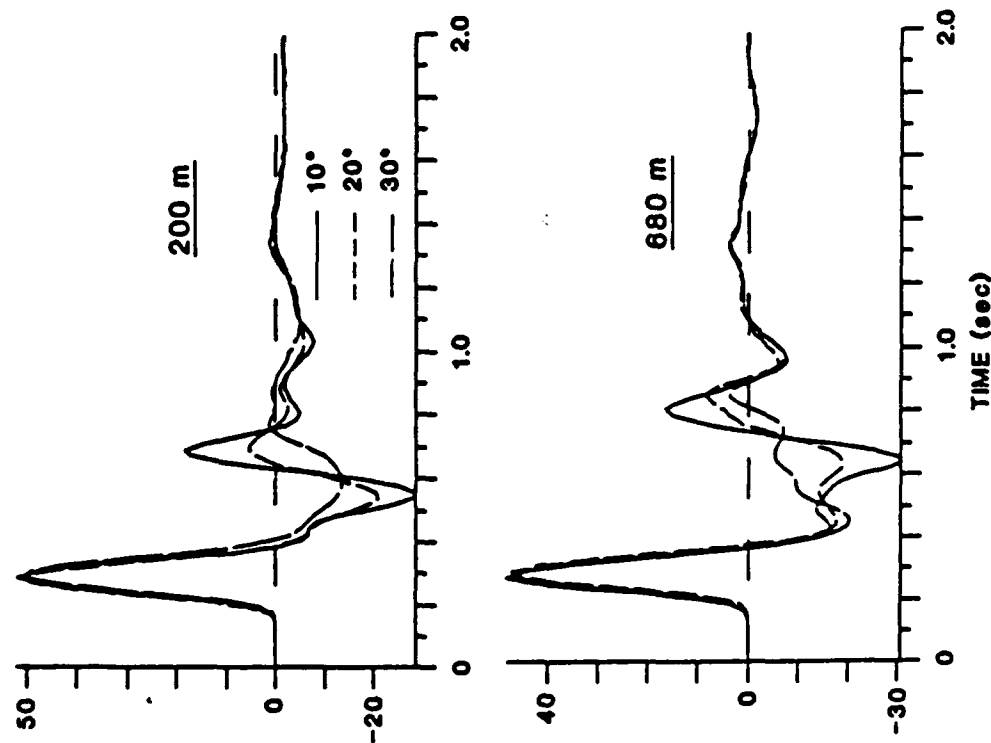


FIGURE 3.3 Observed WWSSN waveform statistics for $\text{Log}(P_{\text{max}}/P_a)$ and $\text{Log}(P_{\text{max}}/P_b)$ are compared to predictions for the non-linear 2-D finite difference calculations for contained and cratering shots in the 100 Kt range. Although the $\text{Log}(P_b/P_a)$ statistic is generally in the correct range, the "c" phase (P_{max}) is generally under estimated by the non-linear calculations.

Far-field P waveforms for 2-D simulations shown as a function of take off angle. No attenuation or instrument response is included.



Deconvolved Source Functions EEKTS Events Recorded at EKA

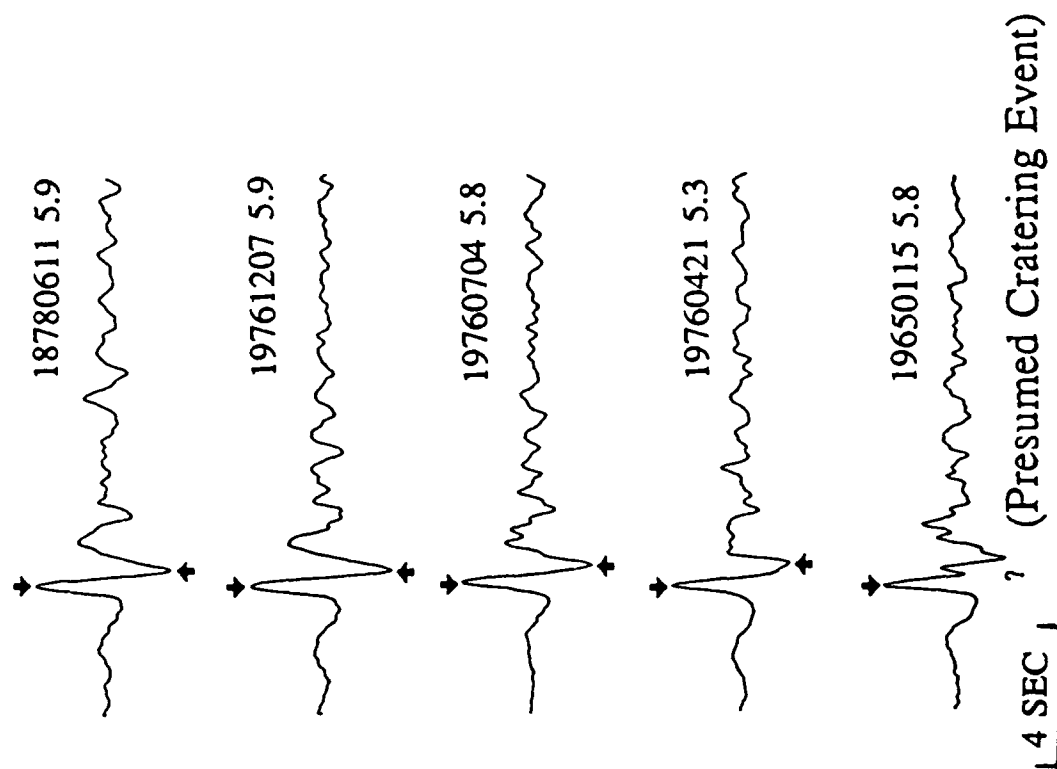


FIGURE 3.4 Comparison of deconvolved Shagan River records to 2-D non-linear simulations.

DEPTH OF BURIAL AND SV GENERATION

Figure 4.1 shows predicted far-field P and SV waveforms (at 30° take off angle) for a 125 Kt explosion buried 200 m, 680 m, and 980m based on 2-D non-linear calculations compared to the placement of an equivalent RDP point source based on a 1-D non-linear calculation. This take off angle which corresponds to regional slownesses for P and S waves illustrates that the 2-D model does not produce substantially larger SV radiation than a point source. From the SV spectra (Figure 4.2) we can see that the 2-D models predict less SV at normal containment depths than the the point source. The primary source of SV appears to be the conversion from the free surface, and the non-linear calculations predict that there will be attenuation above the source. The direct SV from the 2-D source (the negative first arrival on the 2-D waveforms, absent on the 1-D waveforms) is small compared to the converted P-SV (the largest arrival). The cratering explosion exhibits the least amount of SV radiation at this take off angle. There is some suggestion that the non-linear 2-D explosion models predict a "lower" frequency SV source which could contribute to discrimination.

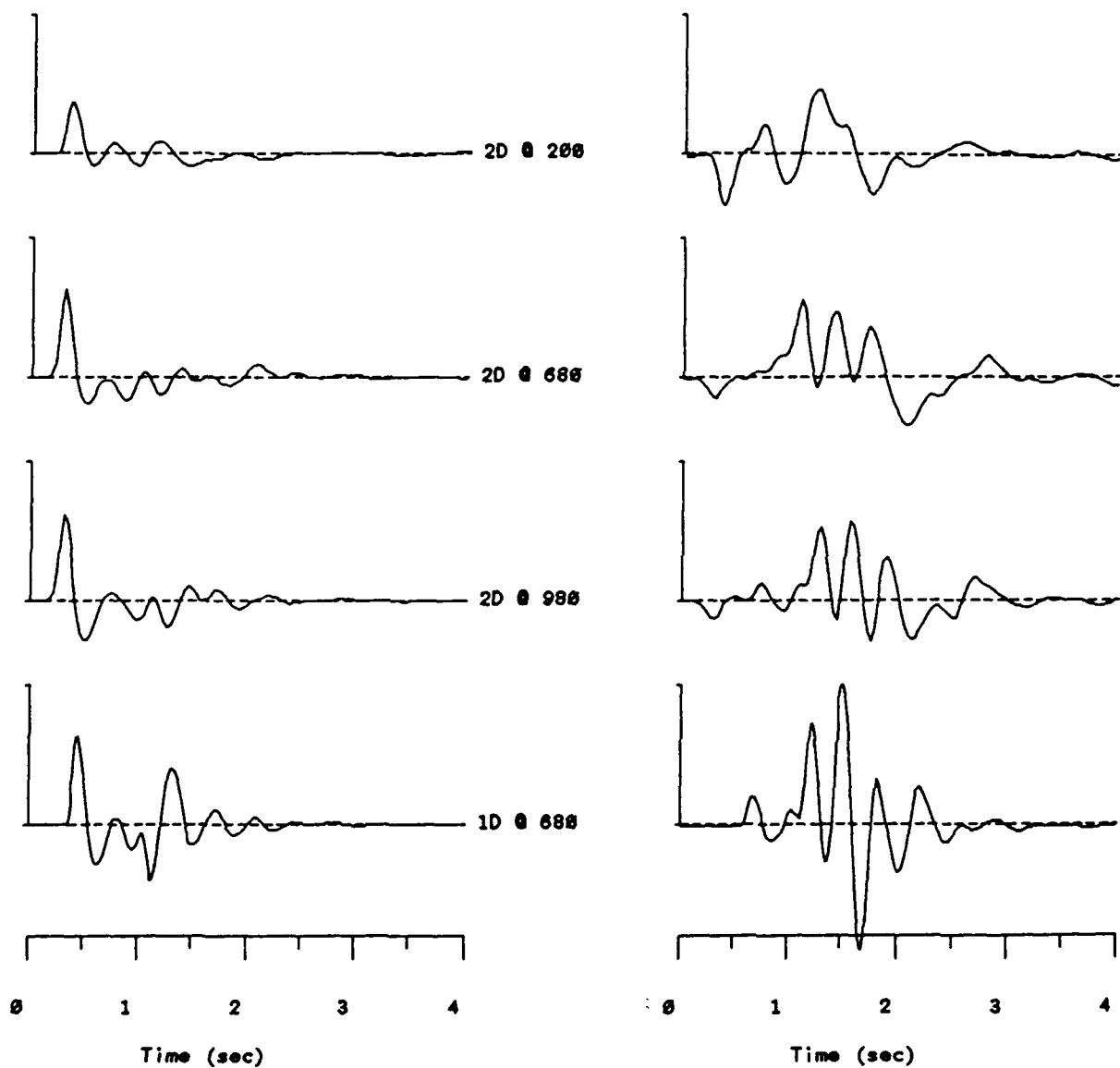


FIGURE 4.1 Far-field P (left) and SV (right) waveforms for 2-D simulations at 200 m (top), 680 m, and 980 m, and a 1-D simulation at 680 m (bottom). Note direct SV from 2-D simulations absent in 1-D simulation (point source Green's function). All waveforms are at the same scale.

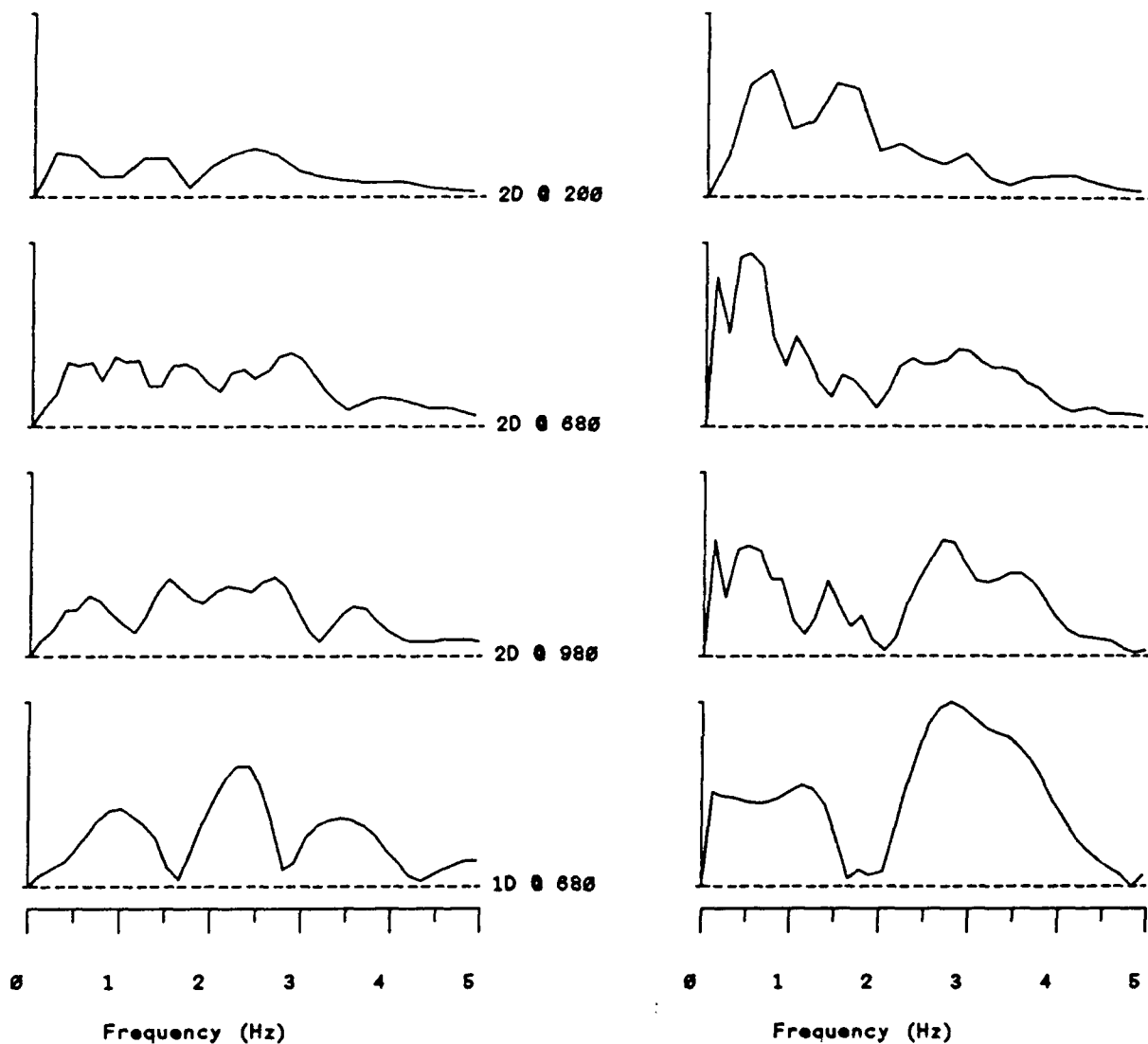


FIGURE 4.2 Spectra (linear-linear) of waveforms in FIGURE 4.1. Note the high frequency SV enhancement for 1-D simulation. Also, the P+pP scalloping is less pronounced for the 2-D simulations. All spectra are shown on the same scale.

GEOPHYSICAL STRUCTURE AT PAHUTE MESA, NEVADA

Poster Presentation for the
10th Annual AFGL/DARPA Seismic Research Symposium

by

John F. Ferguson, Allen H. Cogbill*, Russell J. Heidesch and

Herbert D. Axilrod

The University of Texas at Dallas

Richardson, TX

Contract Number F19628-87-K-0029

Objective: To determine the geophysical structure, above 5 km, on a transect across Pahute Mesa, Nevada. Borehole, gravity and seismic data from a wide angle refraction survey and nuclear tests are used to constrain the geophysical model.

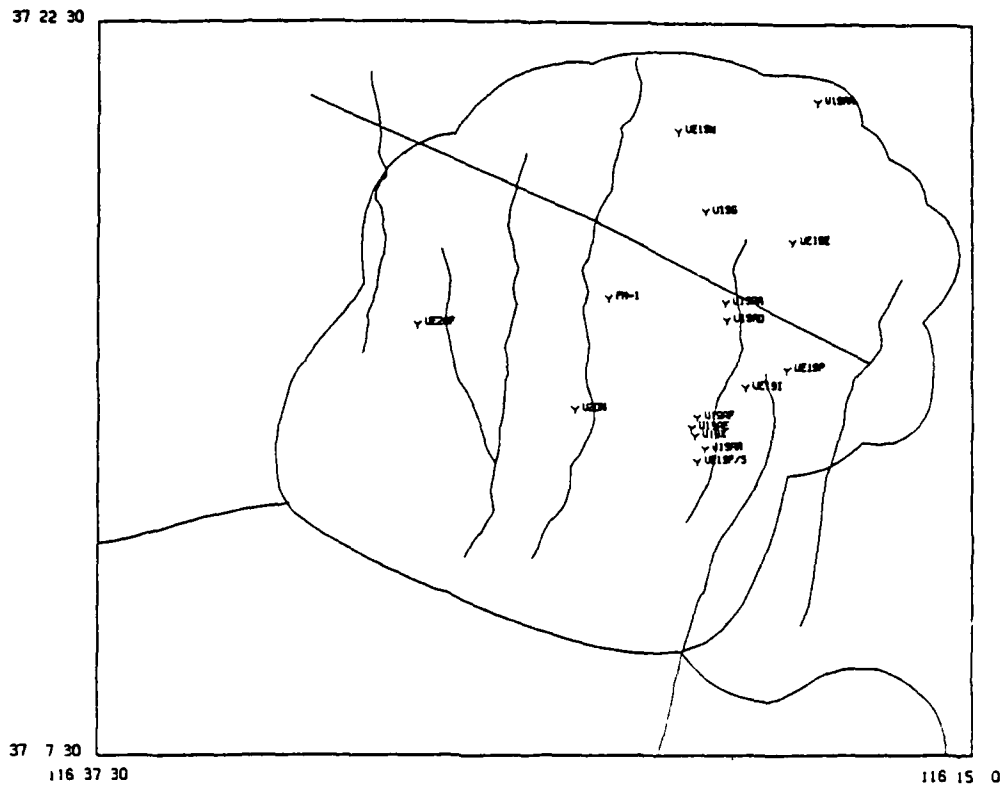
* Los Alamos National Laboratory, Los Alamos, NM

Abstract

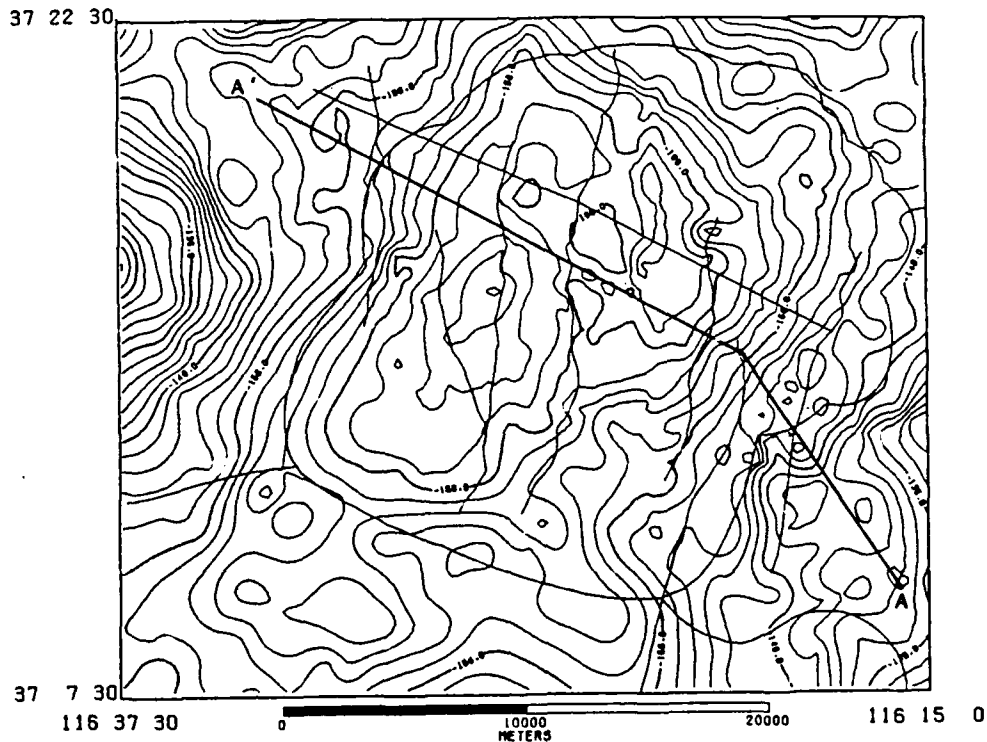
The University of Texas at Dallas and Los Alamos National Laboratory have collaborated in producing new gravity data and a seismic refraction profile, which permit a detailed 2D model of a transect in the southeast portion of the Silent Canyon caldera. The unreversed seismic refraction profile extends 15 km northwest from a single shot point located outside of the Silent Canyon structure. A five unit classification of rocks at this location is possible from an analysis of well logs and other geophysical data. Four volcanic units overlie Belted Range "basement" rocks and Mesozoic intrusives or Paleozoic sediments may underlie the volcanics.

Richard Warren at Los Alamos has compiled a new geologic cross-section along the seismic line, based on extensive petrologic and geochemical studies. This profile has been modified to fit the observed gravity data using the geophysical rock unit classification. Forward modeling exercises using 2D ray tracing and acoustic psuedospectral calculations have further modified the profile to fit the seismic refraction data. The model indicates a thickness of over 1.5 km of younger volcanics over the Belted Range rocks and a sequence of major faults stepping down to the west from the caldera boundary. The parametric model produced by this process should ultimately be useful in seismological studies of explosion source properties.

In February 1988, four seismic stations were occupied on the transect to record the nuclear test Kernville. These data, plus stations recording Almendro, Boxcar, Farm and Scotch, will serve to reverse the seismic line and permit a refined model of the deeper Belted Range structure.

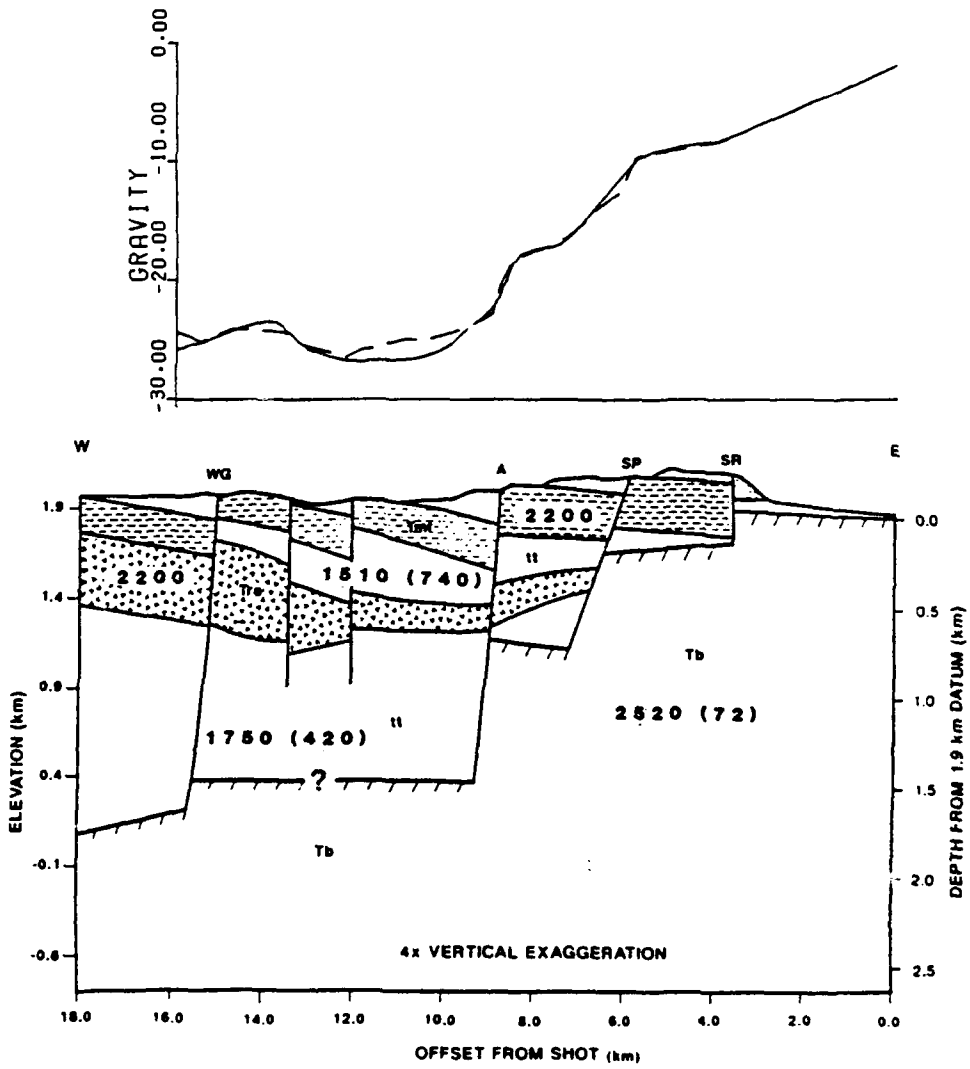


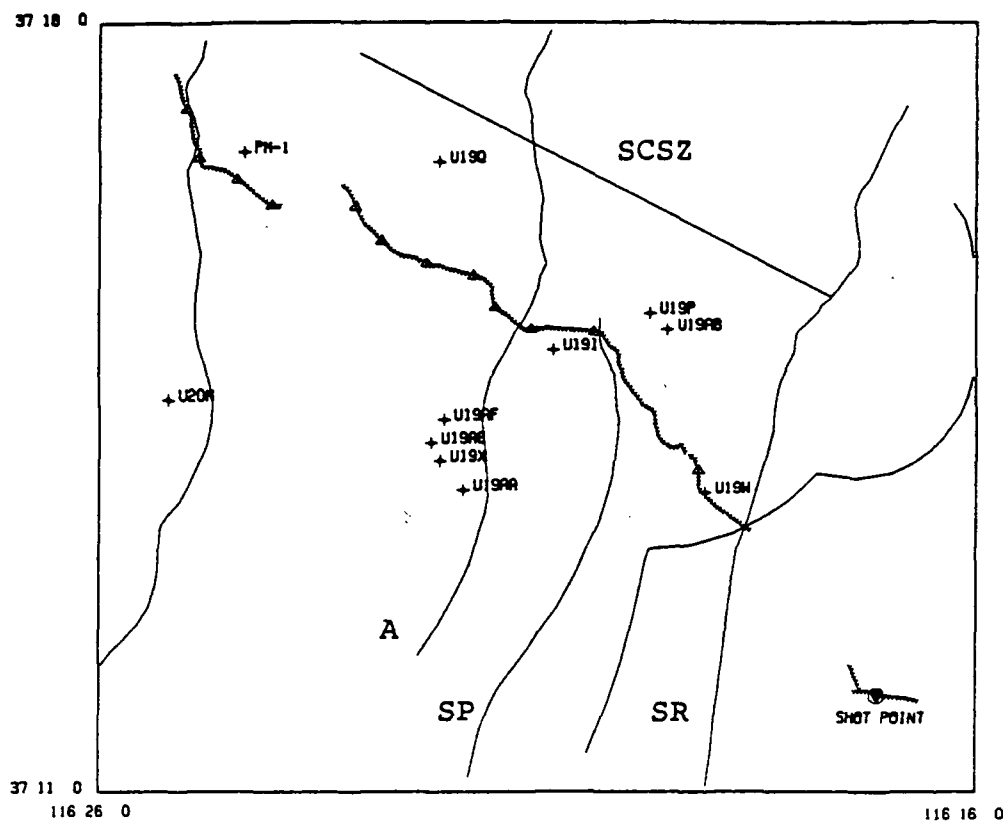
Locations of boreholes used for stratigraphic control and geophysical log analysis.



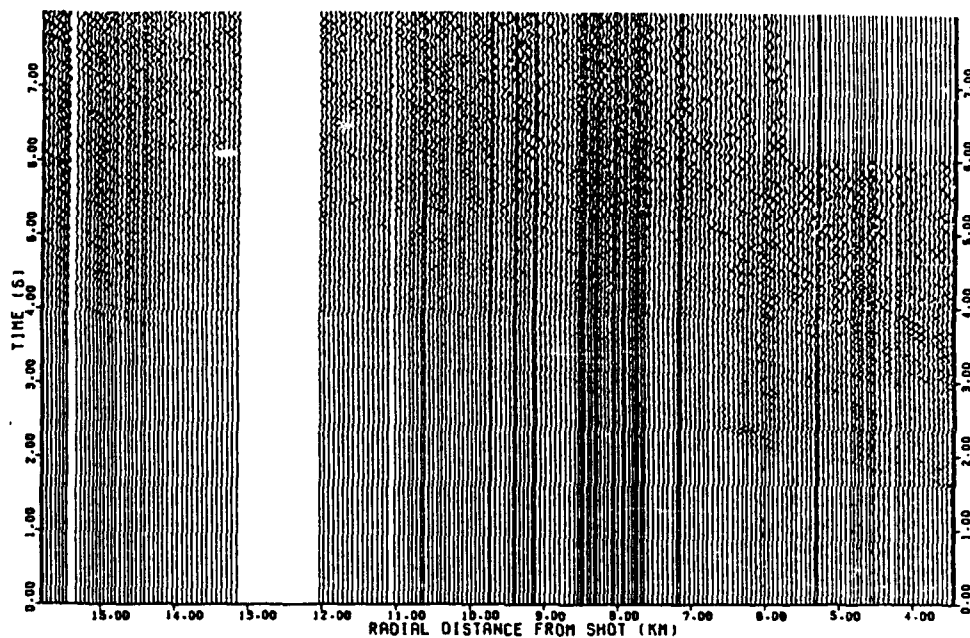
Complete Bouguer anomaly map of Pahute Mesa, Nevada using merged USGS, UTD and LANL gravity data. Contour interval is 2 mGal and the reduction density is 2000 kg/m^3 . The outline of the Silent Canyon caldera and major north-south trending faults are shown for reference. The profile marked A to A' is close to the seismic line and is used to improve the geologic profile through gravity modeling.

Geologic cross section and gravity model along the seismic line. The geologic interpretation is by R. G. Warren at Los Alamos. Important control comes from boreholes PM-1, U19g, U19i, U19p and Ue19w. Indicated faults are Split Ridge (SR), Scrugham Peak (SP), Almendro (A) and West Greeley (WG). Indicated geologic units are Rainier Mesa member of the Timber Mountain tuff (Tmr), caldera fill tuffs (tt, an informal symbol), Area 20 lavas (Tra) and the Belted Range tuff (Tb). The profile is 4 times vertically exaggerated. The observed (solid line) and theoretical (dashed line) residual anomalies are shown above the model. The density functions used in the model are indicated by the surface density value with the gradient (if non-zero) in parentheses. The density functions are based on the log analysis of Ferguson and Reamer (1987). The rms error between observed and theoretical anomalies is 0.7 mGal (2.6% error), with a maximum error of 1.8 mGal (6.7% error). The large misfit between 10 and 12 km offset is a function of shallow high density bodies. The shallow units, especially the Tra, are quite variable, but they have been modeled as homogeneous.

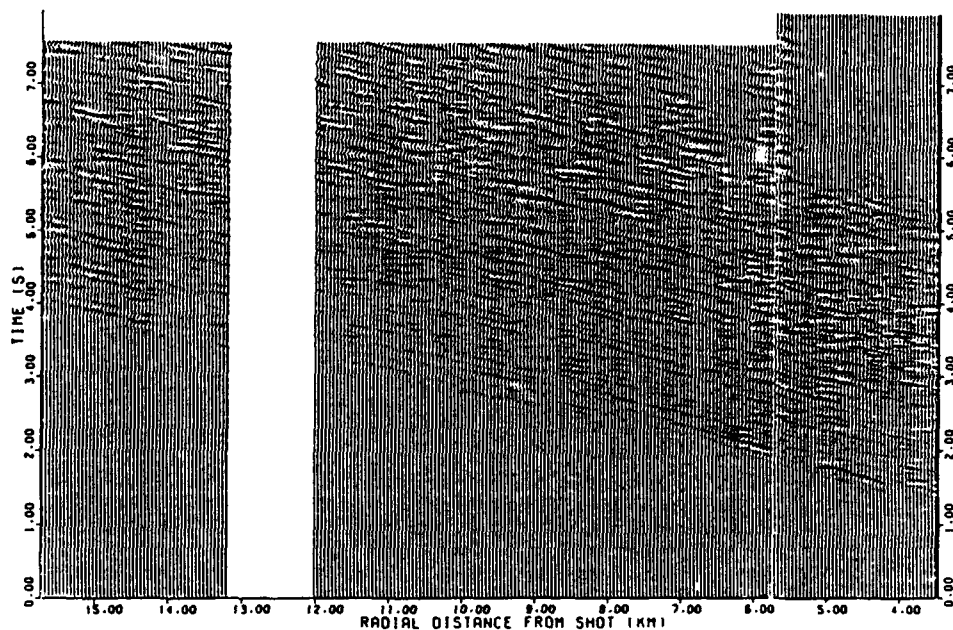




Location map of the 1986 UTD-LANL wide angle seismic survey. The hatched line indicates the geophone group locations and the triangles indicate Dinoseis shot points. The labeled boreholes have geophysical logs for control on the shallow structure. Indicated faults are the Split Ridge (SR), Scrugham Peak (SP), Almendro (A) and Silent Canyon shear zone (SCSZ).

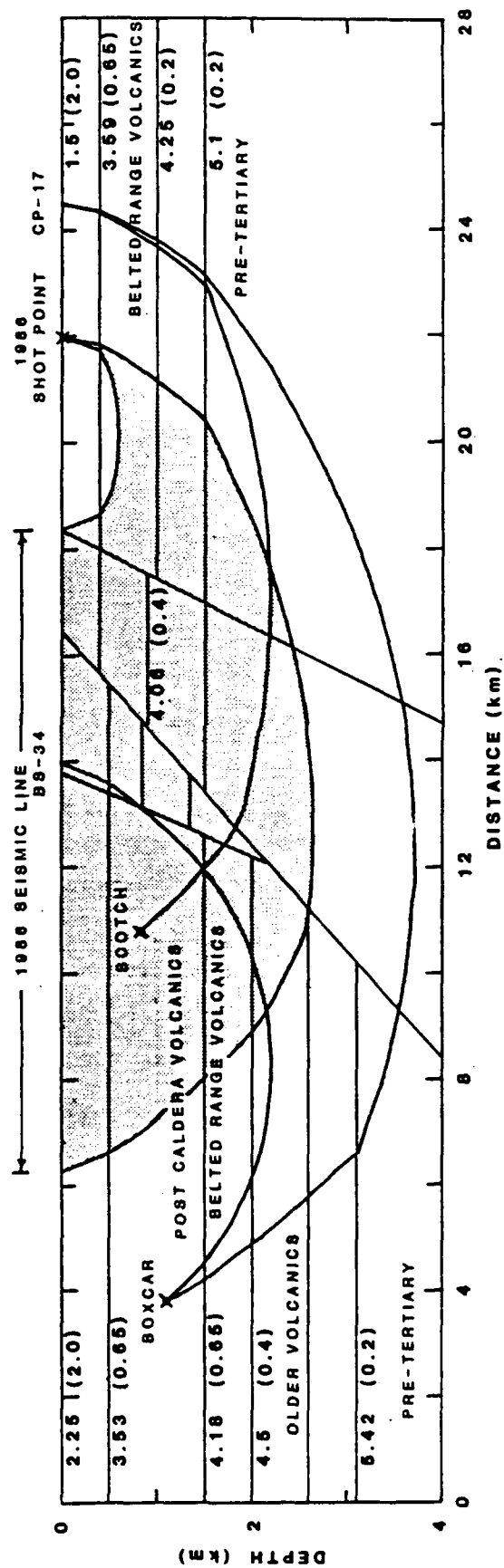


Trace normalized section plot of the 1986 UTD-LANL wide angle seismic survey. The data are corrected to a 1.9 km elevation datum assuming a velocity of 1.3 km/s at the source and 1.9 km/s velocity at the receivers.

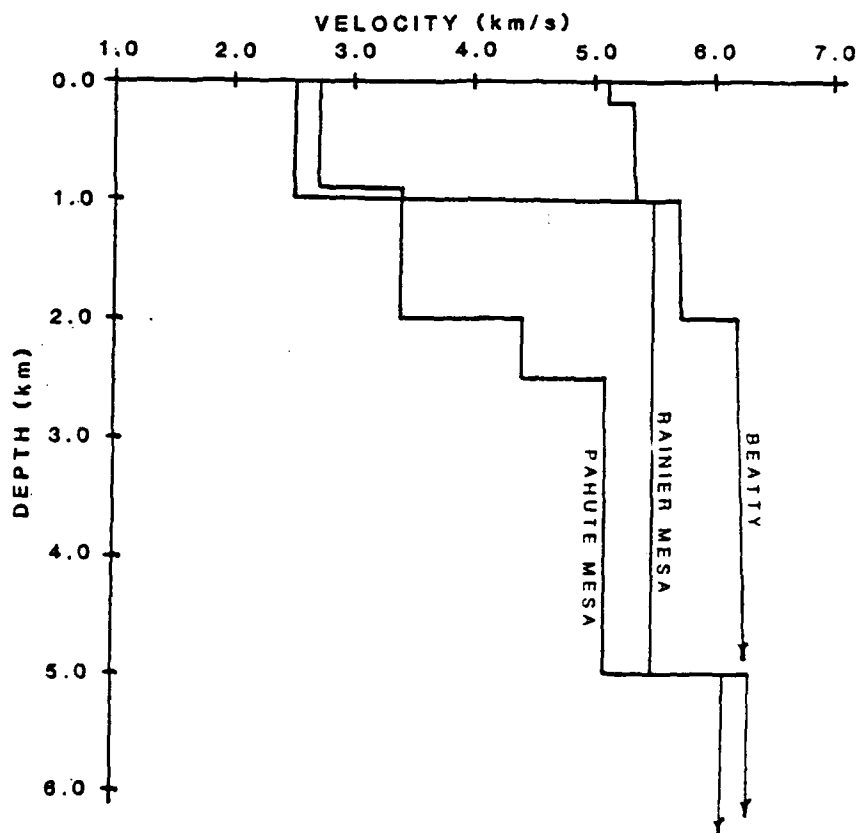
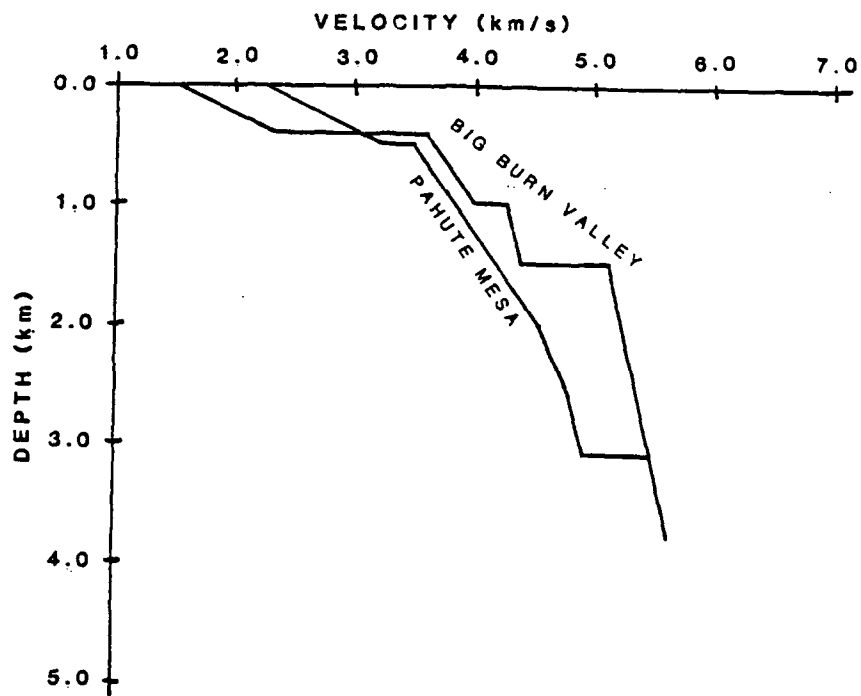


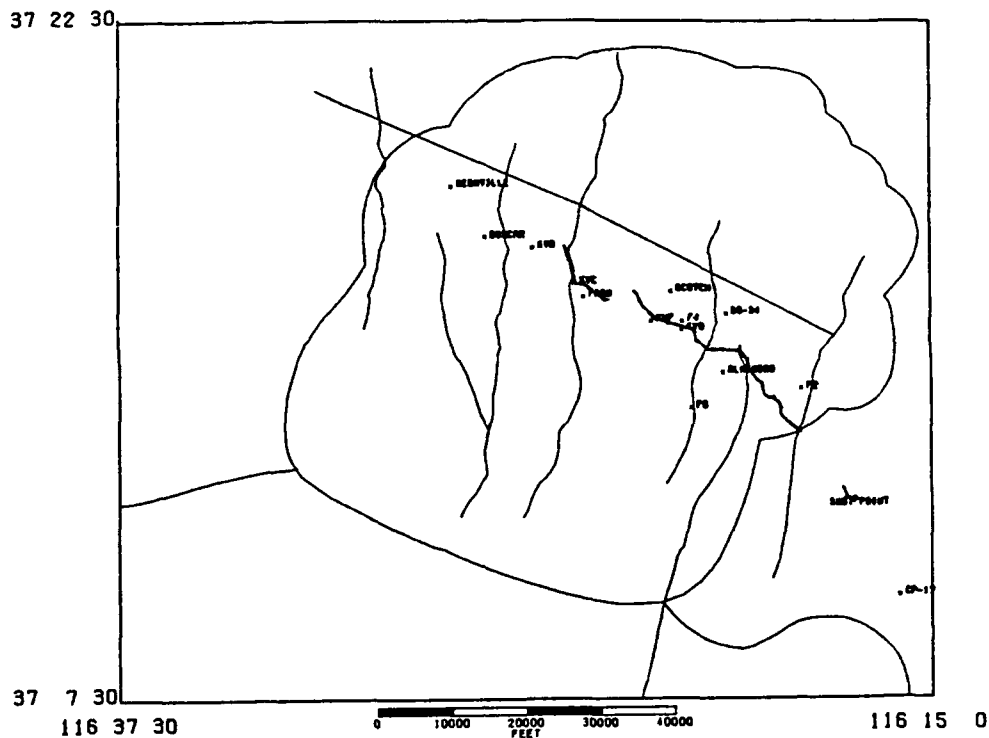
Bandpass and p - τ filtered seismic section. Pass band from 6 to 28 Hz and slowness limits from -0.1 to 0.3 s/km. Events with high phase velocities are enhanced in this section, with incoherent noise somewhat suppressed.

Preliminary P-wave velocity model for the Pahute Mesa transect, based on first arrivals only. The surface is drawn at a 1.9 km elevation datum. Assumed geologic units are indicated. The pre-Tertiary could be variously Paleozoic sediments, Mesozoic intrusives or high velocity Tertiary intrusives under the caldera. The details of the faulting are to be considered schematic only. The model produces agreement with observed travel times to within ± 0.1 s. Structure in the faulted zone is controlled by rays from the 1986 wide angle survey. Deeper structure is controlled by rays from Scotch and Boxcar to CP-17. Within the caldera, data from Farm and Boxcar are in agreement with the velocity structure of Leonard and Johnson (1987).

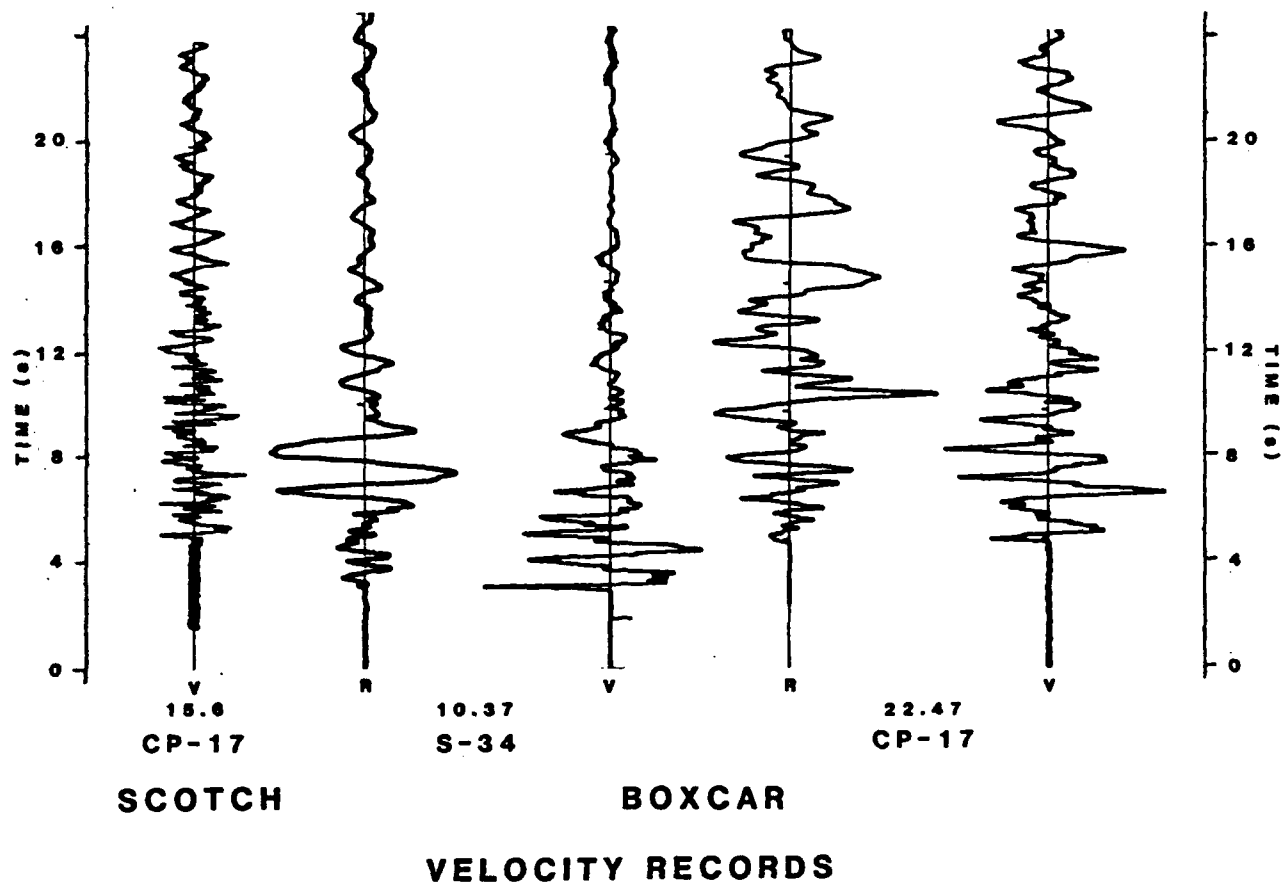


Velocity profiles from the preliminary P-wave velocity model are shown on the top. The curve labeled Pahute Mesa is similar to the model of Leonard and Johnson (1987) with the addition of a high velocity layer below 3 km. The curve labeled Big Burn Valley is from outside the caldera near the 1986 shot point and CP-17. The second curve is derived from the first by assuming 1.6 km of structural relief across the caldera bounding faults. Some reduction of the velocities is necessary to account for depth of burial effects and a very low velocity zone is observed near the surface. The degree of smoothness, of the two curves, is somewhat arbitrary and only general features should be considered valid. On the bottom, 3 other velocity profiles are provided for reference. The Pahute Mesa and Rainier Mesa profiles are from the 3D block, tomographic inversion of Taylor (1983) and the Beatty profile is from Hoffman and Mooney (1983). The Pahute Mesa curve is very similar to the one on the left figure. Very little structural relief exists between Big Burn Valley and Rainier Mesa, so that we have the high velocity basement at about the same elevation at both locations, with some differences in tuff thickness. The Beatty profile is from an area away from the main volcanic centers. The geophysical model is in basic agreement with the geologic scenario presented in Orkild et al. (1968).

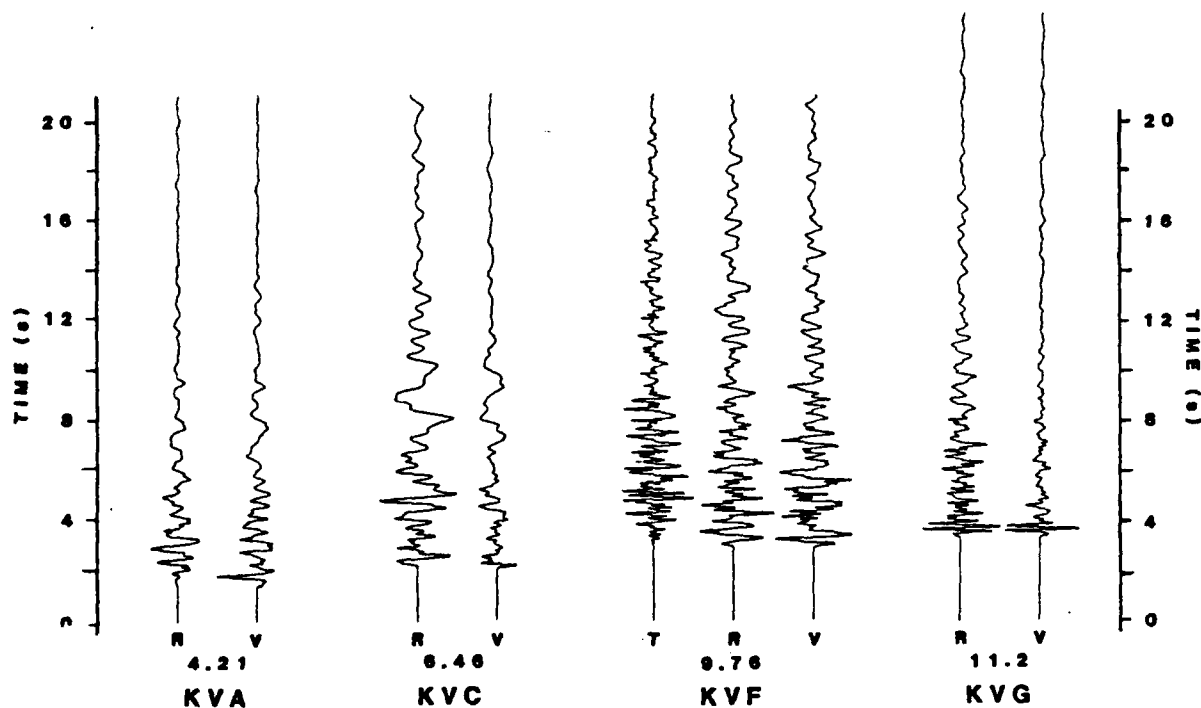




Locations of nuclear and chemical explosive shot points and seismic stations which contribute to the modeling of a structural transect at Pahute Mesa. The 1986 UTD-LANL wide angle seismic survey line is indicated by the hatched line and its shot point is labeled "SHOT POINT". Kernville was recorded at KVA, KVC, KVF and KVG. Boxcar was recorded at BS-34 and CP-17. Scotch was recorded at CP-17. Farm was recorded at F2, F4 and F5. Three stations recording Almedro are not shown.



Records from the nuclear tests Boxcar (4/26/68) and Scotch (5/23/67). These records provide important constraints on the modeling of the 1986 wide angle seismic data. They are recorded in a reverse direction from the 1986 survey and indicate the presence of a high velocity (>5 km/s) material deep under Pahute Mesa and more shallow outside of the Silent Canyon caldera, to the southeast.



KERNVILLE VELOCITY RECORDS

Seismograms from the nuclear test Kernville (2/15/88). Stations KVA and KVC were accelerometers and KVF and KVG were seismometers (velocity transducers). The KVA and KVC seismograms have been integrated to velocity, but no other effort has been made to match the accelerometer and seismometer instrument responses. Very significant differences exist in these records, apparently due to local geologic structure.

References

Ferguson, J. F. and S. K. Reamer, (1987), Geophysical investigations at Pahute Mesa, Nevada, AFGL-TR-87-0242, Univ. Texas Dallas, Richardson, TX.

Heidesch, R. J., (1987), A wide angle seismic investigation of Pahute Mesa, Nevada, M. S. thesis, Univ. Texas Dallas, Richardson, TX.

Hoffman, L. R. and W. D. Mooney, (1983), A seismic study of Yucca Mountain and vicinity, southern Nevada; data report and preliminary results, U. S. Geol. Surv. Open-File Rept. 83-588, Menlo Park, CA.

Leonard, M. A. and L. R. Johnson, (1987), Velocity structure of Silent Canyon caldera, Nevada Test Site, Bull. Seis. Soc. Am., v 77, p 597-613.

Orkild, P. P., F. M. Byers, Jr., D. L. Hoover and K. A. Sargent, (1968), Subsurface geology of Silent Canyon caldera, Nevada Test Site, Nevada, in Nevada Test Site, Mem. 110, E. B. Eckel, Ed., Geol. Soc. Am., Boulder, CO.

Taylor, S. R., (1983), Three-dimensional crust and upper mantle structure at the Nevada Test Site, J. Geophys. Res., v 88, p 2220-2232.

SEA — An Automated Event Analyzer for Seismic Arrays



*Robert M. Searfus, Darrel Lager, Cindy L. Mason,
Tom Canales, Rowland Johnson*

Lawrence Livermore National Laboratory

Abstract



We present a rule based expert system called SEA (Seismic Event Analyzer) that interprets data from regional seismic arrays such as NORESS. SEA was developed to support underground nuclear test ban treaty verification research by automating phase detection, identification, and association, and by applying local and regional knowledge to arrive at interpretations for seismic events. An Assumption Based Truth Maintenance System is used by SEA to emulate the problem solving behavior of the human seismic analyst, and an environment is provided to interactively review the system's chain of reasoning, extend interpretations made by SEA, or manually form a second opinion. Our experience of using SEA with the NORESS array has been very positive – SEA has been successfully used to perform interpretation of NORESS data in real time, act as an intelligent assistant with archived data, and has provided a framework to test new algorithms and strategies. SEA is described in terms of its knowledge representation, reasoning strategy, user interface, and architecture, and our preliminary experience of using SEA with the NORESS array is presented.

Project Personnel



Many people have participated at various times during the development of SEA:

Expert System:

Tom Canales
Rowland Johnson
Darrel Lager
Cindy Mason
Robert Searfus

Seismology:

Fred Followill
Terri Hauk
Steve Jarpe
Steve Taylor

Signal Processing:

Farid Dowla
Dave Harris

Lawrence Livermore National Laboratory



Project History

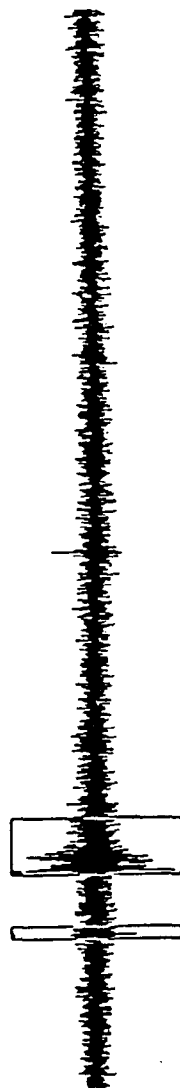
October 1985	<u>Project Initiated</u> Work on SEA began with experimental use of the OPS5 expert system tool. A customized inference engine was eventually written, and was later extended with support for Assumption Based Truth Maintenance. The proof of concept system was developed on a Symbolics LISP Machine, and was written entirely in LISP.
April 1986	<u>RSTNNORESS Research Symposium Demonstration</u> The proof of concept system was demonstrated with archived NORESS array data using a Symbolics 3645 computer.
June 1987	<u>Sun Port of SEA Initiated</u> SEA was ported to the Sun workstation in Common LISP. Parts of the system were rewritten in C or FORTRAN, and the MIT X Window system was used to develop the user interface.
May 1987	<u>Demonstration of Sun Implementation</u> The Sun workstation port of SEA was demonstrated with archived NORESS data during a LLNL Earth Science Department Seminar using a Sun 3/160.
Summer 1987	<u>Real-time Enhancements</u> Enhancements were added to SEA to support real-time interpretation.

Lawrence Livermore National Laboratory

The Problem: Seismic Event Analysis for Treaty Verification

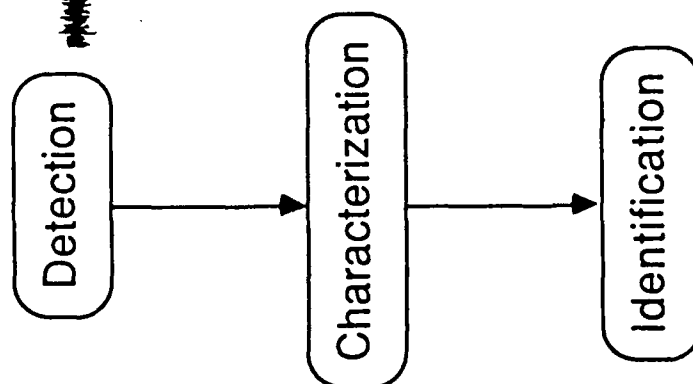


The first step of event analysis is the detection of phase arrivals



The second step is to characterize the event and its component phases

Pn: Azimuth 210° Velocity 7Km/s Amplitude 227 ...
Lg: Azimuth 200° Velocity 3.5Km/s Amplitude 298 ...
Location: 59.1N 10.3E
Magnitude: 1.3
...



Finally, the source of the event must be identified
Chemical Explosion

- A LARGE number of events will require analysis with a low threshold or comprehensive test ban treaty

Lawrence Livermore National Laboratory

Our Solution: AI (Expert Systems)



- Acquire an expert seismologist's knowledge
- Codify the knowledge as rules; develop supporting framework
- Test and refine the expert system
- Advantages
 - Capture an expert's approach to solving the problem
 - Integrate multiple disciplines (seismology, signal processing, ...)
 - Rapid prototyping

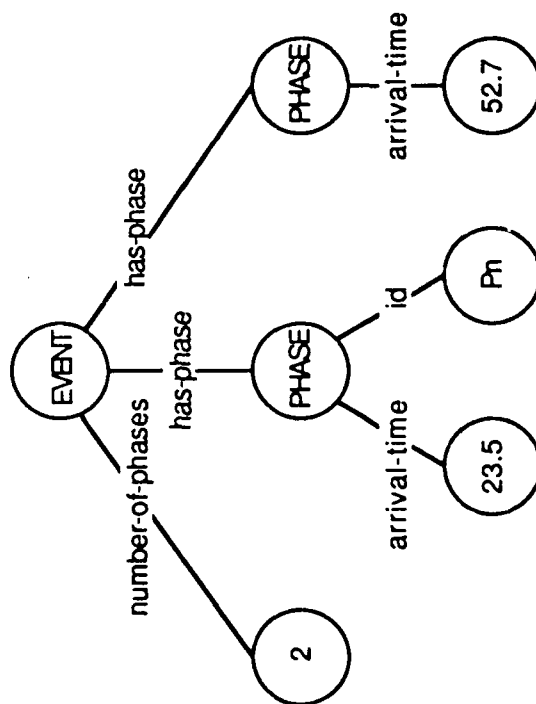


System Overview

- SEA performs phase detection, characterization, and association (does not identify event source).
- A semantic network is used to represent knowledge. Assumption Based Truth Maintenance allows SEA to emulate human problem solving behavior.
- SEA supports two operational modes:
 - Automatic, for online interpretation
 - Interactive, for interpretation review
- SEA is written in Common LISP, C, and FORTRAN, and uses the MIT X Window system.
- SEA is currently based on the Sun workstation family.

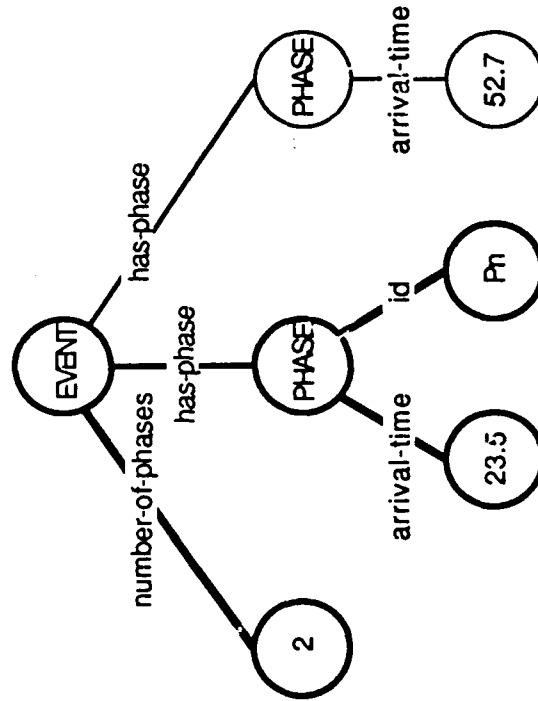
Lawrence Livermore National Laboratory

SEA uses a Semantic Network to Represent Knowledge



- Knowledge is represented as a network of nodes.
- Nodes may be used to represent concepts such as EVENT or PHASE, or may contain attribute values.
- Links represent relationships or attributes.
- Two nodes are joined by a link if a relationship exists between them.

Patterns are used to Match and Extract Information from the Semantic Network



- For example, the pattern:
(EVENT number-of-phases 2)
(EVENT has-phase \$Phase-1)
(\$Phase-1 arrival-time \$Time)
(\$Phase-1 id Pn)
matches the highlighted subnetwork.
- Variables may be used in pattern matching (such as \$Phase-1 or \$Time) to extract information from the network.
- Expressions may be used to constrain pattern matching.

Assumption Based Truth Maintenance is used to Emulate Human Problem Solving Behavior



- Assumptions are made to infer new facts from existing facts.
- Facts derived from assumptions remember the relevant facts on which they are based.
- If a fact is found to be contradictory (disbelieved), all facts based upon the contradictory fact can automatically become disbelieved.

Advantages:

- Allows multiple contexts and solutions.
- Facilitates explanation facility.
- Can be used for efficient inferencing.

Lawrence Livermore National Laboratory

The Expertise and Interpretation Strategy of a Seismologist is Represented in Rules



- Rules have two main parts:
 - A pattern or left-hand side (LHS) that must match to the semantic network before the rule can fire.
 - An action or right-hand side (RHS) that gets executed when the rule fires.
- Patterns are specified by a list of clauses.
- Actions are written in LISP and may call other routines written in LISP, C, or FORTRAN.
- Two types of rules are used by SEA:
 - Inference rules, which create new facts from existing facts.
 - Truth Maintenance rules, which monitor the knowledge base for inconsistencies.

Example Inference Rule



English form:

If there is an event with two phases, and the phases have been identified as Pn and Lg, then compute the distance of the event based on the arrival times.

Rule form:

```
(Compute-Pn-Lg--Event-Distance
  ((EVENT number-of-phases 2)
   (EVENT has-phase $Phase-1)
   ($Phase-1 id Pn)
   ($Phase-1 arrival-time $Time-1)
   (EVENT has-phase $Phase-2)
   ($Phase-2 id Lg)
   ($Phase-2 arrival-time $Time-2))
  (compute-distance-Pn-Lg $Time-1 $Time2))
```

Example Truth Maintenance Rule



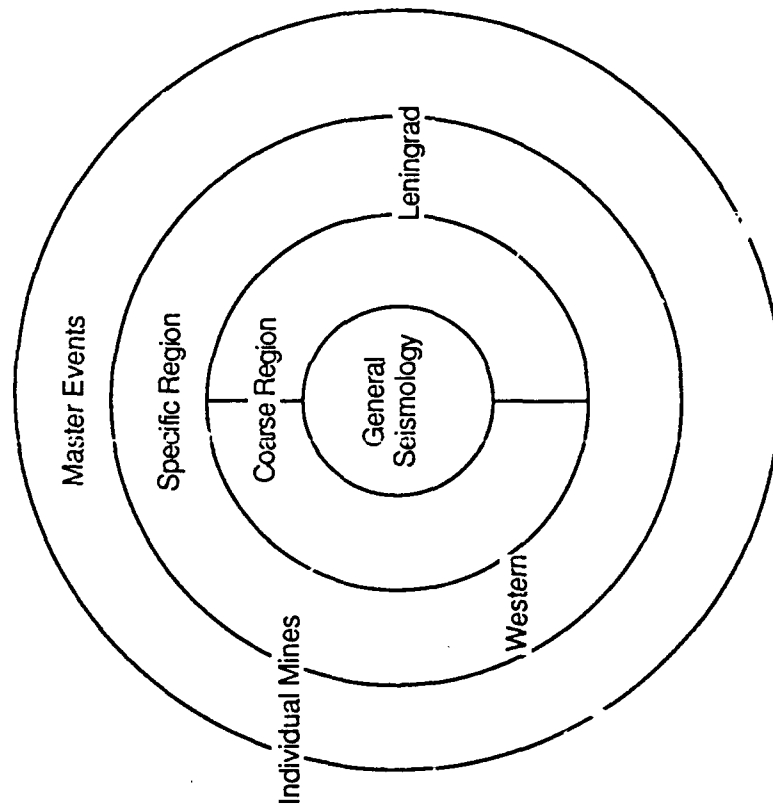
English form:

If there is an event with a Pn phase, and the velocity of the phase is less than an acceptable limit, then the phase is not Pn.

Rule form:

```
(Inconsistent-Pn-Velocity
  ((EVENT has-phase $Phase)
   ($Phase id Pn)
   ($Phase velocity $V)
   (< $V MINIMUM-Pn-VELOCITY))
  (contradict ($Phase id Pn)))
```

Rules are Organized to Cover Increasingly Specific Regions



Lawrence Livermore National Laboratory

AD-A230 066

PROCEEDINGS OF THE ANNUAL DARPA/AFGL SEISMIC RESEARCH

3/3

SYMPOSIUM (10TH) HE. (U) AIR FORCE GEOPHYSICS LAB

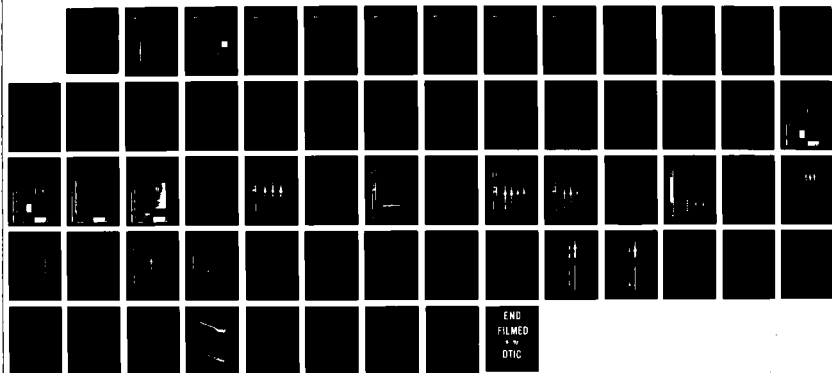
HANSCOM AFB MA J F LENKOWICZ ET AL. 17 DEC 90

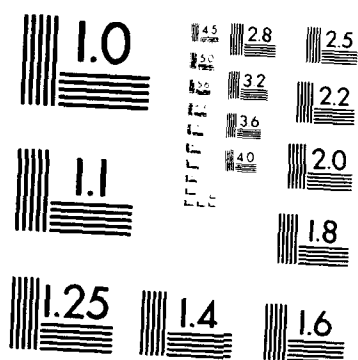
UNCLASSIFIED

GL-TR-90-0332(A) XF-GL

F/G 17/10

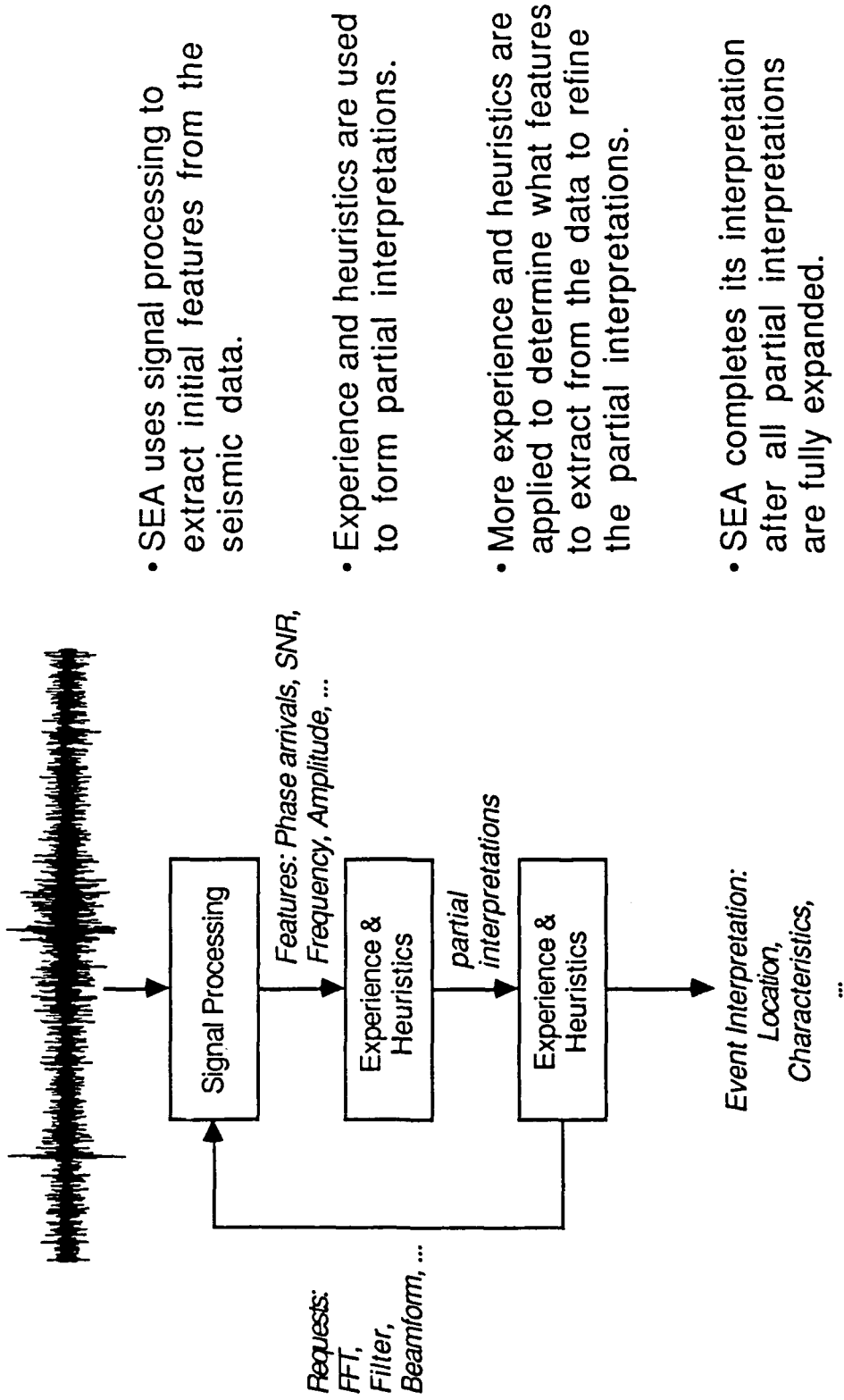
NL





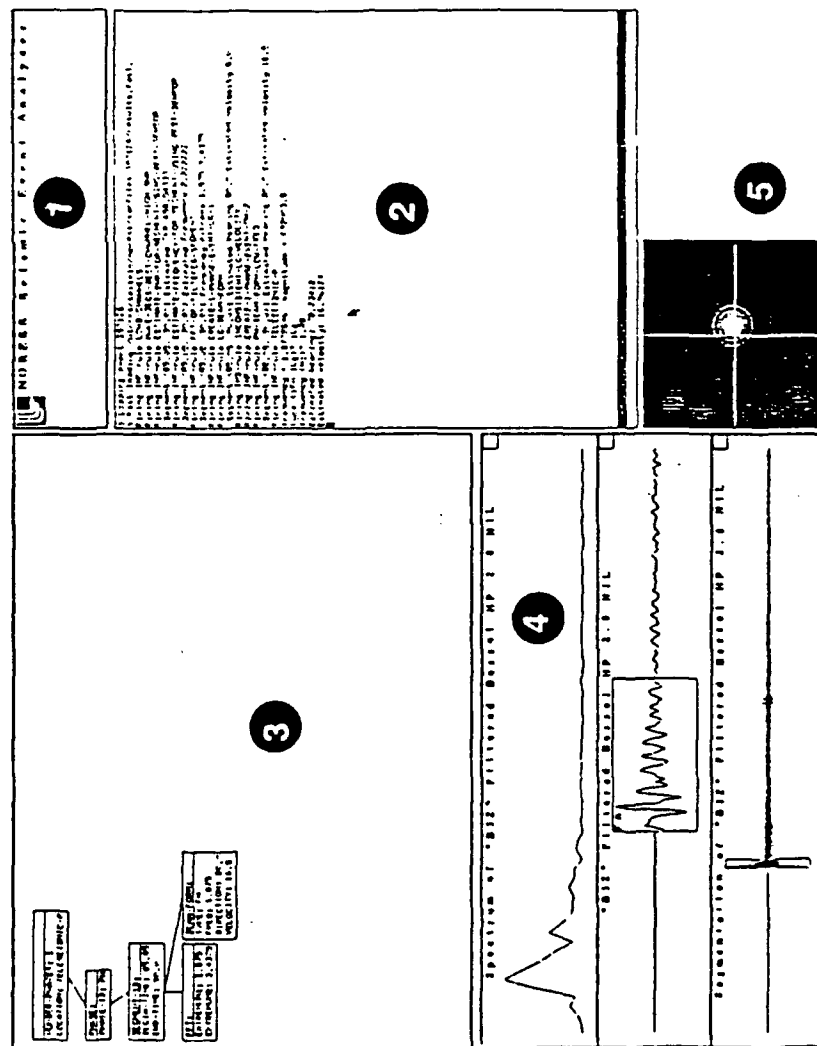
MICROCOPY RESOLUTION TEST CHART
NATIONAL BUREAU OF STANDARDS
STANDARD REFERENCE MATERIAL 1010a
(ANSI and ISO TEST CHART No. 2)

The Reasoning Strategy is to Build and Test Partial Interpretations



Lawrence Livermore National Laboratory

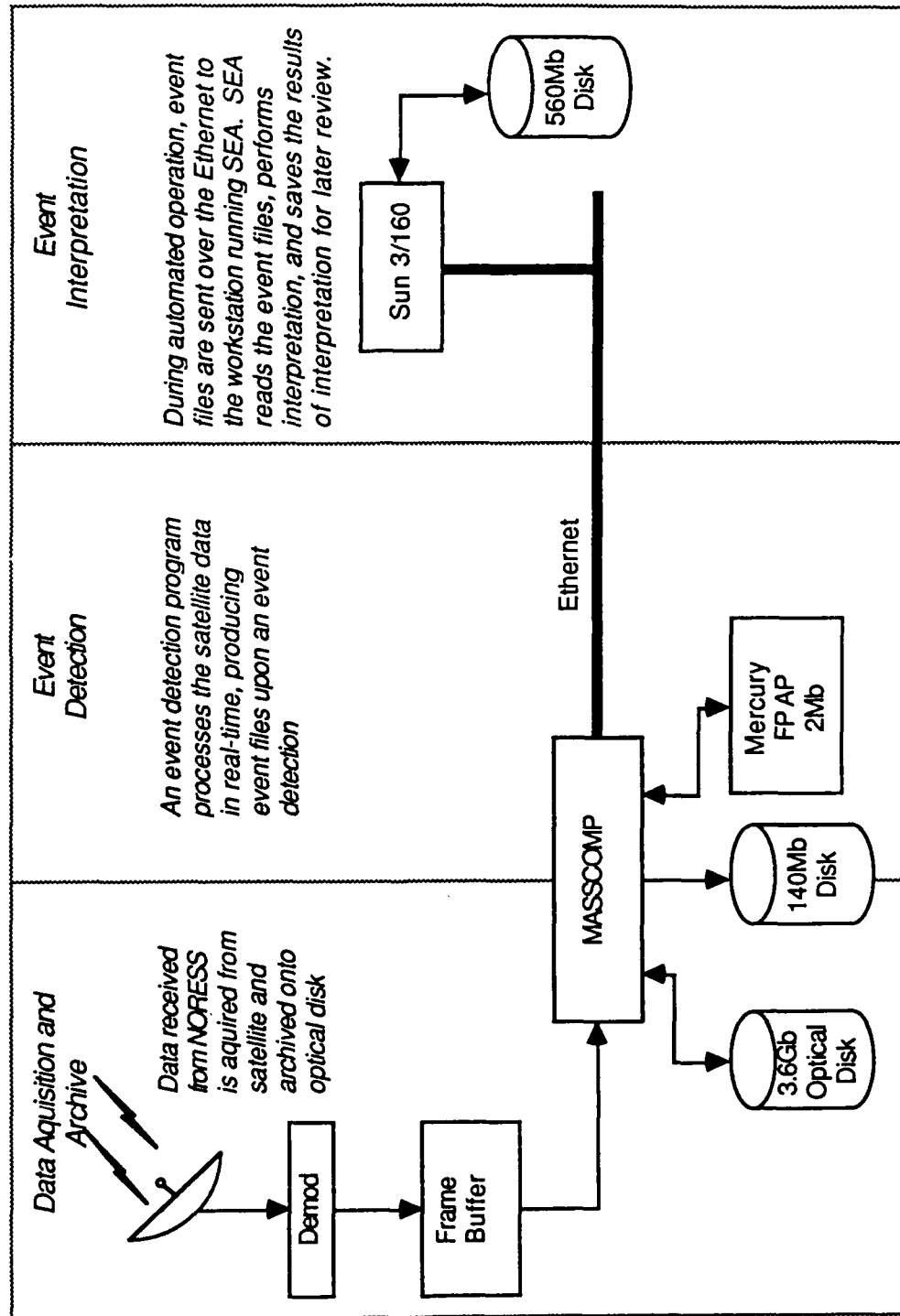
Layout of the SEA Display



1. Logo Window: Displays the LLNL logo along with the system title.
2. Emacs Editor Window: The Editor Emacs is used to interact with SEA, and is also used to edit rules and code.
3. Semantic Network Display Window: During and after interpretation, the information stored in the semantic network (the knowledge data base) is displayed in this window.
4. Waveform Display Stack: Up to three waveforms may be displayed by SEA in this stack of windows.
5. FK Contour/Image Display: The surface resulting from frequency-wavenumber analysis is displayed in this window. On a color display, the surface appears as a contoured image. On monochrome displays, only the surface contours are shown.

Lawrence Livermore National Laboratory

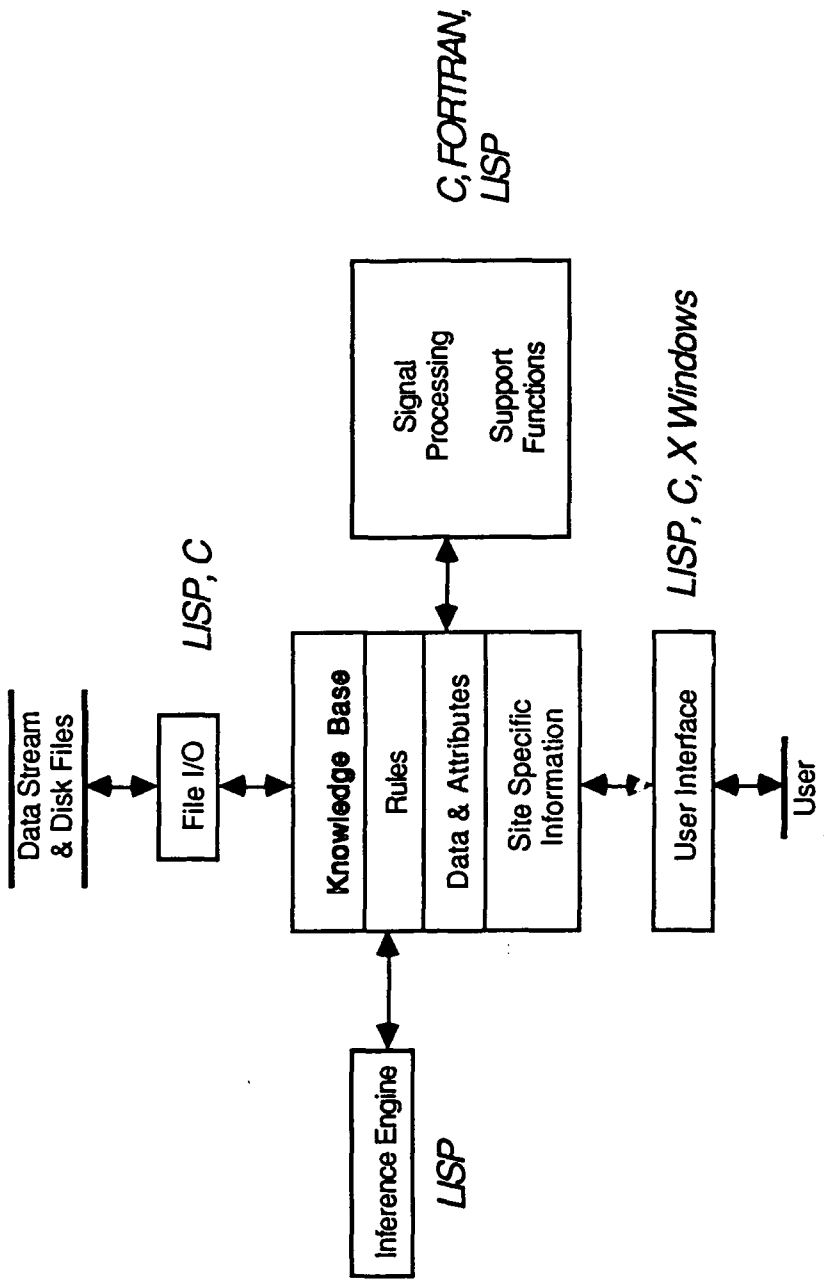
Architecture and Data Flow of the NORESS Interpretation System



Lawrence Livermore National Laboratory



SEA's Architecture and Implementation



- SEA uses standards such as Common LISP, C, FORTRAN, and the MIT X Window system for portability
- Critical software is written in C or FORTRAN for speed

Lawrence Livermore National Laboratory

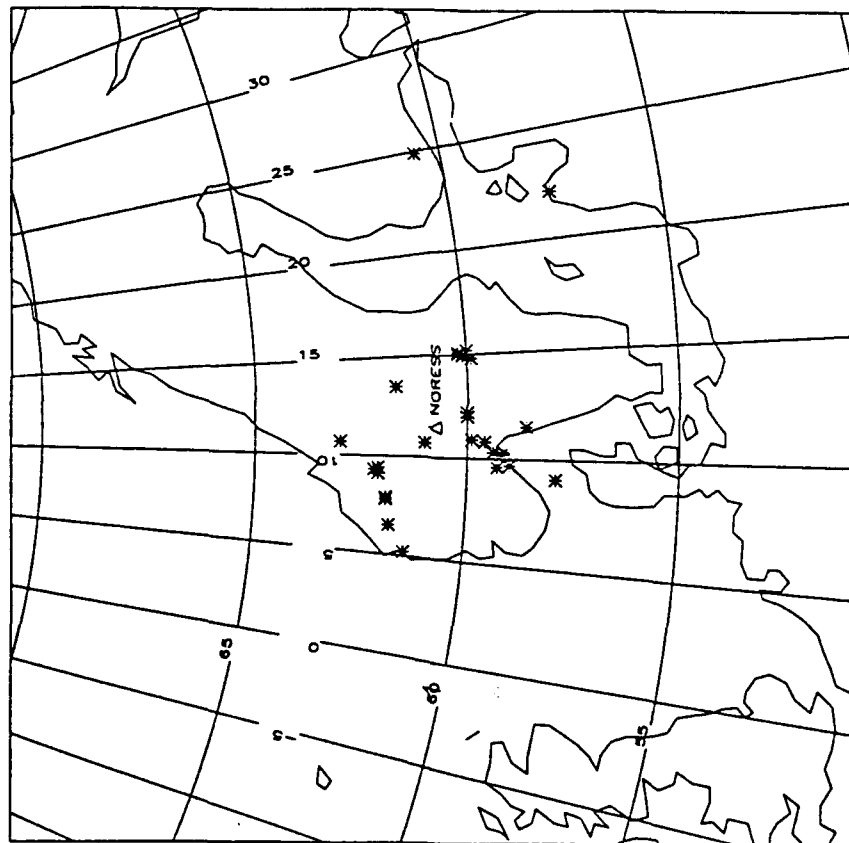
Our Experience with NORESS



- SEA has been run in real-time with NORESS data for evaluation. Interpretation of the detected events often agree with both analyst as well as the NORESS Bulletin.
- Consistently provides good interpretations for high to moderate SNR events.
- Periodic events caused by activities such as mining are tightly grouped.
- Low SNR teleseismic events are sometimes missed.
- A significant number of false alarms may be encountered, depending on run-time parameters and seasonal seismic activity.

Lawrence Livermore National Laboratory

Event Locations Provided by SEA During Preliminary Evaluation



Events shown were interpreted by SEA in real-time during the week of days 239 through 244 1987. Single phase events such as unassociated S phases or teleseismic events are not shown.

Lawrence Livermore National Laboratory

Other Applications of SEA



- SEA has been used as a framework for algorithm and strategy development for seismic arrays.
- SEA has been used to scan large amounts of archived data for events with specified characteristics.
- SEA forms the foundation in the development of an expert system for interpreting data from a network of three-component stations (NetSEA).

Lawrence Livermore National Laboratory

Current Status/Future Research



- We are now performing more detailed performance analysis (to be published).
- Work on the network variant, NetSEA, is ongoing.
- We plan to investigate source discrimination.
- A distributed version of SEA has been built and is being used to research distributed artificial intelligence.

Lawrence Livermore National Laboratory

**DATABASES AND SOFTWARE SUPPORT AT
THE CENTER FOR SEISMIC STUDIES**

Center Staff

Poster Session

10th Annual AFGL/DARPA Seismic Research Symposium

May 4, 1988

DATABASES

Introduction

A major goal of the Center program has been to facilitate the work of contractors in key areas of the nuclear monitoring research program, with the Center supplying data and computer services to external users. The Center currently maintains a sizeable number of databases. Some of these represent a complete set of information of some type and the contents are fixed, while others are undergoing development on a continual basis as new data of the same type arrive.

Status of Primary Databases

All Center databases, a total of 983 Mbytes, are accessed through the *INGRES* relational database management system. Status of the primary databases are given below. Note in relation to the waveform databases that the term "complete" means that the Center has all data available for a particular source; "incomplete" means that additional data may be available from another agency. Some of the waveform data at the Center is in the form of waveform segments for particular events (**GDSN, WAKE, SAFRICA, HDWWSSN, NORSAR, ASPA, NRDC, LRSM, RSTNATTN**), while the remaining data sets contain both continuous and segmented data.

Summary of Primary Center Databases
May 1, 1988

Database	Coverage	No. Tapes	Mbytes (disk)
Parameter Data			
EVENTS	1177 BC to Dec. 31, 1987	0	53.044
ISC	Nov. 1, 1978 to Dec. 31, 1978	0	19.760
ARRIVALS	May 16, 1982 to current	0	173.500
GSETT	Oct. 15, 1984 to Dec. 14, 1984	0	21.524
Waveforms-complete			
GDSN	Jan. 1, 1976 to Dec. 31, 1987	1083	250.282
RSTN	Jan. 1, 1982 to Mar. 31, 1987	3397	172.592
	(dp/pdp Jan. 15, 1984 to Mar. 31, 1987)	0	71.228
WAKE	Sep. 8, 1982 to Dec. 10, 1986	138	4.676
SAFRICA	Mar. 15, 1986 to Jul. 31, 1987	1	0.712
NRDC-Phase I	Jul. 15, 1986 to Nov. 15, 1986	0	0
NRDC-Phase II	Mar. 19, 1987 to Sep. 2, 1987	7	0.580
HDWWSSN	Sep. 13, 1963 to Dec. 27, 1981	4	1.752
Waveforms-incomplete			
NORESS	Oct. 25, 1984 to Feb. 13, 1988	380	28.528
NORESSHF	Dec. 1, 1985 to Dec. 31, 1987	183	1.360
NORSAR	Nov. 6, 1976 to Jun. 6, 1987	100	18.920
ASPA	Dec. 10, 1986 to Apr. 16, 1987	4	0.692
LRSM	Feb. 2, 1962 to Sep. 9, 1966	1	0.620
ARCESS	Jan. 1, 1988 to Feb. 10, 1988		

NORESS Research Data Sets

With the DARPA/GSD program emphasis on advanced research utilizing data from small seismic arrays, the Center has compiled a representative set of NORESS waveform segments for local and regional events over a range of azimuths from the NORESS array, plus waveforms for underground nuclear explosions recorded by the array. These data are archived in three separate data sets.

Data Set I includes selected recordings of 88 small earthquakes and mine blasts in Scandinavia and the western U.S.S.R. representing the various types of events recorded over a range of distance out to 15° and a range of azimuth around the array. The set includes 34 earthquakes, 38 mine blasts and 16 events for which event type was not specified in the local bulletins. Ten of the latter occurred off the southwest coast of Norway on November 20-21, 1985, and were probably earthquakes.

Data Set II includes an additional set of 55 waveform segments for events in southern and western Scandinavia was selected by the SAIC group in La Jolla from events listed in the Bergen, Norway, station bulletin. Selection of these events was based in part on problems identified by the NOR-SAR analyst--probable error in phase association, interfering phases, incorrect identification of Lg phase--as a set of test data for development of expert system analysis tools.

Data Set III includes NORESS recordings for more than 50 presumed underground explosions in the U.S.S.R. and on the Nevada Test Site spanning the time interval from October 1984 through August 13, 1987.

NRDC Database from the Eastern Kazakh Seismic Experiment

The Center is receiving waveform data from the three seismic stations being operated in eastern Kazakh, U.S.S.R., under a cooperative agreement between the Soviet Academy of Sciences and the Natural Resources Defense Council (NRDC). The first seismic station installed under this agreement began operation at Karkaralinsk (KKL) on 15 July 1986, and the others were set up at Bayanaul (BAY) and Karasu (KSU) during the summer and fall of 1986. Distances from the eastern Kazakh test site to these stations range from 100 to 300 km. The stations are in an area of very active mining (taken from analysis of F. Ryall and R. Baumstark), there are numerous events in the area surrounding this network. Most of these appear to be mine blasts.

The Kazakh experiment has been conducted in two phases. In the first phase, from July through December 1986, the stations were temporary and data were recorded on tape cassettes, copied onto IBM/PC floppy disks, and recopied onto 9-track tapes. The data quality during Phase I was very poor, and even after considerable effort by the Center software staff we were not able to make use of it. Phase II data has been better organized and documented than the Phase I data, and the processing and preliminary analysis of this data have proceeded relatively smoothly. The stations are now equipped with Teledyne-Geotech S-750 broadband seismometers emplaced in boreholes, with high- and low-gain output signals sampled at 250 Hz, plus a surface vault containing S-13 short-period and S-1 intermediate-band seismometers, also recording at two gain levels. The data have been of good quality and quite usable.

Waveforms from one or more of the NRDC Kazakh stations have been archived in the Center database for approximately 500 events plus 140 samples of background noise, covering the period through September 2, 1987. Locations of these events are either taken from the NEIS Preliminary Determination of Epicenters listings, or estimated by Center and ENSCO analysts. In the latter case, locations have been determined using the Center's automatic association and epicenter determination program, or estimated from distance and azimuth calculations based on measurements of regional seismic phases for one or two stations.

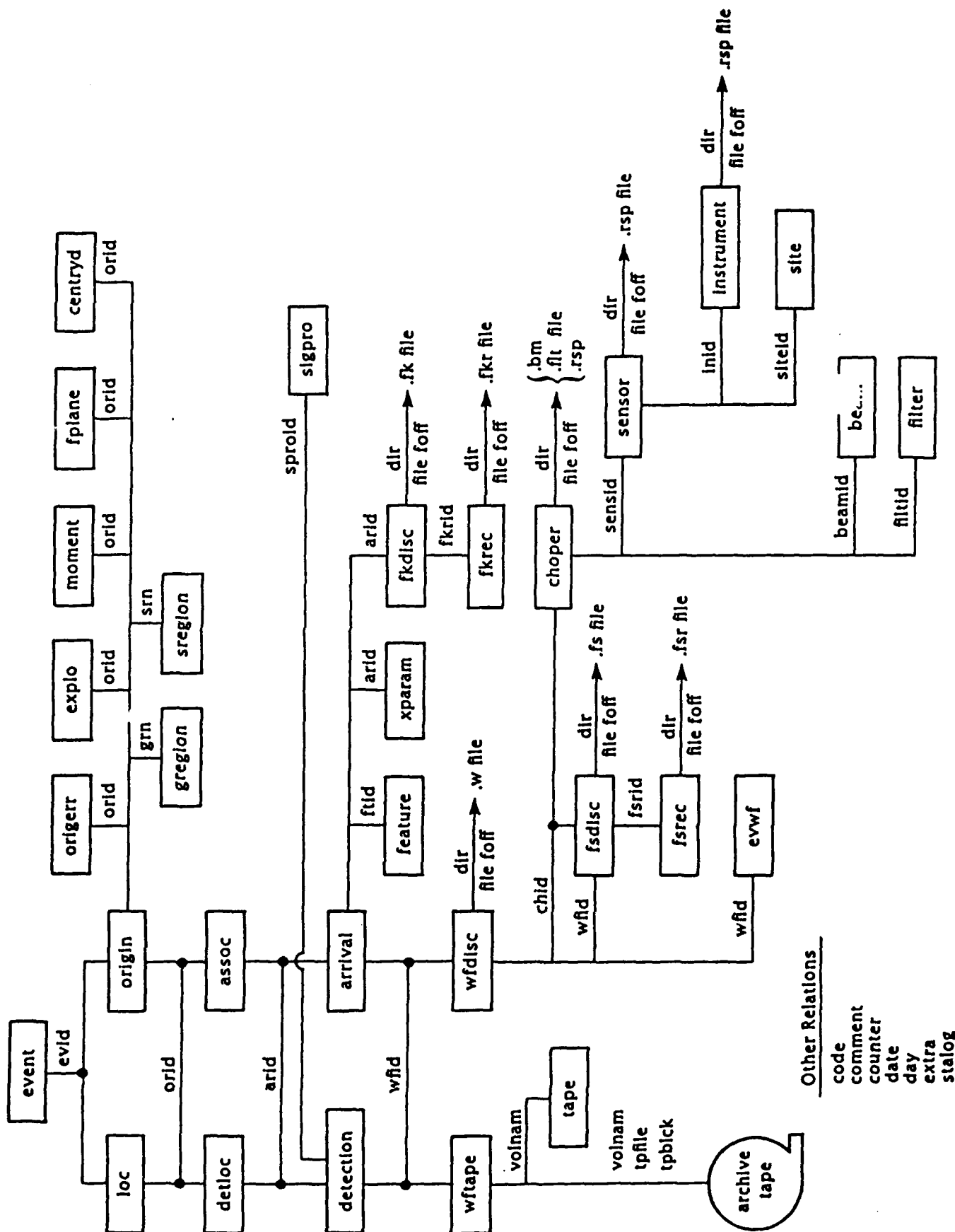
The Center Database Management System (DBMS)

The Center for Seismic Studies currently maintains or is preparing a sizeable number of databases. Some of these represent a complete set of information of some type and the contents are fixed, while others are undergoing development on a continual basis as new data of the same type arrive. An advantage that the Center offers to users is the ability to retrieve windowed waveform segments containing selected events, selected phases, or selected times upon request. These segments are all in a consistent standard format and contain complete identification and calibration information. Due to their size, most of the waveform data reside on tape, but indices to them are on-line, and access to the waveforms is fairly rapid (depending on computer loads).

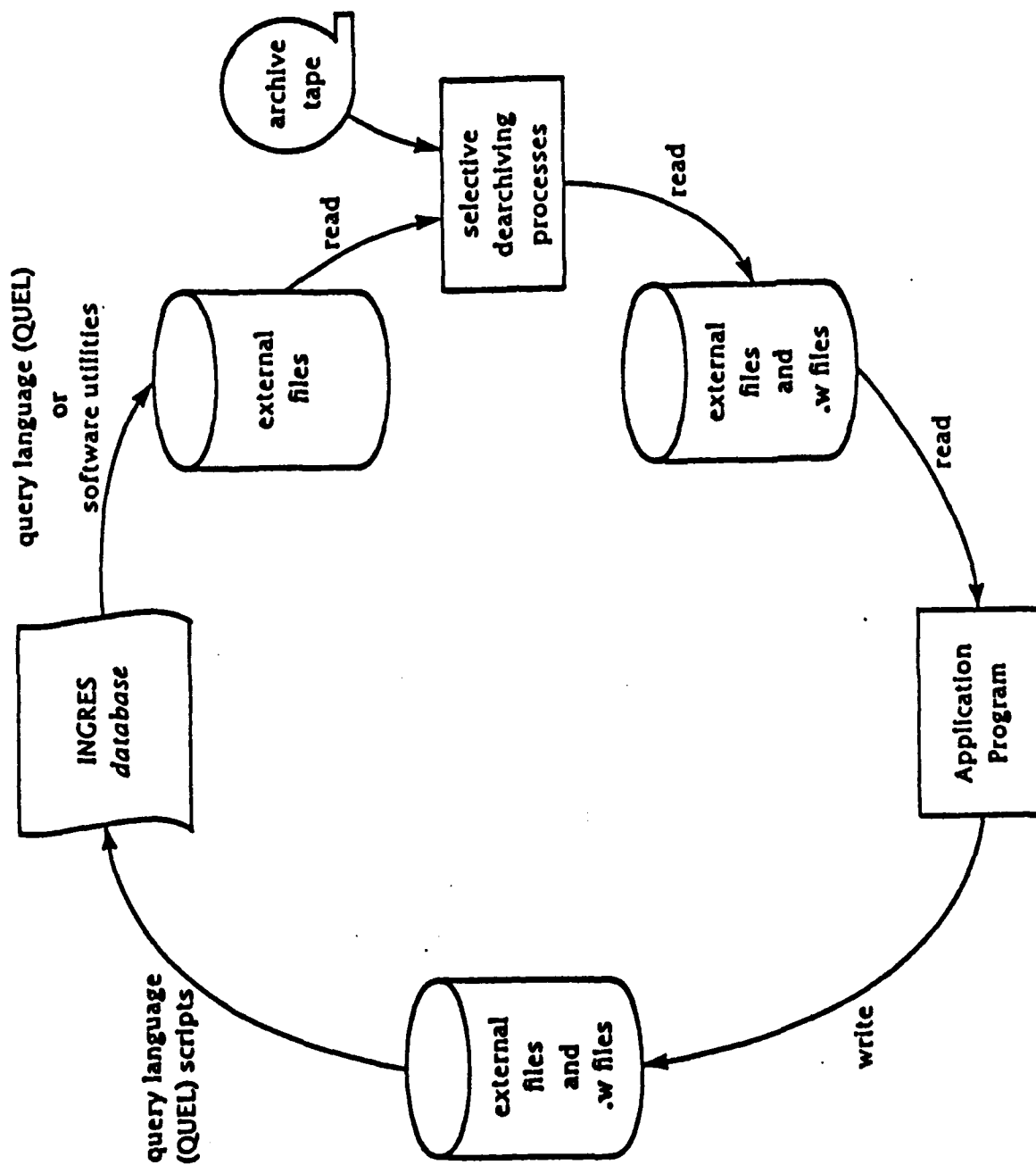
The database structure at the Center is described in Center Report 87-04 (Center for Seismic Studies, 1987). (Copies are available here.) Basically the database management system can be thought of as a collection of tables and a software system for manipulating them. The data management language is called *QUEL* (*QUEry Language*), and it is supported by the *INGRES* relational database management system.

Accessing the Databases

As described by Lees (1985), a number of scripts have been written at the Center to help users who are unfamiliar with *INGRES* find and retrieve data from the databases. For example, a script **helpdb** identifies the types of databases available at the Center (digital waveforms, alphanumeric data, film data), and through a series of queries and user responses takes the user to deeper levels of the script, finally accessing particular databases through *INGRES* to retrieve a list of data available for the event or events of particular interest. Once the user knows which database has pointers to the waveforms or other type of data he wants, other scripts are available to create the files that are needed to dearchive the data from tape. (*Accessing Seismic Data at the Center for Seismic Studies* (Lees, 1985) is available from the Center.

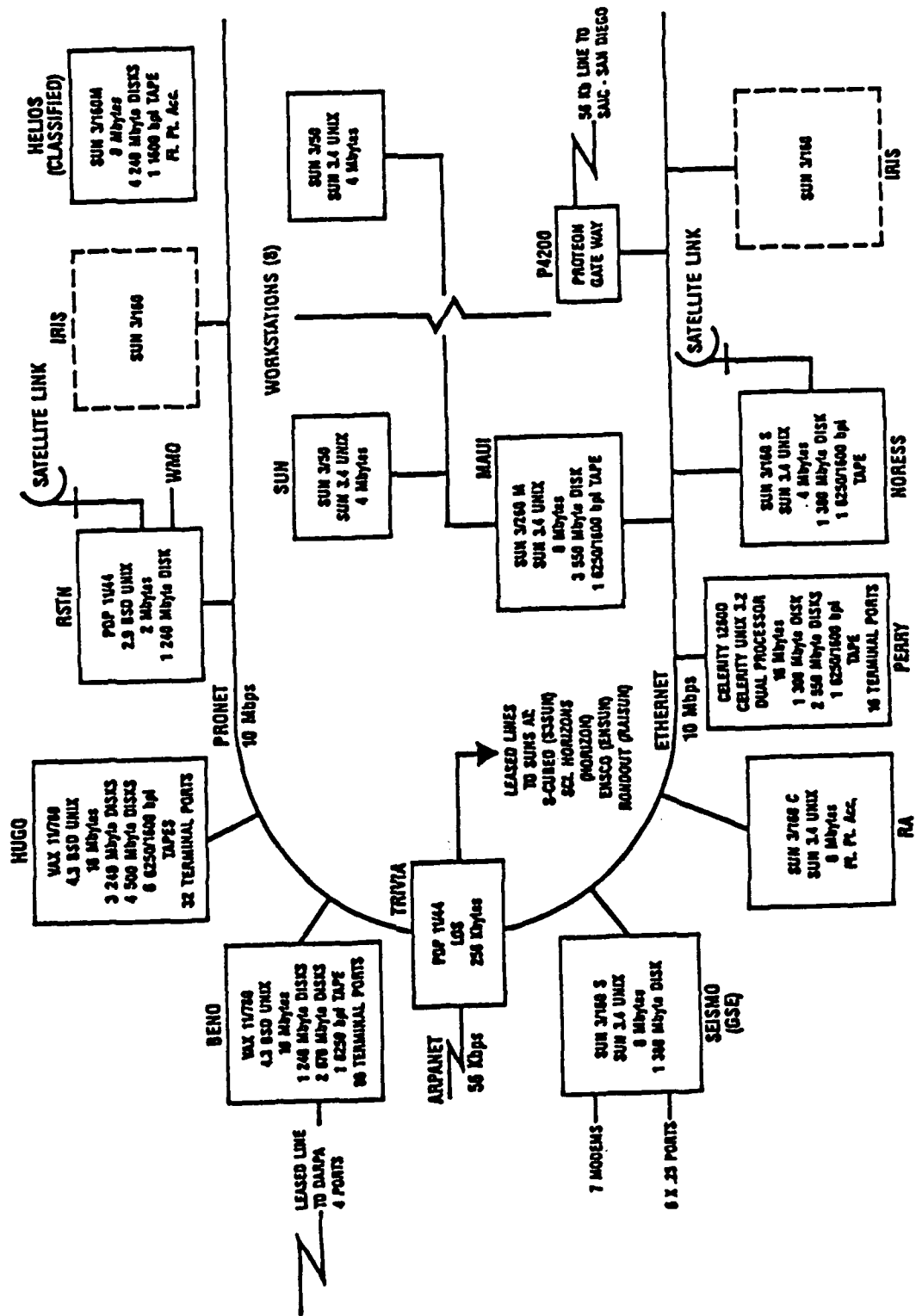


Schematic of Center database structure.



Retrieving and using waveform data.

COMPUTER SYSTEM CONFIGURATION AT CENTER FOR SEISMIC STUDIES



Research and Database Software

Introduction

In addition to the standard UNIX features, a large number of programs, written by the Center staff and other DARPA contractors, have been ported to the Sun computers and are available for research, database building, and seismic data exchange. The Center staff have selected a number of these programs as being particularly useful for research, database building and data exchange.

Grouping of Software by Function

In the tables below, the programs are grouped according to function. For some of the listings, initials in parentheses at the end of the listing indicate the agency that supplied the program:

Initials	Agency
LDGO	Lamont-Doherty Geological Observatory (Roger Davis)
RAI	Rondout Associates (Jerry Carter)
PSR	Pacific Sierra Research (Tony Ciervo)

Manual pages and sample output for some of the more useful waveform processing software are shown here including the interactive seismic analysis package "SUNPICK" developed by Lamont-Doherty Geological Observatory.

Programs Used for General Research

Name	Function
dlaz	Distance, azimuth between two points
etoh	Convert epochal to human time
htoe	Convert human to epochal time
jd	Convert month/day/year to Julian day and vice-versa
locit	Epicenter relocation
qdp	"Quick and dirty" plotting routine
reg	Geographic region number from latitude, longitude
snapt	Seismic network assessment program (PSR)
sta	Station coordinates, description from station code
today	Today's epochal, Julian, standard date
tptotp	Bit-for-bit copy of a tape
trix	Three-station epicenter location
tt	Traveltime table

Programs for Processing Seismic Waveforms and Parameters

Name	Function
3comp	Display three-component waveforms
aa	Automatic association program
apa	Adaptive polarization analysis (RAI)
apdisp	Display data from apa or track programs
beam	Compute and plot array beam in specified passbands
bps	Bandpass filter
cepstrum	Compute and display cepstrum of time series
detect	Plot seismograms, interactively pick arrivals
detector	SRO event detector algorithm
display	Interactive waveform display program (RAI)
dp	Z statistic power detector
filter	Filter seismic data (RAI)
fk	Computer and plot f - k spectra for array data
fseis	Filter and display seismic data
gpm	Interactive seismic waveform analysis program
icorr	Apply instrument corrections to seismic amplitudes
nspec	Plots up to four spectra (RAI)
pdp	Finds first arrival on a seismic waveform
plot_sh	Display seismic traces with associated picks
plot_wfdisc	Display seismic traces with associated picks
polarfilt	Polarization filtering of three-component signals
ppp	Pre- and post-process parameter files
processbeam	Produces (filtered) beams from array data
pslide	Plots autoregressive parameters of seismic signal
pzero	Autoregressive analysis and display program
scanwf	Decimate and display entire waveform file
section	Display record (filtered) section of array signals
sgp	Interactive seismogram plotter (LDGO)
signoise	Plots amplitude spectra for specified times
sigspect	Amplitude, power or phase spectra
slow	Plots waveforms as function of slowness
specgram	Plots power as function of time, frequency (RAI)
threecomp	three-dimensional particle-motion parameters
track	Uses adaptive polarization to track largest motion (RAI)
transform	Transforms time series into frequency domain (RAI)
velspec	Plots velocity spectra (vespagrams) for array data
wdisp	Plots waveforms on Tektronix 4014

Programs Used in Database Building and Checking

Name	Function
aawk	Reformat version 2.8 CSS database files
arc	Program to archive waveforms on tape
arrival.awk	Read, write version 2.8 CSS database files
arseg	Produce waveform segments from arrivals
cmpreq	Compress waveform requests
darc	Recover data from archive tapes
dreq	Process dearchive requests
fea2ori	Convert one type of database file to another
fmt.arrival	Print format for version 2.8 CSS database files
geta	Extract records from version 2.8 CSS database files
lookatt	Displays summary description of a database attribute
lookrel	Look for information about CSS database relations
ori	Keyboard input version 2.8 CSS database files
parse	Produce parameter list for WMO messages
predar	Produces predicted arrival records for specified origins
preview	Predict how much tape an arctwo run will use
reap	Removes duplicate arrivals
renum	Renumbers arid's and ftid's in an arrival file
sptape	Converts AFTAC station processor record to CSS database
stubtap	Stubs off CSS archive tape
taplab	Initializes tape with ANSI label blocks
wfport	Converts waveform file to target machine format
wunseg	Converts segmented waveforms to continuous files

Programs Used in Data Exchange

Name	Function
kermit	File transfer protocol
lev2	Converts version 2.8 CSS waveform to GSE format
pel	Convert version 2.8 database to GSE Event List
wmo	Produces WMO message from CSS .arrival and .feature files

NAME

sunpick - interactive seismic analysis program for Sun workstations

SYNOPSIS

sunpick *prefix per* [-a] [-s *pagesize*]

USAGE

Prefix is the local Center database *prefix*, located in the current directory.

Per is a single-character period identifier used for selecting waveforms from the *wfdisc* relation. *Per* corresponds to first character of the "chan" attribute in the *wfdisc* relation. For example, "s" selects all short-period waveforms, "l" selects all long-period waveforms, etc.

-a If used then the waveforms plotted in the main window are aligned so the first sample of each is at the left edge of the window. The total time plotted is the duration of the longest waveform. If omitted then the waveforms are offset according to their absolute start times. In this case the total time plotted is the duration between the earliest start time and the latest end time of all waveforms.

-s *pagesize*

If used then the main window displays *pagesize* traces per page. Multiple pages of waveforms can be leafed through sequentially (see below). If not used, the default is to plot all the waveforms for all stations on one page.

EXAMPLE

sunpick 85300 s -a -s 9

OVERVIEW

Sunpick is an interactive seismogram analysis program for Sun 3 workstations. **Sunpick** was written primarily at Lamont-Doherty Geophysical Observatory in 1987 and modified at the Center for Seismic Studies. It inputs and outputs Center version 2.8 database relations and waveform files. **Sunpick** accesses the SunView graphics package and runs within or without Suntools on color or monochrome monitors. The best way to use **sunpick** is from a "GraphicsTool" Suntools window, as certain parameters are printed to the standard output. With GraphicsTool the output appears in the text sub-window for immediate viewing. **Sunpick** allows an analyst to display waveforms and add, change or delete arrivals. It uses facilities to scroll, time-align and zoom signals, to compute and overlay signal and noise spectra, to bandpass filter, to compute polarization information and to rotate three-component data. The sampling rate may vary between waveforms. **Sunpick** uses the windowing facilities of SunView to create several sub-windows for specific functions. The following description is organized by the different sub-windows created by **sunpick**.

MAIN WINDOW

The initial window is the **main** window containing a plot of all the waveforms. If the -s *pagesize* option was used in the command line and more than *pagesize* traces are input, then several pages of waveforms are available in the main window. These can be leafed through by placing the pointer on the text stripe at the top of the window and clicking the left mouse button (to leaf forward) or the right mouse button (to leaf backward). The station codes, channels and peak amplitudes in nanometers for traces in the main window are given on the left side. Any arrivals are displayed above the corresponding trace at the correct time. All traces in the main window are plotted with the same time scale and with relative amplitude scales.

Clicking the **left button** in the main window brings up the **display** and **pick**

windows for a detailed waveform analysis. The trace under the pointer when the left button is clicked becomes the active trace in the display and pick windows (see below). A segment of the waveform located at the time position of the pointer is used in the detailed analysis.

Clicking the **middle button** in the main window deletes the trace beneath the pointer; it cannot be accessed again during this run.

main menu

Pressing the **right button** in the main window brings up the **main menu**. Selecting **exit** from the main menu closes all files and terminates **sunpick**. Selecting **list arrivals** from the main menu brings up the **list arrivals** window (see below). Selecting **clear arrivals** from the main menu allows one to delete the arrivals for any waveform. The waveform for which arrivals are deleted is selected by moving the pointer and clicking any button. Selecting the **read arrival file** from the main menu causes **sunpick** to read the arrival relation for the current database. The arrivals need to be read in at the beginning of a session if they are to be reviewed, deleted or modified. If new arrivals will simply be added, then it is not necessary to read the arrival file first. Selecting **write arrival file** from the main menu causes arrivals for all waveforms being analyzed to be immediately written into the arrival relation. If no arrival relation exists then one is created. In a typical session, some arrivals are read from the arrival relation, they are modified, deleted or new ones are created during an analysis, and then they are written back to the arrival relation before exiting. If there are any arrivals in the arrival relation without corresponding waveforms in **sunpick**, they are preserved during a write operation. Don't forget to use **write arrival file** before exiting **sunick** or your work will be lost; **sunpick** does not automatically write your arrivals to the arrival relation.

DISPLAY WINDOW

When a trace is selected in the main window by clicking the left button, both the **display** and **pick** windows appear. The display window is located at the top of the screen and contains the entire waveform selected. The waveform is decimated in this view of the display window, and the decimation factor is computed from the window width and waveform length. The pick window is larger and appears below containing an analysis segment of the selected waveform (plus any other components for this station). The analysis segment is indicated in the display window in reverse video. Its length defaults to 20% of the trace length. However, the analysis segment length can be changed within the pick window (see below). The analysis segment is centered at the time of the pointer during a click. It can be repositioned by pointing to a new time in the display window and clicking the **left button**. Clicking the **middle button** causes **sunpick** to return to the main window. Clicking the **right button** in the display window has no effect.

PICK WINDOW

The pick window is the environment for performing most of the waveform analysis. The pick window contains the segment of data shown in reverse video in the display window above. All components for the selected station are used in the pick window. The station code and channel are given on the left, as is the peak amplitude in nanometers. All channels in the pick window are plotted on the same time and amplitude scales. The time scale is annotated on the x axis and is in units of samples.

The way to return to the **main window** from the **pick window** is by moving the pointer into the **display window** and clicking the middle button.

Clicking the **left button** in the pick window scrolls the data segment so that it becomes centered at the time position of the cross-hair.

function menu

Pressing the **right button** in the pick window brings up the **function menu**. The first four menu items control the time and amplitude scaling for signals plotted in the pick window. Selecting **contract horizontal** followed by any mouse click contracts the time scale to include a longer time segment. The reverse video portion in the display window shows the new segment. The degree of time contraction depends on the button clicked after selecting "contract horizontal"; the left button contracts the time scale by a factor of two, the middle button by a factor of three and the right button by a factor of four. Conversely, selecting **expand horizontal** and clicking a button expands the time scale of the segment a factor of two, three or four, depending on which button is clicked. Similarly, selecting **contract vertical** or **expand vertical** from the function menu followed by a mouse click contracts or expands the vertical scale by a factor of two, three or four if the left, middle or right buttons are clicked, respectively. Selecting **list arrivals** from the function menu brings up the **list arrivals window** (see below). Selecting **amplitude spectra** from the function menu brings up the **spectra window** (see below). Selecting **filter** from the function menu invokes a bandpass filter which is applied to the signals in the pick window. When "filter" is selected, a query appears in the upper left corner asking for the high-pass and low-pass corner frequencies. These need to be entered from the keyboard, first a value for the high-pass frequency (integer or float), a return, a value for the low-pass frequency and another return. If a return is hit without entering a value, the filter is skipped. The filter used is a third-order Butterworth applied in one direction. Selecting **rotate** from the function menu allows a rotation of the horizontal components in the pick window. A query appears in the upper left corner asking for the angle, in degrees clockwise from north, that the north component will be rotated. The angle is entered as an integer or float value followed by a return. The new orientations of the horizontal channels appear on the left side. Note that a "filter" operation can be followed by a "rotate" or "particle motion" operation; these functions cascade if the filtering is done first. Selecting **particle motion** from the function menu invokes a routine to compute the back-azimuth and degree of polarization from three-component data in the pick window. When "particle motion" is selected, a prompt appears in the upper left corner of the pick window. A time must be selected by moving the cross-hair and clicking the left or middle button. If the left button is clicked P-wave motion is computed. If the middle button is clicked Rayleigh-wave motion is computed. The computation segment is centered at the picked time. A reverse-video stripe appears above the trace indicating the computation segment. Results are written to standard output; these can be viewed immediately in the text window if **sunpick** is run from a GraphicsTool. The length of the computation segment for particle motion is fixed by the program and depends on the sampling rate; 2.5 seconds for $\text{sample_rate} > 10$ Hz, 12 seconds for $2 \text{ Hz} < \text{sample_rate} < 10$ Hz, and 60 seconds for $\text{sample_rate} < 2$ Hz. Unless the data are of good quality, filtering should generally be applied before particle motions are computed.

phase menu

Pressing the **middle button** in the pick window brings up the **phase menu**. When a phase is selected from this menu it becomes the current phase. The text line at the top of the pick window is used for manipulating the attributes for the current phase. The channel associated with the current phase is given in brackets at the extreme left. This channel is always the same as the trace in the

display window. The name of the current phase is given on following the character string "phase". Clicking the left button on the character string "time" allows one to select an **arrival time** for the current phase. This is done by moving the cross-hair to the desired time and clicking any button. A vertical line and the name of the phase appear at the selected time. The **quality** of the current phase is set by clicking the left button on the character string "quality". Successive clicks cycle through "_", "l", "e" and "w". The **amplitude** may be measured by clicking the left button on the character string "amp", moving the cross-hair and clicking any button on two amplitude values in the pick window. One-half of the selected amplitude range in nanometers is displayed following the string "amp". Similarly, the **period** for the current phase is measured by clicking the left button on the character string "per", moving the cross-hair and clicking any button on two time values. The absolute difference between the selected times in seconds is displayed following the string "per". Clicking the left button on the character string "delete phase" **deletes** the current phase for this station. The identity of the current phase is given following the string "phase". This nulls the current phase attributes and removes the phase marker from the waveform.

LIST ARRIVALS WINDOW

The **list arrivals** window is invoked by selecting **list arrivals** either from the **main menu** in the main window or from the **function menu** in the pick window. The list arrivals window lists all current arrivals for the stations being analyzed. The list arrivals window simply displays the information; the values cannot be edited or deleted. Clicking on any mouse button in the list arrivals window returns **sunpick** to its previous state.

SPECTRA WINDOW

Selecting **amplitude spectra** from the **function menu** in the pick window brings up the **spectra window** together with the **display window**. An empty spectrum plot appears with log amplitude as the y axis and linear frequency as the x axis. Moving the **left** or **middle button** into the spectrum plot gives a vertical indicator line and a frequency value. This allows one to determine the frequency of any point on the plot.

spectra menu

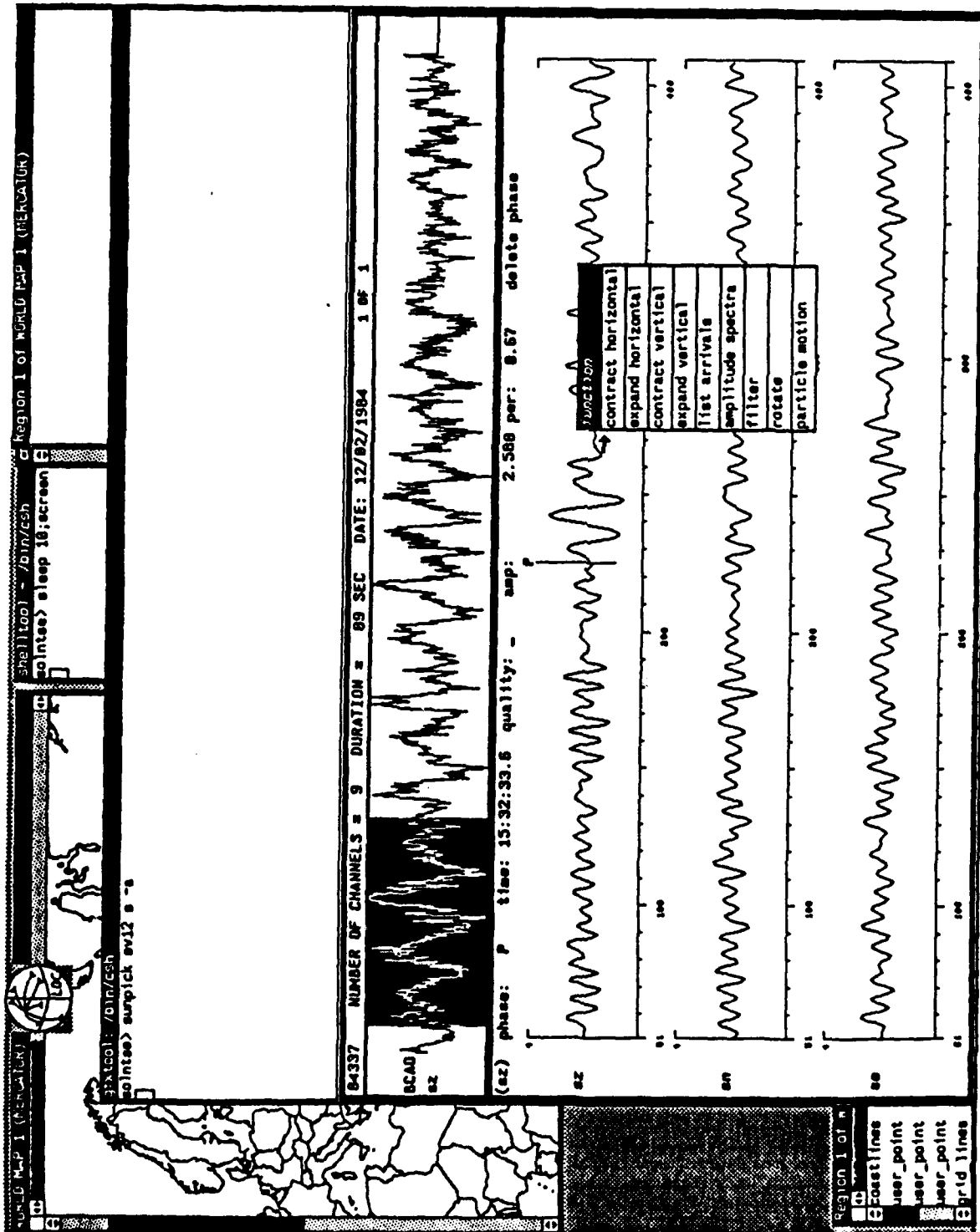
Pressing the **right button** in the spectra window brings up the **spectra menu**. A signal spectrum is computed by selecting **select signal**, moving the pointer into the display window and clicking the left button. A reverse-video time segment appears at the position of the pointer in the display window and the spectrum appears as a solid line in the spectrum plot. A noise spectrum is computed by selecting **select noise**, from the spectra menu, moving the pointer into the display window and clicking the left button. A time segment appears at the position of the pointer in reverse video and a noise spectrum appears on the plot; the area beneath the noise spectrum is shaded in reverse video. Initially the default segment lengths are used for computing the spectra. The segment length can be changed by selecting **time window** from the function menu. A query appears in the lower left corner asking for the new segment length. A value must be entered from the keyboard (float or integer) in units of seconds. Any new spectra computed will now have the new window length. The degree of smoothing of the amplitude spectrum may be changed by selecting **smoothing** from the spectra menu. A query appears asking for a value between 1 and 5 which is entered from the keyboard. Any new spectra computed will have the new degree of smoothing. All amplitude spectra are cleared from the plot by selecting **clear spectra** from the spectra menu. Selecting **return** from the spectra menu returns **sunpick** back to the previous state in **pick** and **display**

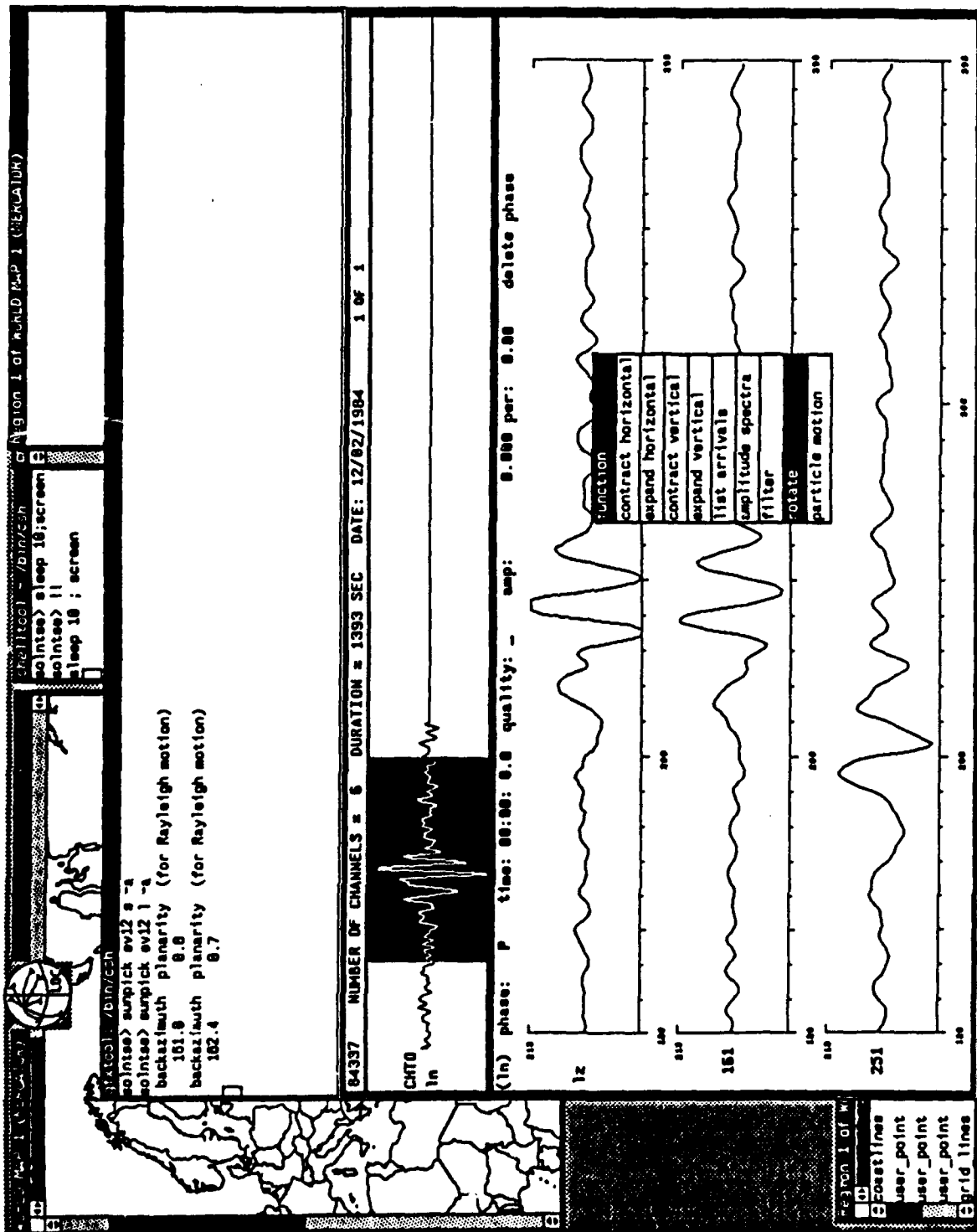
windows.**SEE ALSO**

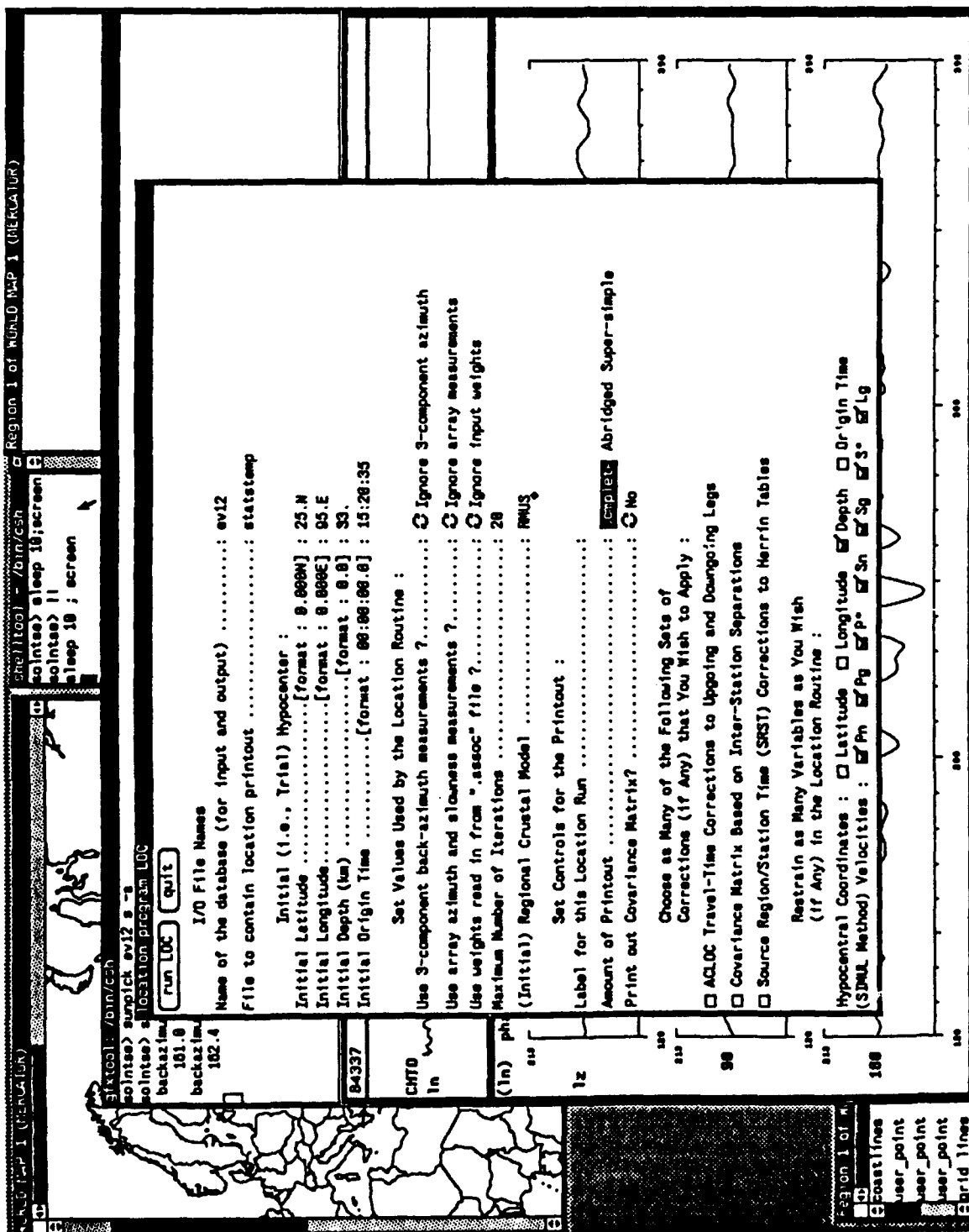
Center for Seismic Studies Database Structure
Version 2.8

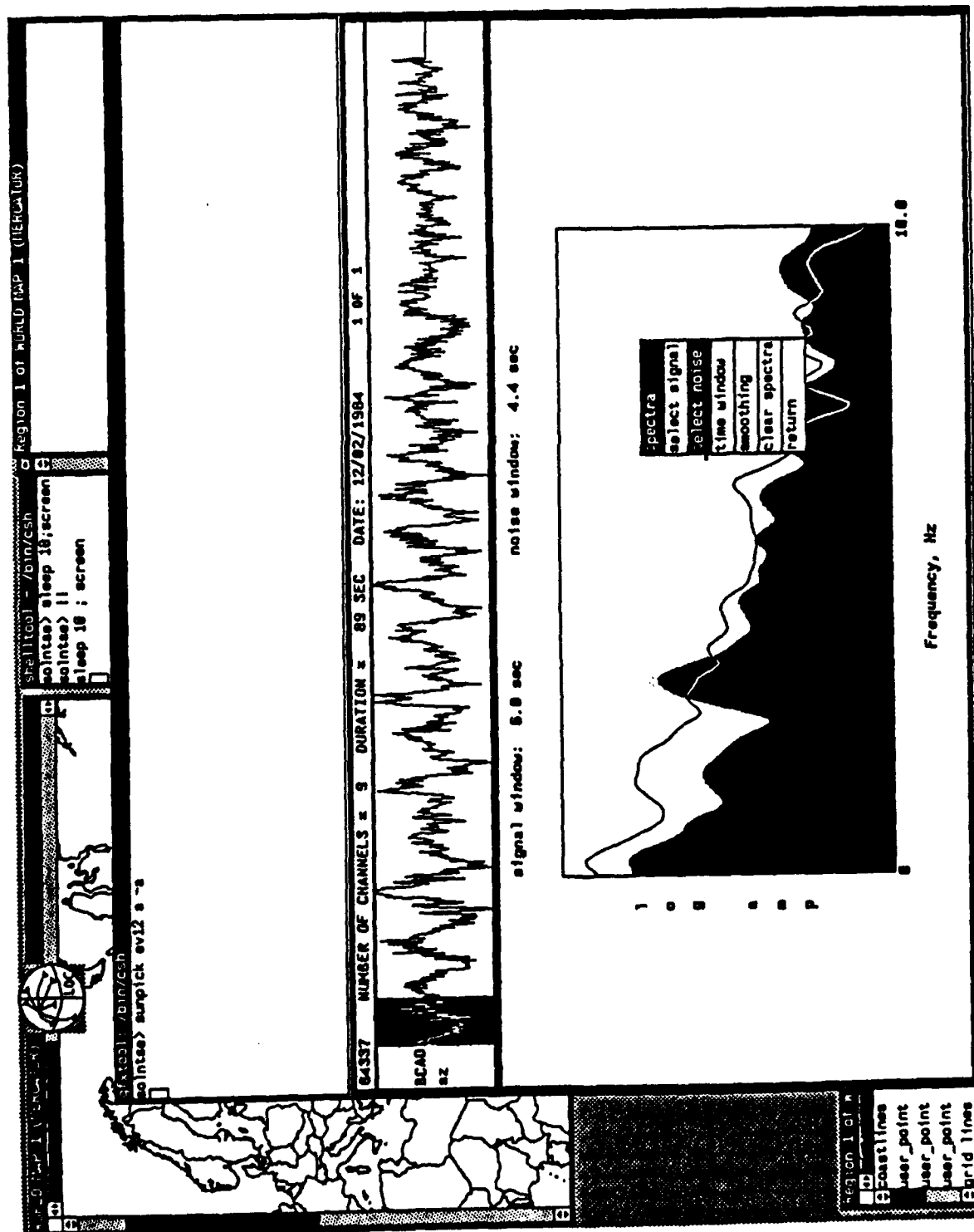
BUGS

Sunpick may fail with a "not enough memory" error when run without the -a option even though it would succeed for the same data set if the -a option is used.









NAME

3comp – display 3-component waveforms, perform filtering and rotation

SYNOPSIS

3comp *database_prefix sz_waveform_id*

INPUT

CSS version 2.7 formatted *.wfdisc*, *.origin*, and *.w* files.

OUTPUT

A plot of the z, n, and e channels or rotated z, r, and t components. Filtering may also be performed.

DESCRIPTION

3comp takes from the command line the database prefix (prefix.wfdisc) and the waveform id of the z channel and then reads the corresponding n and e channels. The program then asks how many seconds to skip in the waveform and how many seconds to retrieve. Filtering can then be performed if needed. The program will then plot either the z, n, and e channels with relative amplitudes preserved between the channels, or it will rotate the data to the backazimuth of the event, determined from the location in the *.origin* file. A time axis is drawn at the bottom of the plot, along with other pertinent information such as the start time of the plot, date, station name, database name, and peak amplitudes in nm/sec. *3comp* is written to be executed within a Sun window.

OPTIONS

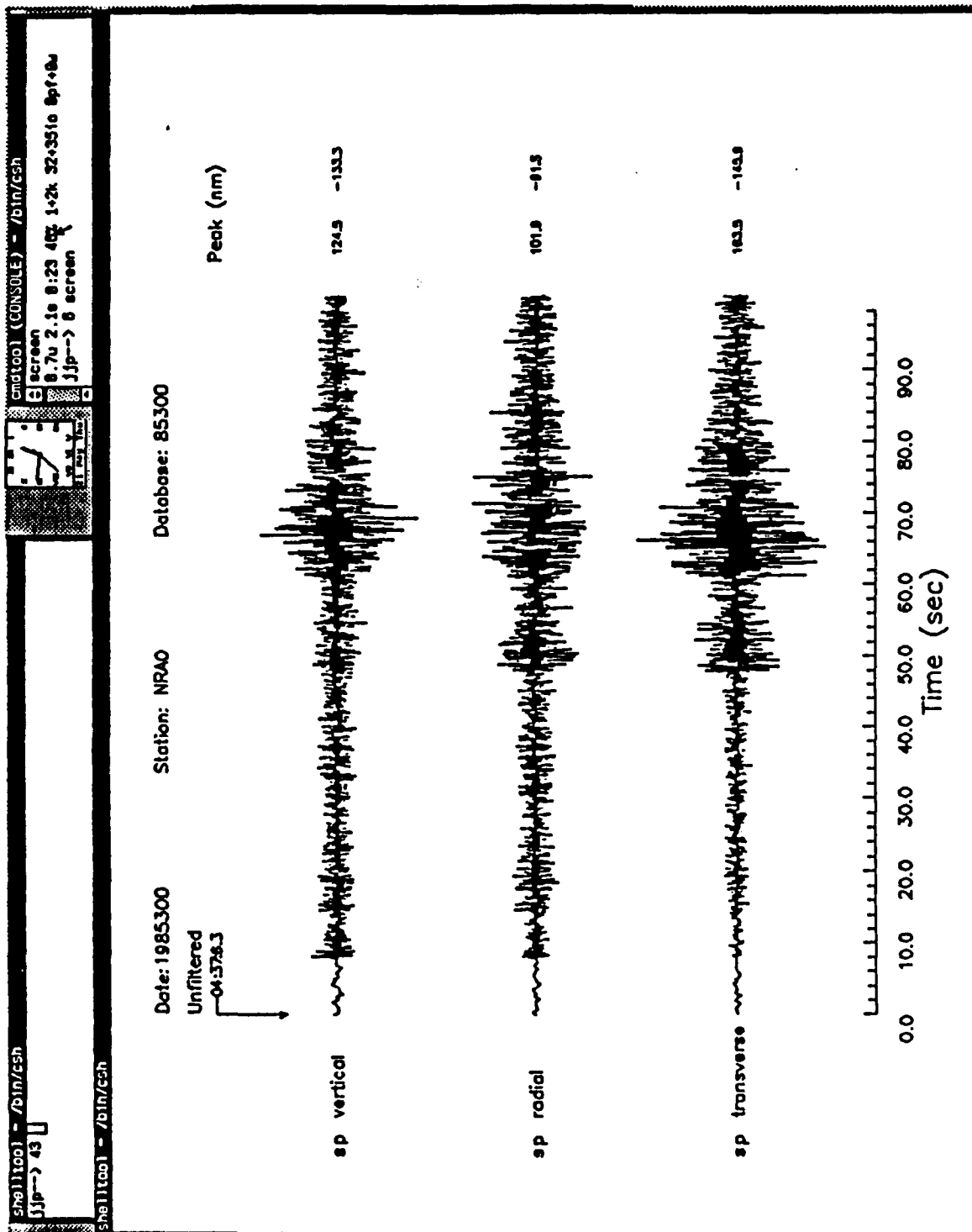
Number of seconds to skip in the *.w* waveform file, number of seconds to plot, and bandpass filtering.

NOTE

This same program is also available on beno with output to the laser printer.

AUTHOR

Jay J. Pulli
Center for Seismic Studies



NAME

section – displays a record section of array data, performs filtering, and produces a beam

SYNOPSIS

section

INPUT

CSS version 2.7 formatted *.wfdisc* and *.w* files.

OUTPUT

A plot of all the vertical component traces from an array, with positive excursions shaded, along with a beam of the data.

DESCRIPTION

section reads from a file called *wfids* in the database directory. This file contains a list of waveform ids and their corresponding moveouts in samples. From this list, it reads each waveform file and displays the trace with positive excursions shaded. Filtering can also be performed. To execute this program, one must first run program *nrbeam*, which reads an azimuth of approach and phase velocity and calculates the moveouts for the array. This program produces a file called *moveouts*. Then, program *mvid* must be run which correlates the output of *moveouts* with that of the *wfdisc* file. It then produces file *wfids*, which has the waveform ids and corresponding moveouts. *section* is written to be executed within a Sun window.

OPTIONS

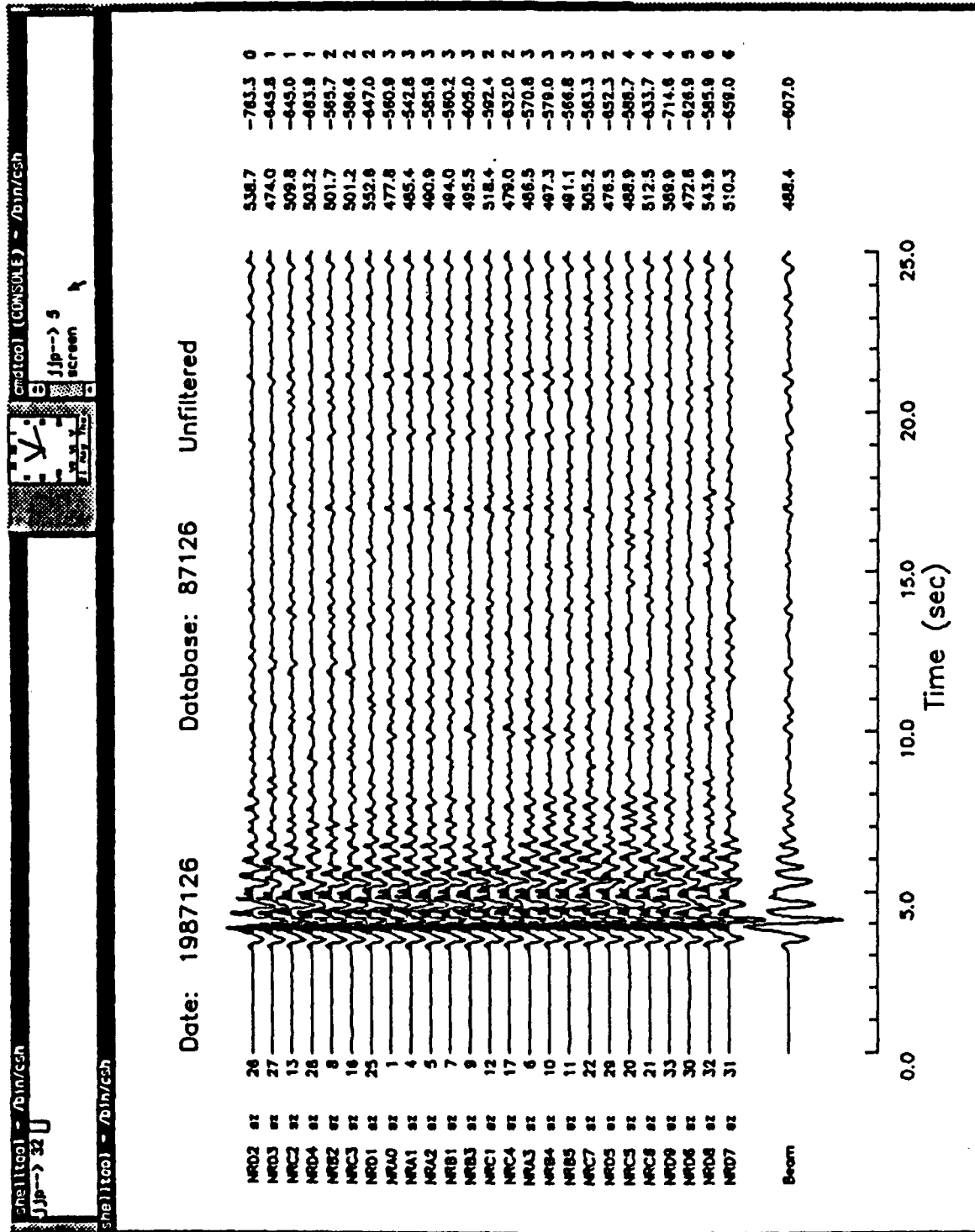
Number of sections to skip and display, filter parameters, and number of waveforms to include in the beam.

NOTE

This same program is also available on beno with output to the laser printer.

AUTHOR

Jay J. Pulli
Center for Seismic Studies



NAME

fsels – displays up to 10 filter bands of a single waveform

SYNOPSIS

fsels *database_prefix* *waveform_number*

INPUT

CSS version 2.7 formatted *.wfdisc*, and *.w* files. File *filter.info* contains the filtering information.

OUTPUT

A plot of the filtered waveforms.

DESCRIPTION

fsels filters and displays the waveform given by the *database_prefix* *wfdisc* file and the *waveform_number* in that file. Up to 10 filters may be used per display. The filter information is stored in the users directory in the file *filter.info*. A time axis is drawn at the bottom of the plot, along with other pertinent information such as the start time of the plot, date, station name, database name, and scaling information. *fsels* must be executed within a Sun window.

OPTIONS

Prompts are given for the number of seconds to skip in the *.w* waveform file, number of seconds to plot, bandpass filtering, and scaling. The filtered waveform can be displayed either to true scale or scaled independently. If independent scaling is chosen, the individual scale factors are shown to the right of each trace.

EXAMPLE

The following command line will plot the second filtered waveform in the data base named *exmpl*:

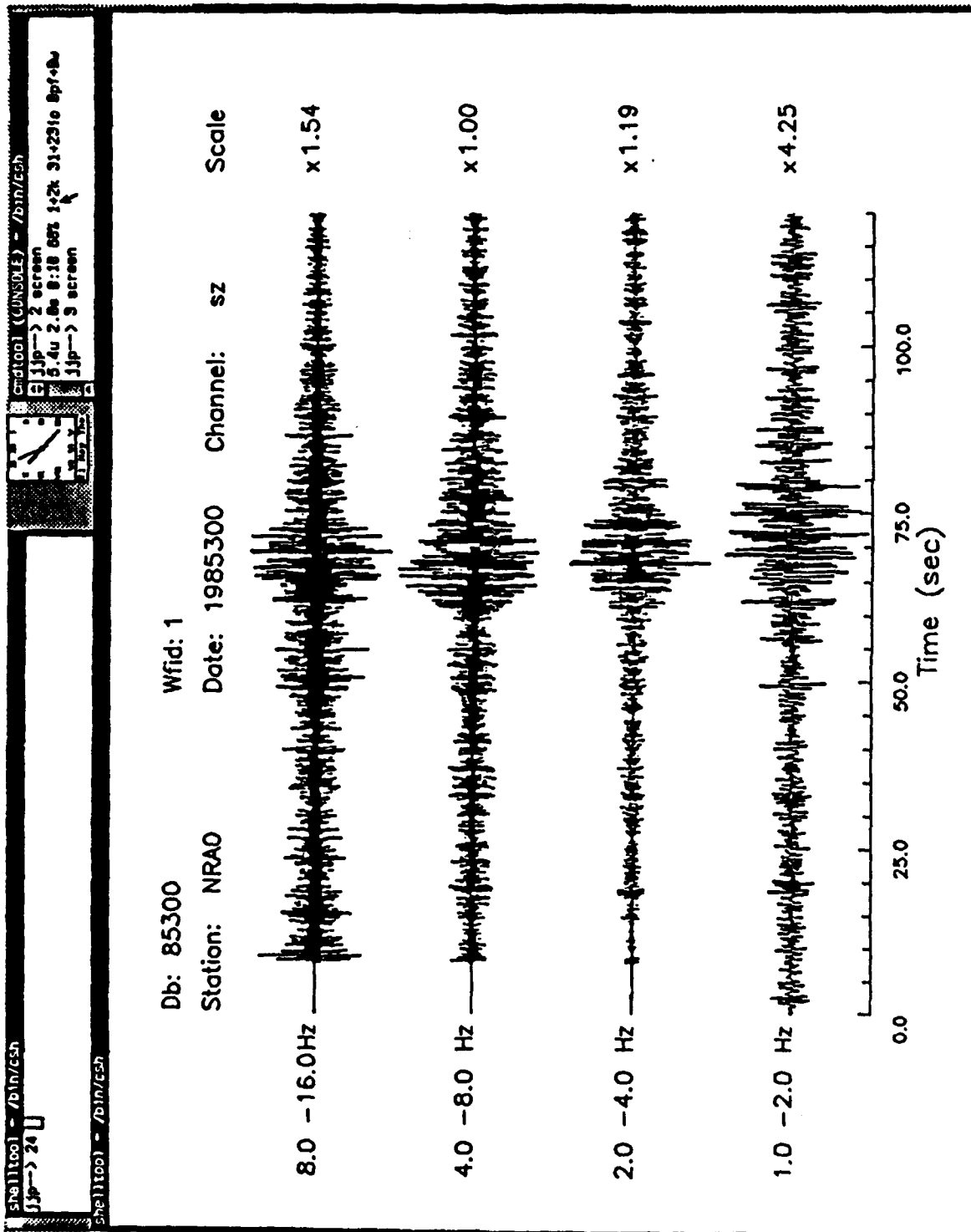
fsels exmpl 2

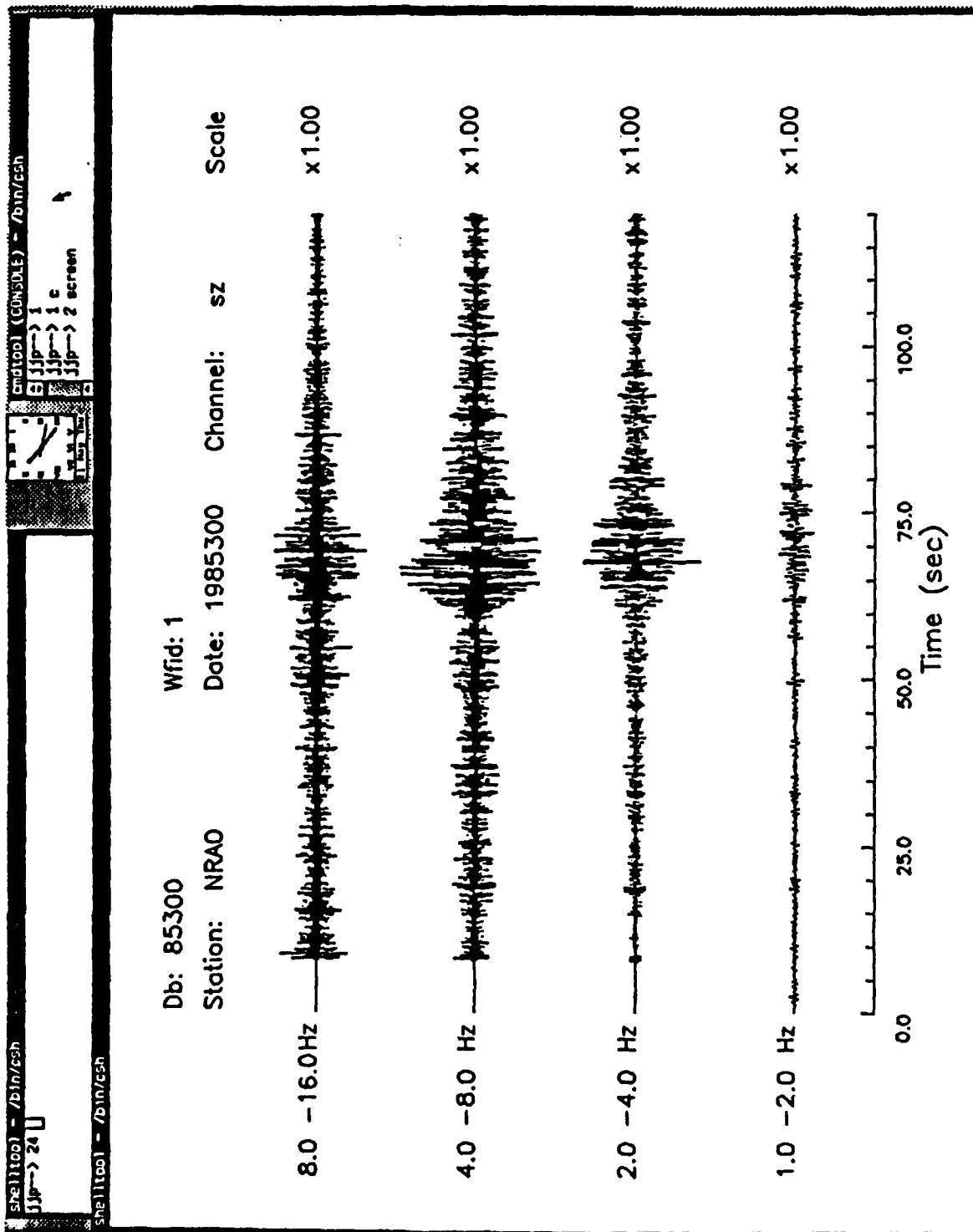
AUTHOR

Jay J. Pulli
Center for Seismic Studies

BUGS

The format and content of the *filter.info* file are not documented. It is assumed that the prefix of the *.wfdisc* and the *.w* files are the same. A friendly "Usage:" message does not occur.





NAME

sigspect – interactive spectral analysis and display program

SYNOPSIS

sigspect

INPUT

CSS version 2.7 formatted *.wfdisc* and *.w* files.

OUTPUT

Plots of the amplitude, power, or phase spectra, and *sigspect.lst* file that echos the input parameters and lists the computed spectral parameters.

DESCRIPTION

sigspect prompts the user for all input, analysis, and display information and computes the amplitude power or phase spectrum of a time series. It also computes the cumulative velocity squared and characteristic frequency for stress drop and source radius calculations.

sigspect is currently written to execute within a sun graphicstool window.

OPTIONS

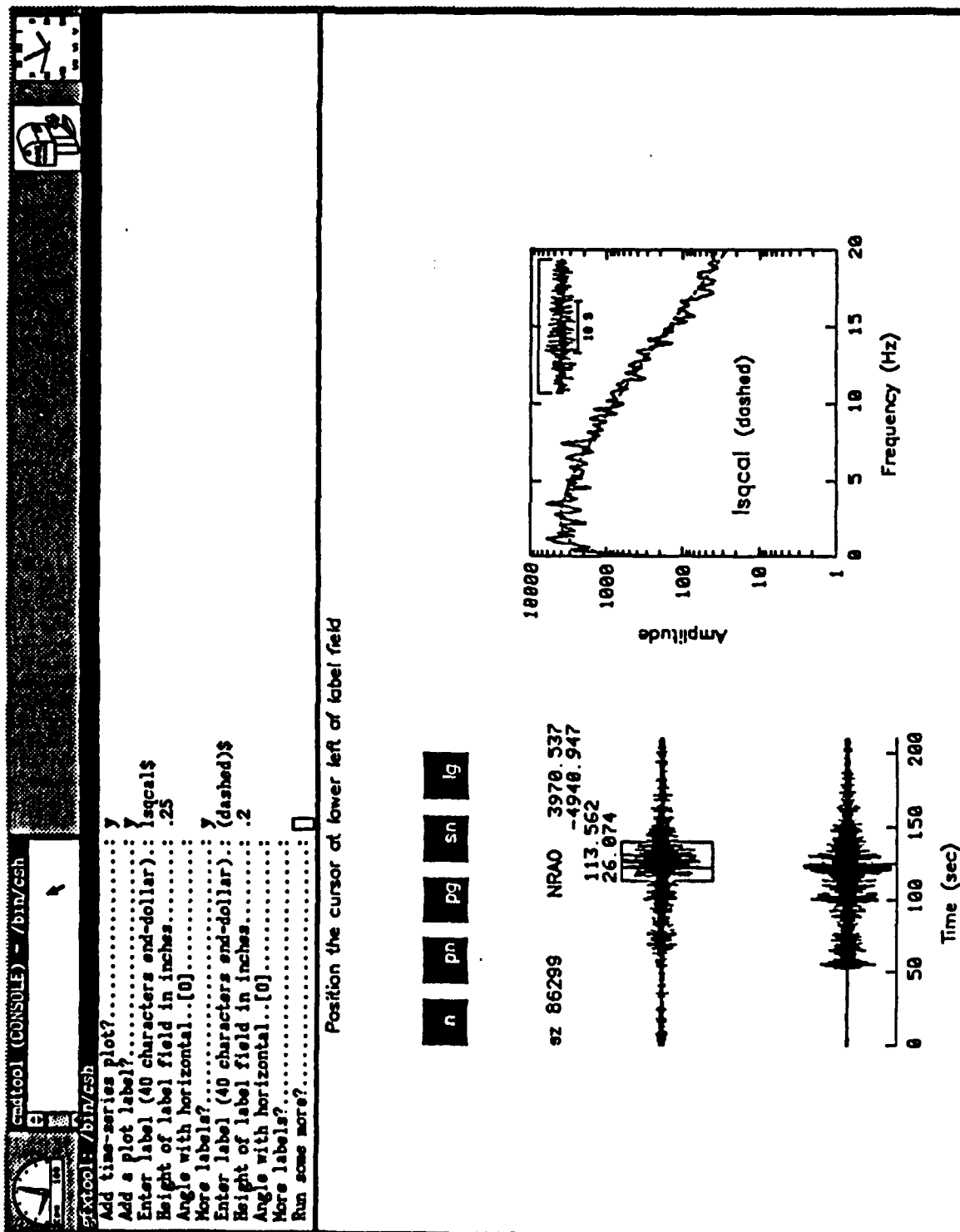
Optional time windowing, bandpass filtering, smoothing, non-linear regression to an asymptotic source model.

NOTE

The main program and associated libraries contain the elements necessary to accomplish the listed options, but these options are generally constrained for a specific application.

AUTHOR

Paul Dysart
Center for Seismic Studies



NAME

threecomp - plot station or array three-component particle motion attributes as a function of time

SYNOPSIS

threecomp

INPUT

CSS version 2.7 formatted *.wfdisc* and *.w* files.

OUTPUT

Graphical display of several particle-motion attributes.

DESCRIPTION

threecomp computes ground particle-motion attributes as a function of time and frequency for a time segment selected by mouse pick. Three-component seismograms are bandpassed and time windowed and the 3x3 covariance matrix is formed for each window. If there are multiple three-component sensors in an array, the covariance matrices from all sensors are averaged. The eigenproblem is then solved for the polarization ellipsoid. Parameters describing the ground particle-motions as a function of time are extracted from the polarization ellipse in each time window. When an array of three-component elements is used, the azimuth and horizontal phase velocity of the plane wave may be input from the file *threecomp.in* in order to improve the time alignment of the time windows at the various sensors before averaging. The sampling rate, number of samples, station, channel and calibration information are obtained from the *wfdisc* file.

Suncore graphics routines are used.

OPTIONS

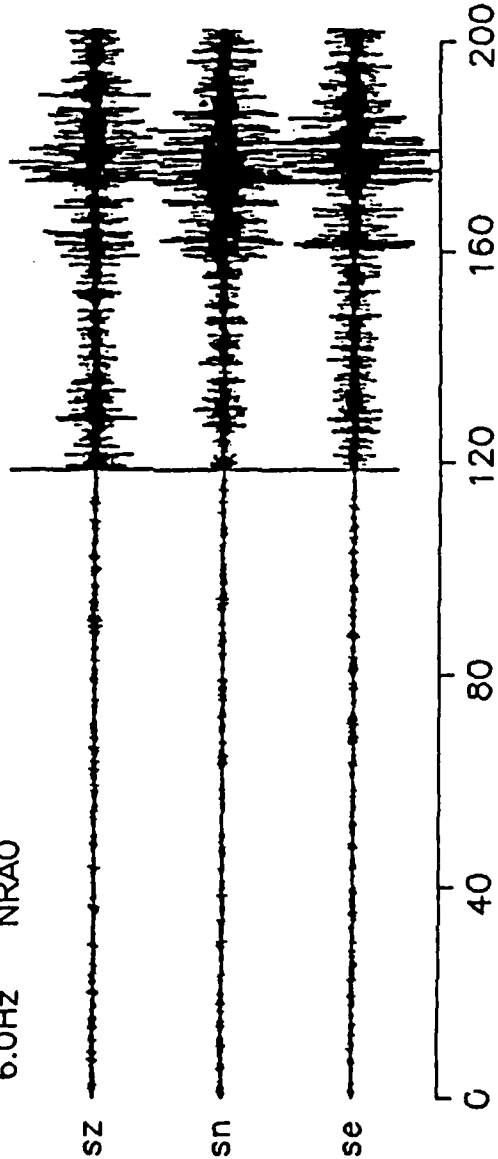
The data segment length, frequency band, time resolution, number of three-component stations and the particle-motion attributes to output are options defined in the file *threecomp.in*.

AUTHOR

Andy Jurkevics
Center for Seismic Studies

use pointer and any button to pick time

6.0Hz NRAO



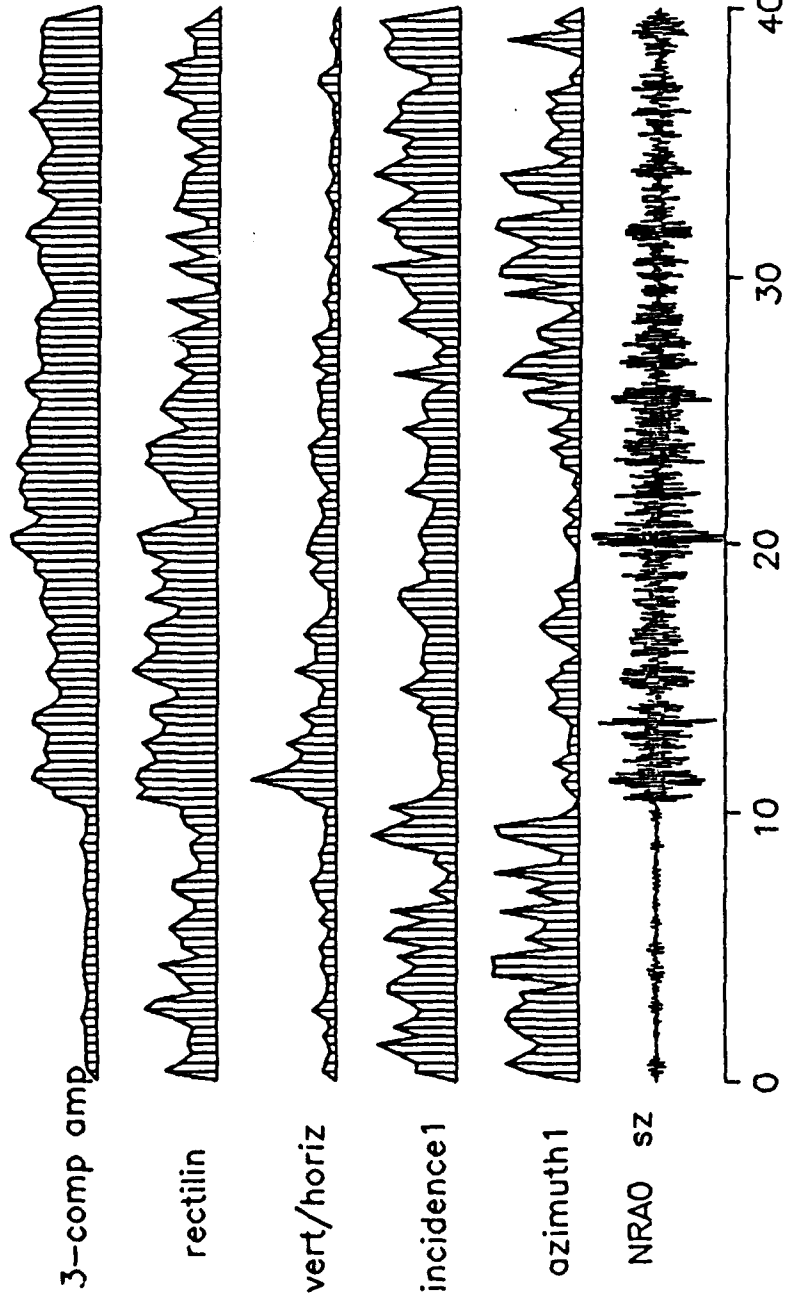
shel1tool - /bin/csh

86C17

1986 day: 17

6.0 Hz

14:11:46.15



NAME

velspec – compute and plot velocity spectra (vespagrams) for array data

SYNOPSIS

velspec

INPUT

CSS version 2.7 formatted *.wfdisc* and *.w* files, and input parameters, station names and coordinates from *velspec.in*.

OUTPUT

A velocity spectra contoured and plotted on the screen. The analysis segment time is selected interactively first.

DESCRIPTION

Velocity spectra (vespagrams) are computed as a function of time. The azimuth is held fixed and the horizontal phase velocity is varied. Array seismograms (vertical components) are input from CSS format local database for a time segment selected by mouse pick. Traces are time-shifted and a normalized multi-channel cross-correlation is computed in short sliding time windows. The data segment length, frequency band and time resolutions are adjustable. The sampling rate, number of samples, station, channel and calibration information are all obtained from the *wfdisc* file.

Suncore interactive graphics routines are used.

OPTIONS

The frequency band, time segment length and stations processed are options.

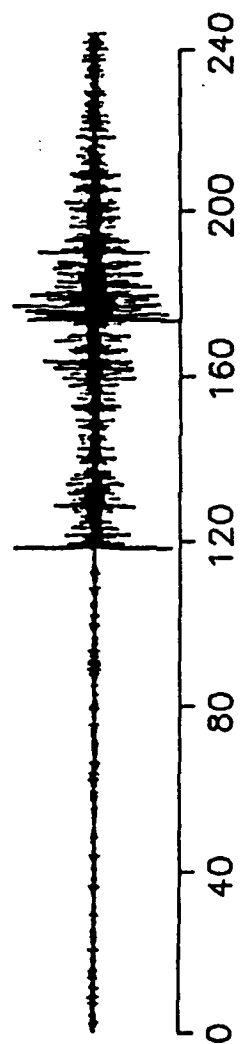
AUTHOR

Andy Jurkevics
Center for Seismic Studies

shelltool - /bin/csh

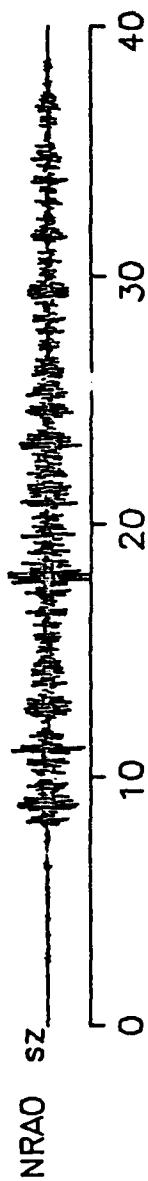
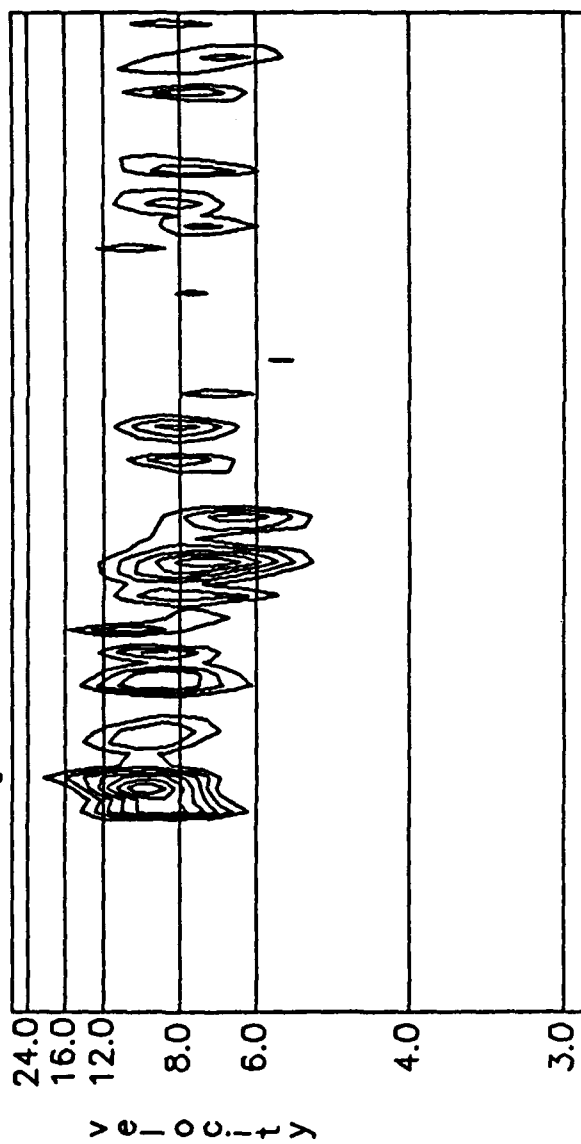
use any button to pick time

6.0Hz NRAO



shelltool - /bin/csh

1986 doy: 17 86017
14:11:48.43
6.0 Hz
225.0 deg



"Data Services" Provided through the Center for Seismic Studies

In addition to serving as an archive for RSTN, GDSN, and NORESS data, the Center for Seismic Studies provides access to certain older, yet still quite valuable, archives of seismic waveforms. These older archives consist of data recorded by, among others, the SRO and ASRO networks, the Very Long Period Experimental Stations and Special Data Collection Experiments, the large-aperture seismic arrays LASA (in Montana), NORSAR (in Norway), ILPA (in Iran), and ALPA (in Alaska), as well as the Long Range Seismic Measurement (LRSM) network and the Project VELA "Geneva-type" small-aperture arrays. Details on the available time frames, stations, and data channels may be obtained from the Center for Seismic Studies or from the Teledyne Geotech Alexandria Laboratories, where the data are stored.

These older archives are still an important source of seismic waveform data for research on both earthquakes and nuclear explosions. The periods of operation of these arrays and networks span the dates of many significant seismic events which are still being studied, and in many respects the utility of these data for research purposes is unsurpassed by that of data from the more recent archives. For instance, the aperture of the large arrays significantly exceeds that of all present-day arrays, and the density of coverage of (permanent, semi-permanent, and temporary) LRSM stations within the continental United States is much greater than that of the sparse RSTN.

A principal task of the Data Services operation of the Center for Seismic Studies is the analog-to-digital (A-D) conversion of the LRSM data. These waveforms were recorded both on film and in FM analog format on magnetic tapes, but they can be converted to the ".w" digital waveform format used at the Center. Currently the A-D conversion is performed in response to large, long-term requests made by DARPA and to smaller requests made by end users of the data. These latter requests are met by Teledyne Geotech, who charge the recipients of the data for the labor involved in retrieving the waveforms and digitizing them. An estimate of the cost of filling any particular data request will be made by Teledyne Geotech prior to accepting an order for the labor. Data requests made by DARPA are paid for in their entirety by the Data Services portion of the Operations and Maintenance contract for the Center.

Users wishing to avail themselves of the data stored in these old archives should note that it is now a policy of the Center for Seismic Studies that the digital waveforms generated as the result of any A-D request will be made available to the Center for addition to the databases of digital seismograms that can be retrieved from off-line storage there.

INSTRUCTIONS FOR PREPARATION OF DATABASES FOR THE CENTER FOR SEISMIC STUDIES

DARPA seismic research contractors are encouraged to provide research projects so that the data may be made readily available to the research community. The following guidance is provided to facilitate the incorporation of research databases into the Center database management system and to make the data available to the community as quickly as possible.

All official databases at the Center are in Center Standard format currently version 2.8 which is documented in Center Technical Report C87-04, "Database Structure, Version 2.8," September 1987.

The Center uses the INGRES relational DBMS licensed by Relational Technology.

Before beginning construction of a database for installation at the Center, the Center database administrator, Richard Baumstark should be contacted at (703) 276-7900 to insure that the data set does not already exist at the Center. He will provide detailed specifications for formatting the data and insuring that all essential information such as calibrations are included correctly.

The actual installation of the database at the Center will be done by the DBA. Once installed as an official Center database, the database will be documented as to author, data type, database relations used, and descriptions of software which may be used to retrieve the data. Users of the Center will then be able to access and use the data provided.

**CONTACTS AT THE
CENTER FOR SEISMIC STUDIES
(703) 276-7900**

**GENERAL INFORMATION ON USE OF
CENTER FACILITIES**

**Dr. Carl F. Romney (Director)
Dr. Alan S. Ryall, Jr. (Director of Research)**

**DETAILED INFORMATION ON DATA,
SOFTWARE AND SYSTEMS**

DATABASE ADMINISTRATOR	Richard Baumstark
SOFTWARE	Mary Ann Brennan
SYSTEMS ADMINISTRATOR	Rick Adams

Discrimination of NTS Explosions and Earthquakes Using High-Frequency Regional Data

Eric P. Chael

Div. 9111, Sandia National Laboratories
Albuquerque, NM 87185

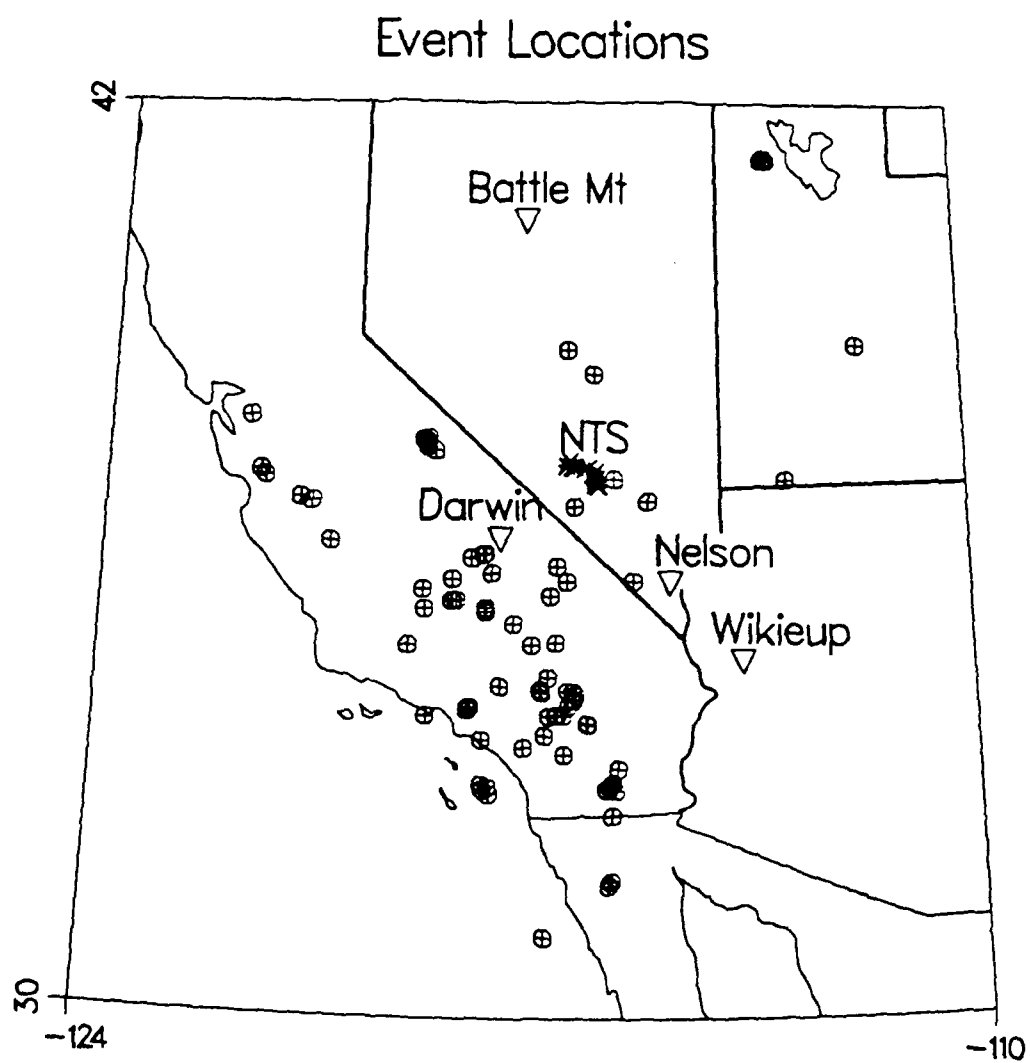
Abstract

To evaluate the potential of high-frequency (HF) monitoring for detecting and identifying nuclear tests, we are operating HF seismic systems at Nelson, NV, Battle Mountain, NV and Darwin, CA. These stations record regional signals from NTS nuclear tests and from earthquakes throughout the Southwest. The earthquake records have substantially stronger signals above 10 Hz than the explosion records, for sources of similar magnitude and distance. Above 25 Hz, NTS explosions are virtually undetectable above the ambient noise. Regional earthquakes, on the other hand, often show clear signals to 40 Hz and above. This directly contradicts the predictions of Evernden et al. (1986), who argued that explosions would be stronger at high frequencies. To quantify the observed spectral differences, we fit straight lines to plots of Pg velocity power density vs. frequency between 4 and 30 Hz. The slopes successfully discriminate the NTS explosions from earthquakes at comparable distances. The slopes are nearly independent of magnitude between M_L 2.5 and 6.0, but they steepen with distance as attenuation removes HF energy. The distance dependence differs markedly between Darwin and Nelson, suggesting differences in Q between the regions around these stations.

High Frequency Seismic Systems

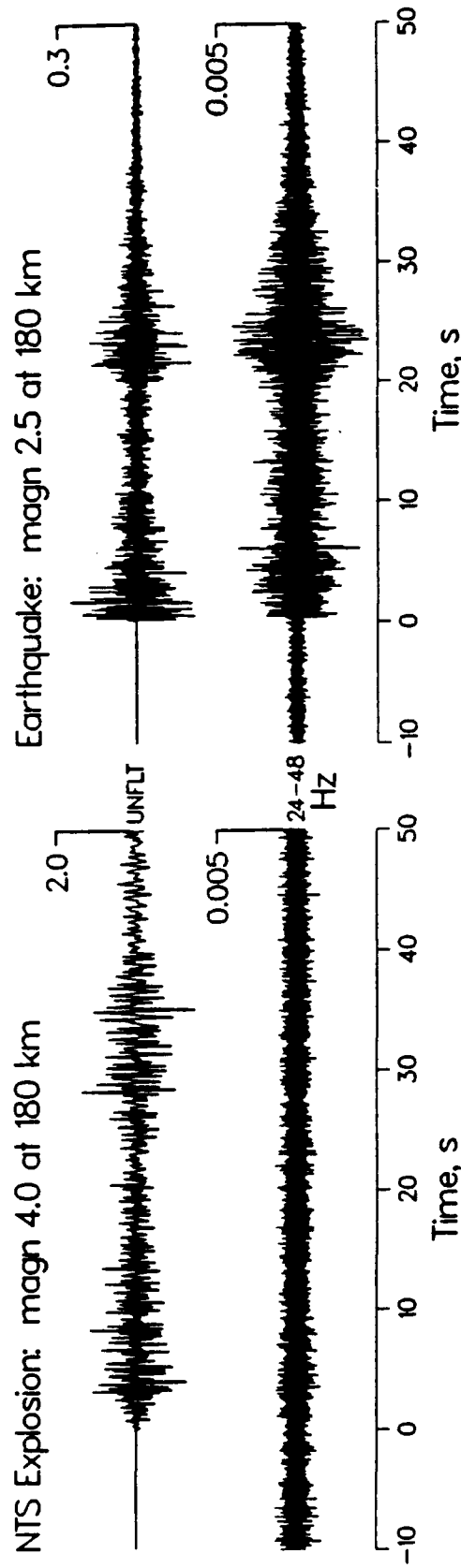
We deployed the HF systems in mine drifts which are used as stations of Sandia's Off-Site Seismic Network. Teledyne-Geotech GS-13 seismometers standing on concrete slabs in the mines detect vertical ground motions. Three signals at different gains are obtained by feeding the seismometer outputs into fixed-gain amplifiers. The highest-gain channels sense ambient earth noise; overall system gain exceeds 120 dB. The signals are sampled 200 times a second with 16-bit A/D converters. DEC 11/73 computers at each station run event detection algorithms to control recording. The data can be accessed from Sandia over a modem.

Spectra of ambient background at Nelson and Darwin have been obtained from noise samples preceeding detected events. Between 1 and 70 Hz, the displacement amplitude spectra roll off approximately as f^{-2} (i. e., white acceleration spectrum). At its quietest, the Darwin site noise is below the quiet Lajitas noise model (Durham, personal communication), while the Nelson site stays somewhat above this reference.



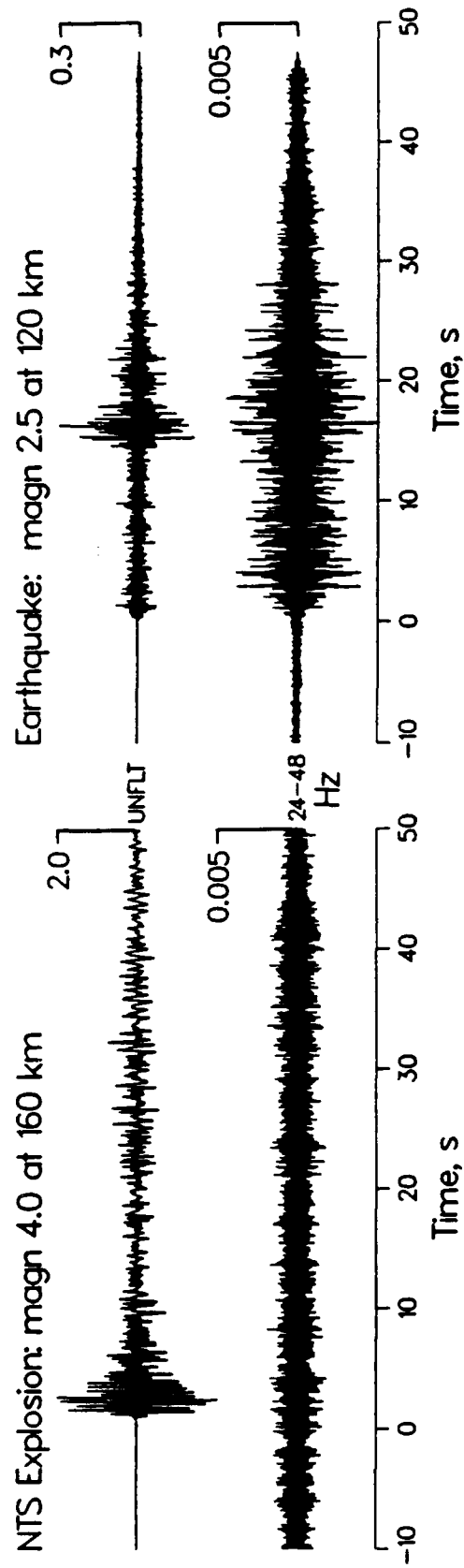
Map of station and event locations used for this study.

Nelson

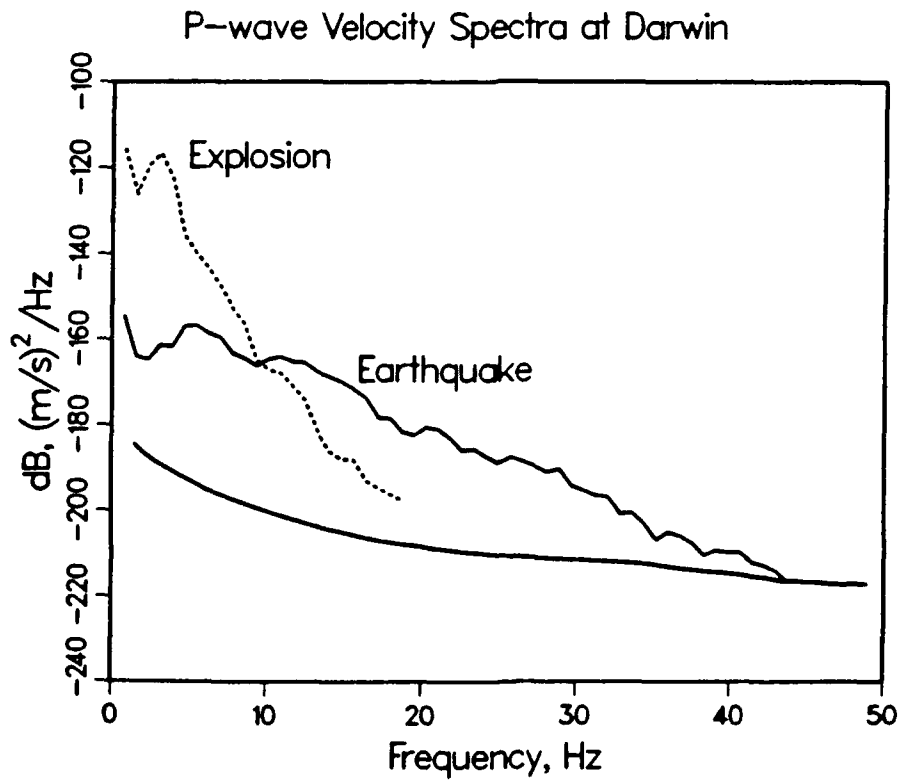
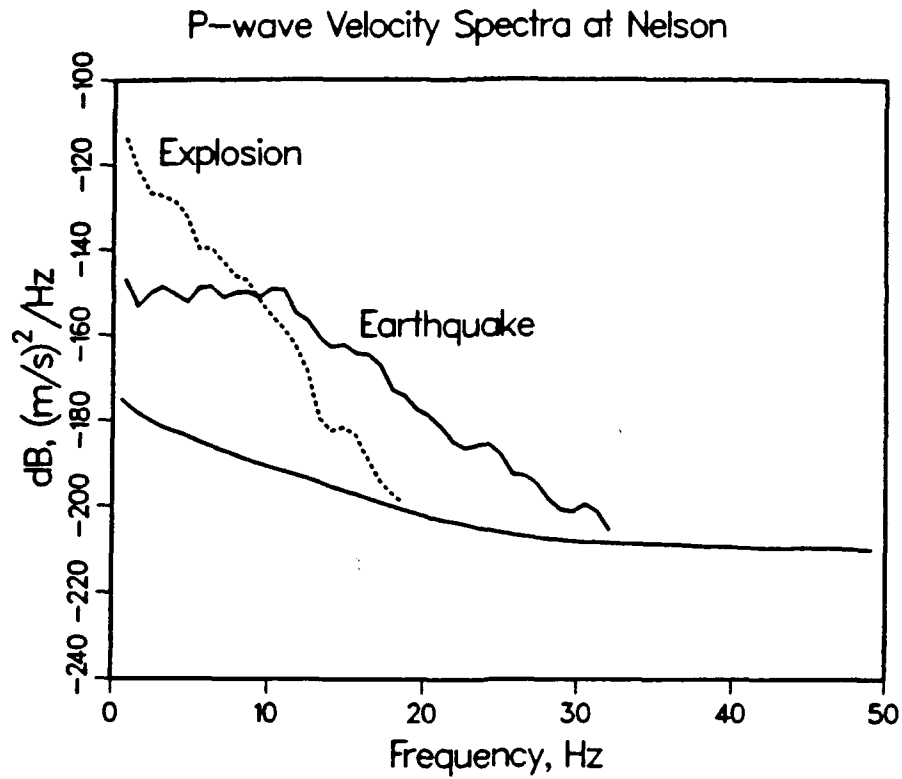


Records obtained at Nelson from the NTS test "Abilene" and an earthquake just southwest of NTS. The upper traces show the signals as originally recorded by the systems, and the lower traces show the HF signals between 24 and 48 Hz, produced by filtering the raw signals. Note that the explosion is larger on the unfiltered trace, but it is lost in the noise at high frequencies.

Darwin

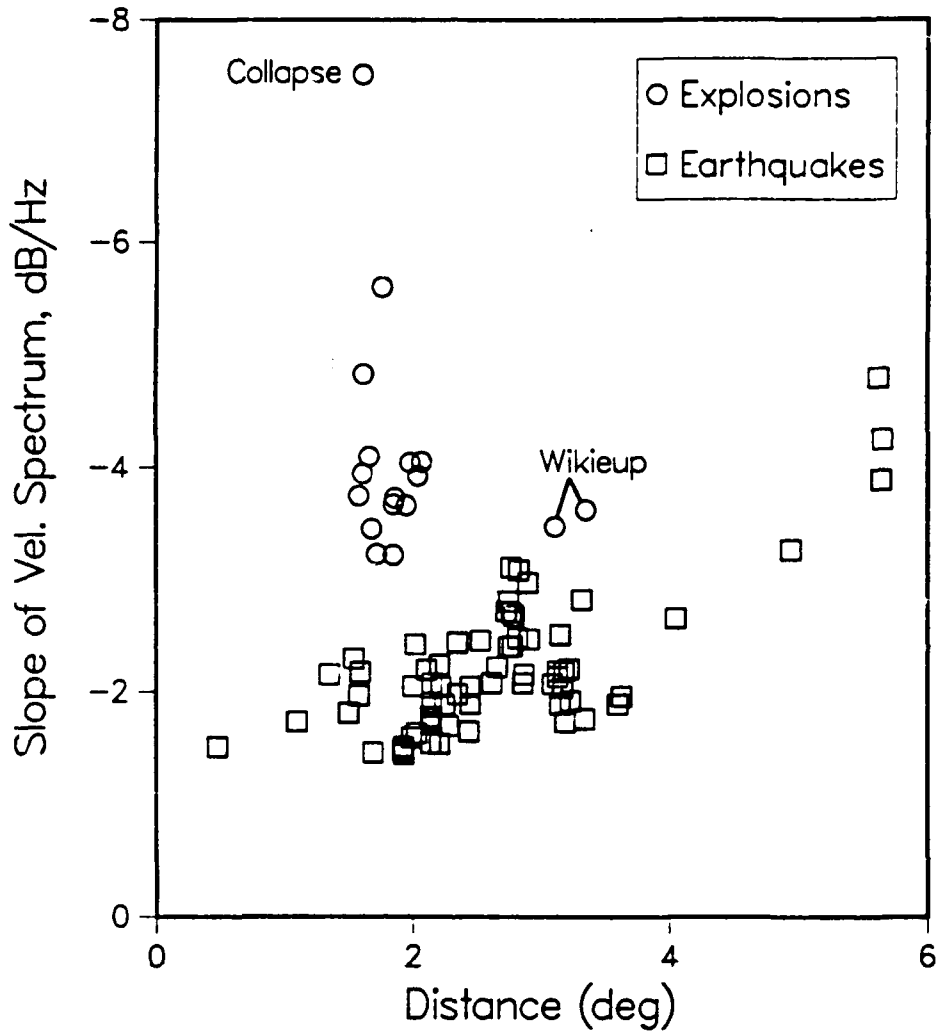


Same as previous figure, for the Darwin station.



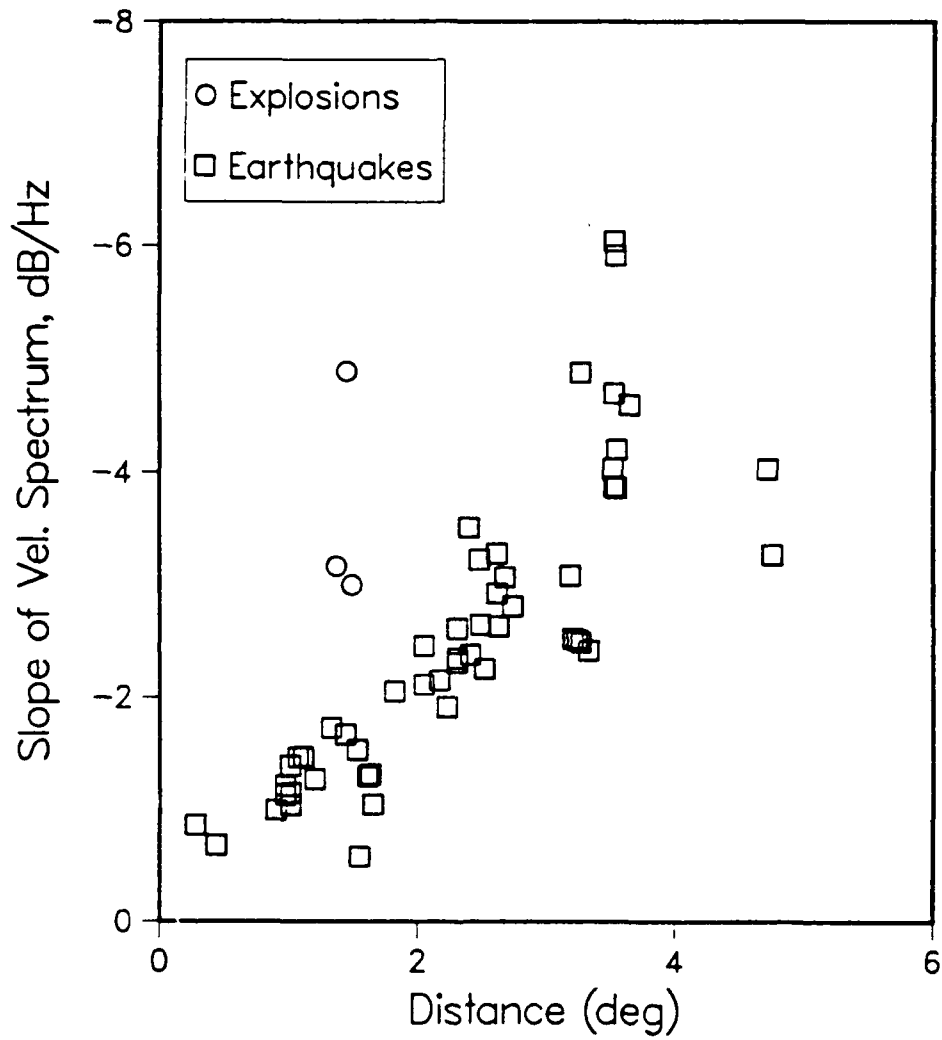
Velocity spectra of the P waves from the earthquake and explosion records shown in the previous figures. The lowermost curves represent typical ambient noise conditions at the stations.

Pg Spectral Slopes at Nelson



Slopes of the Pg velocity spectra of the events we have recorded at Nelson, plotted against epicentral distance. Steeper slopes (less high-frequency energy) plot higher on the figures.

Pg Spectral Slopes at Darwin



Same as previous figure, for the Darwin station.

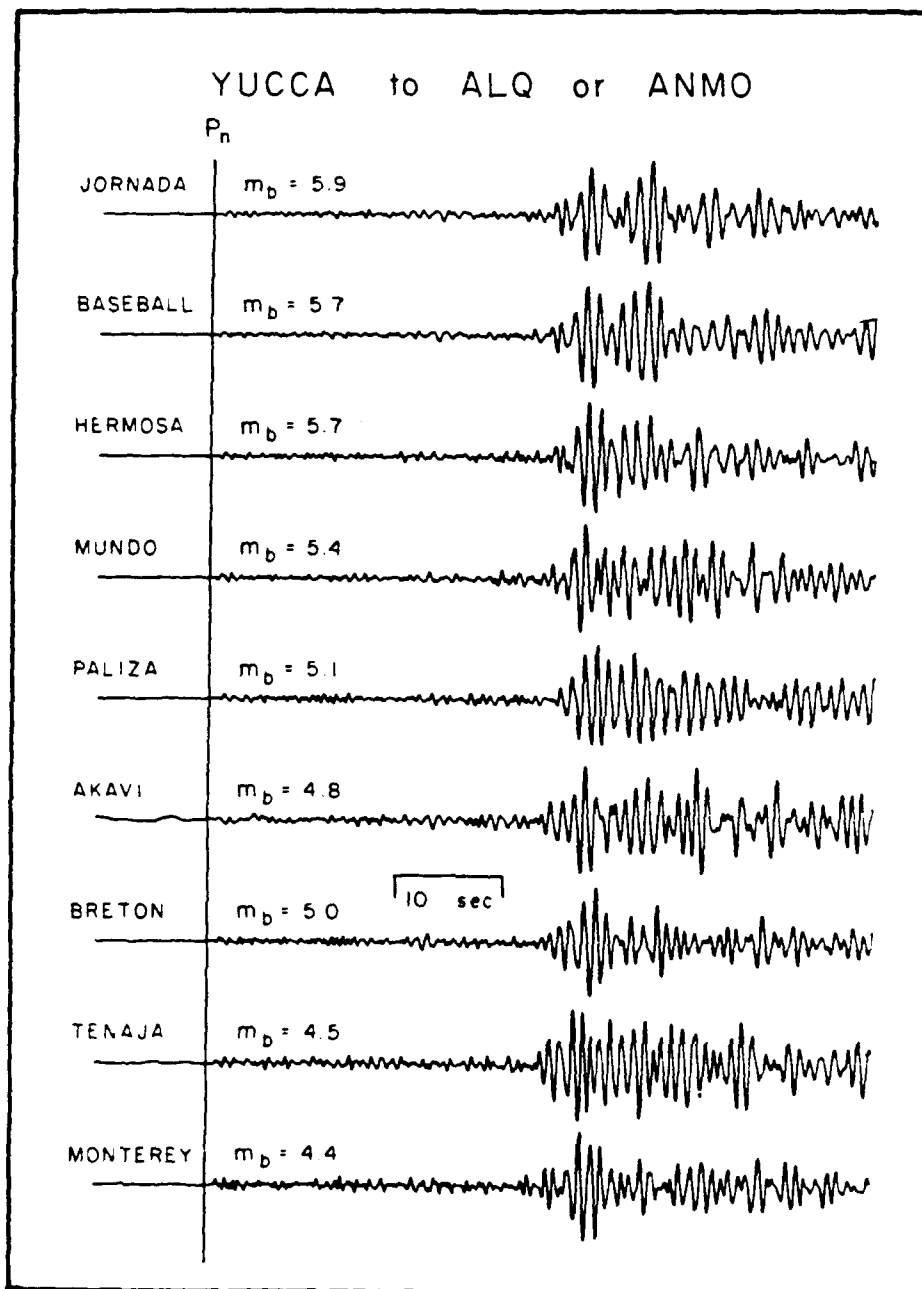


Figure 1.

A subset of the digital $P_n - P_s$ records collected from Yucca events recorded at ANMO or ALQ. There is some hint of a resonance phase pattern in some records, but as usual in short period data the scattering is strong.

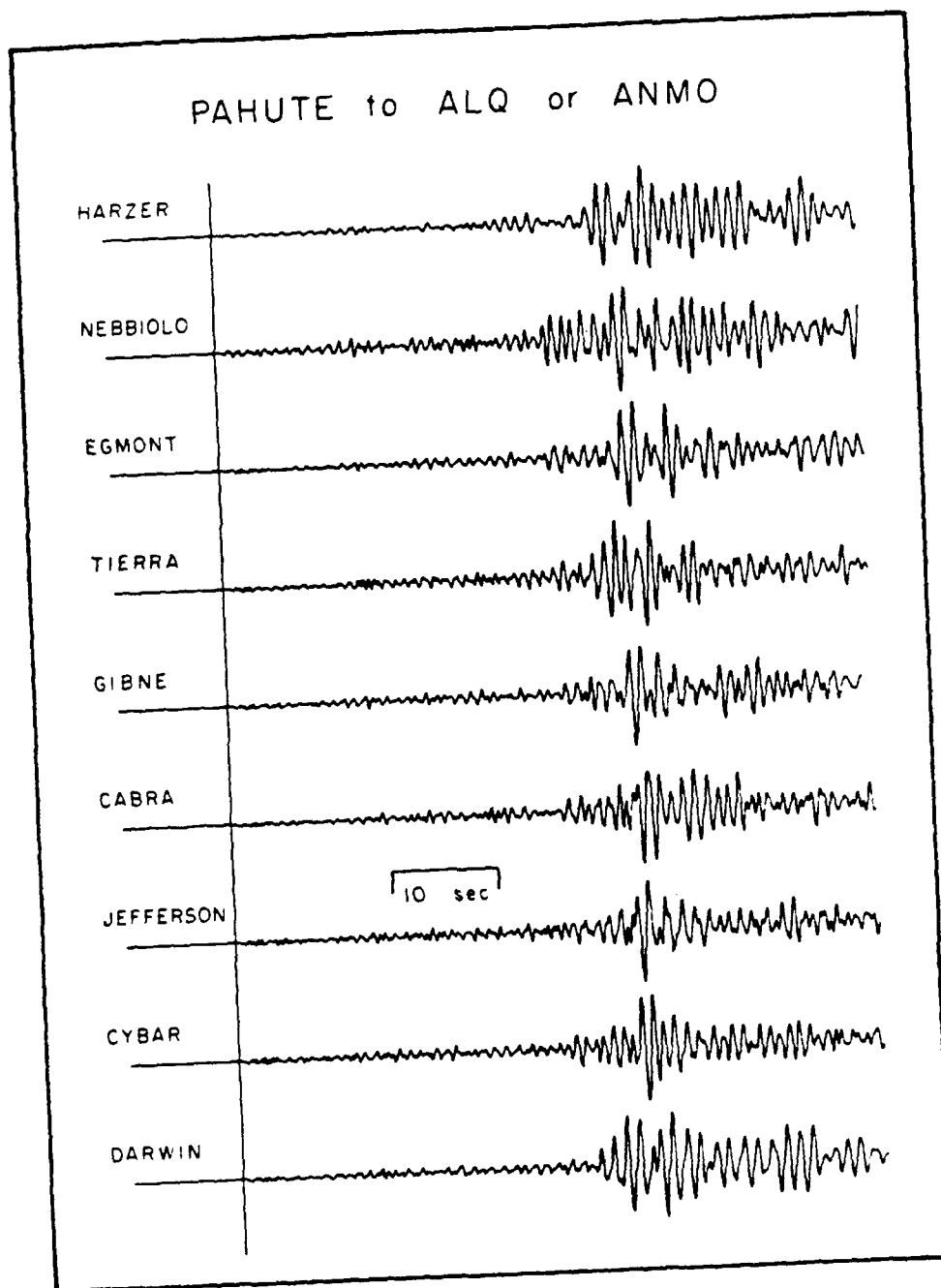
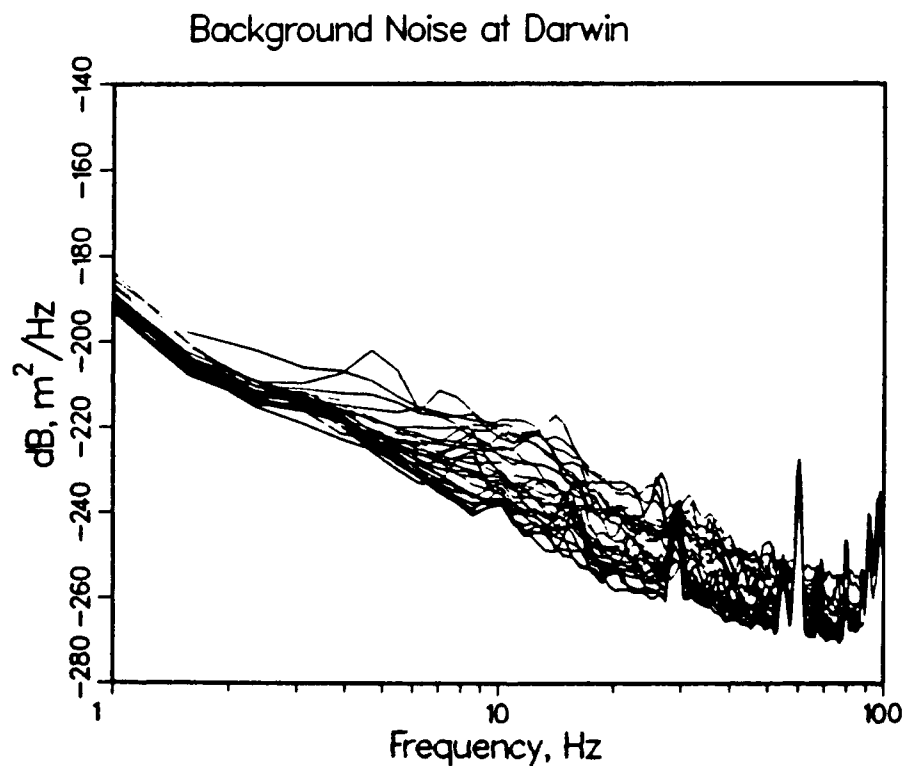
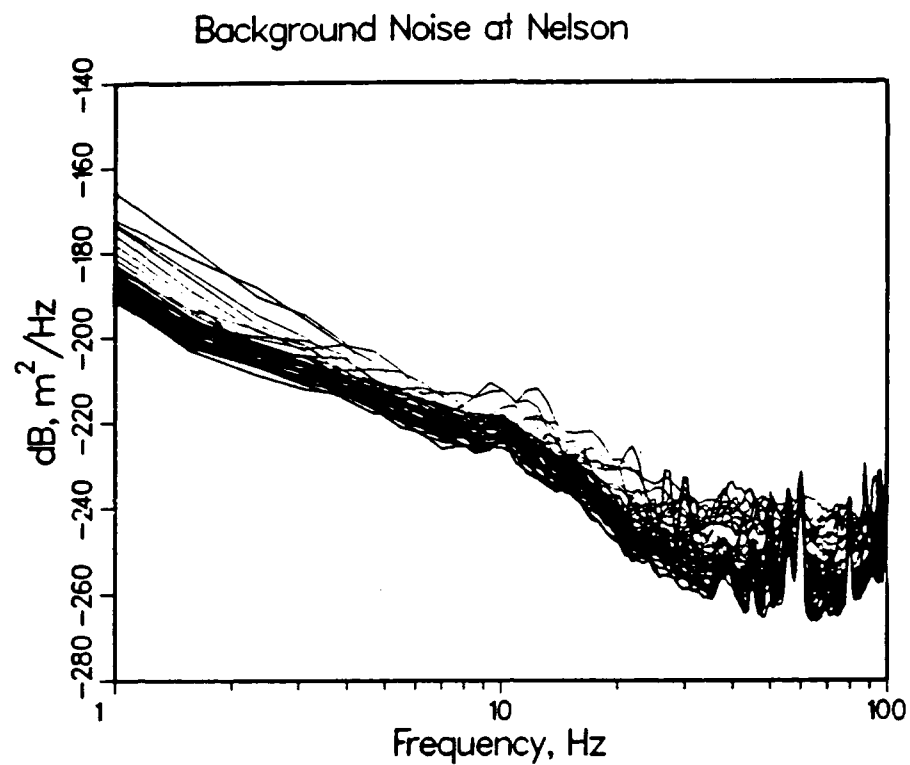


Figure 2.
A subset of the digital $P_n - P_s$ records collected from Pahute events recorded at ANMO or ALQ. Again, though there are indications of resonance phases, the scattered energy dominates.

The simplest portion of a seismogram to interpret is the first arriving energy since it must have traveled the entire path as P without substantial scattering. One way to develop a discriminant would be to test this first energy for the pP arrival which will occur much sooner for explosions than earthquakes. The first arrival from 200 to 1000 km in the Western U.S. is P_n . We have collected appropriate sample explosion P_n waveforms and find they do indeed contain a feature which can be interpreted as pP_n . pP can not usually be observed teleseismically because interference with P is too strong. However, it was observed at some stations in records from the deepest U. S. test CANNIKIN (FIGURE 1). It appears as a distinctive double peak in the "c" swing. If this feature is modeled, it is necessary to artificially delay the pP arrival until after the elastic time. It has been observed in many studies that "effective pP" arrives later than the elastic time and it is believed that this is related to the inelastic processes in the source region. The pP arrival should be more apparent in regional P_n than teleseismic P because small higher frequency sources can be examined, because pP arrives later and because t^* is much higher. We interpret the high frequency P_n arrival as a turning ray in the weak gradient of the lid rather than a true head wave (FIGURE 2).

We gathered observations from JAS (370 km), BKS (525 km) and ALQ (926 km). In virtually all cases for all test sites the first arrival exhibited a double peaked "c" swing (FIGURES 3 4 AND 5). The arrival has the proper sense of moveout for pP in that it is farthest back at JAS, closer to P_n at BKS and closest at ALQ. In some cases, it appears that pP is larger than P in which case it has to be interpreted as a composite elastic-inelastic phase. We have begun to build a discrimination data base using earthquakes occurring near NTS recorded by these same stations. In FIGURES 6 AND 7, we show the first 12 records we obtained. It is clear that in many cases the earthquakes could be discriminated by the absence of pP_n . In FIGURE 8, we compare observations to synthetics computed with a ray parameter appropriate for ALQ. Effective pP is clearly later than elastic pP. In future work, we plan to develop a waveform comparison code that will discriminate explosions from earthquakes objectively.



Displacement power spectra of ambient earth noise recorded at random times at the Nelson and Darwin stations. The upturn in the spectra above 70 Hz results from system noise.

**Report on AFGL/DARPA Research Symposium, May 1988, by Lane
Johnson**

Overall, I thought that this was an excellent symposium and one which will continue to build the reputation of this meeting as one of the best research symposiums on basic seismology that exists in the field, independent of the DARPA emphasis.

The oral presentation part of the program was similar to other years and I would rate that part of the program as good. I believe the presentations are improving each year and the schedule was maintained quite well this year. Although this part of the program is probably necessary, in my opinion it is not the most important part. The good material which is presented will almost always show up in reports (if it has not already) where I can study it more completely and obtain more benefits. The discussions following the talks were somewhat inhibited by the size of the group and the need to maintain a schedule.

The Wednesday morning session concerning perspectives on research issues was excellent and well received. Comparing scientific and political perspectives side-by-side is a good idea. Also, giving the contractors the opportunity to step back, take a wide ranging view, and give their opinions about the directions of the program is a very useful exercise. For instance, Archambeau's ideas generated a lot of discussion during the rest of the meeting. I am sure that everyone realizes that the contractor's views should not be taken as the official position of the program, but they help to generate a general discussion of where the program is and should be going and I believe it is important that everyone think about this.

The poster session also turned out to be very good. The attendance was good and people stayed and talked for a long time. I am in favor of continuing this part of the meeting and would personally prefer to present a paper in the poster session rather than the oral session. Let me throw out an idea which might be worth an experiment. What if one spread out the posters and interspersed a few chairs, tables, and note pads so that people could set down and really get into some useful discussions? Would this generate the type of interaction that we have been thinking about when talking about workshops in the last couple of years?

As always, a very important part of the meeting were the discussions that went on at coffee breaks, meals, and after the sessions ended. Having everyone together with few distractions facilitates this aspect of the meeting, and the environment this year was excellent for this type of activity.

Let me contribute an opinion about your comment during the opening of the meeting in which you said that one purpose of the meeting was to demonstrate to DARPA that the program is producing useful results. While I am sure you are right about that, I do not think that it should be emphasized. My concern is that some contractors might be inhibited by such an emphasis and be less willing to present new

(possibly wrong) ideas or contribute impulsive (possibly dumb) comments during the discussions, and I believe that this would tend to diminish some of the excitement of the meeting. Showing up here is my belief that, in addition to presenting science that has been completed, one of the purposes of this meeting is to actually do new science and this requires a rather permissive atmosphere. I would expect DARPA to be able to recognize the advantages of a stimulating productive meeting with some rough edges over a polished meeting with few new ideas.

I sympathize with your attempts to control the size of the meeting but I fear that you might be a victim of your own success in this area. As an example, this year I brought along one of our students who had reached the stage where a meeting of this type could be a very important stimulant to his career, and I greatly appreciated the opportunity to do that. So, I guess you will have to keep applying the pressure or the size will get out of hand, but it will be a tough job.

In summary, I believe that the meeting this year was very useful, important to the program, and continued the trend of showing improvement over the previous year. You seem to have found a good balance between keeping things that work and experimenting with new ideas which might work.

DARPA/AFGL SEISMIC RESEARCH SYMPOSIUM
2-6 May 1988

An overall assessment of the 10th annual DARPA/AFGL Seismic Research Symposium is that it was very very good. The atmosphere was relaxing and the setting was conducive to a good exchange of information. The meeting rooms were quiet and the microphone and projection facilities were adequate.

The group lunches proved to be an excellent mode of providing continuity of the meeting atmosphere through the entire day. They also prevented excess scattering of the participants so that the start up of the afternoon sessions was not delayed. The dinner Tuesday evening provided a nice social touch after the first day of technical discussions. The open evening on Wednesday allowed participants to form their own private groups for either social or business purposes.

The panel perspectives aired on Wednesday morning provided a nice broadening of the rather narrow view which most researchers have of the issues involved in seismic research.

The IAS overview and demonstration may have been somewhat overdone. While the concepts and capabilities of the system were of general interest, most of the participants will have limited access and/or occasion to use the system, and limited probability of having their own set of HF arrays so that they would have a need for the system.

The poster session was excellent. It provided a loose structure for a free exchange of ideas and also complemented the IAS demonstration limitations. The only problem seemed to be the lack of sufficient space to hold the session in.

The length of the meeting seemed to be about right, although ~~another~~ half day to day of meeting probably would not be too long. The available technical talks and their quality should be the controlling factor. For example, it is difficult to assess whether or not a restoration of the Mt. Palomar Observatory Tour would have warranted extending the meeting another half day. Many people were looking forward to the tour, but were not too upset when it was cancelled.

Some specific problems which could be worked on:

- Slides and viewgraphs - These should be of a professional quality. Virtually everyone has access to a word processor and/or typewriter and Xerox machine. So hand drawn viewgraphs are not necessary. These reflect a general lack of planning and of consideration for the audience.
- Time slot compliance - Most participants did tailor their talks to fit the 20 minute time frame. While it is difficult to control some speakers, there should be some mode of achieving better compliance with the time allocations. Some speakers obviously needed more time to present their research results. Perhaps some talks should be extended to 30 or 45 minutes, either by AFGL or the speakers request - and then scheduled with that time allowance. As with the slides, this should be a matter of professional pride and of consideration for fellow researchers.

In summary, the problems seemed very minor, the activities well organized, and the events well received. I believe that the meeting was extremely informative for everyone involved.

**END
FILMED**

DATE: 3-91

DTIC